UNIVERSITAT POLITÈCNICA DE VALÈNCIA

Department of Mechanical and Materials Engineering

PhD Thesis

Efficient simulation of the pantograph-catenary dynamic interaction. Catenary optimisation and installation error analysis

---

Presented by: Santiago Gregori Verdú

Supervised by: Dr. F. Javier Fuenmayor Fernández

Dr. Manuel Tur Valiente

Valencia, May 2018

PhD Thesis

Efficient simulation of the pantograph-catenary dynamic interaction. Catenary optimisation and installation error analysis

for the degree of

Doctor in Industrial Engineering and Production

presented by

Santiago Gregori Verdú

at the

Department of Mechanical and Materials Engineering

of Universitat Politècnica de València

Supervised by

Dr. F. Javier Fuenmayor Fernández
Dr. Manuel Tur Valiente

Valencia, May 2018

PhD Thesis

Efficient simulation of the pantograph-catenary dynamic interaction. Catenary optimisation and installation error analysis

Presented by: Santiago Gregori Verdú

Supervised by: Dr. F. Javier Fuenmayor Fernández

Dr. Manuel Tur Valiente

QUALIFYING TRIBUNAL

President: Dr. _____

Vocal: Dr. _____

Secretary: Dr. _____

Valencia, May 2018

Abstract

Modelling and simulation of the dynamic interaction between pantograph and catenary has become a powerful tool to expedite the catenary design process since, among other advantages, it helps in reducing the number of the costly experimental in-line tests.

In order to tackle these numerical simulations, in this Thesis the catenary system is modelled by the Finite Element technique, based on the absolute nodal coordinates formulation, while a simple lumped-mass model is used for the pantograph. The interaction between the two systems is accomplished with a penalty formulation. After solving the initial nonlinear configuration problem, the equation of motion is linearised with respect to the static equilibrium position and it is then solved in time by applying the Hilber-Hughes-Taylor (HHT) time integration method. However, dropper slackening and pantograph contact losses are two sources of nonlinearities which must be considered in the solution procedure at the expense of an increase in the computational cost.

The main objectives of this Thesis are both to find optimal catenaries in terms of current collection quality and to analyse the effect of installation errors in the dynamic behaviour of the system. To achieve these goals, it is mandatory to perform a large number of pantograph–catenary dynamic simulations for which the computational cost can become prohibitive.

In order to reduce this computational effort, the first proposal made in this Thesis is to precompute a parametric solution of the pantograph–catenary dynamic interaction for all values of the design variables, by means of the Proper Generalised Decomposition (PGD) technique. Thus, the dynamic response of the system would be instantly available when it is requested by the optimisation or the stochastic algorithms. If dropper lengths are considered as design variables, this parametric approach is successful when applied to the static equilibrium problem. Nevertheless, in the dynamic case, when dropper slackening is considered, the solution exhibits a

great sensitivity to small changes in the parameters and therefore, a huge number of PGD modes are required to obtain the parametric solution with enough accuracy.

The impossibility of having a parametric solution leads the author to propose a fast strategy to simulate the dynamic interaction problem, providing remarkable saves in computational cost. The method is divided into two stages which are based on moving the nonlinear terms to the right hand side of the dynamic equation. In the first stage, the response of the system under unitary forces is precomputed and stored. Then, in the second stage of the method, the treatment of the nonlinearities is condensed into a small system of equations, whose unknowns are now the forces associated with the nonlinearities instead of the nodal displacements of the whole system.

With this proposed algorithm, it is possible to carry out efficient optimisations of the catenary geometry. Specifically, contact wire height and dropper spacing are considered as design variables in order to obtain the most uniform interaction force that leads to the optimal current collection. The optimisation problem is solved by means of a classic Genetic Algorithm, applied to both simple and stitched catenaries. The results obtained show that an optimal catenary design can remarkably improve the current collection quality of the actual catenaries.

Finally, the influence of the installation errors on the dynamic behaviour of the system is analysed under a stochastic approach in which variability in dropper length, dropper spacing and support height are involved in the simulations. The use of a Monte Carlo method allows the propagation of the uncertainty to the magnitudes of interest of the dynamic solution and therefore, to obtain their probability density function. The results of Monte Carlo simulations demonstrate that dropper spacing errors are slightly influential, whilst dropper length and support height installation errors have a strong influence on the dynamic behaviour of the system. Thus, allowing for the variability present in the actual catenaries seems to be important to perform more realistic simulations.

Resumen

El modelado y la simulación de la interacción dinámica entre el pantógrafo y la catenaria se ha convertido en una herramienta imprescindible para agilizar el proceso de diseño de catenarias ferroviarias ya que, entre otras ventajas, es posible reducir el número necesario de los tan costosos ensayos experimentales en vía.

Para la realización de dichas simulaciones numéricas, en esta Tesis la catenaria se modela mediante el método de los Elementos Finitos, con una formulación en coordenadas absolutas, mientras que para modelar el pantógrafo se utiliza un modelo simple de parámetros concentrados. La interacción entre ambos sistemas se trata con un método de penalti. Tras resolver el problema no lineal de configuración inicial, la ecuación del movimiento se linealiza con respecto de la posición de equilibrio estático, y se resuelve en el dominio temporal con el uso de la técnica HHT. Sin embargo, el aflojamiento de las péndolas a compresión y los despegues del pantógrafo son dos fuertes no linealidades que deben ser consideradas en la resolución del problema dinámico, aunque aumenten notablemente el coste computacional de cada simulación.

Los objetivos principales de esta Tesis son encontrar catenarias óptimas en términos de calidad de captación de corriente y analizar los efectos de los errores de montaje de la catenaria en su comportamiento dinámico. Para alcanzar ambos objetivos, es necesario realizar un número elevado de simulaciones de la interacción dinámica entre pantógrafo y catenaria, cuyo coste computacional puede llegar a ser prohibitivo.

Para reducir este coste computacional, la primera propuesta realizada en esta Tesis se basa en el precálculo de una solución paramétrica de la interacción dinámica entre pantógrafo y catenaria, para cualquier valor de las variables de diseño, por medio de la técnica Proper Generalised Decomposition (PGD). De este modo, la respuesta dinámica del sistema puede ser evaluada instantáneamente cuando lo requiera tanto el algoritmo de optimización como el de propagación de incertidumbres. Si las longitudes de las péndolas son consideradas como variables de diseño, la aplicación de este método resulta exitosa en el caso del problema de equilibrio estático. Sin embargo, para el

caso de la dinámica, donde se considera que las péndolas no transmiten fuerzas a compresión, la solución del problema resulta muy sensible ante pequeños cambios de estas variables y por tanto, se requiere de un elevado número de modos PGD para tener una solución paramétrica de suficiente precisión.

La imposibilidad de disponer de una solución paramétrica conduce a proponer una estrategia rápida para resolver el problema de interacción dinámica con la que se reduzca considerablemente el tiempo de cálculo. El algoritmo propuesto se divide en dos fases y se basa en pasar los términos no lineales a la parte derecha de la ecuación de la dinámica del sistema. En la primera fase, se calcula y almacena la respuesta del sistema sometido a fuerzas unitarias. Posteriormente, en la segunda etapa del método, el tratamiento de las no linealidades se condensa en un sistema de ecuaciones pequeño cuyas incógnitas pasan a ser las fuerzas relacionadas con las no linealidades, en vez de los desplazamientos nodales de todo el sistema.

Con este algoritmo eficiente, es posible llevar a cabo la optimización de la geometría de catenarias ferroviarias. En concreto, la altura del cable de contacto y la separación entre péndolas son los parámetros de diseño a optimizar para obtener así una fuerza de interacción entre el pantógrafo y la catenaria lo más uniforme posible y, por lo tanto, conseguir una captación de corriente óptima. El problema de optimización se resuelve mediante un Algoritmo Genético clásico, y se aplica tanto a una catenaria simple como a una catenaria con falso sustentador. Con los resultados obtenidos se demuestra que un diseño óptimo de la geometría puede mejorar notablemente la captación de corriente de las catenarias actuales.

Finalmente, se estudia la influencia que tienen los errores de montaje de la catenaria en el comportamiento dinámico del sistema. Con un planteamiento estocástico del problema, se considera la variabilidad en la longitud de las péndolas, en la separación entre ellas y en la altura de los soportes. Mediante la aplicación de un método clásico de Montecarlo, se propaga la incertidumbre a las magnitudes de interés de la solución dinámica y se obtiene su función de densidad de probabilidad. Los resultados obtenidos muestran que los errores cometidos en la colocación de las péndolas apenas tienen influencia en la respuesta del sistema, mientras que los errores en la longitud de las péndolas y en la altura de los soportes sí que influyen considerablemente en la dinámica del mismo. Por tanto, parece importante tener en cuenta la variabilidad presente en las catenarias para poder realizar simulaciones más realistas.

Resum

El modelatge i la simulació de la interacció dinàmica entre el pantògraf i la catenària ha esdevingut en una ferramenta imprescindible per a agilitzar el procés de disseny de catenàries ferroviàries degut, entre altres coses, a la possibilitat de reduir el nombre dels tan costosos assajos experimentals en via.

Per a la realització d'aquestes simulacions numèriques, en aquesta Tesi la catenària es modela mitjançant el mètode dels Elements Finits, amb una formulació en coordenades nodals absolutes, mentre que per a modelar el pantògraf s'empra un model simple de paràmetres concentrats. La interacció entre ambdós sistemes es tracta amb un mètode de penalti. Després de resoldre el problema no-lineal de configuració inicial, l'equació del moviment es linealitza amb respecte de la posició d'equilibri estàtic, i es resol en el domini del temps amb la tècnica HHT. Tanmateix, l'afluixament de les pèndoles a compressió i la pèrdua de contacte del pantògraf són dues fortes no-linealitats que han de ser considerades en la resolució del problema dinàmic, malgrat l'augment que produeixen del cost computacional de cada simulació.

Els objectius principals d'aquesta Tesi són trobar catenàries òptimes en termes de qualitat de captació de corrent i analitzar els efectes dels errors de muntatge de la catenària en el seu comportament dinàmic. Per a assolir aquests objectius, és necessari realitzar un nombre elevat de simulacions de la interacció dinàmica entre pantògraf i catenària, el que pot comportar un cost computacional prohibitiu.

Per tal de reduir aquest elevat cost computacional, la primera proposta realitzada en aquesta Tesi consisteix a precalcular una solució paramètrica del problema d'interacció dinàmica entre pantògraf i catenària, per a qualsevol valor de les variables de disseny, mitjançant la tècnica Proper Generalised Decomposition (PGD). D'aquesta forma, la resposta dinàmica del sistema pot ser avaluada instantàniament sempre que ho requerisca tant l'algoritme d'optimització com el de propagació de la incertesa. Si les longituds de les pèndoles es consideren com a variables de disseny, l'aplicació d'aquest mètode és exitosa en el cas del problema d'equilibri estàtic. Això

no obstant, per al cas de la dinàmica, on es considera que les pèndoles no poden transmetre força a compressió, la solució del problema és molt sensible davant xicotets canvis d'aquestes variables i per tant, es necessita un elevat nombre de modes PGD per a obtenir una solució paramètrica amb suficient precisió.

L'impediment de no disposar d'una solució paramètrica ens porta a proposar una estratègia ràpida per a resoldre el problema d'interacció dinàmica que reduïsca considerablement el temps de simulació. L'algoritme proposat es divideix en dues fases i es basa a moure els termes no-lineals a la part dreta de l'equació de la dinàmica del sistema. En la primera fase es calcula i s'emmagatzema la resposta del sistema davant forces unitàries. A continuació, en la segona etapa del mètode, el tractament de les no-linealitats es condensa en un xicotet sistema d'equacions les incògnites del qual passen a ser forces en compte de desplaçaments.

Amb aquest algoritme eficient, s'ha pogut realitzar l'optimització de la geometria de catenàries ferroviàries. En concret, l'altura del cable de contacte i la separació entre pèndoles es consideren com a paràmetres a optimitzar per a obtenir una força d'interacció entre el pantògraf i la catenària el més uniforme possible i per tant, aconseguir una òptima captació de corrent. L'optimització es porta a terme mitjançant un Algoritme Genètic clàssic, i s'aplica tant a una catenària simple com a una amb fals sustentador. Amb els resultats obtinguts es demostra que un disseny òptim de la geometria pot millorar notablement la captació de corrent de les actuals catenàries.

Finalment s'estudia la influència que tenen les errades de muntatge de la catenària en el comportament dinàmic del sistema. Aquest plantejament estocàstic del problema considera variabilitat en la longitud de les pèndoles, la separació entre aquestes i l'altura dels suports. Per mitjà d'un mètode clàssic de Montecarlo, es propaga la incertesa a les magnituds d'interés de la solució dinàmica i s'obté la seua funció de densitat de probabilitat. Els resultats obtinguts mostren que hi ha molt poca influència per part de les errades comeses en la col·locació de les pèndoles, mentre que les errades en la longitud de les pèndoles i en l'altura dels suports sí que influeixen considerablement en el comportament dinàmic del sistema. Per tant, és important tenir en compte la variabilitat present en les catenàries per a realitzar simulacions més realistes.

Acknowledgements

First of all, I would like to thank my supervisors Professor Javier Fuenmayor and Professor Manuel Tur for their wise advice and selfless support during these years of study. They welcomed me from the first day with patience, trust and comprehension and their offices' doors were always open for me to raise my doubts.

I would like to extend my gratitude to all my colleagues of the 'Great Hall' and staff of the Department of Mechanical and Materials Engineering. They always offered their help and made me feel as if I were at home. José Manuel, Estivaliz, Onofre, Eva, Luca, Enrique, Camila, José (acho), Tudela, Marta, Ricardo, Xavi, David, Sandra, Vicente, Borja and especially Marga, I really appreciate your support and companionship during these years. Jorge, without your help the cover of this Thesis would not be as it is.

I have to thank very particularly my dear friend Ángel and Professor Paco Chinesta and his group at École Centrale de Nantes for treating me as one of them during my three months research stay. Their contributions definitely helped me to develop a more powerful work.

I cannot forget about my family and friends, specially my girlfriend Jessica, my parents María Ángeles and Vicente, my uncles Francisco and José, and last but not least, my family-in-law, for providing the best atmosphere I could ever have imagined during these four years, being always by my side both in good and not so good times. Without you I would not be who I am.

Finally, I would also like to acknowledge the Spanish society for funding the public education system which provided me with the opportunity of training myself as a researcher in the framework of the FPU grant program.

Thank you very much to all.

Contents

Abstract **vii**

Resumen **ix**

Resum **xi**

Acknowledgements **xiii**

I Thesis report **1**

1 Introduction **3**
1.1 Motivation 3
1.2 Description of a high-speed catenary 5
1.3 Objective 6
1.4 Thesis layout 7

2 State of the art **9**
2.1 Catenary modelling 10
2.2 Pantograph modelling 11
2.3 Coupling modelling and numerical integration 11
2.4 Initial configuration problem 12
2.5 Real-time simulations 13
2.6 Parametric analyses and optimisations 13
2.7 Simulation of irregularities and uncertainties 14
2.8 Other related topics 15

3 Pantograph-catenary dynamic interaction simulation **17**
3.1 Mathematical models . . . 17
3.1.1 Catenary . . . 18
3.1.2 Pantograph . . . 19
3.1.3 Interaction . . . 21
3.2 Static equilibrium and initial configuration problems . . . 22
3.3 Dynamic interaction problem . . . 24

4 Contributions **29**
4.1 Parametric model . . . 30
4.2 Fast simulation algorithm . . . 35
4.2.1 *Offline* stage . . . 35
4.2.2 *Online* stage . . . 37
4.3 Catenary optimisation . . . 40
4.4 Stochastic simulations . . . 45

5 Closure **51**
5.1 Summary and conclusions . . . 51
5.2 Open research lines . . . 52

Bibliography **55**

II Articles **67**

Paper A: Parametric model for the simulation of the railway catenary system static equilibrium problem **69**

Paper B: Fast simulation of the pantograph-catenary dynamic interaction **107**

Paper C: An approach to geometric optimisation of railway catenaries **145**

Paper D: Stochastic Monte Carlo simluations of the pantograph-catenary dynamic interaction to allow for uncertainties introduced during catenary installation **181**

Part I

Thesis report

Chapter 1

Introduction

"Thinking is the hardest work there is, which is probably the reason why so few engage in it"
Henry Ford

1.1. Motivation

Today, the high-speed railway has become one of the most used means of transportation around the world. Specifically, since the inauguration of the Madrid-Sevilla line, Spain has been expanding its infrastructures, becoming the first country in Europe to have 3100 km of high-speed railways.

This large network is endowed with overhead contact line (OCL) equipment, also known as catenary, which provides the required power to the electrical engines of the locomotive. The power supply is carried out by means of a sliding contact between the OCL and the pantograph, the mechanism located on the roof of the locomotive. Technical criteria of such interaction are collected in European standards such as EN 50367 [1] and the Technical Specifications for Interoperability (TSI) [2].

Planning, designing and setting up a new OCL [3] is a tough process that requires a lot of effort and a great economic investment. Current collection performance, which is one of the greatest challenges related to the development of high-speed rail systems, largely depends on the results of this process. However, thanks to the increasing computational power over the last decades, the pantograph–catenary coupled dynamics can be studied by means of numerical simulations. With this option at hand, a wide range of possibilities are opened for the catenary designers, who can simulate the use of different materials, geometric configurations, train speeds, etc., with only the use of a computer. Furthermore, several of the intricate in-line tests which require a great amount and variety of resources can be replaced by numerical simulations.

As previously said, power supply is a key factor in high-speed railway systems. Performance of the supply is strongly related to the force generated in the interaction between the pantograph and the catenary. On the one hand, this interaction force should be high enough to prevent pantograph detachments that cause both interruption in the supply and electrical arcing with the consequent damage to the interfaces. On the other hand, the interaction force should not be too high, as this would produce excessive wear on the sliding surfaces. Thus, an undesirable interaction force will produce damage to the system, shortening the service time and therefore, increasing the maintenance costs. Considering that these costs can be very high, there is an important need to find optimal topologies of catenaries in terms of current collection quality.

Another important aspect is the accuracy of the simulation tools, which must be guaranteed to give validity to the obtained results. In fact, specific standards (EN 50318 [4]) have been developed to validate the simulation tools with the purpose of ensuring certain levels of accuracy. However, all these software follow deterministic approaches, which ignore the uncertainties present in the actual system. For instance, installation errors can have a significant impact on the dynamic behaviour of the system, worsening the current collection performance. For that reason, it is important to have models that account for these sources of variability, providing more reliable results.

The main motivations of this Thesis are:

- The need for efficiently simulating the pantograph–catenary dynamic interaction to reduce time and costs in the OCL design process.
- The high maintenance costs associated with the replacement of damaged elements due to arcing or friction wear produced by poor quality of the power supply.
- The importance of having more realistic simulations allowing for the variability present in the actual catenaries due to installation errors, which can modify the dynamic behaviour of the whole coupled system.

1.2. Description of a high-speed catenary

The OCL is a cabling structure which provides the necessary current to propel electric trains. A picture of a high-speed railway catenary with its main components highlighted is shown in Fig. 1.1.

Among the vast variety of existing topologies of catenaries, from the mechanical point of view, a railway catenary is mainly made of two groups of components: structural elements and cables. Masts with brackets and steady arms are the support points to which the cabling is attached.

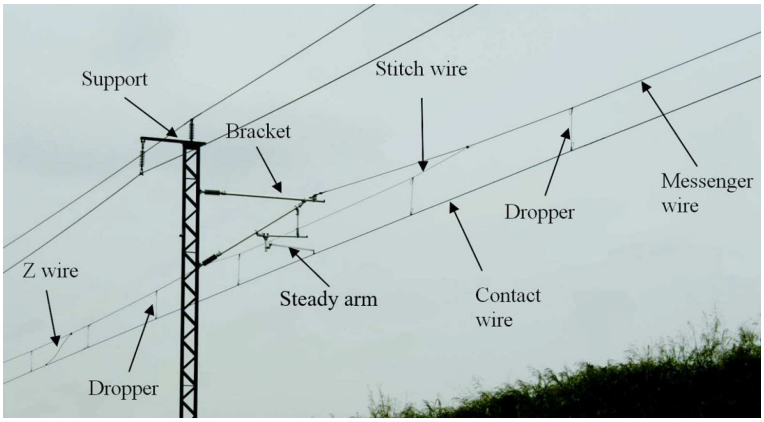

Figure 1.1: Picture of a high-speed railway catenary.

Regarding the cabling, the messenger or carrier cable is directly supported by brackets at regular intervals showing a characteristic catenary curve shape. The section of catenary going from one bracket to another is called the span. The contact wire is in charge of transmitting the electrical current to the locomotive by means of a sliding contact with the collector strips of the pantograph. In order to keep the contact wire at the desired height, it is connected to the messenger cable by means of droppers, whose lengths play an important role in determining the contact wire height profile.

Another interesting feature of a railway catenary is noticed when it is viewed from above. Steady arms pull the contact wire to create a zigzag pattern along the track path. This staggering is essential to assure uniform wear on the contact strips of the pantograph collector.

Near the supports, a catenary usually exhibits higher stiffness. To reduce this unevenness in the vertical stiffness, some types of catenaries include stitch wires,

which provide more flexibility to this area of the system. Other catenaries present the contact wire with some amount of static sag (pre-sag) to keep the contact point, under the action of the pantograph, at a similar height.

To allow maintenance of the overhead line without turning off the entire system and also to facilitate the stringing process, the line is divided into electrically separated portions known as "sections" of approximately one kilometre in length. At the ends of each section there is a compensation system, usually composed of pulleys and counterweights, which keeps the tension of the contact and messenger wires constant, even under dilatations or contractions produced by temperature changes.

1.3. Objective

This Thesis aims to extend and deepen the knowledge of the pantograph–catenary dynamic interaction by means of numerical simulation. To this end, the following two main objectives are proposed:

1. **Optimisation of the geometry of a railway catenary.** When dealing with a high-speed OCL, the current collection performance is directly related to the force produced within the interaction between the pantograph and the contact wire. This dynamic interaction force depends, in turn, on the contact wire height profile among other factors. Thus, optimisation of parameters such as dropper lengths or dropper spacing seems to be crucial to obtain an adequate contact wire height profile. With the achievement of this objective not only the current collection will be improved, but also the wear of the sliding surfaces will be decreased with the consequent reduction in maintenance tasks and costs. The strategy used to optimise the catenary and the obtained results are detailed in Paper C.

2. **Assessment of the uncertainty produced by installation errors.** The current software, which is capable of simulating the pantograph–catenary dynamic interaction, is usually fed by the nominal or design values of the parameters that lead to the initial configuration of the catenary. However, in a real set-up, the stringing process is not prevented from having some little mistakes, thus leading to final geometries which differ from those planned in the design. In order to perform more realistic simulations it is advisable to move from a deterministic to a stochastic modelling, in which installation errors are taken into account and their influence on the dynamic behaviour of the system can be quantified. This objective is thoroughly discussed in Paper D.

The above two main objectives require performing thousands of simulations of the pantograph–catenary dynamic interaction. Thus, if each of these simulations is time-consuming, the objectives set in this Thesis could not be achieved due to the prohibitive computational cost of the simulations. That is why a third objective emerges:

3. **Reduction of the computational cost of the pantograph-catenary dynamic interaction simulation.** Ideally, if the solution of the pantograph–catenary dynamic interaction problem could be precomputed and stored for any value of a given parameter, in an optimisation procedure or in a stochastic scenario each simulation would be instantly performed by only evaluating the precomputed solution with the given values of the parameters. The construction of such a parametric model is presented in Paper A. However, in view of the drawbacks of the aforementioned strategy, another way of achieving this objective consists of modifying the time integration procedure to reduce as much as possible the time invested in finding the solution. Thus, a reliable and fast algorithm is proposed in Paper B.

1.4. Thesis layout

The Thesis is divided into two parts. After these introductory remarks, the remainder of the first part is an overview of the Thesis which includes Chapter 2, with a complete description of the state of the art. A detailed definition and justification of the models chosen to deal with the problem at hand is provided in Chapter 3. Chapter 4 groups and links the main contributions of the Thesis and finally, a summary of the conclusions drawn from this work and further research proposals are presented in Chapter 5.

The second part of the document consists of a compilation of the four papers which provide the scientific contributions of the Thesis. All the papers are presented without journal editing, and the citation of the corresponding journal or some information on the submission is included on the cover of each paper.

Paper A describes the construction of a parametric model of the static equilibrium problem of an overhead line. The model is based on the PGD technique and includes initial dropper lengths as extra-coordinates. A fast strategy to deal with the time integration of the pantograph–catenary dynamic interaction is proposed in Paper B. This algorithm is fully exploited in Paper C in order to find the optimal configurations of high-speed railway catenaries and also in Paper D to evaluate the uncertainty in the dynamic behaviour of a catenary associated with its installation errors.

Chapter 2

State of the art

"The difference between stupidity and genius is that genius has its limits"
Albert Einstein

The great expansion of railways across the world demands an accurate pantograph–catenary interaction that entails cheaper maintenance costs and faster operation of trains. That is the main reason why in the last decades high effort has been put into research on topics related to pantograph–catenary interaction. As stated in [5], the number of papers published on this topic have increased from 19 in 2005 to 80 in 2016.

Good overviews of simulation of the pantograph–catenary dynamic interaction can be found in [5–8]. Also, the recent benchmark exercise [9] brought together ten different simulation codes from nine different countries, providing a detailed picture of the state of the art. Following this line, this section is aimed at providing a review of the literature, paying special attention to the modelling of the pantograph–catenary dynamic interaction, the techniques used to speed up the calculations, the optimisation of the system and the introduction of irregularities and variability into the simulations.

2.1. Catenary modelling

First attempts at describing the catenary dynamics were based on simplified mathematical models, such as lumped-mass models [10] or infinite string models [11]. However, these basic techniques were soon replaced by more complex models enabling reliable simulations of the system behaviour.

More realistic models were introduced to consider the stiffness variation along the span [12–14] or even the apparent mass variation [15,16]. Although low computational cost is required with the use of these simplified models, relevant features such as wave propagation in the wires are not considered, leading to inaccurate results.

In order to consider wave propagation and reflection phenomena, a string model with axial tension was widely used in the past [17, 18], although it is also found in recent publications [19,20]. These string models do not allow for bending stiffness, and reveal a discontinuity in the slope of the wire, which is an unrealistic representation of the physical behaviour. Thus, Euler-Bernoulli beam models became the most used to represent the catenary wires (see for example [21,22]), since shear effects and rotatory inertia are negligible for the usual frequency range of interest [6, 23].

Other components of the catenary are modelled in different ways. Although some authors do not allow for dropper slackening [24–30], it is an important feature that should be regarded in the models as stated in [31], where experimental curves of dropper behaviour are provided. Due to the low bending stiffness of these elements, most dropper models are based on either a mass-spring-damper system with slackening [20, 32–34] or a bar element with slackening [22, 35–38]. These two options are also used to model steady arms [31].

Two approaches are usually used for the numerical treatment of the resulting differential equations: the Finite Difference Method (MDF) and the Finite Element Method (FEM). However, whilst few references are found in which the FDM is used for the spatial discretization of the catenary model [19,28,29,39], the FEM has become the most used method to this end, achieving a good balance between computational effort and accuracy.

The supremacy of the FEM is clearly seen in the benchmark exercise [9], in which nine of the ten different simulation codes used it. The classical beam formulation with rotational degrees of freedom [21, 22, 35, 40, 41] and the Absolute Nodal Coordinates Formulation (ANCF) [38, 42–44] are the two most used formulations. The main advantage of the latter is that large deformation effects can be easily considered. Other less common approaches, use analytical expressions of the elastic cable [45], include torsional effects [46] or are even based on the analytic catenary equation [47].

2.2. Pantograph modelling

In order to model the pantograph, two or three lumped-mass linear models are widely used in the literature [9, 19, 23, 46, 48] whose parameters can be adjusted by experimental tests [49]. These simple models can be improved by the addition of two contact points [50] or more degrees of freedom, such as the rolling motion of the pan-head [33, 41, 51, 52], by the use of modal coordinates to consider the flexibility of the collectors [53], or even by simulating nonlinear elements such as friction dampers or bump stops [36].

However, to take into account more realistic features and geometric nonlinearities, multibody approaches are currently gaining more and more acceptance [21, 54, 55] to model the pantograph. These models are not only composed of rigid bodies [25, 42] but also rigid-flexible hybrid models [56, 57] are used to enlarge the frequency range of validity of the models.

2.3. Coupling modelling and numerical integration

The pantograph–catenary coupling equations must allow for the possible loss of contact between both systems. This is usually carried out either by kinematic constraints with Lagrange multipliers [13,23,50,58] or by the penalty method, which is the most used in the benchmark [9]. The latter ranges from the simplest case with a high-stiffness element [27, 46], accompanied sometimes with a damping element [22, 31], to the more general case of Hertzian type contact with internal damping [55, 59].

Although punctual contact is widely accepted, other formulations can consider distributed contact by means of a density function [23, 50, 60], the lateral component of the contact force [41, 61] or the flexibility of the collectors [57].

Regarding the time integration methods, the central differences method is used in [50], Runge-Kutta is applied in [44] and a explicit two-step method is considered in [39]. However, there is a major consensus in the literature for using the Hilber-Hughes-Taylor (HHT) family of implicit time-integration methods [9,30,35,40], which are unconditionally stable and allow the use of longer time steps.

Modal Superposition Method is an option broadly used [26, 30, 62–65], especially when a fast solution is required. Although the displacement of the contact point can

be calculated without interpolation, the modal truncation error makes this approach not valid to consider more realistic conditions.

Another interesting strategy used by some authors consists of simulating the catenary and pantograph by different codes in which the time integration process is coordinated on both subsystems via a co-simulation procedure [40, 54, 55, 66].

2.4. Initial configuration problem

The initial configuration of the catenary comprises both static equilibrium and design requirements (tensions in wires, arrangement of droppers, initial sag...).

A very simple approach assumes the messenger wire follows a parabola [3], but considers neither mechanical equilibrium nor contact wire sag. To circumvent this drawback, some authors split the catenary into two subsystems (contact wire and messenger cable) and iteratively compute the dropper forces to obtain the desired position of the cabling [22, 36].

Other iterative methods, such as the negative-sag method applied in [34] or the one used in [21, 33], are based on linear formulations and proceed by modifying the dropper lengths at each step of the procedure. Analytic expressions for calculating length of droppers and pre-sag of messenger wire are also found in [43].

An efficient algorithm based on the analytic catenary equation is proposed in [67], whereas in [68] the catenary configuration is continuously evolved by dynamic simulation until an equivalent configuration of the catenary at static equilibrium is computed. Optimisation techniques are also used to find the dropper lengths that hold the contact wire as close as possible to the target position [55].

The above mentioned methods assume that the initial length of messenger and contact wire elements are given. This assumption is not made in [45], where the proposed strategy leads to very accurate results. Finally, one of the most reliable methods present in the current literature was proposed in [69] and it is fully exploited in this Thesis. It is based on the use of ANCF beam elements to build a nonlinear problem in which the nodal coordinates and the initial lengths of certain groups of elements are set as unknowns to fulfil both the static equilibrium and the design requirements.

2.5. Real-time simulations

One of the trends in the last decades is to replace part of the numerical model by the physical system in what is known as Hardware-In-the-Loop (HIL) simulations. In the case of pantograph–catenary interaction, the actual pantograph interacts with a numerical model of the catenary, which needs to have real-time capabilities.

In order to alleviate computational cost when solving the pantograph–catenary dynamic interaction problem, a moving mesh strategy is proposed in [70], a high performance tool was developed in [50] and the modal superposition technique is recommended in [7]. Despite these attempts, to date only very simplified catenary models are able to be used in HIL simulations.

The first papers dealing with HIL simulations for pantograph–catenary interaction present a test rig in which the catenary is modelled by a modal approach [62, 71]. The catenary model used in these works does not consider the slackening of droppers. Similarly, a simple modal-based catenary model is proposed in [7] with real-time capabilities.

Dropper slackening is introduced by modal superposition techniques in [64] along with a shift forward strategy that enables the consideration of only a simplified model of a few spans of the catenary. This strategy also appears in [72] to assess an active control pantograph, in [73] with the introduction of the stagger in the test rig and in [74] to explore a new type of non conventional dropper.

The most recent proposal is found in [28], where the formulation is transformed using moving spatial coordinates. The absorbent boundary conditions to avoid wave reflections on the boundaries of the small scale catenary model introduce significant deviations in the response of the catenary when compared to the use of a full catenary model. Following the same approach, dropper slackening is taken into account in [75] and [29], where different control strategies are discussed.

This short review on real-time simulations reveals the need to put more effort into reducing the computational cost while maintaining a reasonable accuracy of the pantograph–catenary dynamic interaction simulations.

2.6. Parametric analyses and optimisations

The influence on the contact quality of several parameters of pantograph and catenary models has been extensively studied in the literature. From a static point of view, first investigations [76] proposed optimal values of several parameters, such

as tension in the wires, to achieve the most uniform stiffness distribution along the span.

However, dynamic behaviour is more critical for assuring a good current collection performance. Regarding the pantograph, the dynamic sensitivity analysis performed in [77] reveals that the frame and bow masses, along with the damping and stiffness of its attachment with the vehicle roof, are the most influential parameters on the power supply quality. With the use of a direct differentiation method, it is found that the pantograph movement is strongly influenced by the span length according to [78]. The results given in [79] state that the less the pan head mass and the higher the stiffness of the collector bow, the better the contact quality. Furthermore, the influence of the main components of the pantograph is also studied in [27, 66, 79]. Optimisation of the pantograph model parameters is accomplished in [80] using a differential evolutionary algorithm, in [14] with a robust design technique and in [81] applying a genetic algorithm.

Focusing on the catenary system, tension in the wires, pre-sag and arrangement of the end droppers in the span are studied in [82] to find out their best values. The optimal amount of contact wire initial sag is thoroughly discussed in [83], which states that no benefits of pre-sag are found at high speeds. However, dropper spacing is only briefly analysed in [84]. In order to increase the operational speed, the influence of several parameters is revealed in [85], and the best choice from those gave rise to an upgraded catenary. A parametric analysis of catenary geometry, including parameters such as dropper lengths, support heights and wire tensions, is made in [86] with the Sobol index method. Finally, knuckle junctions are optimised in [87] and also studied in [66].

2.7. Simulation of irregularities and uncertainties

Although defects and irregularities are always present in high-speed railway catenaries, dynamic simulations of pantograph–catenary interaction are mainly based on deterministic approaches, disregarding the variability present in the system. Nevertheless, some contributions have been found in recent years.

The topic was first addressed in [88] with the development of a diagnostic procedure based on measurements of the pantograph dynamics and the application of an Extended Kalman Filter to estimate the interaction force. With this procedure, the impact of overhead line irregularity on current collection is discussed in [89].

Other authors have proposed installation guidelines [90] which ensure several parameters characterising the dynamic behaviour to be within acceptable ranges. Local

singularities of contact wire height produced by the length of a single dropper or the height of a single support are investigated in [91] by means of simulations.

Geometric parameters, such as dropper lengths, are statistically identified from a wide set of experimental measurements in [92]. This allowed the introduction of variability into pantograph–catenary dynamic interaction in [93], where the authors reveal the need for further research on the topic.

2.8. Other related topics

Apart from the topics discussed above, there are many more interesting contributions related to pantograph–catenary interaction.

Overlap sections are of major interest when studying the catenary dynamic behaviour. They are successfully simulated in [60, 63, 94] and also in [95], which studies the effect of section insulators too. Furthermore, multiple pantograph operation is commonly found in actual high-speed trains. Effects of the leading pantograph passage to the rear pantograph are analysed in [18, 59].

Pantographs with active control are emerging as a promising solution to increase the operational train speed. Among the several proposals for control laws and system actuators that are found in the literature, [15, 16, 96–99] are especially relevant.

When two surfaces are in sliding contact, analysis and prediction of wear becomes a key aspect for maintenance operations. A model to predict the contact wire wear is proposed in [100, 101] and pantograph collector strips wear is studied in [102, 103].

Other researches focused on the effects of locomotive vibrations on the dynamics of the pantograph–catenary coupled system. While a significant influence is reported in [24], the results given in [104] show that vertical vibrations of the train, caused by irregularities in the track, are not relevant to the pantograph–catenary interaction.

Finally, wind loads also have an important effect on the catenary cabling and the pantograph movement. The galloping instability phenomenon is studied in [105]. Wind tunnel tests are performed in [106] to find the aerodynamic forces acting on the collector of different pantographs. Furthermore, cross-wind action with turbulence is considered in [107] to simulate its effect on the pantograph–catenary system.

Chapter 3

Pantograph-catenary dynamic interaction simulation

"I know that I am intelligent, because
I know that I know nothing"
Socrates

This section is devoted to offering a thorough description of the pantograph and catenary models used in this Thesis and the strategy followed to deal with their dynamic interaction. Starting from the formulation governing each subsystem model, the initial configuration problem and the time integration scheme used are explained in detail.

3.1. Mathematical models

The current collection system is composed of two subsystems that need to be modelled, namely the catenary and the pantograph. Besides, an additional model is also required to consider the sliding contact which couples them.

3.1.1. Catenary

Among the different options identified in Chapter 2, the Finite Element Method (FEM) is the most used method to model realistic catenary behaviour [9]. Specifically, in this work the catenary cables are modelled by beam elements based on the absolute nodal coordinate formulation (ANCF). As previously stated, this formulation has also been used by other authors for railway catenary models [43, 108]. With this formulation, both the initial configuration and the dynamic interaction problems can be dealt with, which is clearly a major benefit.

ANCF applied to very slender beams results in elements which only have six degrees of freedom per node in a three-dimensional problem, taking into account axial and bending deformations. This ANCF beam element is used to model both the messenger cable and the contact wire. Fig. 3.1 shows a sketch of the reference,

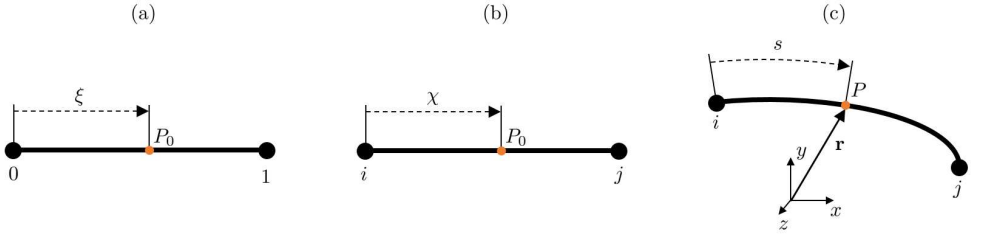

Figure 3.1: Reference (a), undeformed (b) and deformed (c) configurations of the ANCF beam element.

the undeformed and the deformed configurations of a beam element. The position vector in the deformed configuration $\mathbf{r} = [x\ y\ z]^T$ can be interpolated using the shape function matrix as:

$$\mathbf{r} = \mathbf{N}\,\mathbf{q} \tag{3.1}$$

The vector of degrees of freedom for a beam element with nodes i and j is:

$$\mathbf{q}_b = \left[\begin{array}{cccccccccccc} x_i & y_i & z_i & \frac{\partial x_i}{\partial \chi} & \frac{\partial y_i}{\partial \chi} & \frac{\partial z_i}{\partial \chi} & x_j & y_j & z_j & \frac{\partial x_j}{\partial \chi} & \frac{\partial y_j}{\partial \chi} & \frac{\partial z_j}{\partial \chi} \end{array}\right]^T \tag{3.2}$$

where $\chi \in [0,\, l_{ref}]$ is the local coordinate, l_{ref} being the undeformed or initial length of the element. x_i, y_i and z_i are the absolute coordinates of node i while $\frac{\partial x_i}{\partial \chi}$, $\frac{\partial y_i}{\partial \chi}$ and $\frac{\partial z_i}{\partial \chi}$ denote the slopes in each spatial direction. In this case, the absolute position at a given point with local coordinate χ is defined by means of a cubic Hermitian interpolation which guarantees the required C^1 continuity of the solution between

the elements. The shape function matrix can be written as:

$$\mathbf{N}_b(\chi) = [N_{b1}\mathbf{I}_3 \mid N_{b2}\mathbf{I}_3 \mid N_{b3}\mathbf{I}_3 \mid N_{b4}\mathbf{I}_3]$$

$$\begin{array}{ll} N_{b1}(\xi) = 1 - 3\xi^2 + 2\xi^3 & N_{b2}(\xi) = l_{ref}(\xi - 2\xi^2 + \xi^3) \\ N_{b3}(\xi) = 3\xi^2 - 2\xi^3 & N_{b4}(\xi) = l_{ref}(-\xi^2 + \xi^3) \end{array} \tag{3.3}$$

where the normalized local coordinate $\xi = \chi/l_{ref} \in [0, 1]$ and $\mathbf{I}_3$ is the 3×3 identity matrix.

Steady arms, droppers and stitch wires are modelled by nonlinear bar elements. In this case, their degrees of freedom are only the absolute position of the two nodes of the element, that is:

$$\mathbf{q}_a = \begin{bmatrix} x_i & y_i & z_i & x_j & y_j & z_j \end{bmatrix}^T \tag{3.4}$$

For these elements, as no bending deformations are taken into account, we use the linear interpolation

$$\mathbf{N}_a(\chi) = [N_{a1}\mathbf{I}_3 \mid N_{a2}\mathbf{I}_3]$$

$$N_{a1}(\xi) = -\frac{\xi - 1}{2} \quad N_{a2}(\xi) = \frac{\xi + 1}{2} \tag{3.5}$$

in which the normalised coordinate is $\xi \in [-1, 1]$ in this case.

Fig. 3.2 shows a picture of the FE model of a straight catenary section in which all the modelled components are highlighted and supports have been replaced by suitable boundary conditions (triangles). In this model we also consider the dropper clamps as punctual masses. The x direction is aligned with the track and the vertical direction is on the z axis. The y direction is chosen perpendicular to them to form an Euclidean coordinate system.

The displacements of the initial and final points of the messenger cable and contact wire (red triangles) are restricted like those of the ends of the steady arms connected to the brackets (orange triangles). The points where the messenger cable is connected to the supports (black triangles) have the displacements in y direction restricted and two options are possible regarding z direction: i) the displacement is also restricted, or ii) a spring-damper system is placed instead. Displacement in x direction is allowed in these connections except for the anchor point, usually located on the central support of the section (yellow triangle), in which it is also restricted.

3.1.2. Pantograph

A vast number of different pantograph models can be found in the bibliography, as explained in Chapter 2. Although there are some models based on FEM or multi-

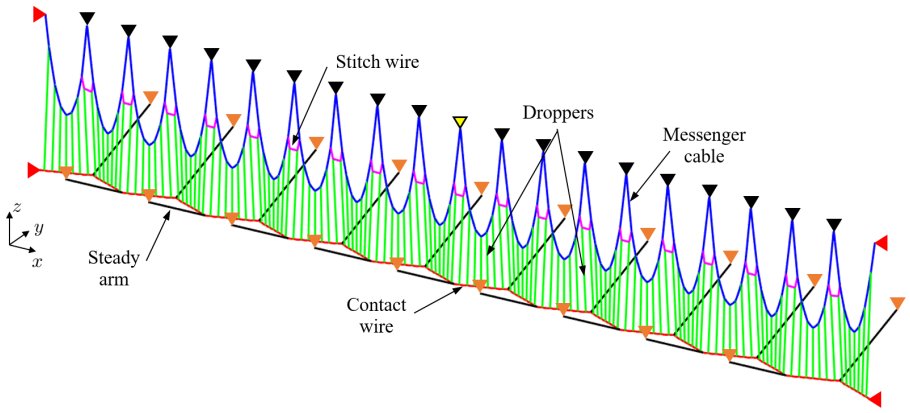

Figure 3.2: FE catenary model with boundary conditions.

body approaches [109, 110], the most widely used is a 'low-order' pantograph model composed of lumped parameters. In this work, a model with three vertical degrees of freedom has been chosen, as depicted in Fig. 3.3.

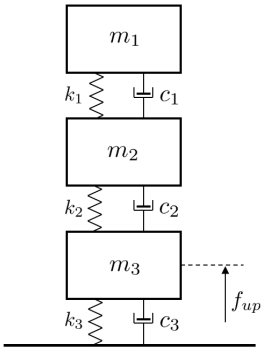

Figure 3.3: Lumped mass pantograph model.

The validity of this model is restricted to the usual studied frequency range (< 20 Hz). The external force f_{up} is acting on the bottom mass, simulating the force exerted by the uplift mechanism. Other forces such as the aerodynamic force can also be included in this simple model.

3.1.3. Interaction

In order to couple the dynamics of the pantograph and the catenary models, some approaches have been revisited in Chapter 2. In this Thesis the pantograph–catenary interaction is simulated by the simple and widely used penalty method. This method introduces a high stiffness elastic element which connects the pantograph head with the contact wire and accomplishes the impenetrability constraint. A scheme of this type of interaction is represented in Fig. 3.4.

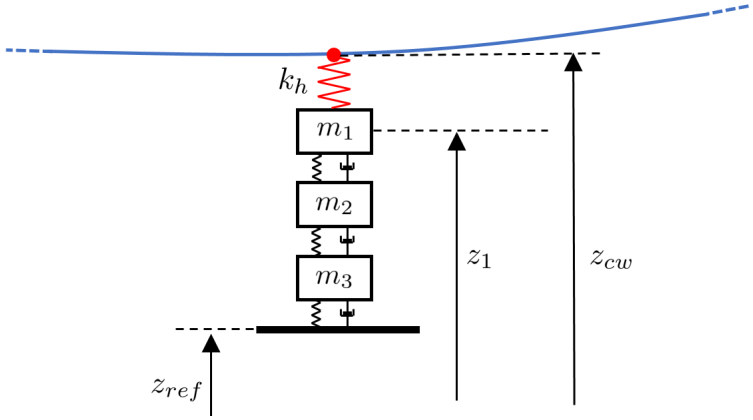

Figure 3.4: Pantograph–catenary interaction scheme.

According to the reference model given in [4] and most of the references in [9], the value of the penalty stiffness is set at $k_h = 50$ kN/m in tension and null in compression, which would imply a contact loss. The contact or interaction force is assumed to be punctual and vertically oriented. If z_1 and z_{cw} are the vertical absolute coordinates of the upper mass of the pantograph and the contact point on the contact wire respectively, the value of the interaction force is computed as:

$$f_{inter} = \begin{cases} k_h(z_1 - z_{cw}) & \text{if} \quad z_1 \geq z_{cw} \\ 0 & \text{if} \quad z_1 < z_{cw} \end{cases} \tag{3.6}$$

3.2. Static equilibrium and initial configuration problems

As in any cabling structure, when dealing with a railway catenary it is necessary to differentiate the two following problems. On the one hand, given a catenary model in which all the lengths of the elements are known, the static equilibrium problem consists of finding the nodal coordinates which fulfil the force equilibrium equations. On the other hand, the initial configuration problem is devoted to obtaining not only the nodal coordinates, but also the length of the elements in order to satisfy both static equilibrium and some constraints imposed in the catenary stringing.

The static equilibrium problem, in which the undeformed lengths of all the elements are given, can be set by the virtual work principle. This is a nonlinear problem due to the large displacements undergone by the cabling structure.

Let Ω be defined as the spatial domain of a certain railway catenary system, which is discretised into N_e elements of length l^e_{ref}, such that $\Omega = \cup_e^{N_e} \Omega_e$ and $\Omega_e \cap \Omega_d = \emptyset$, $e \neq d$, where $\Omega_e = [0,\, l^e_{ref}]$. The total virtual work, produced by internal and external forces, is obtained as the contribution of each element, so that:

$$\delta W = \sum_{e=1}^{N_e} (\delta W^e_{int} - \delta W^e_{ext}) \tag{3.7}$$

For an element e, with Young's modulus E, cross-sectional area A and second moment of area I, the contribution to the internal work comes from both axial and bending strains [111],

$$\delta W^e_{int} = \int_{\Omega^e} (EA\,\varepsilon_L\,\delta\varepsilon_L + EI\,\kappa\,\delta\kappa)\; d\chi \tag{3.8}$$

where ε_L and κ represent the longitudinal deformation and the curvature of the element, respectively. The former can be defined using the Green strain tensor as:

$$\varepsilon_L = \frac{1}{2}\left(\mathbf{r}' \cdot \mathbf{r}' - 1\right) \tag{3.9}$$

where $'$ represents the derivative with respect to the reference coordinate χ, namely $\mathbf{r}' = \frac{d\mathbf{r}}{d\chi} = \frac{1}{l_{ref}} \frac{d\mathbf{r}}{d\xi}$.

The latter, from the Frenet-Serret frame, is defined as [111]:

$$\kappa = \left| \frac{d^2\mathbf{r}}{ds^2} \right| = \frac{|\mathbf{r}' \times \mathbf{r}''|}{|\mathbf{r}'|^3} \tag{3.10}$$

where s is the local coordinate in the deformed configuration as shown in Fig. 3.1. However, as the axial strains within the catenary wires are observed to be small, $ds \approx d\chi$ and the curvature can be approximated by [112]:

$$\kappa \approx |\mathbf{r}''| \tag{3.11}$$

If we compute the axial deformation and the curvature produced by a virtual displacement, and replace them into Eq. (3.8), the virtual work of internal forces results in:

$$\delta W_{int}^e = \int_{\Omega^e} \left[EI\delta\mathbf{r}'' \cdot \mathbf{r}'' + \frac{EA}{2}\delta\mathbf{r}' \cdot \mathbf{r}' \left(\mathbf{r}' \cdot \mathbf{r}' - 1\right) \right] d\chi \tag{3.12}$$

Regarding the external forces acting on the catenary, the gravity must be taken into account. For a single element e, the virtual work caused by the gravity force is:

$$\delta W_{ext}^e = \int_{\Omega^e} \delta\mathbf{r} \cdot \mathbf{f}_g \, d\chi \tag{3.13}$$

where $\mathbf{f}_g = \{0 \;\; 0 \;\; -gA\rho\}^T$, g is the gravitational constant and ρ is the density of the material.

Finally, the weak form of the static equilibrium problem is obtained by placing Eqs. (3.12) and (3.13) into Eq. (3.7) to consider the contributions of all the elements. It consists of finding $\mathbf{r}(\chi)$ for all the admissible $\delta\mathbf{r}$, such that:

$$\sum_{e=1}^{N_e} \int_{\Omega^e} \left[EI\delta\mathbf{r}'' \cdot \mathbf{r}'' + \frac{EA}{2}\delta\mathbf{r}' \cdot \mathbf{r}' \left(\mathbf{r}' \cdot \mathbf{r}' - 1\right) - \delta\mathbf{r} \cdot \mathbf{f}_g \right] d\chi = 0, \quad \forall\delta\mathbf{r} \tag{3.14}$$

Introducing the FE interpolation defined in Eq. (3.1), the internal and gravitational force vectors for the element e are:

$$\begin{aligned} \mathbf{f}_{int}^e &= \int_{\Omega^e} \left[EI\, \mathbf{N}''^T \mathbf{N}'' \mathbf{q} + \frac{EA}{2} \left(\left(\mathbf{N}'^T \mathbf{N}' \mathbf{q} \right) \left(\mathbf{q}^T \mathbf{N}'^T \mathbf{N}' \mathbf{q} - 1 \right) \right) \right] d\chi \\ \mathbf{f}_g^e &= \int_{\Omega^e} \mathbf{N}^T \mathbf{f}_g \, d\chi \end{aligned} \tag{3.15}$$

After the usual assembly process, the static equilibrium equation for the whole catenary system reads:

$$\mathbf{F}_{int}(\mathbf{q}) + \mathbf{F}_g = \mathbf{0} \tag{3.16}$$

which can be solved using for example the Newton-Raphson method.

The second type of problem, the initial configuration problem, also known as the 'shape-finding' problem, consists of obtaining the nodal coordinates and the initial length of each element which fulfil both the static equilibrium equations and certain constraints imposed by design. In this work, the method proposed in [69] is fully adopted.

In this method, as the number of unknowns must be equal to the number of equations, some groups of elements are defined whose reference length l^e_{ref} is modified by a factor κ_l. Thus, the static equilibrium equation (3.16) incorporates not only the nodal coordinates $\mathbf{q}$, but also the factor κ_l of each group of elements as unknowns, that is:

$$\mathbf{F}_{int}(\mathbf{q}, \boldsymbol{\kappa}_l) + \mathbf{F}_g(\boldsymbol{\kappa}_l) = \mathbf{0} \tag{3.17}$$

Additionally, the final equilibrium position must fulfil that certain elements such as those modelling the messenger cable, the contact wire and the stitch wire, are pre-stressed with a given tension T. For the element e, this constraint is defined as:

$$c_I(\mathbf{q}, \kappa_l) = (f^e_{int_x})^2 + (f^e_{int_y})^2 + (f^e_{int_z})^2 - T^2 = 0 \tag{3.18}$$

where $f^e_{int_j}$ is the j component of the internal nodal force vector. Other constraints are related to the right placement of certain elements of the catenary. These point-wise restrictions enforce the height of the contact wire at dropper connections, the position of droppers within the span, the position of supports along the track and also the coordinates of the points at which stitch wires and steady arms are connected to the cables. This type of constraint can be defined with the following expression:

$$c_{II}(\mathbf{q}) = q_i - P = 0 \tag{3.19}$$

where q_i, for $i = x$, y, z, is the nodal coordinate enforced to have a value of P.

If static equilibrium equations (3.17) and constraints $\mathbf{c}(\mathbf{q}, \mathbf{l}^e_{ref})$ are put together, the nonlinear initial configuration problem reads:

$$\left.\begin{aligned} \mathbf{F}(\mathbf{q}, \boldsymbol{\kappa}_l) &= 0 \\ \mathbf{c}(\mathbf{q}, \boldsymbol{\kappa}_l) &= 0 \end{aligned}\right\} \tag{3.20}$$

Again, it can be solved by the Newton-Raphson method to obtain both the nodal absolute positions $\mathbf{q}$ and the factors $\boldsymbol{\kappa}_l$ (or equivalently the initial length of the elements $\mathbf{l}^e_{ref}$), which fulfil not only the static equilibrium but also the restrictions imposed by the catenary stringing.

3.3. Dynamic interaction problem

The dynamic behaviour of the catenary when interacting with the pantograph is characterized by small displacements of the cables. Unlike in the static equilibrium problem, it is common to linearise the catenary dynamic equations with respect to the static equilibrium position of the catenary, $\mathbf{r}_0$, obtained from Eq. (3.16). Thus,

the absolute position of an arbitrary point $\mathbf{r} = [x\ y\ z]^T$ can be obtained as $\mathbf{r} = \mathbf{r}_0 + \mathbf{v}$, $\mathbf{v} = \mathbf{N}\mathbf{u}^e$ being the displacements with respect to the configuration in which the system has been linearised, and $\mathbf{u}^e$ the nodal displacements for a beam element with nodes i and j as follows:

$$\mathbf{u}^e = \left[\begin{array}{cccccccccccc} u_i & v_i & w_i & \frac{\partial u_i}{\partial \chi} & \frac{\partial v_i}{\partial \chi} & \frac{\partial w_i}{\partial \chi} & u_j & v_j & w_j & \frac{\partial u_j}{\partial \chi} & \frac{\partial v_j}{\partial \chi} & \frac{\partial w_j}{\partial \chi} \end{array} \right]^T \tag{3.21}$$

If Eq. (3.14) is linearised and the inertial term is considered, the dynamics of the catenary system without any applied external force is described by:

$$\sum_{e=1}^{N_e} \int_{\Omega^e} \left[\rho A \delta \mathbf{v} \cdot \ddot{\mathbf{v}} + EI \delta \mathbf{v}'' \cdot \mathbf{v}'' + \frac{EA}{2} \delta \mathbf{v}' \cdot \left[2\mathbf{r}_0' \left(\mathbf{v}' \cdot \mathbf{r}_0' \right) + \mathbf{v}' \left(\mathbf{r}_0' \cdot \mathbf{r}_0' - 1 \right) \right] \right] d\chi = 0 \tag{3.22}$$

for all admissible $\delta\mathbf{v}$, where the dot symbol $\dot{}$ denotes a time derivative.

After introducing the FE interpolation, the mass and stiffness matrices of the catenary are:

$$\begin{aligned} \mathbf{M}_{cat} &= \mathop{\mathsf{A}}_{e}^{N_e} \int_{\Omega^e} \rho A \mathbf{N}^T \mathbf{N} \, d\chi \\ \mathbf{K}_{cat} &= \mathop{\mathsf{A}}_{e}^{N_e} \int_{\Omega^e} \Big[EI \mathbf{N}''^T \mathbf{N}'' + EA \Big(\left(\mathbf{N}'^T \mathbf{N}' \mathbf{q}_0 \right) \left(\mathbf{q}_0^T \mathbf{N}'^T \mathbf{N}' \right) + \\ &\qquad \frac{1}{2} \left(\mathbf{N}'^T \mathbf{N}' \right) \left(\mathbf{q}_0^T \mathbf{N}'^T \mathbf{N}' \mathbf{q}_0 - 1 \right) \Big) \Big] d\chi \end{aligned} \tag{3.23}$$

where A is the assembly operator.

Regarding the damping, a proportional Rayleigh model is considered, which leads to the catenary damping matrix:

$$\mathbf{C}_{cat} = \alpha_r \mathbf{M}_{cat} + \beta_r \mathbf{K}_{cat} \tag{3.24}$$

where α_r and β_r are the damping coefficients. Hence, the linear dynamic equation of the catenary system can be expressed in matrix form as:

$$\mathbf{M}_{cat} \ddot{\mathbf{u}}_{cat} + \mathbf{C}_{cat} \dot{\mathbf{u}}_{cat} + \mathbf{K}_{cat} \mathbf{u}_{cat} = \mathbf{0} \tag{3.25}$$

The lumped mass model chosen for the pantograph is a linear model which only introduces vertical displacements (w_i) with respect to a given reference height z_{ref} (see Fig. 3.4). The equation of motion of this system is:

$$\mathbf{M}_{pan} \ddot{\mathbf{w}}_{pan} + \mathbf{C}_{pan} \dot{\mathbf{w}}_{pan} + \mathbf{K}_{pan} \mathbf{w}_{pan} = \mathbf{F}_{pan} \tag{3.26}$$

Finally, the interaction model couples Eqs. (3.25) and (3.26). Using a penalty method, the virtual work produced by the interaction force f_{inter} is:

$$(\delta z_1 - \delta z_{cw}) k_h (z_1 - z_{cw}) = (\delta w_1 - \delta w_{cw}) k_h (z_{ref} + w_1 - z_{0,cw} - w_{cw}) \tag{3.27}$$

where $z_{0,cw}$ is the vertical coordinate of the contact point of the contact wire in the static equilibrium configuration. This value changes as the pantograph moves forward. If the contact point is located on the local coordinate χ_c of a beam element with nodes i and j, and the FE interpolation is introduced, Eq. (3.27) leads to:

$$\mathbf{f}_{inter} = \mathbf{k}_{inter}\mathbf{u}_{inter} + \mathbf{f}_{0,inter} = \\ k_h \left(\begin{array}{cccc|c} N_{b1}^2 & N_{b12} & N_{b13} & N_{b14} & -N_{b1} \\ N_{b21} & N_{b2}^2 & N_{b23} & N_{b24} & -N_{c2} \\ N_{b31} & N_{b32} & N_{b3}^2 & N_{b34} & -N_{c3} \\ N_{b41} & N_{b42} & N_{b43} & N_{b4}^2 & -N_{b4} \\ \hline -N_{b1} & -N_{b2} & -N_{b3} & -N_{b4} & 1 \end{array}\right) \begin{pmatrix} w_i \\ w_i' \\ w_j \\ w_j' \\ \hline w_1 \end{pmatrix} + k_h(z_{ref} - z_{0,cw}) \begin{pmatrix} -N_{b1} \\ -N_{b2} \\ -N_{b3} \\ -N_{b4} \\ \hline 1 \end{pmatrix} \tag{3.28}$$

where $N_{bij} = N_{bi}N_{bj}$ and all the shape functions are evaluated in χ_c.

If the global vector of displacements is defined as $\mathbf{u} = [\mathbf{u}_{cat}\ \mathbf{w}_{pan}]^T$, Eq. (3.28) can be expanded to the global size. That is:

$$\mathbf{F}_{inter} = \mathbf{K}_{inter}\mathbf{u} + \mathbf{F}_{0,inter} \tag{3.29}$$

At this point, all the matrices are available to be combined, leading to the differential equation which governs the coupled dynamics of the pantograph–catenary system, namely:

$$\mathbf{M}\ddot{\mathbf{u}} + \mathbf{C}\dot{\mathbf{u}} + \mathbf{K}\mathbf{u} = \mathbf{F} \tag{3.30}$$

where

$$\mathbf{M} = \begin{pmatrix} \mathbf{M}_{cat} & \mathbf{0} \\ \mathbf{0} & \mathbf{M}_{pan} \end{pmatrix} \quad \mathbf{C} = \begin{pmatrix} \mathbf{C}_{cat} & \mathbf{0} \\ \mathbf{0} & \mathbf{C}_{pan} \end{pmatrix} \quad \mathbf{K} = \begin{pmatrix} \mathbf{K}_{cat} & \mathbf{0} \\ \mathbf{0} & \mathbf{K}_{pan} \end{pmatrix} + \mathbf{K}_{inter} \tag{3.31}$$

and

$$\mathbf{F} = \begin{pmatrix} \mathbf{0} \\ \mathbf{F}_{pan} \end{pmatrix} - \mathbf{F}_{0,inter} = \mathbf{F}_{ext} - \mathbf{F}_{0,inter} \tag{3.32}$$

The first step to solve Eq. (3.30) consists of finding the initial conditions necessary to begin with the time integration scheme. In order to obtain the initial position $\mathbf{r}^0 = \mathbf{r}_0 + \mathbf{u}^0$, the static problem $\mathbf{K}\mathbf{u}^0 = \mathbf{F}$ is solved. Regarding the initial velocity, $\dot{\mathbf{u}}^0$, it is assumed to be null and finally, the initial acceleration $\ddot{\mathbf{u}}^0$ can be obtained from Eq. (3.30).

With the initial conditions of the movement at hand, the Hilber-Hughes-Taylor (HHT) time integration scheme [113] is used to obtain the dynamic response of the system. This time integrator can be seen as a generalization of the well-known Newmark method. It uses a constant time step Δt and the parameters α, β and γ which control the stability and the numerical damping introduced by the method.

Despite the linear assumption in the dynamics of the cables, this problem includes two sources of nonlinearities. The first comes from the unilateral behaviour of droppers shown in Fig. 3.5. Droppers have stiffness k_d in traction, while under compression it is assumed to be null. In this figure, f_d represents the internal force of the dropper and $f_{0,d}$ is its traction force in the static equilibrium configuration in which the equations are linearised. $\delta_{0,d}$ is the elongation that the dropper suffers in the static equilibrium position.

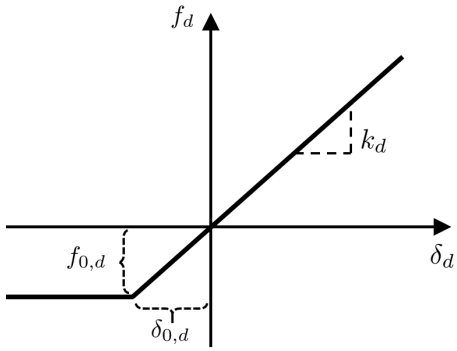

Figure 3.5: Force - elongation curve for dropper d.

The second nonlinearity comes from the fact that the pantograph can be detached from the contact wire inducing a null interaction force. These two features require the use of an iterative scheme in order to obtain the solution in each time step.

By applying the HHT algorithm to Eq. (3.30), the displacements at time step t, $t = 1, ..., N_{stp}$, and iteration j are obtained by solving the following linear system of equations:

$$\mathbf{A}_j^t \mathbf{u}_j^t = \mathbf{b}_j^t \tag{3.33}$$

where

$$\begin{aligned} \mathbf{A}_j^t &= (1+\alpha)\left[\mathbf{K}_j^t + b_4 \mathbf{C}_j^t\right] + b_1 \mathbf{M} \\ \mathbf{b}_j^t &= -\alpha \mathbf{F}^{t-1} + (1+\alpha)\mathbf{F}_j^t + \mathbf{F}_{IC}^t \end{aligned} \tag{3.34}$$

and

$$\begin{aligned} \mathbf{F}_{IC}^t = \alpha\left(\mathbf{K}^{t-1}\mathbf{u}^{t-1} + \mathbf{C}^{t-1}\dot{\mathbf{u}}^{t-1}\right) + \mathbf{M}\left(b_1\mathbf{u}^{t-1} - b_2\dot{\mathbf{u}}^{t-1} - b_3\ddot{\mathbf{u}}^{t-1}\right) + \\ (1+\alpha)\mathbf{C}_j^t\left(b_4\mathbf{u}^{t-1} - b_5\dot{\mathbf{u}}^{t-1} - b_6\ddot{\mathbf{u}}^{t-1}\right) \end{aligned} \tag{3.35}$$

All the constants b_i, $i = 1, ..., 6$ depend on the time step and the method's parameters β and γ as follows:

$$\begin{aligned} b_1 &= \frac{1}{\beta\Delta t^2} & b_2 &= \frac{1}{\beta\Delta} & b_3 &= 1 - \frac{1}{2\beta} \\ b_4 &= \gamma\Delta t\, b_1 & b_5 &= 1 + \gamma\Delta t\, b_2 & b_6 &= \Delta t(1 + \gamma b_3 - \gamma) \end{aligned} \tag{3.36}$$

Once $\mathbf{u}_j^t$ is obtained, the state of all the N_d droppers must be checked. To this end, given a dropper d, it is necessary to compute its internal force. If $\mathbf{k}_d$ is the stiffness matrix of the element, and $\mathbf{u}_{d,j}^t$ is the vector of element displacements, then:

$$\mathbf{f}_{d,j}^t = \left[\mathbf{k}_d \mathbf{u}_{d,j}^t\right]_k \tag{3.37}$$

where the operator $[\ ]_k$ selects only the components of the force vector that are applied on the node n of the dropper, whose modulus is $f_{d,j}^t$. The slackening criterion is stated as:

$$\begin{aligned} &\text{if } f_{d,j}^t + f_{0,d} \leq 0 \text{ then dropper } d \text{ is slackened} \\ &\text{if } f_{d,j}^t + f_{0,d} > 0 \text{ then dropper } d \text{ is tensioned} \end{aligned} \tag{3.38}$$

from which the the slackening state vector, $\mathcal{D}_j^t$, is defined with ones for the N_{sd}^t slackened droppers and zeros for the remaining droppers.

In this direct integration method, the slackened droppers' stiffness and damping are removed from the global matrices and their internal force in the static equilibrium position must be included in the next iteration $j+1$ to account for this new slackening state. Then, the required updates for the next iteration are:

$$\mathbf{K}_{j+1}^t = \mathbf{K}^t - \sum_d^{N_{sd}^t} \mathbf{K}_d \qquad \mathbf{C}_{j+1}^t = \mathbf{C}^t - \sum_d^{N_{sd}^t} \mathbf{C}_d \qquad \mathbf{F}_{j+1}^t = \mathbf{F}^t + \sum_d^{N_{sd}^t} \mathbf{F}_{0,d} \tag{3.39}$$

where $\mathbf{K}_d$, $\mathbf{C}_d$ and $\mathbf{F}_{0,d}$ are the stiffness and damping matrices and the force vector in static equilibrium position of dropper d, respectively, expanded to the global size of the problem.

In addition, before moving to the next iteration, the value of the interaction force, f_{inter}, must be obtained according to Eq. (3.6) to define the contact loss state $\mathcal{C}_j^t$. This is set to zero if contact exists, $f_{inter} > 0$, or to one in case of contact loss, leading to a null interaction force.

The iterative process keeps going until both the dropper slackening state $\mathcal{D}^t$ and the contact loss state $\mathcal{C}^t$ are identical in two consecutive iterations. In that case, we can also move to the next time step $t + 1$.

Chapter 4

Contributions

"It always seems impossible until it's done"
Nelson Mandela

This chapter is an overview of the main contributions of the Thesis, focusing on their novel aspects and key ideas.

As pointed out in Section 1.3, the two main objectives of this Thesis, namely the optimisation of the geometry and the simulation of the installation errors of a railway catenary, have the common feature of requiring thousands of simulations of the pantograph–catenary dynamic interaction. Following the procedure described in Chapter 3, each of those simulations can take long time, which makes it infeasible from a practical point of view to be applied in optimisation and uncertainty propagation algorithms. For example, the dynamic simulation of a conventional catenary section when the pantograph moves at 300 km/h during 10 s, takes about 30 minutes using an Intel® Xeon® CPU E5-1660 v3 processor. Hence, the first efforts were made to devise an efficient simulation algorithm that enables the proposed objectives to be achieved with a reasonable computational cost.

Each of the following four sections of the current chapter is directly linked with a paper included in Part II of this document. In Section 4.1, a parametric model of the pantograph–catenary dynamic interaction is proposed (see Paper A). Due to the drawbacks of this model, an efficient strategy to deal with the nonlinearities of the problem is presented in Section 4.2 (see Paper B). With the obtained high-performance tool for the simulation of the pantograph–catenary dynamic interaction,

optimisation of the catenary geometry is carried out in Section 4.3 (see Paper C). Finally, assessment and analysis of the most common installation errors found in actual catenaries are accomplished in Section 4.4 (see Paper D).

4.1. Parametric model

Dropper lengths are parameters with direct influence on the contact wire height and therefore, on the dynamic behaviour of the coupled pantograph–catenary system. Due to their major effects, they are seen as good candidates to be optimised to build catenaries with an optimal behaviour and also, to analyse the effects of accidentally installing droppers with different lengths than those planned in the design.

The analysis of the influence of undeformed dropper lengths on the dynamics of the coupled system would require a great number of simulations for different combinations of these parameters, which would be infeasible in practice with traditional finite element technology. One of the novelties proposed in this Thesis (see Paper A) consists of finding a parametric solution of the pantograph–catenary dynamic interaction problem, so that it is computed only once for all dropper lengths. Thus, when a simulation of a particular catenary is required, it can be directly obtained by only evaluating the precomputed parametric solution with the value of its dropper lengths.

The above mentioned parametric solution can be built by means of the Proper Generalised Decomposition (PGD) technique [114]. The PGD allows the solving of parametric models defined in high dimensional spaces, such as the problem at hand, in which undeformed dropper lengths are introduced as new coordinates of the problem. The PGD is an *a priori* Model Order Reduction (MOR) technique which can be easily used to solve a wide range of problems in a multidimensional framework [115]. The main pillar of the PGD is to include parameters as extra-coordinates into the weak formulation in order to circumvent the so-called *curse of dimensionality* when a large number of parameters are considered.

In order to obtain a parametric solution to the dynamic problem, it is first necessary to have at hand the parametric solution to the static equilibrium problem. This can be obtained by applying the PGD technique to the nonlinear Eq. (3.14), in which some initial dropper lengths l^d_{ref}, $d = 1, ..., \mathscr{N}$ are not treated as parameters any more, but as coordinates. Thus, $\mathbf{r} = \mathbf{r}(\chi, l^1_{ref}, ..., l^{\mathscr{N}}_{ref})$, where $\chi \in [0,\, l^e_{ref}]$ is the local coordinate of the element (see Fig. 3.1).

The PGD technique proposes approximating the solution to a summation of modes in which the separation of variables is applied as follows:

$$\mathbf{r}(\chi, l^1_{ref}, ..., l^{\mathscr{N}}_{ref}) \approx \mathbf{r}^n = \mathbf{r}^{n-1} + \mathbf{R}_n(\chi)\, L^1_n(l^1_{ref}) \dots L^{\mathscr{N}}_n(l^{\mathscr{N}}_{ref}) \tag{4.1}$$

where the previous modes

$$\mathbf{r}^{n-1} = \sum_{i=1}^{n-1} \mathbf{R}_i(\chi)\, L_i^1(l_{ref}^1) \dots L_i^{\mathscr{N}}(l_{ref}^{\mathscr{N}}) \tag{4.2}$$

are assumed to be known.

If Eq. (4.1) is introduced into the variational form of the static problem (see Eq. (3.14) for its discretised counterpart), the unknowns are now the functions $\mathbf{R}_n(\chi)$ and $L_n^d(l_{ref}^d)$ for $d = 1, ..., \mathscr{N}$. These functions can be obtained iteratively by means of an alternating fixed-point strategy, in which at each iteration a three-dimensional problem and $\mathscr{N}$ one-dimensional problems are solved to obtain $\mathbf{R}_n$ and L_n^d respectively. Thus, instead of a multidimensional problem to obtain $\mathbf{r}(\chi, l_{ref}^1, ..., l_{ref}^{\mathscr{N}})$, a sequence of lower dimensional problems are dealt with using classical discretisation techniques.

One of the main features of a catenary is the inability of droppers in transmitting compressive forces. This unilateral behaviour is also included within the PGD framework, which also represents a challenging new contribution to the field. A good overview of the PGD constructor is given in [114] and the details of its application to the catenary static equilibrium problem are provided in Paper A.

Table 4.1: Material and geometrical properties of the elements.

Element	$\mathbf{E}(Pa)$	$\boldsymbol{\rho}(kg/m^3)$	$\mathbf{A}(mm^2)$	$\mathbf{I}(mm^4)$
Messenger wire	9114	$1.1 \cdot 10^{11}$	94.8	1237.2
Contact wire	9160	$1.1 \cdot 10^{11}$	150	2170
Droppers	9114	$1.1 \cdot 10^{11}$	10	0

Although in Paper A there are more realistic numerical examples, the performance of the method is tested here through an academic problem. The spatial domain Ω of this 2D catenary span model, which only includes two droppers, is shown in Fig. 4.1. Material and geometrical properties of the elements are listed in Table 4.1. The two droppers are considered to have a variable undeformed length l_{ref}^1 and l_{ref}^2. In order to explore all the capabilities of the method, both variables are defined in the same domain, $\Omega_l^1 = \Omega_l^2 = [1.15, 1.25]\ m$, which ensures droppers are compressed in certain regions of it. This domain is uniformly discretised into 20 values. The x and z coordinates of the ends of both wires are imposed as boundary conditions.

The parametric solution is obtained under two different assumptions: i) droppers are able to transmit compressive forces and ii) droppers slacken under compression. Let us define the global error of the parametric solution with n modes as:

$$E_{glob}^n = \int_{\Omega^1 \times \dots \times \Omega^{\mathscr{N}}} \frac{\|\mathbf{r}_{FEM} - \mathbf{r}_{PGD}^n\|}{\|\mathbf{r}_{FEM}\|}\, dl_{ref}^1 \dots dl_{ref}^{\mathscr{N}} \tag{4.3}$$

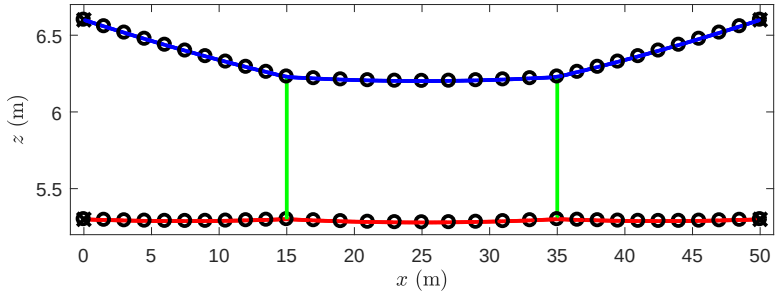

Figure 4.1: Academic example spatial mesh.

where $\mathbf{r}_{FEM}$ and $\mathbf{r}^n_{PGD}$ are the absolute position fields obtained from the FE standard approach and the PGD parametric solution with n modes, respectively.

Fig. 4.2 shows a plot of the global error versus the number of modes included in the parametric solution. If the enrichment procedure is stopped when $E_{glob} < 10^{-3}$, the parametric solution converges very fast with only 11 modes when dropper slackening is not considered (Fig. 4.2a). However, the strong nonlinearity of dropper slackening notably slows down the speed of convergence, since with 11 modes $E^{11}_{glob} \approx 0.33$, as can be seen in Fig. 4.2b. Hence, although affordable, a remarkable computational effort is necessary to obtain parametric solutions of the catenary static equilibrium problem when allowing for dropper slackening.

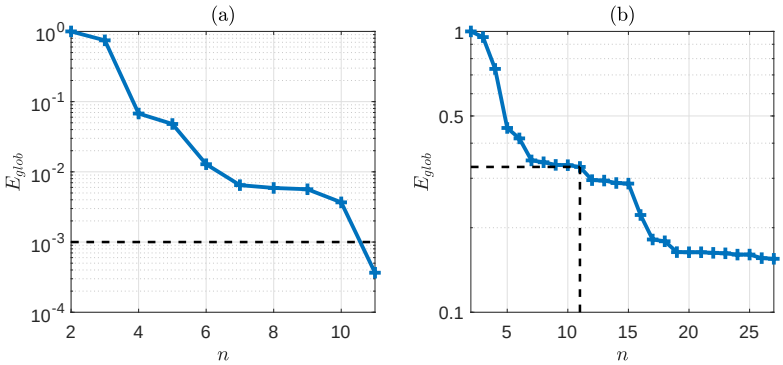

Figure 4.2: E_{glob} of PGD parametric solution. (a) Dropper slackening is not considered and (b) dropper slackening is allowed for.

Moving to the dynamic interaction problem, the PGD technique can also be applied to introduce dropper lengths as extra coordinates. In this case, the absolute

position field reads:

$$\mathbf{r}(\chi, t, l^1_{ref}, ..., l^{\mathscr{N}}_{ref}) = \mathbf{r}_0^{n_0} + \mathbf{u}^{n-1} + \mathbf{U}_n(\chi, t)\, \mathscr{L}^1_n(l^1_{ref}) \dots \mathscr{L}^{\mathscr{N}}_n(l^{\mathscr{N}}_{ref}) \tag{4.4}$$

where $\mathbf{r}_0^{n_0}$ is the parametric solution of the static equilibrium problem in which the dynamics have been linearised, and $\mathbf{u}^{n-1}$ is the solution with $n-1$ modes, which is assumed to be known.

Again, by introducing Eq. (4.4) into the weak form of Eq. (3.30), the functions $\mathbf{U}_n(\chi, t)$ and $\mathscr{L}^d_n(l^d_{ref})$ for $d = 1, ..., \mathscr{N}$ become the unknowns of the parametric problem. If the fixed-point method is applied, these functions are obtained iteratively by solving a time-spatial problem and a sequence of univariate problems, respectively. The former is solved with the HHT time integration scheme, and the latter are solved with a traditional FE discretisation technique.

This strategy is applied to the example defined above, disregarding dropper slackening and pantograph contact loss, so that the problem is fully linear. In this example, we use the pantograph model defined in [9], which moves forward at 300 km/h. The convergence of the parametric solution is checked in Fig. 4.3 in which the interaction force f_{inter}, obtained from the standard FE approach, is depicted in a dashed black line. This force is compared with those obtained with the PGD technique, including $n = 1, ..., 4$ modes. A great convergence is observed in both cases, in which the solution has been evaluated with two different dropper length sets, since only three modes are necessary to achieve a high accuracy in the results.

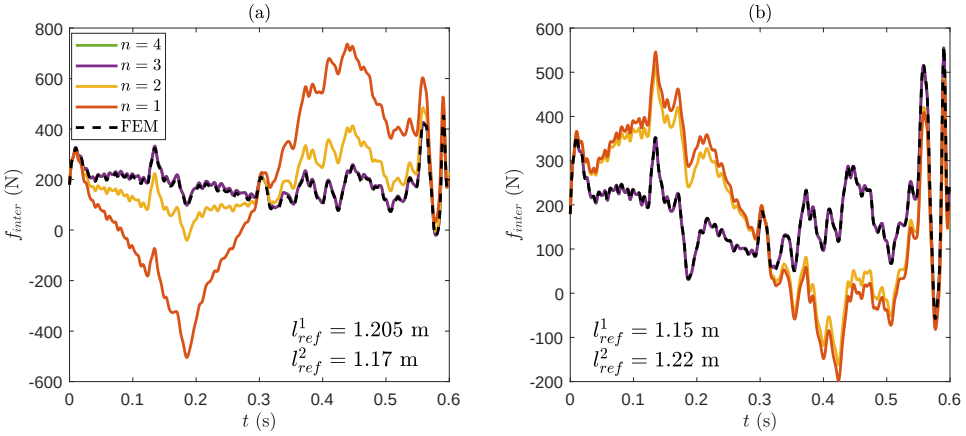

Figure 4.3: Comparison of the interaction force between the parametric solution, with different number of modes n, and the reference FE solution for two specific points in Ω_l. (a) $l^1_{ref} = 1.205$ m and $l^2_{ref} = 1.17$ m, (b) $l^1_{ref} = 1.15$ m and $l^2_{ref} = 1.22$ m.

Despite this good convergence of the parametric solution, in a more realistic problem allowing for dropper slackening and pantograph contact losses, the scenario

changes radically. In this case, the system dynamics become very sensitive to little changes in the value of dropper lengths. To exemplify this behaviour, Fig. 4.4 shows the interaction force value for the time at which the pantograph passes under the second dropper ($t = 420$ ms), in the parametric domain $\Omega_l^1 \times \Omega_2^1$.

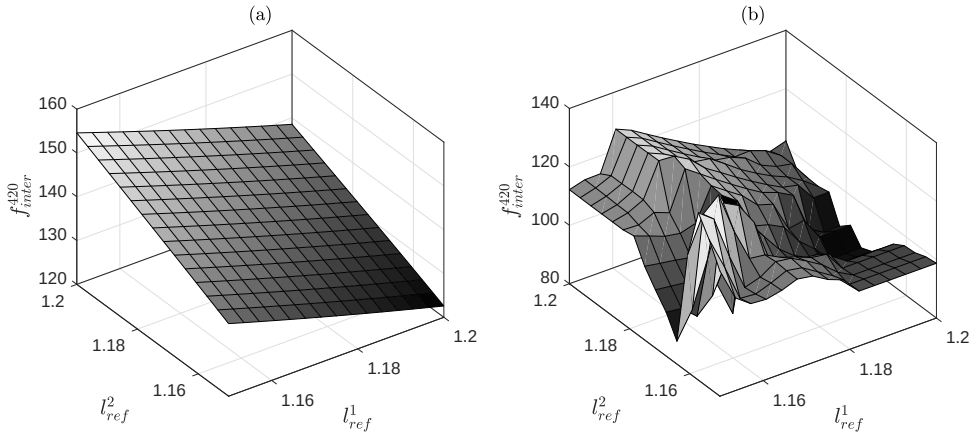

Figure 4.4: Interaction force at instant 420 ms for the whole parametric domain $\Omega_l^1 \times \Omega_l^2$. (a) Linear behaviour of droppers, (b) dropper slackening is considered.

Fig. 4.4a is obtained if dropper slackening is not considered, while in Fig. 4.4b, droppers slacken under compressive forces. Crucial differences between them are observed. If droppers behave linearly, dropper length variations produce a smooth tendency in the interaction force. In contrast, if considering a bilinear behaviour in droppers (see Fig. 3.5), the interaction force varies abruptly and is very sensitive to small changes in the parametric domain.

This fact was already intuited when solving the parametric static equilibrium problem, but it becomes even worse in the dynamic case. Thus, due to the non-separable nature of the dynamic problem observed when nonlinear droppers are considered, obtaining an accurate enough parametric solution of the dynamic problem, as stated in Eq. (4.4), becomes infeasible due to the huge number of required modes.

4.2. Fast simulation algorithm

Due to the major difficulties found when dealing with the parametric dynamic interaction problem, other strategies must be conceived to have a solver which allows to efficiently apply optimisation and stochastic techniques.

As previously said, dropper slackening and pantograph–contact wire interaction, are the two sources of nonlinearities present in the dynamic problem. In this Thesis we propose a new strategy in which, after moving the nonlinear terms to the right hand side of the dynamic equation (3.30) as proposed in [31], the use of the superposition principle to transfer the unknowns from the displacements to the forces is its basic pillar. Hence, the nonlinearities are dealt with iteratively but now, the size of the nonlinear system to be solved in each time step is equal to the number of elements with nonlinear behaviour (slackened droppers and penalty stiffness element) in lieu of the global size of the problem.

The method is divided into two stages, namely the *Offline* and the *Online*. In the first stage, the response of the catenary in a single time step Δt, subject to unitary forces, is computed and stored. Then, in the *Online* stage, by applying the superposition principle, the time integration is carried out making use of the information computed in the *Offline* stage so that the nonlinearities are efficiently treated in each time step.

4.2.1. *Offline* stage

As the nonlinear terms are moved to the right hand side of the dynamic equation, damping and stiffness matrices become constant in time and therefore the HHT integration matrix

$$\mathbf{A} = (1+\alpha)\left[\begin{pmatrix}\mathbf{K}_{cat} & \mathbf{0}\\ \mathbf{0} & \mathbf{K}_{pan}\end{pmatrix} + b_4\begin{pmatrix}\mathbf{C}_{cat} & \mathbf{0}\\ \mathbf{0} & \mathbf{C}_{pan}\end{pmatrix}\right] + b_1\begin{pmatrix}\mathbf{M}_{cat} & \mathbf{0}\\ \mathbf{0} & \mathbf{M}_{pan}\end{pmatrix} = \begin{pmatrix}\mathbf{A}_{cat} & \mathbf{0}\\ \mathbf{0} & \mathbf{A}_{pan}\end{pmatrix} \tag{4.5}$$

does not change in time either (see Eq. (3.34)).

In the *Offline* stage, the catenary is treated as a fully linear system, and three different problems are solved in order to obtain the single time-step response of the system under unitary external loads and null initial conditions. They are:

1. A unitary force pushing upwards at the interaction point on the contact wire (blue arrow in Fig. 4.5b). If $\mathbf{A}_{cat}$ is taken from the elements of matrix $\mathbf{A}$ only related to the degrees of freedom of the catenary, the problem:

$$\mathbf{A}_{cat}\mathbf{u}^{*,t}_{inter,cat} = \mathbf{F}^{*,t}_{inter,cat} \quad \forall t \in [1, N_{stp}] \tag{4.6}$$

must be solved N_{stp} times, in each of which $\mathbf{F}^{*,t}_{inter,cat}$ is the result of assembling $\mathbf{f}^{*}_{inter,cat}$, which is applied to the corresponding interaction point on the contact wire.

2. A unitary force compressing each dropper (black arrows in Fig. 4.5b). Therefore, the linear problem:

$$\mathbf{A}_{cat}\mathbf{u}^{*}_{d} = \mathbf{F}^{*}_{d} \quad \forall d \in [1, N_d] \tag{4.7}$$

needs to be solved N_d times in which, $\mathbf{f}^{*}_{d}$ is applied on a different dropper and assembled in vector $\mathbf{F}^{*}_{d}$.

3. A unitary force pushing downwards on the upper mass of the pantograph in which, the interaction with the contact wire takes place (blue arrow in Fig. 4.5a). If $\mathbf{A}_{pan}$ extracts the elements of matrix $\mathbf{A}$ related to the degrees of freedom of the pantograph, the problem:

$$\mathbf{A}_{pan}\mathbf{w}^{*}_{inter,pan} = \mathbf{F}^{*}_{inter,pan} \tag{4.8}$$

where $\mathbf{F}^{*}_{inter,pan}$ results from assembling $\mathbf{f}^{*}_{inter,pan}$, needs to be solved only once.

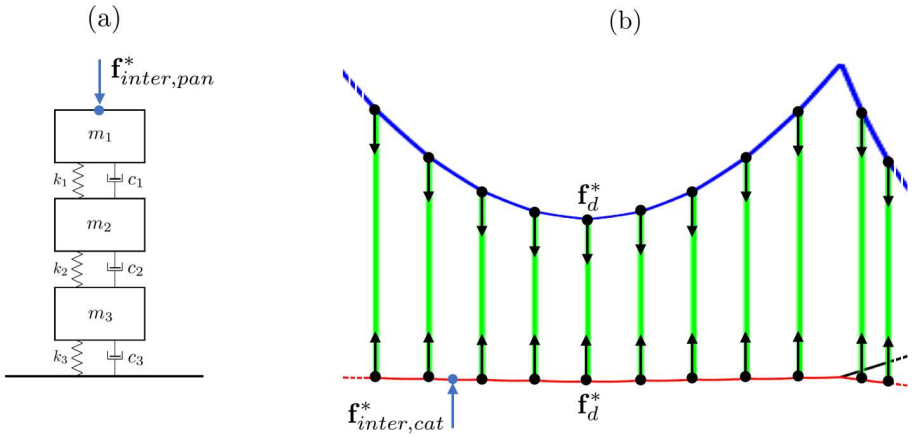

Figure 4.5: Unitary external forces applied in the *Offline* stage. (a) Pantograph and, (b) Catenary.

As $\mathbf{A}_{cat}$ is constant, it can be prefactorised in order to obtain substantial computational cost savings when solving Eqs. (4.6) and (4.7). Additionally, velocities and accelerations of all the aforementioned problems are also computed and stored following the rules of the HHT time integrator.

4.2.2. *Online* stage

In the *Online* stage, the time integration is carried out taking into account the nonlinearities introduced by dropper slackening and pantograph contact loss. Starting from Eq. (3.33) at time step t, the nonlinear sources are moved to the right hand side of the equation, which results in:

$$\mathbf{A}\,\mathbf{u}^t = \mathbf{F}_{IC}^t + \mathbf{F}_{ext} - \alpha\mathbf{F}_{nl}^{t-1} + (1+\alpha)\mathbf{F}_{nl}^t \tag{4.9}$$

where $\mathbf{F}_{IC}^t$ contains information of the previous time step and $\mathbf{F}_{ext}$ considers the constant external uplift force applied onto the pantograph. If there are N_{sd}^t slackened droppers in the current time step, the nonlinear force term is:

$$\mathbf{F}_{nl}^t = -\mathbf{F}_{0,inter}^t - \mathbf{K}_{inter}^t\mathbf{u}^t + \sum_{d}^{N_{sd}^t}\left(\mathbf{F}_{0,d}^t + \mathbf{K}_d^t\mathbf{u}^t + \mathbf{C}_d^t\dot{\mathbf{u}}^t\right) \tag{4.10}$$

in which $\mathbf{F}_{0,inter}^t + \mathbf{K}_{inter}^t\mathbf{u}^t$ is the interaction force and $\mathbf{F}_{0,d}^t + \mathbf{K}_d^t\mathbf{u}^t + \mathbf{C}_d^t\dot{\mathbf{u}}^t$ is the correction force of the slackened dropper d.

With this rearrangement, there is no coupling between pantograph and catenary degrees of freedom in the system of equations. The known and unknown terms can be grouped as

$$\mathbf{A}\,\mathbf{u}^t = \mathbf{F}_{kn}^t + (1+\alpha)\left(\mathbf{F}_{inter}^t + \sum_{d}^{N_{sd}^t}\mathbf{F}_d^t\right) \tag{4.11}$$

where

$$\begin{aligned}\mathbf{F}_{kn}^t &= \mathbf{F}_{IC}^t + \mathbf{F}_{ext} - \alpha\mathbf{F}_{nl}^{t-1}\\ \mathbf{F}_{inter}^t &= -\mathbf{F}_{0,inter}^t - \mathbf{K}_{inter}^t\mathbf{u}^t\\ \mathbf{F}_d^t &= \mathbf{F}_{0,d}^t + \mathbf{K}_d^t\mathbf{u}^t + \mathbf{C}_d^t\dot{\mathbf{u}}^t\end{aligned} \tag{4.12}$$

$\mathbf{F}_{kn}^t$ contains all the known forces, but the interaction force $\mathbf{F}_{inter}^t$ and the correction forces of the slackened droppers $\mathbf{F}_d^t$ remain unknown since they depend on the sought displacements $\mathbf{u}^t$.

By applying the superposition principle, the total response of the system can be computed as the sum of the responses caused by the three forces in Eq. (4.12) acting separately, that is:

$$\mathbf{u}^t = \mathbf{u}_{F_{kn}}^t + (1+\alpha)\left(\mathbf{u}_{F_{inter}}^t + \sum_{d}^{N_{sd}^t}\mathbf{u}_{F_d}^t\right) \tag{4.13}$$

or equivalently, taking benefit from the responses under unitary forces calculated in the *Offline* stage, and explicitly splitting the system in terms of catenary and

pantograph:

$$\begin{pmatrix} \mathbf{u}_{cat}^t \\ \mathbf{w}_{pan}^t \end{pmatrix} = \mathbf{u}_{F_{kn}}^t + (1+\alpha)\left(f_{inter}^t \begin{pmatrix} \mathbf{u}_{inter,cat}^{*,t} \\ \mathbf{w}_{inter,pan}^{*} \end{pmatrix} + \sum_{d}^{N_{sd}^t} f_d^t \begin{pmatrix} \mathbf{u}_d^* \\ \mathbf{0} \end{pmatrix} \right) \tag{4.14}$$

Now, the magnitude of the interaction force, f_{inter}^t, and the correction forces of the slackened droppers, f_d^t for $d = 1, ..., N_{sd}^t$, are the set of unknowns of the problem at the current time step t.

The displacements coming from initial conditions can be directly computed from

$$\begin{aligned} \mathbf{A}_{cat}\mathbf{u}_{F_{kn},cat}^t &= \mathbf{F}_{kn,cat}^t \\ \mathbf{A}_{pan}\mathbf{w}_{F_{kn},pan}^t &= \mathbf{F}_{kn,pan}^t \end{aligned} \tag{4.15}$$

in which $\mathbf{A}_{cat}$ has been factorised in the *Offline* stage into two sparse triangular matrices. Thus, solving the whole system consists of applying forward and backward solvers which are computationally very efficient.

To deal with the nonlinearities, by including Eq. (4.14) into the last two equations in (4.12) it is possible to define a linear system of equations whose unknowns are f_{inter}^t and f_d^t for $d = 1, ..., N_{sd}^t$. Although this is a linear system in itself, the nonlinearity is present in the number of equations of which it is composed, because N_{sd}^t depends upon the solution of the system. Further details for the construction of this system are provided in Section 4.3.2 of Paper B.

This small system can be iteratively solved at each time step, which is much more efficient than solving iteratively a global sized system with displacements as unknowns. After obtaining the unknown forces, the slackening (3.38) and the contact loss states must be checked out. As in the direct approach, the procedure lasts until in two consecutive iterations the slackening state $\mathcal{D}$ and the contact loss state $\mathcal{C}$ are equal. When the iterative procedure finishes, one can move to the next time step of the time integration scheme, as summarised in Algorithm 1.

If the proposed strategy is compared with respect to the direct approach defined in Section 3.3, the solution of the dynamic interaction problem is obtained with the same accuracy in both strategies; however, the *Offline*/*Online* approach is much more efficient in terms of computational cost.

In order to highlight the benefits of the procedure, four catenary models are defined. Cat.1, Cat.2 and Cat.3 are three-dimensional models with five, ten and 18 spans, respectively. Cat.4 is the two-dimensional version of Cat.3. The computational time required for the direct time integration procedure, for the *Offline* stage and for the *Online* stage are shown in Table 4.2 for both the HHT and the Newmark time integrators.

As revealed by these values, a simulation of the pantograph–catenary dynamic interaction is performed with the proposed strategy from about 25 to 30 times faster than with the direct procedure explained in Section 3.3. Furthermore, no deterioration

Algorithm 1 *Offline/Online* time integration.

OFFLINE stage:
  Assemble $\mathbf{A}_{cat}$ and calculate its LU factorisation;
  Solve the N_{stp} problems (4.6): $\mathbf{u}^{*,t}_{inter,cat}$;
  Solve the N_d problems (4.7): $\mathbf{u}^{*}_{d}$;
  Solve the equation (4.8): $\mathbf{w}^{*}_{inter,pan}$;

ONLINE stage:
Initializations: $\mathcal{D}^0 = 0$; $\mathcal{C}^0 = 0$
for $t = 1...N_{stp}$ **do**
  Obtain the response to the initial conditions (4.15): $\mathbf{u}^{t}_{F_{kn},cat}$, $\mathbf{w}^{t}_{F_{kn},pan}$;
  Set: $j = 1$; $\mathcal{D}^t_{j-1} = \mathcal{D}^t_j = \mathcal{D}^{t-1}$; $\mathcal{C}^t_{j-1} = \mathcal{C}^t_j = \mathcal{C}^{t-1}$;
  while $\left(\mathcal{D}^t_{j-1} \neq \mathcal{D}^t_j \text{ and } \mathcal{C}^t_{j-1} \neq \mathcal{C}^t_j\right)$ or $j = 1$ **do**
    $j = j + 1$;
    $\mathcal{D}^t_{j-1} = \mathcal{D}^t_j$; $\mathcal{C}^t_{j-1} = \mathcal{C}^t_j$;
    Set the linear system of $N_{sd} + 1$ equations;
    Apply the slackening criterion (3.38): $\mathcal{D}^t_j$;
    Apply the contact loss criterion: $\mathcal{C}^t_j$;
  end while
  With Eq. (4.13) obtain the total displacements $\mathbf{u}^t$;
end for

Table 4.2: Computational time comparison.

	Cat.1	**Cat.2**	**Cat.3**	**Cat.4**
d.o.f.	5996	11986	21570	14385
Simulated time (s)	3	5	10	10
HHT				
Direct (s)	56.05	205.38	802.80	412.46
Offline stage (s)	0.76	2.39	9.83	5.28
Online stage (s)	1.74	5.22	19.27	10.86
Offline/*Online* (s)	2.5	7.61	29.1	16.14
Newmark				
Direct (s)	52.69	218.74	785.10	417.60
Offline stage (s)	0.79	2.50	9.64	5.19
Online stage (s)	1.37	4.48	15.75	9.10
Offline/*Online* (s)	2.16	6.98	25.39	14.29

in the accuracy of the results is introduced with the fast simulation algorithm. If we only focus on the *Offline* stage, in which the time integration is carried out, some simulations can even be performed in real-time. This feature allows the algorithm to be used in Hardware-In-the-Loop (HIL) [116] simulations in which the mathematical model of the pantograph is replaced by a real pantograph mechanism.

4.3. Catenary optimisation

Once we already have an efficient algorithm to simulate the pantograph–catenary dynamic interaction, optimisation of the catenary system can be addressed with reasonable computational cost.

Current collection quality is influenced by many parameters, such as the mass of the pan-head, the contact wire tension, the uplift force applied to the pantograph or the speed of the train. Some recent attempts in optimising the current collection performance are found in the literature [14, 81], but most of them are focused on the parameters of the pantograph model.

In this Thesis, a first attempt to find the optimal catenary geometry, in terms of current collection quality, is made by exploring alternatives such as the contact wire height profile and the dropper spacing. To characterise the quality of the interaction, the coefficient of variation of the interaction force is usually used. It is defined as the quotient between the standard deviation and the mean of this force $\nu = \sigma\left(f_{inter}\right)/\mu(f_{inter})$.

Following the standard [1], the maximum mean contact force applied to the contact wire must fulfil the relationship:

$$\mu(f_{inter}) \leq 0.00097v^2 + 70 \tag{4.16}$$

for an alternating current catenary, in which $200 < v < 320$ km/h. To guarantee the fulfilment of Eq. (4.16), the uplift force f_{up}, is properly tuned in each simulation. Additionally, before computing ν, the interaction force is low-pass filtered at 20 Hz according to the standard [1].

Thus, for a given train speed v, if contact wire height or dropper spacing are considered as the optimisation variables $\mathbf{p}$, the optimisation problem reads:

$$\begin{aligned} &\min_{\mathbf{p}} \quad \nu\left(f_{inter}(\mathbf{p})\right) \\ &\text{s.t.} \\ &p_i^{min} \leq p_i \leq p_i^{max} \quad i = 1, ..., N_p \end{aligned} \tag{4.17}$$

where p_i^{min} and p_i^{max} are the lower and upper bounds of each of the N_p parameters, respectively.

To solve the problem (4.17), a metaheuristic method is required because the use of gradient-based strategies would require the computation of the derivatives of the objective function with respect to the optimisation variables, which would be cumbersome in this case. Specifically, a Genetic Algorithm (GA) is chosen due to its wide range of applicability, even for highly nonlinear or discontinuous objective functions.

The GA used in this Thesis is that included in the MATLAB® software. An initial population evolves towards better solutions from generation to generation following the principles of natural selection, crossover and mutation (see Fig.4.6). Selection is ruled by a stochastic uniform process. The three best-scored parents are considered as elite and are moved directly to the next generation. A crossover fraction of 0.8 is set to guarantee that the 80% of children come from a random combination of parameters of their parents. The remaining children are randomly obtained by mutation of the parameters of a single parent.

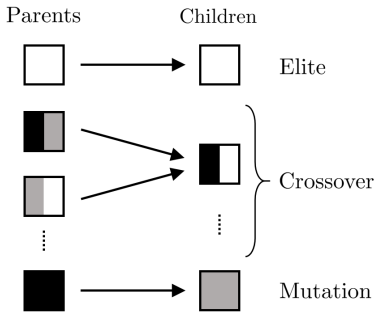

Figure 4.6: Scheme of the next generation creation process.

In this problem, the N_p optimisation variables are taken as discrete variables in order to make a finite size space of search.

In order to evaluate the objective function, it is necessary to solve both the initial configuration problem (3.20) and the dynamic interaction problem by means of the method described in Section 4.2. Nonetheless, during these evaluations some combinations of parameters $\mathbf{p}$ could produce non-desirable catenaries from a practical point of view. In these cases, individuals that fulfil one of the following conditions are excluded from the population:

- If a contact loss is detected the individual is not valid any more.
- If any dropper is slackened in the static equilibrium position, this catenary is no longer admissible.

Other restrictions, such as a maximum steady arm uplift, could be incorporated into the previous list without any further consideration.

Although a thorough discussion of the optimised catenaries is made in Paper C, for the purpose of enlightening the potential of the results, the optimisation of the contact wire height profile of a simple type catenary and a stitched catenary is presented here. The simple catenary model matches with that used in the benchmark [9]. The stitched catenary model is described in Appendix A of Paper C. Both models are composed of 20 spans each, although f_{inter} is measured on the ten central spans to prevent boundary effects. The optimisations are carried out at a train speed of 300 km/h.

Regarding the simple catenary, as there are nine droppers per span and the catenary must be symmetric, the optimisation problem is set with only five variables corresponding to the contact wire height at the connection points with droppers (black points in Fig. 4.7). Therefore, $\mathbf{p} = [z_{cw}^1 \dots z_{cw}^5]$ is defined from $p_i^{min} = -0.06$ m to $p_i^{max} = 0.02$ m for $i = 1, ..., 5$, at intervals of 1 mm.

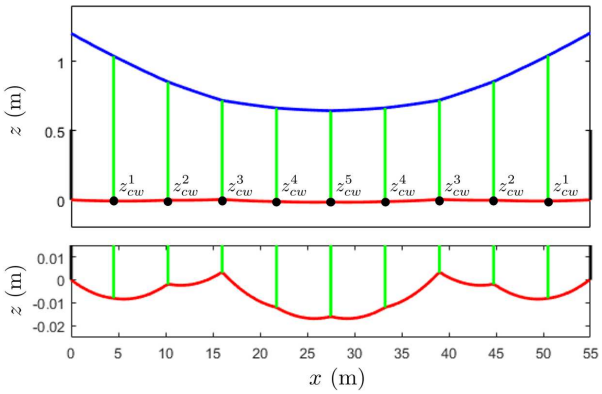

Figure 4.7: Optimised simple catenary with zoom of the contact wire in the bottom picture.

After 120 generations of the GA with a population of 100 individuals, a span of the optimised simple catenary is shown in Fig. 4.7, in which a zoom of the contact wire height profile is provided in the bottom image.

The stitched catenary has only seven droppers per span and therefore, four variables suffice to define the contact wire height (black points in Fig. 4.8), with the same bounds as in the previous case. With a population of 80 individuals, the GA took 90 generations to obtain the optimised stitched catenary shown in Fig. 4.8.

To sum up, Table 4.3 presents, for the two studied catenaries, the optimal values of the contact wire height at dropper connections, the minimum value of the objective function, and its reduction with respect to that obtained from the reference catenaries. The 56% of decrease in $\nu(f_{inter})$, from a simple catenary with a standard pre-sag of 1/1000 of the span length to the proposed optimal contact wire height profile,

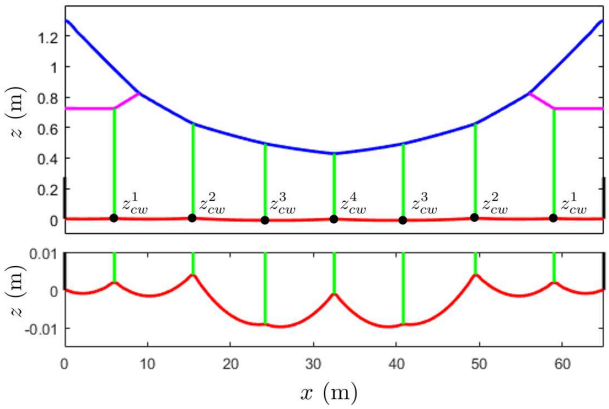

Figure 4.8: Optimised stitched catenary with zoom of the contact wire at the bottom picture.

is remarkable. This reduction is 37% for the case of the stitched catenary when compared to its reference model with a completely horizontal contact wire.

Table 4.3: Contact wire height optimisation results.

Catenary	Optimal values (m)	$\nu(f_{inter})$ (N)	Reduction (%)
Simple	-0.008 -0.002 0.003 -0.012 -0.016	0.1126	56.52
Stitched	0.002 0.004 -0.009 -0.001	0.0899	36.60

The vertical stiffness along a catenary span is depicted in Fig. 4.9. Especially for the simple catenary, a more uniform stiffness is found for the optimised catenaries when compared to that of the reference models.

Other magnitudes to be analysed are the forces carried by droppers in the static equilibrium position. While droppers in the reference catenaries are almost uniformly loaded (Figs. 4.10a and 4.10c), the forces in the optimised catenaries notably differ from one dropper to another (Figs. 4.10b and 4.10d).

How the optimised catenaries behave at different train speeds is another interesting point to be analysed. To this end, $\sigma(f_{inter})$ is plotted for both the simple and stitched catenaries in Figs. 4.11a and 4.11b, respectively.

The conclusions drawn from these results are that there are more benefits in optimising the simple catenary since, as seen in Fig. 4.11a, not only is there a greater reduction at the optimisation speed (300 km/h) but also the behaviour at other speeds is similar to that shown by the reference catenary. However, this feature is not observed for the stitched catenary in Fig. 4.11b.

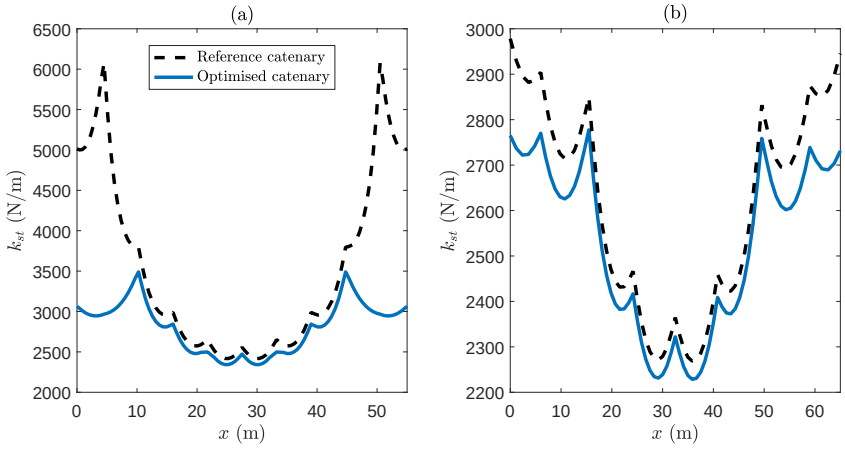

Figure 4.9: Vertical stiffness of the simple catenary span (a), and the stitched catenary span (b).

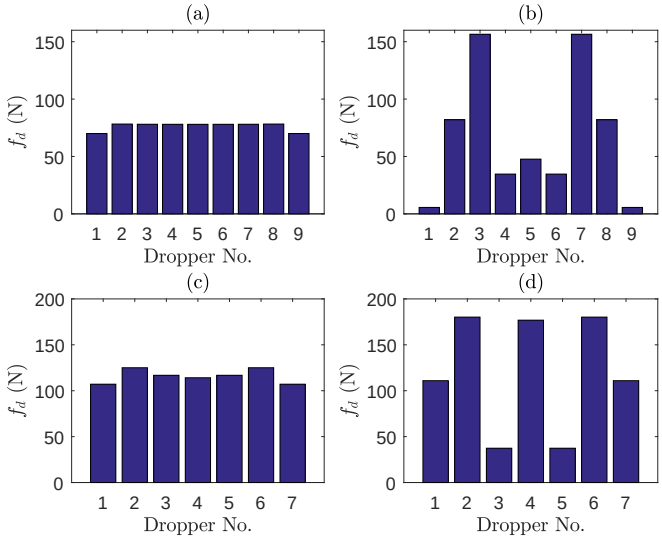

Figure 4.10: Dropper forces in the static configuration of the reference simple catenary (a), the optimised simple catenary (b), the reference stitched catenary (c), and the optimised stitched catenary (d).

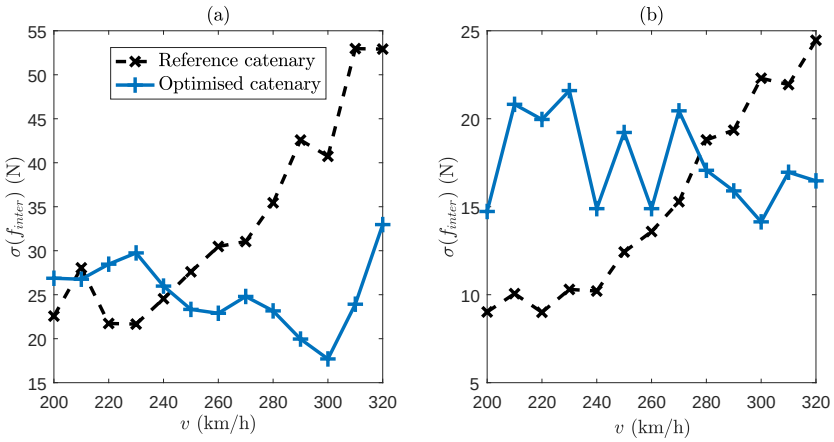

Figure 4.11: Comparison of the standard deviation of the interaction force between the reference and the optimised catenaries at different train speeds. (a) Simple catenary and, (b) Stitched catenary.

This contribution reveals to the catenary designers that there are other promising alternatives apart from the usual pre-sag in order to have better catenaries in which interaction force fluctuations can be remarkably reduced.

4.4. Stochastic simulations

Simulations of the pantograph–catenary dynamic interaction usually provide deterministic results in which the output magnitudes, such as the interaction force or the steady arm uplift, do not allow for the variability present in the system. Although there are countless sources of variability, the catenary installation procedure itself and some human faults made during the installation, lead to a final catenary configuration that differs from the designed one.

These discrepancies can have a high impact on the dynamic performance of the system. Very few works in the literature deal with uncertainties when simulating the dynamic behaviour of the catenary, as can be seen in Chapter 2. Among them, guideline values for certain installation error rates based on real measured data were proposed in [90], whereas variability in contact wire wear, aerodynamic effects and geometry irregularities are introduced in [93].

In this Thesis, an approach is proposed to account for the variability introduced by installation errors. Specifically, dropper lengths (dl), dropper spacing (ds) and support height (sh) errors are considered due to their main role in determining the contact wire height. A sketch of these installation errors is depicted in Fig. 4.12.

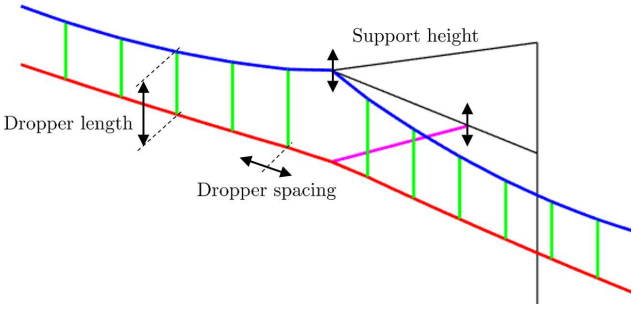

Figure 4.12: Sketch of the installation errors considered in the analysis.

The three different errors considered are assumed to be normally distributed with null mean and standard deviations $\sigma_{dl} = 0.0066$ m, $\sigma_{ds} = 0.02$ m and $\sigma_{sh} = 0.02$ m, respectively. These values agree with those measured in [86]. Technical details for the modelling of these errors from the computational point of view are provided in Section 4 of Paper D.

The classic version of the Monte Carlo method (MC) [117] has been chosen to propagate the aforementioned uncertainties. It consists of evaluating the model a sufficiently large times N, with a random sampling of the input quantities $\mathbf{x}_r$ for $r = 1, ..., N$, from their probability density function (PDF). As a result of each simulation, the output quantities $\mathbf{y}_k$ for $k = 1, ..., M$, are measured and their PDF can be built.

This large number of simulations N, is achievable thanks to the efficient simulation strategy presented in Section 4.2. However, it is important to quantify the value of N which provides enough accuracy in both the mean and standard deviation of the PDFs of the output quantities.

If $\nu = \sigma(f_{inter})/\mu(f_{inter})$ is considered as the output parameter of main interest, the central limit theorem states that the sample mean $\bar{\nu}$ is normally distributed with mean $\mu(\nu)$ and standard deviation $\frac{\sigma(\nu)}{\sqrt{N}}$ for a large enough N. Thus, with a confidence level α, and assuming an absolute error d, the population size can be determined by:

$$N = z_{\alpha/2}^2 \frac{\sigma(\nu)^2}{d^2} \tag{4.18}$$

where $z_{\alpha/2}$ is the value with an occurrence probability lower than $\frac{\alpha}{2}$ in a normal standard distribution.

Following again a central limit approach for the sample standard deviation $S(\nu)$, for a confidence level α and an assumable relative error $e = \frac{|S(\nu)^2 - \sigma(\nu)^2|}{\sigma(\nu)^2}$, the popu-

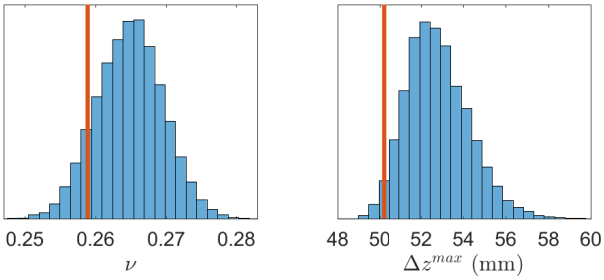

Figure 4.13: PDFs of ν_{dl} ($\bar{\nu}_{dl} = 0.2649$, $S(\nu)_{dl} = 4.71 \cdot 10^{-3}$) and Δz^{max}_{dl} obtained when uncertainty in dropper lengths is considered. Vertical lines indicate the ν and Δz^{max} obtained from the nominal catenary.

lation size is now determined by:

$$N = z^2_{\alpha/2} \frac{\gamma(\nu) - 1}{e^2} \tag{4.19}$$

where $\gamma(\nu)$ is the kurtosis, which can be estimated from a large enough population.

Thus, to obtain $\bar{\nu}$ with less than 1% of error with respect to $\mu(\nu)$ 99% of times, it suffices with $N = 50$. However, if $S(\nu)$ is sought with an accuracy of 3.4% with respect to $\sigma(\nu)$ and a 99% of confidence level is considered, $N = 10000$ simulations are needed. It is remarkable the large population size required to obtain an accurate standard deviation if compared with that required to obtain the mean with acceptable accuracy.

To reveal the power of the method, it is applied to the simple type catenary defined in [9]. Although the model is composed of 20 spans, the results are only taken from the ten central spans to avoid boundary effects. The output parameters of interest are in this case the coefficient of variation ν of the 20 Hz low-pass filtered interaction force, and the maximum steady arm uplift, Δz^{max}. The examples are carried out at 300 km/h, with an uplift force of $f_{up} = 168.47$ N to meet the requirement of Eq. 4.16.

Figs. 4.13, 4.14 and 4.15 show the PDFs of ν and Δz^{max} when dropper length, dropper spacing and support height errors are considered, respectively. The reference values of ν and Δz^{max}, obtained from the nominal catenary without installation errors, are indicated by a vertical red line. Besides, the values of $\bar{\nu}$ and $S(\nu)$ are given in the three cases.

The first conclusion drawn from these results is the little influence of dropper spacing errors if compared with the other two sources of variability. Dropper length and support height errors provide similar dispersion in ν and Δz^{max}, but the former presents a mean value $\bar{\nu}_{dl}$ higher than the reference value of ν, while the latter produces a PDF of ν centred to the reference value. Therefore, dropper length error can be seen as the most harmful installation error, even though the variability of the obtained

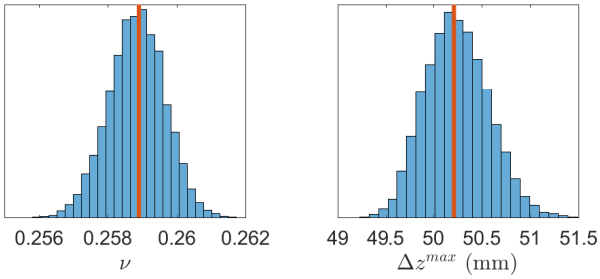

Figure 4.14: PDFs of ν_{ds} ($\bar{\nu}_{ds} = 0.2588$, $S(\nu)_{ds} = 8.14 \cdot 10^{-4}$) and Δz_{ds}^{max} obtained when uncertainty in dropper spacing is considered. Vertical lines indicate the ν and Δz^{max} obtained from the nominal catenary.

results increases if the two most influential installation errors are considered together. This last scenario is fully explored in Paper D.

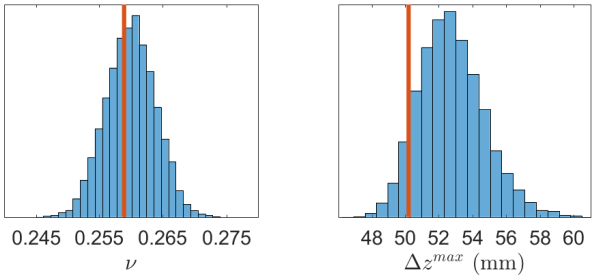

Figure 4.15: PDFs of ν_{sh} ($\bar{\nu}_{sh} = 0.2599$, $S(\nu)_{sh} = 6.01 \cdot 10^{-3}$) and Δz_{sh}^{max} obtained when uncertainty in support height is considered. Vertical lines indicate the ν and Δz^{max} obtained from the nominal catenary.

Another option that offers this methodology is to perform parametric studies by considering the mean value of the parameter instead of its deterministic value. For example, it is possible to investigate how $\bar{\nu}$ changes with respect to variations in the amount of contact wire pre-sag.

As previously stated, 50 individuals are enough to accurately determine $\bar{\nu}$. Fig. 4.16 shows these values obtained from 12 catenaries with different pre-sag, allowing for both dropper length and support height installation errors, when the pantograph moves forward at 250 km/h. This is a clear example in which considering the uncertainty of the installation procedure produces significant differences in the results if compared with those obtained from the deterministic approach. Specifically, the optimal pre-sag was approximately 35 mm with classical deterministic simulations,

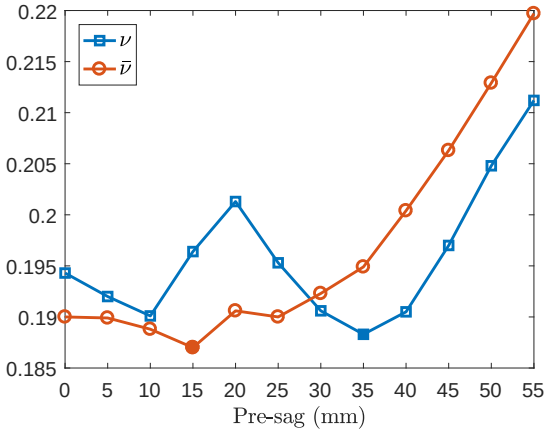

Figure 4.16: Comparative between ν and $\bar{\nu}$ for different pre-sag values when the train runs at 250 km/h. 50 catenaries with dropper length and support height errors are simulated to obtain $\bar{\nu}$.

but when installation errors are taken into account, the optimal pre-sag is found to be around 15 mm.

Thus, this last contribution of the Thesis reveals the importance of treating the pantograph–catenary dynamic interaction from a stochastic point of view to have better consideration of the features present in the actual installed catenaries.

Chapter 5

Closure

"If I have seen further than others, it is by standing upon the shoulders of giants"
Isaac Newton

The main contributions and conclusions of this Thesis and the opened lines of research are summarised in the following two sections.

5.1. Summary and conclusions

In this Thesis an efficient strategy for solving the pantograph–catenary dynamic interaction is introduced. This high-performance tool is fully exploited to perform optimisations of the catenary geometry and to involve installation errors within simulations. The key points of the work done in the Thesis can be summarised as follows:

- A first attempt to achieve a parametric solution of the pantograph–catenary dynamic interaction problem is made by considering dropper lengths as extra-coordinates. The Proper Generalised Decomposition technique is successfully applied in both the static equilibrium problem and the dynamic interaction

problem only if droppers are modelled as linear bars. However, when the unilateral nonlinearity of dropper slackening is considered, the solution becomes very sensitive to small changes in dropper lengths, thus preventing obtaining the separate solution sought.

- Given the difficulty in obtaining a parametric solution, a highly efficient strategy is proposed to reduce the computational cost required for the time integration of the pantograph–catenary coupled system. It consists of two stages, namely the *Offline* and the *Online*. The method begins by moving the nonlinear terms to the right hand side of the dynamic equation. Then, by applying the superposition principle, the nonlinearities can be solved in terms of forces instead of displacements, which notably reduces the size of the system to be solved iteratively. This strategy allows the dynamic problem to be solved from about 25 to 30 times faster than with the use of the direct procedure.
- The fast time integration strategy is first used to optimise the catenary geometry. Dropper lengths and dropper spacing are chosen as the optimisation parameters. The use of a standard Genetic Algorithm allowed optimal configurations to be found in terms of current collection quality, measured by the ratio between the standard deviation and the mean of the interaction force. The results obtained, for both simple and stitched catenaries, reveal reductions of about 40% of this ratio when compared to their respective reference catenary geometry, even with the use of fewer droppers per span.
- Finally, a simple Monte Carlo method is applied to include in the simulations the variability produced by certain installation errors. Specifically, dropper length, dropper spacing and support height errors are taken into account. The method allows the probability density function of several magnitudes of interest to be obtained. The results demonstrate the little influence that dropper spacing errors have on the current collection quality. However, dropper length and support height errors are notably influential on the dynamic behaviour of the system, being more critical for higher speeds.

5.2. Open research lines

This work has opened up several lines of research on pantograph–catenary dynamic interaction simulation as follows:

- In order to be closer to the actual system, the pantograph–catenary model used in this Thesis can be further improved by adding more elements such

as the mechanical compensating system, overlap sections, multiple pantograph operation, curved tracks, the vibration of the locomotive or the wind action on both the cables and the pantograph. These features will be included in the code to widen the knowledge about the system as well as to analyse their effect on the current collection performance.

- Another research line is related to further reducing the computational cost of the simulations with no loss of accuracy in the results. Some options such as the use of modal basis combined with the *Offline/Online* strategy or the application of machine learning techniques, such as kernel Principal Component Analysis (kPCA) or Locally Linear Embedding (LLE), are being considered to speed up the code. This will allow a test rig to be built to perform Hardware-In-the-Loop simulations, with which different pantographs can be tested or eventually validated without expensive in-line tests.

- In this Thesis the catenary has been optimised following a deterministic approach for a single train speed. Future investigations will be focused on finding the optimum for a range of pantograph speeds and different options for the objective functions must be tested. Furthermore, robust optimizations in which, optimization techniques are combined with stochastic methods, will be needed to consider the uncertainty coming from installation errors in the optimisation process. This achievement will provide useful and practical information to catenary designers.

Bibliography

[1] EN 50367, "Railway applications. Current collection systems. Technical criteria for the interaction between pantograph and overhead line," *European Committee for Electrotechnical Standardization*, 2012. 1.1, 4.3, 4.3

[2] European Union Agency for Railways, "Technical specifications for interoperability relating to the 'energy' subsystem of the rail system in the Union," *Official Journal of the European Union*, 2014. 1.1

[3] F. Kiebling, R. Puschmann, and A. Schmieder, *Contact lines for electrical railways: planning-design-implementation*. Erlangen: Publicis Corporate Publishing, 2002. 1.1, 2.4

[4] EN 50318, "Railway applications. Current collection systems. Validation of simulation of the dynamic interaction between pantograph and overhead contact line," *European Union Agency for Railways*, 2003. 1.1, 3.1.3

[5] S. Bruni, G. Bucca, M. Carnevale, A. Collina, and A. Facchinetti, "Pantograph–catenary interaction: recent achievements and future research challenges," *International Journal of Rail Transportation*, pp. 1–26, 2017. 2

[6] G. Poetsch, J. Evans, R. Meisinger, W. Kortüm, W. Baldauf, A. Veitl, and J. Wallaschek, "Pantograph/catenary dynamics and control," *Vehicle System Dynamics*, vol. 28, no. 2-3, pp. 159–195, 1997. 2, 2.1

[7] S. H. Kia, F. Bartolini, A. Mpanda-Mabwe, and R. Ceschi, "Pantograph-catenary interaction model comparison," in *IECON 2010-36th Annual Conference on IEEE Industrial Electronics Society*, pp. 1584–1589, IEEE, 2010. 2, 2.5

[8] Z. Liu, Y. Song, Y. Han, H. Wang, J. Zhang, and Z. Han, "Advances of research on high-speed railway catenary," *Journal of Modern Transportation*, pp. 1–23, 2016. 2

[9] S. Bruni, J. Ambrosio, A. Carnicero, Y. H. Cho, L. Finner, M. Ikeda, S. Y. Kwon, J. P. Massat, S. Stichel, and M. Tur, "The results of the pantograph-catenary interaction benchmark," *Vehicle System Dynamics*, vol. 53, no. 3, pp. 412–435, 2015. 2, 2.1, 2.2, 2.3, 3.1.1, 3.1.3, 4.1, 4.3, 4.4

[10] H. Nibler, "Dynamisches verhalten von fahrleitung und stromabnehmer bei elektrischen hauptbahnen," *Elektrische Bahnen*, vol. 21, no. 10, pp. 234–241, 1950. 2.1

[11] G. Gilbert and H. Davies, "Pantograph motion on a nearly uniform railway overhead line," in *Proceedings of the Institution of Electrical Engineers*, vol. 113, pp. 485–492, IET, 1966. 2.1

[12] T. X. Wu and M. J. Brennan, "Basic analytical study of pantograph-catenary system dynamics," *Vehicle System Dynamics*, vol. 30, no. 6, pp. 443–456, 1998. 2.1

[13] J. L. Maroño, A. Carnicero, and O. López-García, "Modelo simplificado para la simulación de la interacción dinámica catenaria-pantógrafo," *Revista internacional de métodos numéricos para cálculo y diseño en ingeniería*, vol. 23, no. 1, pp. 15–33, 2007. 2.1, 2.3

[14] J. W. Kim and S. N. Yu, "Design variable optimization for pantograph system of high-speed train using robust design technique," *International Journal of Precision Engineering and Manufacturing*, vol. 14, no. 2, pp. 267–273, 2013. 2.1, 2.6, 4.3

[15] A. Pisano and E. Usai, "Contact force regulation in wire-actuated pantographs," *Modern Sliding Mode Control Theory*, pp. 447–463, 2008. 2.1, 2.8

[16] A. Balestrino, O. Bruno, A. Landi, and L. Sani, "Innovative solutions for overhead catenary-pantograph system: wire actuated control and observed contact force," *Vehicle System Dynamics*, vol. 33, no. 2, pp. 69–89, 2000. 2.1, 2.8

[17] A. Hobbs, I. Illingsworth, and A. Peters, "New developments in understanding the dynamics of overhead current collection equipment for electric railways," *Closed Loop*, vol. 1, pp. 3–9, 1977. 2.1

[18] K. Manabe and Y. Fujii, "Overhead system resonance with multi-pantographs and countermeasures," *Railway Technical Research Institute, Quarterly Reports*, vol. 30, no. 4, 1989. 2.1, 2.8

[19] M. Arnold and B. Simeon, "Pantograph and catenary dynamics: a benchmark problem and its numerical solution," *Applied Numerical Mathematics*, vol. 34, no. 4, pp. 345–362, 2000. 2.1, 2.2

[20] A. Metrikine and A. Bosch, "Dynamic response of a two-level catenary to a moving load," *Journal of Sound and Vibration*, vol. 292, no. 3, pp. 676–693, 2006. 2.1

[21] J. P. Massat, E. Balmes, J. P. Bianchi, and G. Van Kalsbeek, "OSCAR statement of methods," *Vehicle System Dynamics*, vol. 53, no. 3, pp. 370–379, 2015. 2.1, 2.2, 2.4

[22] M. Ikeda, "'Gasen-do FE' statement of methods," *Vehicle System Dynamics*, vol. 53, no. 3, pp. 357–369, 2015. 2.1, 2.3, 2.4

[23] G. Teichelmann, M. Schaub, and B. Simeon, "Modelling and simulation of railway cable systems," *ZAMM-Journal of Applied Mathematics and Mechanics*, vol. 85, no. 12, pp. 864–877, 2005. 2.1, 2.2, 2.3

[24] W. Zhai and C. Cai, "Effect of locomotive vibrations on pantograph-catenary system dynamics," *Vehicle System Dynamics*, vol. 29, no. S1, pp. 47–58, 1998. 2.1, 2.8

[25] W. Zhang, G. Mei, and J. Zeng, "A study of pantograph/catenary system dynamics with influence of presag and irregularity of contact wire," *Vehicle System Dynamics*, vol. 37, no. sup1, pp. 593–604, 2002. 2.1, 2.2

[26] W. Zhang, Y. Liu, and G. Mei, "Evaluation of the coupled dynamical response of a pantograph–catenary system: contact force and stresses," *Vehicle System Dynamics*, vol. 44, no. 8, pp. 645–658, 2006. 2.1, 2.3

[27] N. Zhou and W. Zhang, "Investigation on dynamic performance and parameter optimization design of pantograph and catenary system," *Finite Elements in Analysis and Design*, vol. 47, no. 3, pp. 288–295, 2011. 2.1, 2.3, 2.6

[28] D. Ritzberger, E. Talic, and A. Schirrer, "Efficient simulation of railway pantograph/catenary interaction using pantograph-fixed coordinates," *IFAC-PapersOnLine*, vol. 48, no. 1, pp. 61–66, 2015. 2.1, 2.5

[29] A. Schirrer, G. Aschauer, E. Talic, M. Kozek, and S. Jakubek, "Catenary emulation for hardware-in-the-loop pantograph testing with a model predictive energy-conserving control algorithm," *Mechatronics*, vol. 41, pp. 17–28, 2017. 2.1, 2.5

[30] S. Sorrentino, D. Anastasio, A. Fasana, and S. Marchesiello, "Distributed parameter and finite element models for wave propagation in railway contact lines," *Journal of Sound and Vibration*, vol. 410, pp. 1–18, 2017. 2.1, 2.3

[31] A. Collina and S. Bruni, "Numerical simulation of pantograph-overhead equipment interaction," *Vehicle System Dynamics*, vol. 38, no. 4, pp. 261–291, 2002. 2.1, 2.3, 4.2

[32] J. H. Seo, H. Sugiyama, and A. A. Shabana, "Three-dimensional large deformation analysis of the multibody pantograph/catenary systems," *Nonlinear Dynamics*, vol. 42, no. 2, pp. 199–215, 2005. 2.1

[33] Y. H. Cho, "SPOPS statement of methods," *Vehicle System Dynamics*, vol. 53, no. 3, pp. 329–340, 2015. 2.1, 2.2, 2.4

[34] N. Zhou, Q. Lv, Y. Yang, and W. Zhang, "TPL-PCRUN statement of methods," *Vehicle System Dynamics*, vol. 53, no. 3, pp. 380–391, 2015. 2.1, 2.4

[35] Y. H. Cho, "Numerical simulation of the dynamic responses of railway overhead contact lines to a moving pantograph, considering a nonlinear dropper," *Journal of Sound and Vibration*, vol. 315, no. 3, pp. 433–454, 2008. 2.1, 2.3

[36] P. A. Jönsson, S. Stichel, and C. Nilsson, "CaPaSIM statement of methods," *Vehicle System Dynamics*, vol. 53, no. 3, pp. 341–346, 2015. 2.1, 2.2, 2.4

[37] C. Sánchez-Rebollo, A. Carnicero, and J. R. Jiménez-Octavio, "CANDY statement of methods," *Vehicle System Dynamics*, vol. 53, no. 3, pp. 392–401, 2015. 2.1

[38] M. Tur, L. Baeza, F. Fuenmayor, and E. García, "PACDIN statement of methods," *Vehicle System Dynamics*, vol. 53, no. 3, pp. 402–411, 2015. 2.1

[39] L. Finner, G. Poetsch, B. Sarnes, and M. Kolbe, "Program for catenary-pantograph analysis, PrOSA statement of methods and validation according EN 50318," *Vehicle System Dynamics*, vol. 53, no. 3, pp. 305–313, 2015. 2.1, 2.3

[40] F. G. Rauter, J. Pombo, J. Ambrósio, J. Chalansonnet, A. Bobillot, and M. S. Pereira, "Contact model for the pantograph-catenary interaction," *Journal of System Design and Dynamics*, vol. 1, no. 3, pp. 447–457, 2007. 2.1, 2.3

[41] J. Benet, "An efficient method for the mechanical study of pantograph-catenary interaction," *Proceedings of the Tenth International Conference on Computational Structures Technology*, 2010. 2.1, 2.2, 2.3

[42] J. H. Seo, S. W. Kim, I. H. Jung, T. W. Park, J. Y. Mok, Y. G. Kim, and J. B. Chai, "Dynamic analysis of a pantograph–catenary system using absolute nodal coordinates," *Vehicle System Dynamics*, vol. 44, no. 8, pp. 615–630, 2006. 2.1, 2.2

[43] J. H. Lee and T. W. Park, "Development of a three-dimensional catenary model using cable elements based on absolute nodal coordinate formulation," *Journal of Mechanical Science and Technology*, vol. 26, no. 12, pp. 3933–3941, 2012. 2.1, 2.4, 3.1.1

[44] J. H. Lee, T. W. Park, H. K. Oh, and Y. G. Kim, "Analysis of dynamic interaction between catenary and pantograph with experimental verification and performance evaluation in new high-speed line," *Vehicle System Dynamics*, vol. 53, no. 8, pp. 1117–1134, 2015. 2.1, 2.3

[45] Y. Song, Z. Liu, H. Wang, X. Lu, and J. Zhang, "Nonlinear modelling of high-speed catenary based on analytical expressions of cable and truss elements," *Vehicle System Dynamics*, vol. 53, no. 10, pp. 1455–1479, 2015. 2.1, 2.4

[46] M. Oumri and A. Rachid, "A mathematical model for pantograph-catenary interaction," *Mathematical and Computer Modelling of Dynamical Systems*, vol. 22, no. 5, pp. 463–474, 2016. 2.1, 2.2, 2.3

[47] M. Such, J. R. Jiménez-Octavio, A. Carnicero, and O. López-García, "An approach based on the catenary equation to deal with static analysis of three dimensional cable structures," *Engineering Structures*, vol. 31, no. 9, pp. 2162–2170, 2009. 2.1

[48] O. Vo Van, J. P. Massat, and E. Balmes, "Waves, modes and properties with a major impact on dynamic pantograph-catenary interaction," *Journal of Sound and Vibration*, vol. 402, pp. 51–69, 2017. 2.2

[49] S. P. Jung, Y. G. Kim, J. S. Paik, and T. W. Park, "Estimation of dynamic contact force between a pantograph and catenary using the finite element method," *Journal of Computational and Nonlinear Dynamics*, vol. 7, no. 4, 2012. 2.2

[50] A. Alberto, J. Benet, E. Arias, D. Cebrian, T. Rojo, and F. Cuartero, "A high performance tool for the simulation of the dynamic pantograph–catenary interaction," *Mathematics and Computers in Simulation*, vol. 79, no. 3, pp. 652–667, 2008. 2.2, 2.3, 2.5

[51] W. Zhang, Z. Shen, and J. Zeng, "Study on dynamics of coupled systems in high-speed trains," *Vehicle System Dynamics*, vol. 51, no. 7, pp. 966–1016, 2013. 2.2

[52] P. Nåvik, A. Rønnquist, and S. Stichel, "Variation in predicting pantograph–catenary interaction contact forces, numerical simulations and field measurements," *Vehicle System Dynamics*, pp. 1–18, 2017. 2.2

[53] A. Collina, A. Lo Conte, and M. Carnevale, "Effect of collector deformable modes in pantograph–catenary dynamic interaction," *Proceedings of the Institution of Mechanical Engineers, Part F: Journal of Rail and Rapid Transit*, vol. 223, no. 1, pp. 1–14, 2009. 2.2

[54] J. Ambrósio, J. Pombo, M. Pereira, P. Antunes, and A. Mósca, "A computational procedure for the dynamic analysis of the catenary–pantograph interaction in high-speed trains," *Journal of Theoretical and Applied Mechanics*, vol. 50, no. 3, pp. 681–699, 2012. 2.2, 2.3

[55] J. Ambrósio, J. Pombo, P. Antunes, and M. Pereira, "PantoCat statement of methods," *Vehicle System Dynamics*, vol. 53, no. 3, pp. 314–328, 2015. 2.2, 2.3, 2.4

[56] J. Ambrósio, F. Rauter, J. Pombo, and M. S. Pereira, "A flexible multibody pantograph model for the analysis of the catenary–pantograph contact," in *Multibody Dynamics*, pp. 1–27, Springer, 2011. 2.2

[57] N. Zhou, W. H. Zhang, and R. P. Li, "Dynamic performance of a pantograph-catenary system with the consideration of the appearance characteristics of contact surfaces," *Journal of Zhejiang University-Science A*, vol. 12, no. 12, pp. 913–920, 2011. 2.2, 2.3

[58] O. López-García, A. Carnicero, and J. Maroño, "Influence of stiffness and contact modelling on catenary–pantograph system dynamics," *Journal of Sound and Vibration*, vol. 299, no. 4, pp. 806–821, 2007. 2.3

[59] J. Pombo and J. Ambrósio, "Multiple pantograph interaction with catenaries in high-speed trains," *Journal of Computational and Nonlinear Dynamics*, vol. 7, no. 4, 2012. 2.3, 2.8

[60] J. Benet, A. Alberto, E. Arias, and T. Rojo, "A mathematical model of the pantograph–catenary dynamic interaction with several contact wires," *International Journal of Applied Mathematics*, vol. 37, no. 2, 2007. 2.3, 2.8

[61] J. Benet, N. Cuartero, F. Cuartero, T. Rojo, P. Tendero, and E. Arias, "An advanced 3D-model for the study and simulation of the pantograph catenary system," *Transportation Research Part C: Emerging Technologies*, vol. 36, pp. 138–156, 2013. 2.3

[62] W. Zhang, G. Mei, X. Wu, and Z. Shen, "Hybrid simulation of dynamics for the pantograph-catenary system," *Vehicle System Dynamics*, vol. 38, no. 6, pp. 393–414, 2002. 2.3, 2.5

[63] G. Mei, W. Zhang, H. Zhao, and L. Zhang, "A hybrid method to simulate the interaction of pantograph and catenary on overlap span," *Vehicle System Dynamics*, vol. 44, no. sup1, pp. 571–580, 2006. 2.3, 2.8

[64] F. Resta, A. Facchinetti, A. Collina, and G. Bucca, "On the use of a hardware in the loop set-up for pantograph dynamics evaluation," *Vehicle System Dynamics*, vol. 46, no. S1, pp. 1039–1052, 2008. 2.3, 2.5

[65] A. Rønnquist and P. Nåvik, "Dynamic assessment of existing soft catenary systems using modal analysis to explore higher train velocities: a case study of a norwegian contact line system," *Vehicle System Dynamics*, vol. 53, no. 6, pp. 756–774, 2015. 2.3

[66] J. P. Massat, C. Laurent, J. P. Bianchi, and E. Balmès, "Pantograph catenary dynamic optimisation based on advanced multibody and finite element co-simulation tools," *Vehicle System Dynamics*, vol. 52, no. sup1, pp. 338–354, 2014. 2.3, 2.6

[67] O. López-García, A. Carnicero, and V. Torres, "Computation of the initial equilibrium of railway overheads based on the catenary equation," *Engineering Structures*, vol. 28, no. 10, pp. 1387–1394, 2006. 2.4

[68] C. Yang, W. Zhang, J. Zhang, G. Mei, N. Zhou, and G. Ren, "Static form-finding analysis of a railway catenary using a dynamic equilibrium method based on flexible multibody system formulation with absolute nodal coordinates and controls," *Multibody System Dynamics*, vol. 39, no. 3, pp. 221–247, 2017. 2.4

[69] M. Tur, E. García, L. Baeza, and F. Fuenmayor, "A 3D absolute nodal coordinate finite element model to compute the initial configuration of a railway catenary," *Engineering Structures*, vol. 71, pp. 234–243, 2014. 2.4, 3.2

[70] J. R. Jiménez-Octavio, A. Carnicero, C. Sánchez-Rebollo, and M. Such, "A moving mesh method to deal with cable structures subjected to moving loads and its application to the catenary–pantograph dynamic interaction," *Journal of Sound and Vibration*, vol. 349, pp. 216–229, 2015. 2.5

[71] W. Zhang, G. Mei, X. Wu, and L. Chen, "A study on dynamic behaviour of pantographs by using hybrid simulation method," *Proceedings of the Institution of Mechanical Engineers, Part F: Journal of Rail and Rapid Transit*, vol. 219, no. 3, pp. 189–199, 2005. 2.5

[72] A. Facchinetti and M. Mauri, "Hardware-in-the-loop overhead line emulator for active pantograph testing," *IEEE Transactions on Industrial Electronics*, vol. 56, no. 10, pp. 4071–4078, 2009. 2.5

[73] A. Facchinetti, L. Gasparetto, and S. Bruni, "Real-time catenary models for the hardware-in-the-loop simulation of the pantograph–catenary interaction," *Vehicle System Dynamics*, vol. 51, no. 4, pp. 499–516, 2013. 2.5

[74] S. Bruni, G. Bucca, A. Collina, and A. Facchinetti, "Numerical and hardware-in-the-loop tools for the design of very high speed pantograph-catenary systems," *Journal of Computational and Nonlinear Dynamics*, vol. 7, no. 4, p. 041013, 2012. 2.5

[75] A. Schirrer, G. Aschauer, and S. Jakubek, "High-dynamic accurate railway catenary emulation by real-time mechanical impedance control for pantograph testing," in *Simulation and Testing for Vehicle Technology*, pp. 277–295, Springer, 2016. 2.5

[76] G. Galeotti and P. Toni, "Overhead contact line elasticity optimization for railway high speed running," *Computers & Structures*, vol. 65, no. 6, pp. 975–983, 1997. 2.6

[77] T. J. Park, C. S. Han, and J. H. Jang, "Dynamic sensitivity analysis for the pantograph of a high-speed rail vehicle," *Journal of Sound and Vibration*, vol. 266, no. 2, pp. 235–260, 2003. 2.6

[78] J. W. Kim, H. C. Chae, B. S. Park, S. Y. Lee, C. S. Han, and J. H. Jang, "State sensitivity analysis of the pantograph system for a high-speed rail vehicle considering span length and static uplift force," *Journal of Sound and Vibration*, vol. 303, no. 3, pp. 405–427, 2007. 2.6

[79] J. Pombo and J. Ambrósio, "Influence of pantograph suspension characteristics on the contact quality with the catenary for high speed trains," *Computers & Structures*, vol. 110, pp. 32–42, 2012. 2.6

[80] J. H. Lee, Y. G. Kim, J. S. Paik, and T. W. Park, "Performance evaluation and design optimization using differential evolutionary algorithm of the pantograph for the high-speed train," *Journal of Mechanical Science and Technology*, vol. 26, no. 10, pp. 3253–3260, 2012. 2.6

[81] J. Ambrósio, J. Pombo, and M. Pereira, "Optimization of high-speed railway pantographs for improving pantograph–catenary contact," *Theoretical and Applied Mechanics Letters*, vol. 3, no. 1, 2013. 2.6, 4.3

[82] A. Bobillot, J. P. Massat, and J. P. Mentel, "Design of pantograph–catenary systems by simulation," in *9th World Congress on Railway Research (WCRR)*, 2011. 2.6

[83] Y. H. Cho, K. Lee, Y. Park, B. Kang, and K. N. Kim, "Influence of contact wire pre-sag on the dynamics of pantograph–railway catenary," *International Journal of Mechanical Sciences*, vol. 52, no. 11, pp. 1471–1490, 2010. 2.6

[84] M. L. Yu, W. Z. Liu, J. Zhang, and C. Y. Yan, "Influence of dropper spacing on quality of pantograph–catenary current collection," in *Applied Mechanics and Materials*, vol. 654, pp. 78–81, Trans Tech Publ, 2014. 2.6

[85] P. Nåvik, A. Rønnquist, and S. Stichel, "The use of dynamic response to evaluate and improve the optimization of existing soft railway catenary systems for higher speeds," *Proceedings of the Institution of Mechanical Engineers, Part F: Journal of Rail and Rapid Transit*, vol. 230, no. 4, pp. 1388–1396, 2016. 2.6

[86] O. Vo Van, E. Balmes, A. Capitaine, and X. Lorang, "Sensitivity analysis of catenary geometry on current collection quality," in *The Third International Conference on Railway Technology: Research, Development and Maintenance, Cagliari, Sardinia, Italy*, 2016. 2.6, 4.4

[87] C. Gómez, R. Saa, A. García, F. García-Carballeira, and J. Carretero, "A model to obtain optimal designs of railway overhead knuckle junctions using simulation," *Simulation Modelling Practice and Theory*, vol. 26, pp. 16–31, 2012. 2.6

[88] A. Collina, F. Fossati, and F. Resta, "An innovative OHL diagnosis procedure based on the pantograph dynamics measurements," in *World Congress on Railway Research, Koln*, 2001. 2.7

[89] A. Collina, F. Fossati, M. Papi, and F. Resta, "Impact of overhead line irregularity on current collection and diagnostics based on the measurement of pantograph dynamics," *Proceedings of the Institution of Mechanical Engineers, Part F: Journal of Rail and Rapid Transit*, vol. 221, no. 4, pp. 547–559, 2007. 2.7

[90] M. Aboshi and M. Tsunemoto, "Installation guidelines for Shinkansen high speed overhead contact lines," *Quarterly Report of RTRI*, vol. 52, no. 4, pp. 230–236, 2011. 2.7, 4.4

[91] R. Huan, G. Pan, and W. Zhu, "Dynamics of pantograph–catenary system considering local singularities of contact wire with critical wavelengths," in *Proceedings of the 1st International Workshop on High-Speed and Intercity Railways*, vol. 1, p. 319, Springer, 2012. 2.7

[92] O. Vo Van, E. Balmès, and J. P. Massat, "Statistical identification of geometric parameters for high speed train catenary," in *International Conference on Noise and Vibration Engineering*, 2014. 2.7

[93] O. Vo Van, J. P. Massat, C. Laurent, and E. Balmes, "Introduction of variability into pantograph–catenary dynamic simulations," *Vehicle System Dynamics*, vol. 52, no. 10, pp. 1254–1269, 2014. 2.7, 4.4

[94] J. P. Massat, J. Laine, and A. Bobillot, "Pantograph–catenary dynamics simulation," *Vehicle System Dynamics*, vol. 44, no. sup1, pp. 551–559, 2006. 2.8

[95] P. Harell, L. Drugge, and M. Reijm, "Study of critical sections in catenary systems during multiple pantograph operation," *Proceedings of the Institution of Mechanical Engineers, Part F: Journal of Rail and Rapid Transit*, vol. 219, no. 4, pp. 203–211, 2005. 2.8

[96] G. Diana, F. Fossati, and F. Resta, "High speed railway: collecting pantographs active control and overhead lines diagnostic solutions," *Vehicle System Dynamics*, vol. 30, no. 1, pp. 69–84, 1998. 2.8

[97] Y. J. Huang, "Discrete fuzzy variable structure control for pantograph position control," *Electrical Engineering*, vol. 86, no. 3, pp. 171–177, 2004. 2.8

[98] A. Collina, A. Facchinetti, and F. Resta, "A feasibility study of an aerodynamic control for a high speed pantograph," in *Advanced intelligent mechatronics, 2007 IEEE/ASME international conference*, pp. 1–6, IEEE, 2007. 2.8

[99] Y. Song, H. Ouyang, Z. Liu, G. Mei, H. Wang, and X. Lu, "Active control of contact force for high-speed railway pantograph–catenary based on multi-body pantograph model," *Mechanism and Machine Theory*, vol. 115, pp. 35–59, 2017. 2.8

[100] A. Collina, S. Melzi, and A. Facchinetti, "On the prediction of wear of contact wire in OHE lines: a proposed model," *Vehicle System Dynamics*, vol. 37, no. 1, pp. 579–592, 2002. 2.8

[101] F. J. González, J. A. Chover, B. Suárez, and M. Vázquez, "Dynamic analysis using finite elements to calculate the critical wear section of the contact wire in suburban railway overhead conductor rails," *Proceedings of the Institution of Mechanical Engineers, Part F: Journal of Rail and Rapid Transit*, vol. 222, no. 2, pp. 145–157, 2008. 2.8

[102] A. Shing and P. Wong, "Wear of pantograph collector strips," *Proceedings of the Institution of Mechanical Engineers, Part F: Journal of Rail and Rapid Transit*, vol. 222, no. 2, pp. 169–176, 2008. 2.8

[103] G. Bucca and A. Collina, "A procedure for the wear prediction of collector strip and contact wire in pantograph–catenary system," *Wear*, vol. 266, no. 1, pp. 46–59, 2009. 2.8

[104] A. Carnicero, J. R. Jiménez-Octavio, C. Sánchez-Rebollo, A. Ramos, and M. Such, "Influence of track irregularities in the catenary–pantograph dynamic interaction," *Journal of Computational and Nonlinear Dynamics*, vol. 7, no. 4, p. 041015, 2012. 2.8

[105] M. Stickland, T. Scanlon, I. Craighead, and J. Fernández, "An investigation into the mechanical damping characteristics of catenary contact wires and their effect on aerodynamic galloping instability," *Proceedings of the Institution of Mechanical Engineers, Part F: Journal of Rail and Rapid Transit*, vol. 217, no. 2, pp. 63–71, 2003. 2.8

[106] M. Bocciolone, F. Resta, D. Rocchi, A. Tosi, and A. Collina, "Pantograph aerodynamic effects on the pantograph–catenary interaction," *Vehicle System Dynamics*, vol. 44, no. sup1, pp. 560–570, 2006. 2.8

[107] J. Pombo, J. Ambrósio, M. Pereira, F. Rauter, A. Collina, and A. Facchinetti, "Influence of the aerodynamic forces on the pantograph–catenary system for high-speed trains," *Vehicle System Dynamics*, vol. 47, no. 11, pp. 1327–1347, 2009. 2.8

[108] J. Seo, A. S. Kim, I. Jung, T. Park, J. Mok, Y. Kim, and J. Chai, "Dynamic analysis of a pantograph–catenary system using absolute nodal coordinates," *Vehicle System Dynamics*, vol. 44, no. 8, pp. 615–630, 2006. 3.1.1

[109] J. Ambrósio, F. Rauter, J. Pombo, and M. Pereira, "A flexible multibody pantograph model for the analysis of the catenary–pantograph contact," *Multibody Dynamics*, vol. 23, pp. 1–27, 2011. 3.1.2

[110] A. Collina and A. L. C. M. Carnevale, "Effect of collector deformable modes in pantograph-catenary dynamic interaction," *Proceedings of the Institution of Mechanical Engineers, Part F: Journal of Rail and Rapid Transit*, vol. 223, no. 1, pp. 1–14, 2009. 3.1.2

[111] J. Gerstmayr and A. A. Shabana, "Analysis of thin beams and cables using the absolute nodal co-ordinate formulation," *Nonlinear Dynamics*, vol. 45, no. 1-2, pp. 109–130, 2006. 3.2, 3.2

[112] M. Berzeri and A. Shabana, "Development of simple models for the elastic forces in the absolute nodal co-ordinate formulation," *Journal of Sound and Vibration*, vol. 235, no. 4, pp. 539–565, 2000. 3.2

[113] H. M. Hilber, T. J. R. Hughes, and R. L. Taylor, "Improved numerical dissipation for time integration algorithms in structural dynamics," *Earthquake Engineering & Structural Dynamics*, vol. 5, no. 3, pp. 283–292, 1977. 3.3

[114] F. Chinesta, R. Keunings, and A. Leygue, *The Proper Generalized Decomposition for Advanced Numerical Simulations: A Primer*. Springer Publishing Company, Incorporated, 2013. 4.1, 4.1

[115] F. Chinesta, P. Ladeveze, and E. Cueto, "A short review on model order reduction based on proper generalized decomposition," *Archives of Computational Methods in Engineering*, vol. 18, no. 4, p. 395, 2011. 4.1

[116] M. Matar, D. Paradis, and R. Iravani, "Real-time simulation of modular multilevel converters for controller hardware-in-the-loop testing," *IET Power Electronics*, vol. 9, no. 1, pp. 42–50, 2016. 4.2.2

[117] N. Metropolis and S. Ulam, "The Monte Carlo method," *Journal of the American Statistical Association*, vol. 44, no. 247, pp. 335–341, 1949. 4.4

Part II

Articles

PAPER A

Parametric model for the simulation of the railway catenary system static equilibrium problem

S. Gregori, M. Tur, E. Nadal, F. J. Fuenmayor and F. Chinesta

Finite Elements in Analysis and Design
Volume 115, Pages 21–32, 2016
DOI: 10.1016/j.finel.2016.02.007

Abstract

Dynamic simulations of pantograph–catenary interaction are nowadays essential for improving the performance of railway locomotives, by achieving better current collection at higher speeds and lower wear of the collecting parts. The first step in performing these simulations is to compute the static equilibrium of the overhead line. The initial dropper lengths play an important role in hanging the contact wire at an appropriate height. From a classical point of view, if one wants to obtain the static equilibrium configuration of the system for different combinations of dropper lengths, one static problem must be solved for each combination of lengths, which involves a prohibitive computational cost. In this paper we propose a parametric model of the catenary, including the undeformed dropper lengths as extra-coordinates of the problem. This multidimensional problem is efficiently solved by means of the Proper Generalized Decomposition (PGD) technique, avoiding the *curse of dimensionality* issue. The capabilities and performance of the proposed method are shown by numerical examples.

Key words

Railway catenary; Model order reduction; Dropper slackening; Static equilibrium problem

Contents

1 Introduction **75**

2 Description of the overhead line **76**

3 Catenary finite element model **77**

4 Static equilibrium problem **80**

5 Proper Generalized Decomposition approach **82**
5.1 PGD formulation 82
5.2 Generalization to $\mathscr{N}$ extra-coordinates 85
5.3 PGD formulation: Dropper slackening 86
5.4 PGD formulation: Linearized static problem 88

6 Numerical examples **89**
6.1 Example 1: Academic example 90
6.2 Example 2: Variable pre-sag 94
6.3 Example 3: Multidimensional catenary span 96

7 Conclusions **99**

A The PGD constructor **99**
A.1 Computing $\mathbf{R}_{n+1}(\tilde{\chi})$ from $L_{n+1}(l_p)$ 100
A.2 Computing $L_{n+1}(l_p)$ from $\mathbf{R}_{n+1}(\tilde{\chi})$ 100

B Separation of the h function **102**

Bibliography **103**

1. Introduction

The overhead line equipment, or the so called overhead catenary, is the system responsible for providing electric energy to railway locomotives by means of the pantograph. As a result of the pantograph–contact wire interaction and the dynamic response of the system, a time-varying contact force is generated. The overhead line is wished to operate at the smallest possible contact force (to minimize wear due to friction) but maintaining at least a minimum value to ensure that the pantograph always remains pushing the contact wire. The numerical models used to simulate this system are a useful tool in catenary design for achieving better high-speed current collection [1–3]. Fig. 1 shows the main elements of a typical railway catenary.

Many factors influence the dynamics of the overhead system and affect the contact force. These include dropper lengths, which are parameters that can be easily modified in engineering practice using the current catenary-stringing technology. The static position of the contact wire largely depends on the length and position of the droppers. Thus, the interaction of the pantograph with the contact wire and the contact force generated also depend on the dropper lengths. In fact, some amount of the so-called pre-sag of the contact wire (deviations of the contact wire height from the horizontal position) has been shown to improve catenary performance at high-speeds [4, 5]. It is still an open question whether or not there are optimal dropper lengths for a certain pantograph and train speed that provides the best performance in terms of contact force. Numerical simulation tools can help in solving this issue. However, at the present time, the analysis of the influence of undeformed dropper lengths on the dynamics of the system would require a great number of simulations for different combinations of these parameters, which would be infeasible in practice with traditional finite element technology.

The aim of this paper is to present a numerical method able to perform this type of analysis at a reasonable computational cost. In particular, there is an especial interest in finding the static equilibrium position of the railway catenary system for any combination of dropper lengths. By using the Proper Generalized Decomposition (PGD) technique it is possible to solve parametric models that are defined in high dimensional spaces, such as in the problem at hand, in which undeformed dropper lengths are introduced as extra-coordinates.

PGD [6] is a Model Order Reduction (MOR) technique which can easily solve multidimensional problems. PGD has already successfully addressed a variety of problems, including shell-type geometries [7,8], shape optimization problems [9], computational rheology [10], linear elastic fracture mechanics [11] or mechanic simulation for biological tissues [12, 13] among others, in a multidimensional framework. Space-time decompositions are also dealt with in [14] under a PGD approach. The errors of the PGD solutions are studied in [15]. PGD is thus able to provide a multiparametric

solution of the problem that explicitly depends on the parameters to be identified (in this case dropper lengths) and avoids the *curse of dimensionality* issue when a large number of parameters are considered. The interested reader is addressed to [16] and the references therein for a deeper analysis of this technique.

The main interest of the proposed method is to obtain a solution of the static equilibrium position, required to simulate the dynamic interaction, for any combination of dropper lengths. With the parametric solution it is possible to perform an efficient geometry optimization process of the catenary, based on different criteria, such as the minimal standard deviation of the contact force. With a parametric dynamic solution of the problem, the effect of wrong stringing, which leads to a static configuration other than the one designed, can be reproduced and analysed

The paper is organized as follows. The overhead line and the elements which compose the catenary are described in Section 2. In Section 3 the finite element model of the catenary is introduced. This model is based on the absolute nodal coordinate formulation (ANCF). On the basis of the virtual work principle, in Section 4 the static equilibrium problem is presented from a classical point of view. In Section 5 the static equilibrium problem is dealt with the PGD approach. The proposed formulation is given in two versions: i) without considering dropper slackening and ii) including the effect of dropper slackening. A linearised problem is also presented in order to reduce the computational cost. The accuracy and performance of the method is analysed in Section 6 through some numerical examples. Finally, the conclusions are summarized in Section 7.

2. Description of the overhead line

Fig. 1 shows a high-speed train catenary. The catenary is mainly composed of two groups of components, structural elements and cables. Masts, brackets and registration arms are responsible for supporting the entire cabling in the desired position. The cables include the messenger or carrier wire, droppers and contact wire. The messenger wire hangs from the brackets at regular intervals. Its main aim is to hold the contact wire at the required height from the track. This can be achieved by means of droppers clamped to the messenger and contact wire at certain points in every span. The contact wire transmits electrical power to the locomotive through the pantograph head on the locomotive roof. Some types of catenaries include stitch wires near the masts in order to reduce the variation of the stiffness along the span. Both the messenger and contact wires are prestressed and keep the tension constant with the aid of a compensation system located at both ends of each section along the overhead line.

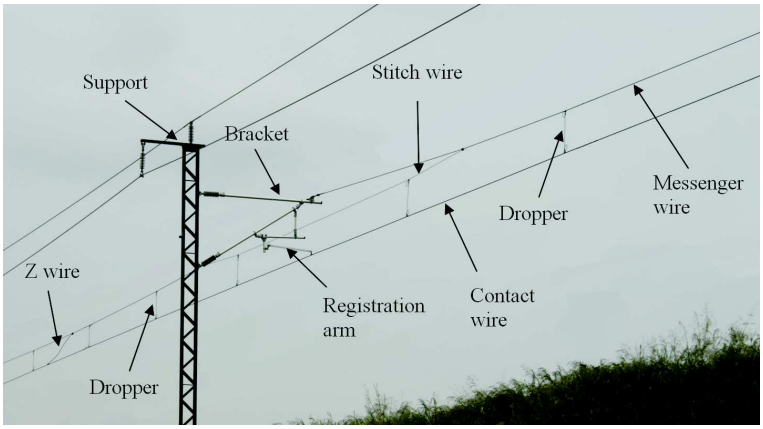

Figure 1: Picture of a high-speed railway catenary.

Viewed from above, the catenary follows a zigzag pattern from one bracket to another. This stagger is designed to guarantee uniform wear on the contact strip of the pantograph collectors. Another important geometric issue in many catenaries is their pre-sag, which reduces the variations in contact force caused by the reduced stiffness in the central region of the spans, and is controlled by means of appropriate dropper lengths.

It is important to point out that small changes in certain parameters, such as the undeformed dropper lengths, may change the height of the contact wire and therefore affect interaction with the pantograph. Also, if the initial length of a dropper is larger than a certain value, the dropper can slacken and fail to hold the contact wire in the static position.

3. Catenary finite element model

The catenary system was modelled by finite elements. Only the main features of the model are summarized here (for further information see [17]). An example of this model is depicted in Fig. 2, in which the nodes are plotted as circles. A beam element based on the absolute nodal coordinate formulation (ANCF) is employed to model the cables. The original 3D ANCF element was proposed in [18, 19] and used for railway catenary models in [20, 21]. For the interested reader, a good comparison between this element and the elements based on the classical formulation can be found in [22].

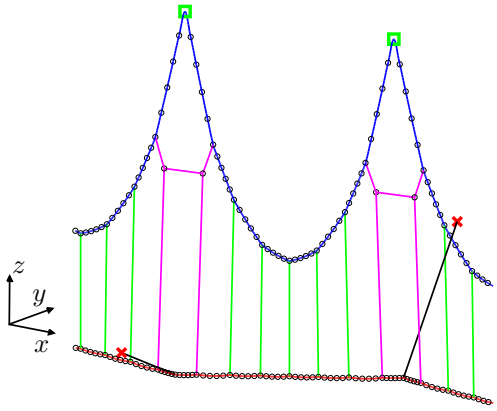

Figure 2: Finite element model of the catenary.

Catenary wires are much longer than their cross-sectional area, so that the torsional effects can be neglected. This results in the element introduced in [23] with only 6 degrees of freedom per node, taking into account axial and bending deformations. In this paper, this type of element is called 'cable element' and is used to model both the messenger and the contact wires. Droppers and registration arms are modelled as single large displacement nonlinear elements called 'bar element' throughout the paper. The nonlinear bar element is only capable of transmitting axial forces in traction and slackens under compressive forces.

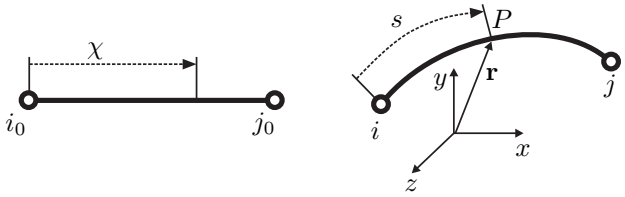

Figure 3: Undeformed and deformed configurations of the ANCF element.

In this model the masts and brackets are replaced by suitable boundary conditions. Dirichlet boundary conditions are applied at the ends of the registration arms joined to the brackets (nodes marked with a cross in Fig. 2). Spring-damping elements can be used to simulate the supports (nodes marked with a square in Fig. 2).

Fig. 3 shows a scheme of the reference and deformed configurations of an ANCF cable element. The vector of degrees of freedom of a cable element of nodes i and j containing the coordinates and their gradient is:

$$\mathbf{q}_c = \left[\begin{array}{cccccccccccc} x_i & y_i & z_i & \frac{\partial x_i}{\partial \chi} & \frac{\partial y_i}{\partial \chi} & \frac{\partial z_i}{\partial \chi} & x_j & y_j & z_j & \frac{\partial x_j}{\partial \chi} & \frac{\partial y_j}{\partial \chi} & \frac{\partial z_j}{\partial \chi} \end{array} \right]^T \tag{1}$$

where $\chi \in [0, l_0]$ is the local coordinate, l_0 being the length of the undeformed element. In a deformed configuration, the absolute position coordinates $\mathbf{r}(\chi)$ are defined by means of a cubic polynomial that can be written as:

$$\mathbf{r}(\chi) = \mathbf{S}_c(\chi)\, \mathbf{q}_c \tag{2}$$

The interpolation is defined as:

$$\mathbf{S}_c(\chi) = \left[\begin{array}{cccccccccccc} S_{c1} & 0 & 0 & S_{c2} & 0 & 0 & S_{c3} & 0 & 0 & S_{c4} & 0 & 0 \\ 0 & S_{c1} & 0 & 0 & S_{c2} & 0 & 0 & S_{c3} & 0 & 0 & S_{c4} & 0 \\ 0 & 0 & S_{c1} & 0 & 0 & S_{c2} & 0 & 0 & S_{c3} & 0 & 0 & S_{c4} \end{array} \right] \tag{3}$$

where

$$\begin{array}{ll} S_{c1}(\xi) = 1 - 3\xi^2 + 2\xi^3 & S_{c2}(\xi) = l_0(\xi - 2\xi^2 + \xi^3) \\ S_{c3}(\xi) = 3\xi^2 - 2\xi^3 & S_{c4}(\xi) = l_0(-\xi^2 + \xi^3) \end{array} \tag{4}$$

The coordinate $\xi = \chi / l_0 \in [0, 1]$ denotes the normalized local coordinate. These Hermite cubic polynomials guarantee the C^1 continuity between elements.

The element vector of degrees of freedom of the bar element contains only the absolute positions of the two nodes as:

$$\mathbf{q}_b = \left[\begin{array}{cccccc} x_i & y_i & z_i & x_j & y_j & z_j \end{array} \right]^T \tag{5}$$

The interpolation used for this element is linear, and the length of the undeformed element does not appear explicitly in the shape functions, that is:

$$\mathbf{S}_b(\chi) = \left[\begin{array}{cccccc} S_{b1} & 0 & 0 & S_{b2} & 0 & 0 \\ 0 & S_{b1} & 0 & 0 & S_{b2} & 0 \\ 0 & 0 & S_{b1} & 0 & 0 & S_{b2} \end{array} \right] \tag{6}$$

in which

$$S_{b1}(\xi) = -\frac{\xi - 1}{2} \quad S_{b2}(\xi) = \frac{\xi + 1}{2} \tag{7}$$

For the sake of clarity, in the following sections the equations are particularized for cable elements, since they are directly applicable to bar elements only by neglecting the term of bending deformations. Subscripts c and b are deleted for simplicity in the notation.

4. Static equilibrium problem

This section introduces the classical FEM formulation to solve the static equilibrium configuration of a railway catenary under gravitational effects. In a catenary system, before computing the static equilibrium position, the so-called 'shape-finding' or initial configuration problem must be solved. The goal of this problem is to compute the undeformed lengths of the elements fulfilling the force equilibrium equations and all the constraints introduced during the catenary stringing. The tension in the messenger and the contact wire, and the height of the latter are the main constraints taken into account. A thoroughly detailed explanation of a method for dealing with the 'shape-finding' problem of the overhead line can be found in [17]. In this contribution, it is assumed that the initial configuration problem is solved, i.e. the undeformed length of all the cables is given. It is the static equilibrium position under gravitational forces what is sought for any value of initial dropper lengths.

The formulation of the static equilibrium problem is obtained by using the virtual work principle. Let Ω be defined as the spatial domain of a certain railway catenary system, i.e. the catenary components modelled by FE. If Ω is discretised into N_e elements such that $\Omega = \cup_i^{N_e} \Omega_i^e$ and $\Omega_i^e \cap \Omega_j^e = \emptyset$, $i \neq j$, the total virtual work of internal forces obtained as the combination of each element is:

$$\delta W_{int} = \sum_{e=1}^{N_e} \delta W_{int}^e \tag{8}$$

For an element, this work is due to the contribution of the axial and the bending strains, that is

$$\delta W_{int}^e = \int_{\Omega^e} \left(EA\, \delta\varepsilon_L\, \varepsilon_L + EI\, \delta\kappa\, \kappa \right) d\chi \tag{9}$$

where E represents the Young's modulus, A denotes the cross-sectional area, I is the second moment of area and, ε_L and κ represent the axial deformation and the

curvature of the element, respectively. The axial strain can be defined using the Green strain tensor as:

$$\varepsilon_L = \frac{1}{2}\left(\frac{d\mathbf{r}}{d\chi}\cdot\frac{d\mathbf{r}}{d\chi} - 1\right) \tag{10}$$

From the Frenet-Serret frame, the curvature [24] is defined as:

$$\kappa = \left|\frac{d^2\mathbf{r}}{ds^2}\right| = \frac{\left|\frac{d\mathbf{r}}{d\chi}\times\frac{d^2\mathbf{r}}{d\chi^2}\right|}{\left|\frac{d\mathbf{r}}{d\chi}\right|^3} \tag{11}$$

where s is the local coordinate in the deformed configuration as showed in Fig. 3. Since on the catenary wires the axial strains are observed to be small, $ds \approx d\chi$ and the definition of curvature can be approximated by [19]:

$$\kappa \approx \left|\frac{d^2\mathbf{r}}{d\chi^2}\right| \tag{12}$$

After computing the variations of the axial deformation and the curvature and replacing them into (9), the virtual work of the internal forces results in:

$$\delta W^e_{int} = \int_{\Omega^e}\left[EI\frac{d^2\delta\mathbf{r}}{d\chi^2}\cdot\frac{d^2\mathbf{r}}{d\chi^2} + \frac{EA}{2}\frac{d\delta\mathbf{r}}{d\chi}\cdot\frac{d\mathbf{r}}{d\chi}\left(\frac{d\mathbf{r}}{d\chi}\cdot\frac{d\mathbf{r}}{d\chi} - 1\right)\right] d\chi \tag{13}$$

On the other hand, the force of gravity acts on the catenary. For an element, the virtual work caused by this external force is:

$$\delta W^e_{ext} = \int_{\Omega^e}\delta\mathbf{r}\cdot\mathbf{g}\, d\chi \tag{14}$$

where $\mathbf{g} = \{0 \;\; 0 \;\; -gA\rho\}^T$, being g the gravitational constant and ρ the density of the element.

Finally, the weak form of the static problem is obtained by equating (13) and (14) and accounting for all the element contributions. It consists of finding $\mathbf{r}(\chi)$ for all the admissible $\delta\mathbf{r}$, such that:

$$\sum_{e=1}^{N_e}\int_{\Omega^e}\left[EI\frac{d^2\delta\mathbf{r}}{d\chi^2}\cdot\frac{d^2\mathbf{r}}{d\chi^2} + \frac{EA}{2}\frac{d\delta\mathbf{r}}{d\chi}\cdot\frac{d\mathbf{r}}{d\chi}\left(\frac{d\mathbf{r}}{d\chi}\cdot\frac{d\mathbf{r}}{d\chi} - 1\right) - \delta\mathbf{r}\cdot\mathbf{g}\right] d\chi = 0, \quad \forall\delta\mathbf{r} \tag{15}$$

After the usual assembly process taking into account all the Dirichlet boundary conditions, a nonlinear algebraic system of equations is obtained. The static equilibrium equation for the whole catenary system reads:

$$\mathbf{f}(\mathbf{q}) = \mathbf{0} \tag{16}$$

It can be solved using for example the Newton-Raphson method. Note that if one wish to obtain the static equilibrium position for different sets of initial dropper lengths, the domain Ω changes, therefore a new static problem (Eq. (15)) must be solved.

5. Proper Generalized Decomposition approach

The objective of this section is to solve the static equilibrium problem (15) for any initial configuration of dropper lengths. For this purpose the PGD model order reduction technique is used. In this approach the geometrical parameters 'dropper lengths' are considered as extra-coordinates of the problem. Thus, the unknown field of absolute positions, and also its variations, now depends on both the spatial and dropper length coordinates, $\mathbf{r} = \mathbf{r}(\chi, l_{p1}, l_{p2}, ...)$. For the sake of simplicity, in this section the presented formulation only includes one undeformed dropper length as extra-coordinate of the static equilibrium problem, so that $\mathbf{r}(\chi, l_p)$. In the last part of the current section, the proposed formulation is generalized to $\mathscr{N}$ undeformed dropper lengths extra-coordinates.

Remark: Note the difference between l_0, the constant value of the undeformed length of an element, and l_p, which represents any possible value of the undeformed dropper length in an given interval.

5.1. PGD formulation

With the addition of one dropper length as extra-coordinate, $l_p \in \Omega_l = [l_p^-, l_p^+]$, l_p^- and l_p^+ are the lower and upper bounds of the interval Ω_l for which it is desired to obtain the static equilibrium position. Now, the variational problem (15) is extended to the whole geometry of the catenary, Ω and to the domain Ω_l. The new problem consists of finding the absolute position $\mathbf{r}(\chi, l_p)$ such that for all virtual displacement $\forall \delta\mathbf{r}$:

$$\sum_{e=1}^{N_e} \int_{\Omega_l} \int_{\Omega^e} \left[EI \frac{d^2\delta\mathbf{r}}{d\chi^2} \cdot \frac{d^2\mathbf{r}}{d\chi^2} + \frac{EA}{2} \frac{d\delta\mathbf{r}}{d\chi} \cdot \frac{d\mathbf{r}}{d\chi} \left(\frac{d\mathbf{r}}{d\chi} \cdot \frac{d\mathbf{r}}{d\chi} - 1 \right) - \delta\mathbf{r} \cdot \mathbf{g} \right] d\chi \, dl_p = 0 \quad (17)$$

Note that the spatial domain Ω depends on the initial length of the dropper l_p, which is problematic for the proposed formulation. In the same way as in [9], the

following change of variable is applied to (17) in order to circumvent this problem:

$$\chi = l_p\,\tilde{\chi}\,,\quad \tilde{\chi}\in[0,1] \tag{18}$$

With the introduced change of variable, the contribution of an element to the static equilibrium reads:

$$\int_{\Omega_l}\int_0^1 \left[\frac{EI}{l_p^2}\frac{d^2\delta\mathbf{r}}{d\tilde{\chi}^2}\cdot\frac{d^2\mathbf{r}}{d\tilde{\chi}^2}+\frac{EA}{2l_p^2}\frac{d\delta\mathbf{r}}{d\tilde{\chi}}\cdot\frac{d\mathbf{r}}{d\tilde{\chi}}\left(\frac{1}{l_p^2}\frac{d\mathbf{r}}{d\tilde{\chi}}\cdot\frac{d\mathbf{r}}{d\tilde{\chi}}-1\right)-\delta\mathbf{r}\cdot\mathbf{g}\right] l_p\,d\tilde{\chi}\,dl_p \tag{19}$$

which is possible to be solved with the PGD technique. PGD is based on a separate representation of the unknown field. In this case:

$$\mathbf{r}(\tilde{\chi},l_p)\approx\mathbf{r}^n=\sum_{i=1}^{n}\mathbf{R}_i(\tilde{\chi})L_i(l_p) \tag{20}$$

where each mode is composed of an $\mathbf{R}_i(\tilde{\chi})$ function that only depends on the spatial coordinate $\tilde{\chi}$, and an $L_i(l_p)$ function that depends on the extra-coordinate l_p.

In order to account for the non-homogeneous Dirichlet boundary conditions (the absolute position of the points that connect the wires with the fixed structure), let us consider a function $\mathbf{d}$ that satisfies these conditions. It is possible to state $\mathbf{d}(\tilde{\chi},l_p)$ in a separate form

$$\mathbf{d}(\tilde{\chi},l_p)=\mathbf{D}_\chi(\tilde{\chi})D_l(l_p) \tag{21}$$

where $\mathbf{D}_\chi(\tilde{\chi})$ is the FE solution of problem (15) for a particular value of the dropper lengths and $D_l(l_p)$ is a constant function with unitary value in all Ω_l. Considering $\mathbf{R}_1(\tilde{\chi})=\mathbf{D}_\chi(\tilde{\chi})$ and $L_1(l_p)=D_l(l_p)$, the remaining functions $\mathbf{R}_i(\tilde{\chi})$ and $L_i(l_p)$, for $i>1$, are calculated with homogeneous Dirichlet boundary conditions. The interested reader is referred to [25,26] for a detailed explanation of the PGD construction algorithm for problems with homogeneous Dirichlet boundary conditions.

The solution enrichment process starts from the assumed computed $\mathbf{r}^n,\ n\geq 1$, and then the next term of the separated solution is sought

$$\mathbf{r}^{n+1}=\sum_{i=1}^{n}\mathbf{R}_i(\tilde{\chi})L_i(l_p)+\mathbf{R}_{n+1}(\tilde{\chi})L_{n+1}(l_p) \tag{22}$$

with an admissible variation

$$\delta\mathbf{r}=\delta\mathbf{R}_{n+1}L_{n+1}+\mathbf{R}_{n+1}\delta L_{n+1} \tag{23}$$

Introducing (22) and (23) in (19) leads to a nonlinear expression in which $\mathbf{R}_{n+1}$ and L_{n+1} are the unknown functions. A widely used procedure to find these functions is based on an alternating fixed point strategy [10, 25, 26]. In each iteration of the proposed algorithm, two problems have to be solved in order to obtain both the $\mathbf{R}_{n+1}(\tilde{\chi})$ and $L_{n+1}(l_p)$ functions. These problems are detailed in Appendix A and are briefly described below:

- *Calculation of* $\mathbf{R}_{n+1}(\tilde{\chi})$. In this problem, $\mathbf{r}^n$ is known and $L_{n+1}(l_p)$ comes from either the previous iteration of the alternating strategy or it is randomly chosen in the case of the first iteration. Introducing Eq. (22) into (19) and integrating over Ω_l, $\mathbf{R}_{n+1}(\tilde{\chi})$ is the only unknown of the problem. If

$$\delta\mathbf{r} = \delta\mathbf{R}_{n+1} L_{n+1} \tag{24}$$

is considered to be the test function, the element contribution to the static equilibrium is:

$$\begin{aligned}
&\int_0^1 \Big[EI\,\delta\mathbf{R}^{''} \cdot \left(\omega_i \mathbf{R}_i^{''} + \pi \mathbf{R}_{n+1}^{''}\right) + \frac{EA}{2}\delta\mathbf{R}^{'} \cdot \Big[\alpha_{ijk}\mathbf{R}_i^{'}\left(\mathbf{R}_j^{'}\cdot\mathbf{R}_k^{'}\right) + \\
&\beta_{ij}\left(2\mathbf{R}_i^{'}\left(\mathbf{R}_j^{'}\cdot\mathbf{R}_{n+1}^{'}\right) + \mathbf{R}_{n+1}^{'}\left(\mathbf{R}_i^{'}\cdot\mathbf{R}_j^{'}\right)\right) + \\
&\gamma_i\left(2\mathbf{R}_{n+1}^{'}\left(\mathbf{R}_i^{'}\cdot\mathbf{R}_{n+1}^{'}\right) + \mathbf{R}_i^{'}\left(\mathbf{R}_{n+1}^{'}\cdot\mathbf{R}_{n+1}^{'}\right)\right) + \\
&\theta\mathbf{R}_{n+1}^{'}\left(\mathbf{R}_{n+1}^{'}\cdot\mathbf{R}_{n+1}^{'}\right) - \omega_i\mathbf{R}_i^{'} - \eta\mathbf{R}_{n+1}^{'}\Big] - \tau\rho A\delta\mathbf{R}\cdot\mathbf{g}\Big]\, d\tilde{\chi}
\end{aligned} \tag{25}$$

where $\mathbf{R}^{'}$ and $\mathbf{R}^{''}$ are the first and second derivatives of $\mathbf{R}$ respect to $\tilde{\chi}$, and the repeated subscripts i, j, k represent summations from 1 to n, following the Einstein notation. The coefficients α_{ijk}, β_{ij}, γ_i, θ, ω_i, η and τ are the integrals in Ω_l described in Appendix A. Finally, this second order nonlinear boundary value problem is solved for $\mathbf{R}_{n+1}(\tilde{\chi})$ using the FEM discretization described in Section 3.

- *Calculation of* $L_{n+1}(l_p)$. $\mathbf{r}^n$ is again known and $\mathbf{R}_{n+1}(\tilde{\chi})$ is the just-computed function. Introducing Eq. (22) into (19) and integrating over $\tilde{\chi}$, $L_{n+1}(l_p)$ remains the only unknown of the problem. In this case,

$$\delta\mathbf{r} = \mathbf{R}_{n+1}\delta L_{n+1} \tag{26}$$

is the test function which leads to the following element contribution:

$$\begin{aligned}
&\int_{\Omega_l} \Big[\frac{\delta L}{l_p}\Big[I_{2i}L_i + I_1 L_{n+1} + \frac{1}{l_p^2}\left(\alpha_{ijk}L_iL_jL_k + \left(\beta_{1ij}+\beta_{2ij}\right)L_{n+1}L_iL_j + \right. \\
&\left.\left(\gamma_{1i}+\gamma_{2i}\right)L_{n+1}^2 L_i + \theta L_{n+1}^3\right) - \omega_i L_i - \eta L_{n+1}\Big] - \delta L\tau l_p\Big]\, dl_p
\end{aligned} \tag{27}$$

The coefficients I_1, I_{2i}, α_{ijk}, β_{1ij}, β_{2ij}, γ_{1i}, γ_{2i}, θ, ω_i, η and τ are the integrals in the variable $\tilde{\chi}$ given in Appendix A. Finally, a nonlinear algebraic problem is obtained, which in this paper is solved for $L_{n+1}(l_p)$ using an appropriate discretization technique.

Both functions obtained at fixed point iteration p are compared with the same functions at the previous step $p-1$. The iterative process proceeds until its relative

difference becomes smaller than a certain prefixed value ε, that is,

$$\frac{\left\|\mathbf{R}_{n+1}^{p}L_{n+1}^{p}-\mathbf{R}_{n+1}^{p-1}L_{n+1}^{p-1}\right\|}{\left\|\mathbf{R}_{n+1}^{p-1}L_{n+1}^{p-1}\right\|}<\varepsilon \tag{28}$$

The solution enrichment process ends when the error $\Sigma(n)$ is small enough, $\Sigma(n) < \tilde{\varepsilon}$. Among the existing stopping criteria, for its simplicity and short calculation time, we chose

$$\Sigma(n)=\frac{\|\mathbf{R}_n L_n\|}{\|\mathbf{R}_k L_k\|} \tag{29}$$

where k is 2 if the first mode is employed to enforce the non-homogeneous Dirichlet boundary conditions, or 1 otherwise.

When the just described separated representation constructor is used in nonsymmetric problems, the obtained solution contains more modes than those provided by the Singular Value Decomposition (SVD) (or its multidimensional counterpart, the High Order Singular Value Decomposition (HOSVD)) applied to the problem solution computed by using standard discretization techniques. Thus, the decomposition provided by the PGD constructor is not optimal [27]. This reveals that some modes do not make an important contribution to the solution reconstruction and are not necessary in the reduced basis.

Therefore, a post-compression should be envisaged in order to express the solution in a more compact form (see [27] and [26]). If $\mathbf{r}^{\hat{n}}$ is the PGD solution of the original problem with $\hat{n}$ modes, the post-compression is carried out by solving the following problem:

$$\int_{\Omega_l}\int_{\Omega}\delta\mathbf{r}_c\left[\mathbf{r}_c(\tilde{\chi},l_p)-\mathbf{r}^{\hat{n}}(\tilde{\chi},l_p)\right]d\tilde{\chi}\,dl_p=0 \tag{30}$$

in which $\mathbf{r}_c(\tilde{\chi},l_p)$ is the unknown field. The PGD is here applied only for approximation purposes. With this technique the number of modes of the approximated solution $\mathbf{r}_c^n$ are usually fewer than those making up the original solution, i.e. $n \leq \hat{n}$. Therefore, post-processing the PGD solution requires a lighter computational effort.

5.2. Generalization to $\mathscr{N}$ extra-coordinates

It is straightforward to extrapolate the previous method to a more general case in which there are $\mathscr{N}$ different undeformed dropper lengths extra-coordinates. In this case, the domain $\Omega_l = \Omega_{l_1} \times \Omega_{l_2} \times ... \times \Omega_{l_{\mathscr{N}}}$, in which $\Omega_{l_i} = [l_{pi}^-, l_{pi}^+]$, $i = 1, ..., \mathscr{N}$. The separated representation of the absolute position field is:

$$\mathbf{r}(\tilde{\chi},l_{p1},...,l_{p\mathscr{N}})\approx\mathbf{r}^n=\sum_{i=1}^{n}\mathbf{R}_i(\tilde{\chi})\prod_{j=1}^{\mathscr{N}}L_{i,j}(l_{pj}) \tag{31}$$

Assuming $\mathbf{r}^n(\tilde{\chi}, l_{p1}, ..., l_{p\mathscr{N}})$ to be known, the next term of the separated representation is:

$$\mathbf{r}^{n+1} = \mathbf{r}^n + \mathbf{R}_{n+1}(\tilde{\chi}) \prod_{j=1}^{\mathscr{N}} L_{n+1,j}(l_{pj}) \tag{32}$$

and the virtual displacements field can be chosen as:

$$\delta\mathbf{r} = \delta\mathbf{R}_{n+1} \prod_{j=1}^{\mathscr{N}} L_{n+1,j}(l_{pj}) + \mathbf{R}_{n+1} \sum_{i=1}^{\mathscr{N}} \delta L_{n+1,i} \prod_{\substack{j=1 \\ j\neq i}}^{\mathscr{N}} L_{n+1,j} \tag{33}$$

Replacing Eqs. (32) and (33) in (19) and applying the fixed point iterative strategy, the resolution of $\mathscr{N}+1$ one dimensional problems at each fixed point iteration must be performed in order to calculate the functions $\mathbf{R}_{n+1}(\tilde{\chi})$, $L_{n+1,1}$, ..., $L_{n+1,\mathscr{N}}$ respectively.

5.3. PGD formulation: Dropper slackening

In the formulation presented in the previous section the droppers are allowed to be in compression due to the forces applied by the messenger and contact wires. However, this is not strictly true, since the droppers behave as cables and they can slacken when the pantograph pushes them upwards. In the case of the static configuration problem, they may have some combinations of undeformed dropper lengths that result in the slackening of some droppers in the static equilibrium position. Although this is not desirable in a railway catenary, if the model could take it into account it would be possible to simulate mistakes in the assembly process or failures in the design.

In a classic FEM approach it is easy to account for this effect by neglecting the axial strain term in Eq. (15) for the droppers whose deformed length is shorter than its undeformed length. When the problem is solved by the PGD approach there is not a straightforward solution. Here, we propose the following procedure to capture dropper slackening in the separate solution:

1. Solve the PGD problem described in Section 5.1, in which droppers work in compression.
2. For each dropper p, identify the combinations of extra-coordinates in which the dropper is compressed. For this pupose, the function $h^p \in \Omega_l$ is defined, which takes the value of 1 when the dropper is stretched and is set to 0 otherwise.
3. If there is more than one extra-coordinate, separate each h^p function in a summation of the product of one dimensional functions:

$$h^p = \sum_{i=1}^{N_p} H_{i,1}(l_{p1}) H_{i,2}(l_{p2}) ... H_{i,\mathscr{N}}(l_{p\mathscr{N}}) \tag{34}$$

4. Solve a PGD static problem in which, for the dropper p, the axial strain term of the element contribution to the static equilibrium (19) is multiplied by its respective separate h^p function.

In practice, in a real catenary with a realistic range of variation of dropper lengths, if we focus on a single dropper, its slackening can be assumed to depend only on its initial length and the undeformed length of its two neighbor droppers. With this assumption, each h^p function depends, at most, on three extra-coordinates. Otherwise, in problems with several extra-coordinates, it would be challenging to explore all Ω_l to identify the dropper slackening due to computational memory limitations.

Let us assume that there are p droppers in the spatial domain Ω but, for simplicity in the notation, only the undeformed length of the first two droppers are considered as extra-coordinates, namely l_{p1} and l_{p2}. By solving the problem posted in Section 5.1 but now with these two extra-coordinates, the separated absolute position field is obtained:

$$\mathbf{r}_{PGD}(\tilde{\chi}, l_{p1}, l_{p2}) = \sum_{i=1}^{n} \mathbf{R}_i(\tilde{\chi}) L_{i,1}(l_{p1}) L_{i,2}(l_{p2}) \tag{35}$$

Next, for each dropper p the domain $\Omega_l = \Omega_{l_1} \times \Omega_{l_2}$ is explored and the h^p function is built. Specifically, for dropper 2:

$$h^2(l_{p1}, l_{p2}, l_{03}) = \begin{cases} 1 & if \quad \frac{l_{def2}}{l_{p2}} \geq 1 \\ 0 & if \quad \frac{l_{def2}}{l_{p2}} < 1 \end{cases} \tag{36}$$

where l_{def2} is the deformed length of dropper 2 and l_{03} denotes the undeformed length of dropper 3, which is assumed to be constant in this case.

Following the procedure described in Appendix B, all of these h^p functions are exactly represented with n_p modes in a separate form:

$$h^p(l_{p1}, l_{p2}) = \sum_{i=1}^{n_p} H_{i,1}(l_{p1}) H_{i,2}(l_{p2}) \tag{37}$$

The last step of the proposed strategy consists of solving a PGD static equilibrium problem with the use of the h^p functions, in order to cancel the axial force of the droppers for all the combinations of l_{p1} and l_{p2} that make them slacken. The procedure for obtaining the separated representation of the absolute position field is exactly the same as described in Section 5.1. However, in this case, for a dropper p with variable initial length l_{p1}, its contribution to the static equilibrium (Eq. (19)) becomes:

$$\int_{\Omega_l} \int_0^1 \left[H_{m,1}(l_{p1}) H_{m,2}(l_{p2}) \frac{EA}{2l_{p1}^2} \frac{d\delta\mathbf{r}}{d\tilde{\chi}} \cdot \frac{d\mathbf{r}}{d\tilde{\chi}} \left(\frac{1}{l_{p1}^2} \frac{d\mathbf{r}}{d\tilde{\chi}} \cdot \frac{d\mathbf{r}}{d\tilde{\chi}} - 1 \right) - \delta\mathbf{r} \cdot \mathbf{g} \right] l_{p1} \, d\tilde{\chi} \, dl_{p1} \, dl_{p2} \tag{38}$$

where the subscript m denotes a summation.

This method leads to accurate results in spite of having some drawbacks. For example, when the high nonlinearity of the dropper slackening is introduced into the problem, the fixed-point alternating strategy needs more iterations to converge, with a consequently higher computational cost. Moreover, looking at expression (38), when the separated field (22) is introduced there is a summation whose number of terms depends cubically on the previous computed modes, and linearly on the number of terms in the separated h^p function.

It is true that these calculations are performed offline and only once, however they can require excessive computational time. For this reason, we propose the linearization of the problem (15) with respect to one static equilibrium position computed from a given value of dropper lengths. The linear solution is close to the nonlinear solution, as will be seen in Section 6, but the time required to obtain this solution is orders of magnitude lower.

5.4. PGD formulation: Linearized static problem

In a classic FEM approach, in order to linearise the static equilibrium problem, the first step is to calculate the static equilibrium configuration for which the problem is linearised This involves solving the problem stated in (15) for a certain values of undeformed dropper lengths $\mathbf{l}_{ref}$ defining the reference catenary spatial domain Ω_{ref}. This provides $\mathbf{r}_{ref}(\chi)$, the reference equilibrium position field. For a different set of undeformed dropper lengths $\mathbf{l}_0$ defining the spatial domain Ω, the new equilibrium position can be expressed as $\mathbf{r} = \mathbf{r}_{ref} + \mathbf{u}$, where $\mathbf{u}(\chi)$ is the displacement field with respect to the reference solution $\mathbf{r}_{ref}(\chi)$. Therefore, the linearised static equilibrium problem consists of solving for all admissible $\delta\mathbf{u}$:

$$\sum_{e=1}^{N_e} \int_{\Omega^e} \left[EI \frac{d^2\delta\mathbf{u}}{d\chi^2} \cdot \frac{d^2\mathbf{u}}{d\chi^2} + \frac{EA}{2} \frac{d\delta\mathbf{u}}{d\chi} \cdot \left[2\frac{d\mathbf{r}_{ref}}{d\chi} \left(\frac{d\mathbf{u}}{d\chi} \cdot \frac{d\mathbf{r}_{ref}}{d\chi} \right) + \frac{d\mathbf{u}}{d\chi} \left(\frac{d\mathbf{r}_{ref}}{d\chi} \cdot \frac{d\mathbf{r}_{ref}}{d\chi} \right) + \frac{d\mathbf{r}_{ref}}{d\chi} \left(\frac{d\mathbf{r}_{ref}}{d\chi} \cdot \frac{d\mathbf{r}_{ref}}{d\chi} \right) - \frac{d\mathbf{u}}{d\chi} - \frac{d\mathbf{r}_{ref}}{d\chi} \right] - \rho A \delta\mathbf{u} \cdot \mathbf{g} \right] d\chi = 0, \quad \forall \delta\mathbf{u} \tag{39}$$

In order to apply the PGD to such a variational problem, the reference solution $\mathbf{r}_{ref}(\chi)$, which only depends on the spatial coordinate, is obtained again solving Eq. (15), in which $\mathbf{l}_{ref}$ are now defined as the intermediate values of the undeformed dropper lengths in Ω_l. From now on, the same steps as detailed in Section 5.1 must be followed. The displacements field also depends on all the extra-coordinates, so the change of variable defined in (18) is introduced. Taking only one extra-coordinate for simplicity in the notation, the element contribution to the linearised static equilibrium

problem reads:

$$\int_{\Omega_l}\int_0^1 \frac{1}{l_p^3}\left[EI\frac{d^2\delta\mathbf{u}}{d\tilde{\chi}^2}\cdot\frac{d^2\mathbf{u}}{d\tilde{\chi}^2}+\frac{EA}{2}\frac{d\delta\mathbf{u}}{d\tilde{\chi}}\cdot\left[2\frac{d\mathbf{r}_{ref}}{d\tilde{\chi}}\left(\frac{d\mathbf{u}}{d\tilde{\chi}}\cdot\frac{d\mathbf{r}_{ref}}{d\tilde{\chi}}\right)+\right.\right.$$
$$\left.\frac{d\mathbf{u}}{d\tilde{\chi}}\left(\frac{d\mathbf{r}_{ref}}{d\tilde{\chi}}\cdot\frac{d\mathbf{r}_{ref}}{d\tilde{\chi}}\right)+\frac{d\mathbf{r}_{ref}}{d\tilde{\chi}}\left(\frac{d\mathbf{r}_{ref}}{d\tilde{\chi}}\cdot\frac{d\mathbf{r}_{ref}}{d\tilde{\chi}}\right)-l_p^2\left(\frac{d\mathbf{u}}{d\tilde{\chi}}+\frac{d\mathbf{r}_{ref}}{d\tilde{\chi}}\right)\right]- \tag{40}$$
$$\left.\rho A l_p\,\delta\mathbf{u}\cdot\mathbf{g}\right]\,d\tilde{\chi}\,dl_p$$

The separated form of the unknown field is:

$$\mathbf{u}(\tilde{\chi},l_p)\approx\mathbf{u}^n=\sum_{i=1}^{n}\mathbf{U}_i(\tilde{\chi})L_i(l_p) \tag{41}$$

where $\mathbf{U}(\tilde{\chi})$ is a function that only depends on the normalized spatial coordinate $\tilde{\chi}$, and $L(l_p)$ is a function which depends on the extra-coordinate l_p. As the Dirichlet boundary conditions are fulfilled by the reference static solution $\mathbf{r}_{ref}$, the linearised problem is solved with homogeneous Dirichlet boundary conditions.

In order to obtain the next mode $\mathbf{u}^{n+1}$, the procedure used is again the same as described in Section 5.1. In order to account for the dropper slackening, the procedure explained in Section 5.3 is applied combined with the linearised problem defined above, considering now that Eq.(36) becomes:

$$h^p(l_{p1},l_{p2})=\begin{cases}1 & if \quad f^p_{int}(l_{p1},l_{p2})\geq f^p_{ref}\\ 0 & if \quad f^p_{int}(l_{p1},l_{p2})<f^p_{ref}\end{cases} \tag{42}$$

in which f^p_{int} is the projected internal force of the dropper element p in its axial direction for a given value of l_{p1} and l_{p2}, and f^p_{ref} is the internal force of the same element in the reference configuration.

By using the linearised formulation, when solving the problem defined in $\Omega\times\Omega_l$ with the fixed-point algorithm, the number of terms involved in the internal forces increases linearly with the number of already evaluated modes. On the other hand, if the nonlinear formulation is used, the number of terms increases cubically with the evaluated modes. This means there is a considerable reduction in computational cost when the linearised formulation is employed.

6. Numerical examples

In this section, the proposed method is checked through some numerical examples. The first one is quite simple, allowing all the FEM static solutions to be obtained

and thus making it possible to compare the whole nonlinear PGD solution with the solutions obtained from the FE analysis. The second example includes a more real catenary geometry, with which a more realistic application of the algorithm is shown. Finally, the third example reveals that when the nonlinear formulation includes dropper slackening, the solution process is very expensive in terms of computational cost, so that the linearised approach is used and validated.

6.1. Example 1: Academic example

The proposed method is validated with the first numerical example. The spatial domain Ω of this 2D academic example is shown in Fig.4. It simulates a single span with two droppers, in which the contact and messenger wires are discretized into 30 elements each. The material and geometrical properties of these elements are listed in Table 1. Regarding the Dirichlet boundary conditions, the vertical and horizontal displacements of the nodes located at the ends of both cables are constrained. Altogether, there are 240 spatial degrees of freedom. The two droppers are considered with variable undeformed length. The domains of the extra-coordinates l_{p1} and l_{p2} are $\Omega_{l_1} = \Omega_{l_2} = [1.15, 1.25]\ m$, which ensure dropper slackening in certain regions of Ω_l. The domains of each extra-coordinate are discretized into 20 elements of the same length.

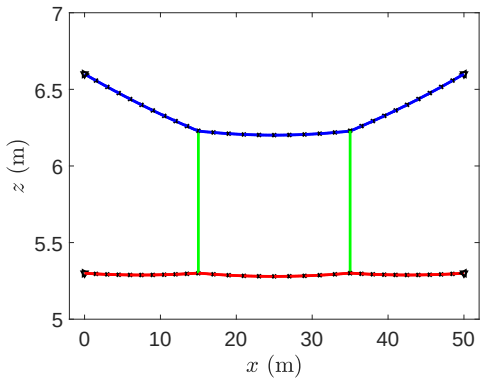

Figure 4: Academic example spatial mesh.

The first PGD solution is obtained allowing the dropper elements to work in compression. The iterative process converges with 12 modes. Fast convergence of fixed-point alternating strategy was observed (around 8 iterations each mode) and short computational time was required.

Table 1: Material and geometrical properties of the elements.

Element	$\mathbf{E}(Pa)$	$\boldsymbol{\rho}(kg/m^3)$	$\mathbf{A}(mm^2)$	$\mathbf{I}(mm^4)$
Messenger wire	9114	$1.1 \cdot 10^{11}$	94.8	1237.2
Contact wire	9160	$1.1 \cdot 10^{11}$	150	2170
Droppers	9114	$1.1 \cdot 10^{11}$	10	0

From this solution, the h^1 and h^2 functions are calculated. It should be remembered that the h^p function controls whether or not the dropper p is under compression $(h = 0)$ or $(h = 1)$ for any combination of variable undeformed dropper lengths. These functions are plotted in Fig. 5. The magenta area is the region of the domain Ω_l, in which the respective dropper is stretched, while the cyan area shows the values of the extra-coordinates at which the dropper is compressed.

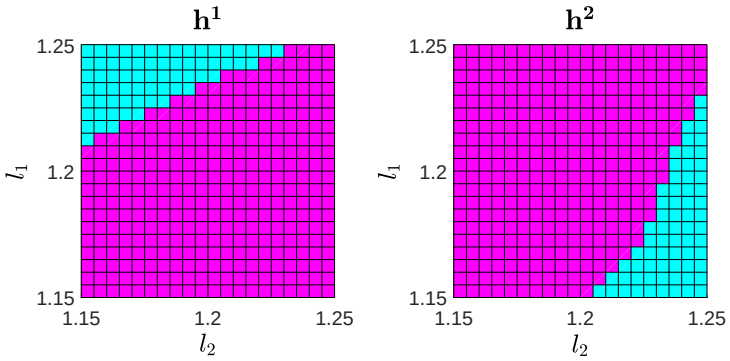

Figure 5: h function for droppers 1 and 2. $h = 0$ in cyan, $h = 1$ in magenta.

Focusing on h^1, it can be seen that when dropper 1 becomes longer it tends to slacken, while on the other hand, dropper 1 is more likely to slacken when dropper 2 becomes shorter. The same conclusions can be drawn for dropper 2, looking at h^2.

The separation of h^1 results in a summation of 9 terms and h^2 is separated properly with 10 modes. The next step of the calculation is to compute the PDG solution, taking dropper slackening into account. The strong nonlinearity introduced by the h^p functions slows down the speed of convergence of the fixed-point strategy. Furthermore, the number of modes necessary to obtain a similar error to the case of droppers without slacking increases hugely, as can be seen in Fig. 6. For these reasons, the computational cost required to solve this problem is much higher than that required to solve the PGD problem without dropper slackening.

Let us define the local error of the separated solution with N modes and for specific values of the extra-coordinates, as:

$$E^N_{loc}(l_{p1},...,l_{p\mathcal{N}}) = \frac{\left\|\mathbf{r}_{EX}(l_{p1},l_{p2},...,l_{p\mathcal{N}}) - \mathbf{r}^N_{PGD}(l_{p1},l_{p2},...,l_{p\mathcal{N}})\right\|}{\left\|\mathbf{r}_{EX}(l_{p1},l_{p2},...,l_{p\mathcal{N}})\right\|} = \frac{\sqrt{\sum_{i=1}^{N_e}\int_0^{l_0}\left|\mathbf{r^i}_{EX}(l_{p1},l_{p2},...,l_{p\mathcal{N}}) - \mathbf{r^i}^N_{PGD}(l_{p1},l_{p2},...,l_{p\mathcal{N}})\right|^2 d\chi}}{\sqrt{\sum_{i=1}^{N_e}\int_0^{l_0}\left|\mathbf{r^i}_{EX}(l_{p1},l_{p2},...,l_{p\mathcal{N}})\right|^2 d\chi}} \tag{43}$$

where $\mathbf{r}_{EX}$ and $\mathbf{r}^N_{PGD}$ are the absolute position field from the FEM solution and the PGD solution, respectively. To account for all Ω_l, a global error is defined as the integral of the local error in this domain:

$$E^N_{glob} = \int_{\Omega_l} E^N_{loc}(l_{p1},l_{p2},...,l_{p\mathcal{N}})\, dl_{p1}\, dl_{p2} \ldots dl_{p\mathcal{N}} \tag{44}$$

In Fig. 6 is shown a plot of the global error versus the number of PGD modes. The graph on the left shows the case without dropper slackening and the one on the right gives the error of the problem which accounts for dropper slackening. As mentioned above, the speed of convergence to the reference FEM solution is noticeably slower than the case without dropper slackening.

The twenty-seven computed modes of the separated solution can be compressed into a few modes using (30) with almost the same accuracy, as shown in Fig. 7.

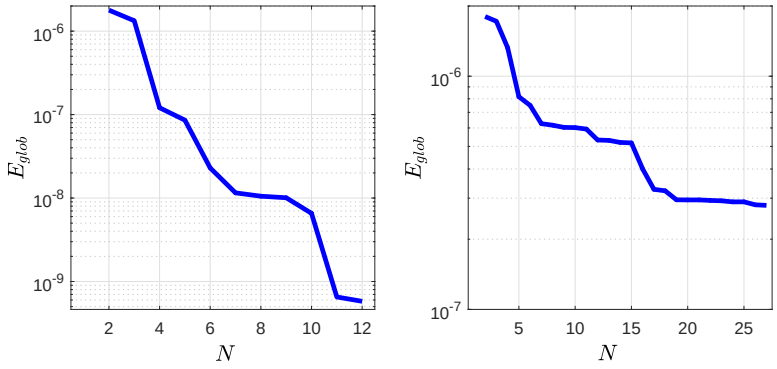

Figure 6: E_{glob} of PGD solution without dropper slackening (left) and with dropper slackening (right).

A comparison between the solutions considering (blue line) and obviating (red line) the slackening of dropper 1 is shown in Fig. 8. In both cases, the values of the

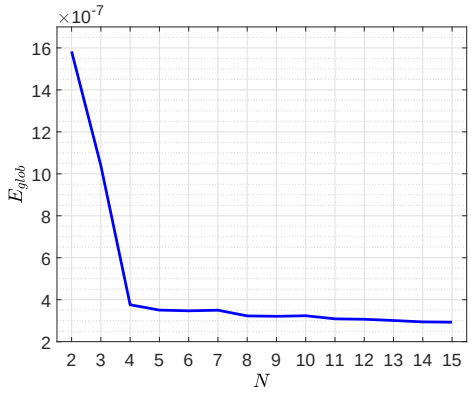

Figure 7: E_{glob} of PGD post-compressed solution.

undeformed lengths are $l_{p1} = 1.25\,m$ and $l_{p2} = 1.15\,m$. The difference in the static equilibrium position is quite clear, and it becomes even more apparent in the dynamic interaction problem. Thus, it is necessary to include dropper slackening into the PGD approach to obtain realistic solutions.

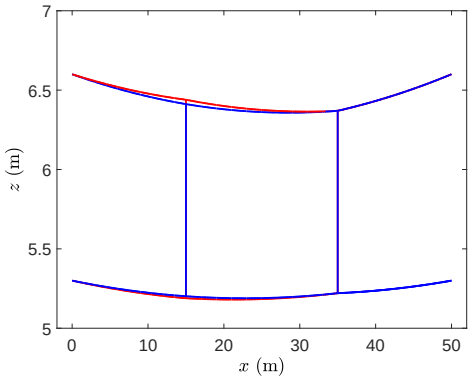

Figure 8: Static position for $l_{p1} = 1.25\,m$ and $l_{p2} = 1.15\,m$. With dropper slackening (blue), without dropper slackening (red).

6.2. Example 2: Variable pre-sag

In this case, a real span of an overhead line set-up is studied. The span consists of 9 droppers, and the messenger and contact wires are discretized into 100 elements each. As in the previous example, the vertical and horizontal displacements of the nodes at the ends of both cables are constrained.

In a real railway catenary the presence of a certain amount of pre-sag is fairly common. Pre-sag is defined as the vertical deflection, in the static equilibrium configuration, of the contact wire at the midspan, as shown in Fig. 9.

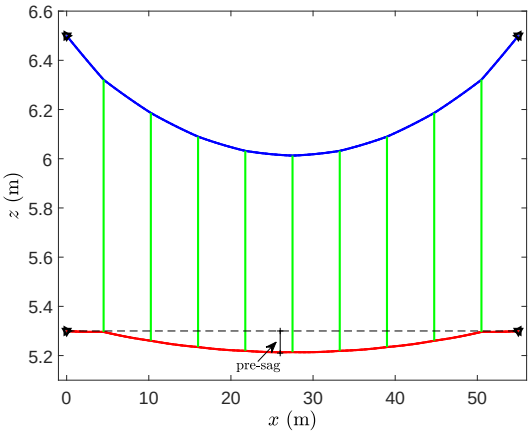

Figure 9: Geometric model of a real span, with defined pre-sag.

The method described in this paper not only allows the undeformed dropper lengths to be directly included as extra-coordinates, but also it allows to consider a parameter on which the undeformed dropper lengths depend, i.e. for a certain dropper i, $l_{pi} = f_i(parameter)$. Since the amount of pre-sag is defined with the initial dropper lengths, it is possible to include an extra-coordinate of the problem that controls the pre-sag. Each undeformed length of droppers 2 to 8 is variable and depends on the x coordinate of the dropper, on the undeformed dropper length that leads to a static position in which the pre-sag is null, and finally on the new variable $psg \in \Omega_{psg} = [0, 0.18]\, m$. This range of values of the extra-coordinate psg is equivalent to a pre-sag of $[0, 85]\, mm$. The domain of the extra-coordinate is discretized into 20 uniform distributed elements.

The PGD solution to this problem, in which any dropper slackens, is accurate enough with 5 modes, as showed in Fig. 10.

In Fig. 11 the $L_i(psg)$, $i > 1$ normalized functions are plotted. It is notorious that $L_i(0) = 0$, $i = 2, ..., 5$. This is because the first mode $R_1(\tilde{\chi})L_1(psg)$ introduced

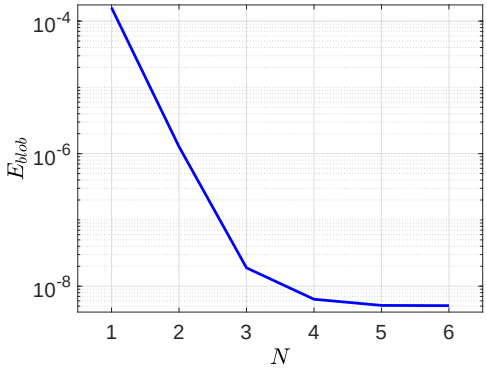

Figure 10: Global error for PGD solution with variable pre-sag.

into the solution to fulfill the Dirichlet boundary conditions is the FEM solution of the static equilibrium problem for zero pre-sag. Therefore, as expected, the following PGD modes do not change the solution for $psg = 0$.

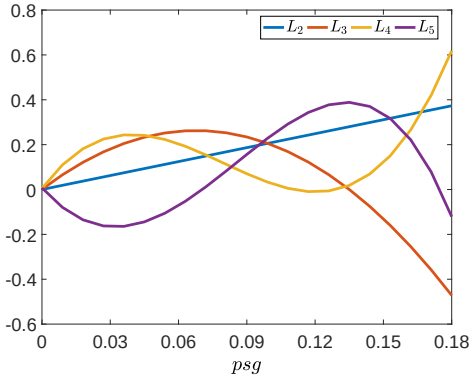

Figure 11: $L_i(psg),\ i > 1$ normalized functions.

Once the solution is obtained, we have to check if there are any compressed droppers. For the case at hand, all the h^p functions are null because all droppers are tensioned in all Ω_l. This example shows what is expected to take place in a real railway catenary static configuration. The values of the initial dropper lengths are designed so that in the static equilibrium configuration all the droppers work under tension. This PGD solution could therefore be used as the initial modes of the solution of a parametric dynamic simulation problem following the PGD approach.

Table 2: Definition of the domains for each extra-coordinate.

Dropper	Extra-coordinate	Range (m)
1-9	l_{p1}	1.00 - 1.05
2-8	l_{p2}	0.82 - 0.87
3-7	l_{p3}	0.70 - 0.75
4-6	l_{p4}	0.62 - 0.68
5	l_{p5}	0.59 - 0.64

6.3. Example 3: Multidimensional catenary span

The same geometrical model of the catenary span used in the example 2 is also used in this case. The nine droppers in the span are considered as elements with variable initial length. In particular, as regards the span symmetry, the symmetric droppers are related to the same extra-coordinate, and so five extra-coordinates are introduced. The range of variation of each variable and the droppers related to them are listed in Table 2. The 5D domain Ω_l is composed of the product of the 1D domains Ω_{li}, which are discretized into 20 uniform elements each.

The first step deals with the PGD problem without dropper slackening, using the nonlinear formulation of the static equation. In the current case, due to its high dimensionality, it is not possible to generate a reference solution with classical methods, so that the local and global error cannot be evaluated. As all the $L_{i,j}$ $(i = 1, ..., N;\ j = 1, ..., 5)$ functions are normalized, the weight of the mode n is defined as $w_n = \|\mathbf{R}_n\|$. Fig. 12 represents the weight of the first 30 modes, where its decreasing tendency can be seen.

When building the h^p functions the nine droppers are compressed in certain regions of Ω_l. Therefore, the next step is to solve the static equilibrium problem, including dropper slackening. However, even if this is performed offline, using the nonlinear formulation takes an excessive time. Consequently, when there are several extra-coordinates, the linearised formulation is highly advantageous in terms of computational cost without major changes in the required accuracy.

In Fig. 13 there is a comparison of the static equilibrium position obtained after solving the nonlinear and the linearised problem. The maximum values are used for the l_p coordinates, so that this case is the furthest case from the reference solution, i.e. the distance between Ω_{ref} and Ω is maximum for the current Ω_l. Even so, the largest differences observed in the height of the contact wire are around $1\,mm$. These discrepancies are perfectly assumable and confirm the validity of the linearised static formulation for this Ω_l.

When computing the PGD solution with dropper slackening, using the linearised formulation, 225 modes are computed to achieve good accuracy in the separate so-

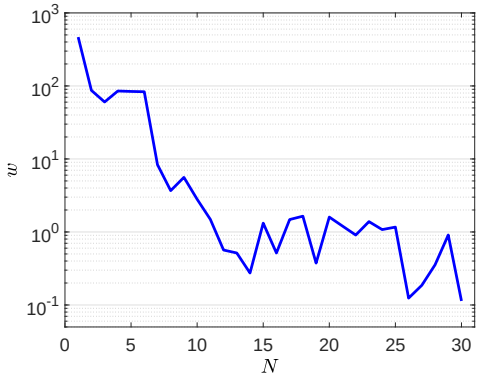

Figure 12: Weight of the PGD modes of the nonlinear problem without dropper slackening.

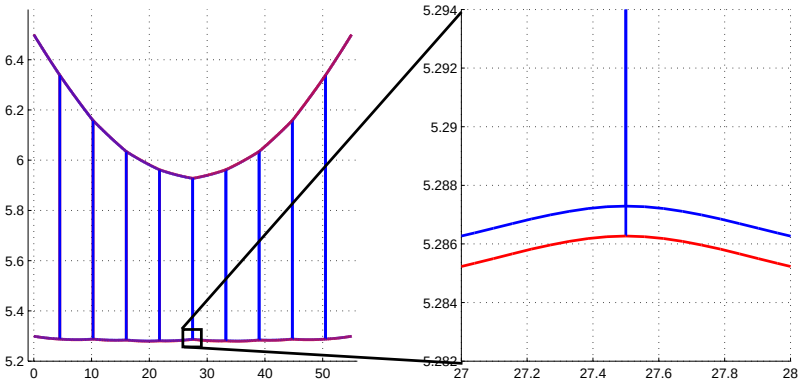

Figure 13: Comparison of linear and nonlinear static equilibrium positions.

lution. This amount of modes would be challenging to obtain with the nonlinear formulation, whilst it requires little computational cost with the linearised problem.

Fig. 14 shows the weights of the computed modes for the original solution (left) and the post-compressed solution (right). Although there are some peaks, the general trend is to reduce the weight of the modes while the PGD solution tends to the exact solution of the problem. This tendency is clearly improved when the post-compressor problem (30) is solved. However, for the established accuracy, the number of modes required is not reduced when the solution is compressed, which means that every mode plays an important role in the reconstruction of the solution.

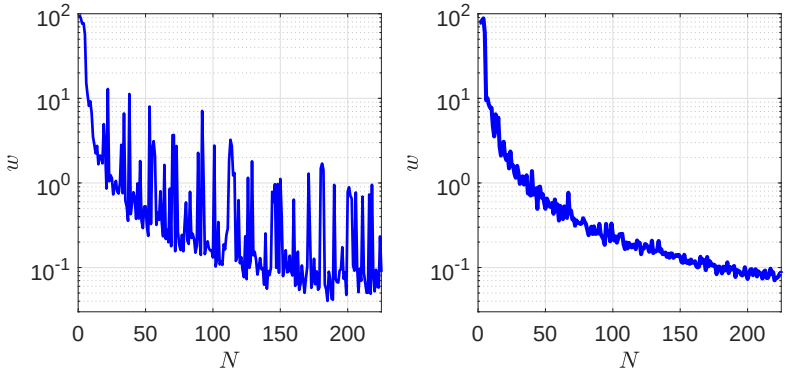

Figure 14: Weight of the PGD modes of the linear problem solution, with slackening. Original solution (left), post-compressed solution (right).

Finally, in order to emphasize the effect of considering dropper slackening, Fig. 15 shows the static equilibrium configuration for $l_{p1} = 1\,m$, $l_{p2} = 0.82\,m$, $l_{p3} = 0.75\,m$, $l_{p4} = 0.62\,m$ and $l_{p5} = 0.64\,m$. On the blue plot, droppers 2, 4, 6 and 8 are compressed, while on the red plot they are slackened.

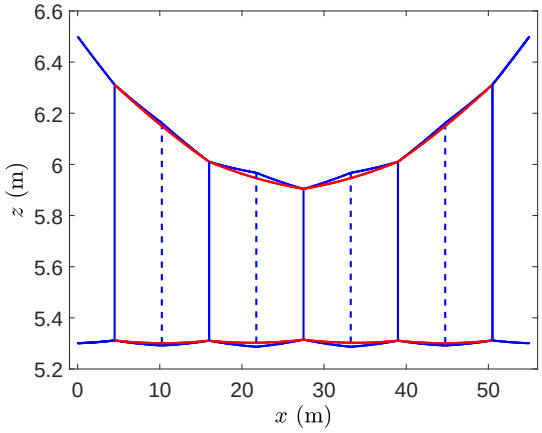

Figure 15: Static equilibrium with compressed droppers and slackened droppers.

7. Conclusions

This paper addresses the static equilibrium problem of a railway catenary. The catenary system was modelled by FE according to the absolute nodal coordinate formulation. The undeformed dropper lengths were introduced into the nonlinear formulation as extra-coordinates in order to obtain a general solution valid for any value of undeformed dropper length, using PGD. The proposed strategy was applied to an academic example showing good convergence and accuracy.

Not only undeformed dropper lengths can be added as extra-coordinates, but also any parameter on which these lengths depend. In order to demonstrate the method's capabilities, pre-sag was included as an extra-coordinate in the model. The proposed method also allows for the strong nonlinearity of dropper slackening. This high nonlinear effect has a remarkable influence in the number of modes needed for the solution and thus, it increases the required computational time. In order to make the separated construction more efficient, a linearised formulation of the problem, which provides a similar level of accuracy in the results, is also proposed.

This work constitutes the first step towards the major objective of optimizing the geometry of the catenary, which normally requires a large number of dynamic catenary simulations for different values of the parameters to be optimized, e.g. undeformed dropper lengths. With the parametric solution provided by the PGD approach, i.e. the dynamic response of the system for any combination of undeformed dropper lengths, addressing the optimization problem would be faster because one dynamic simulation would be substituted by a evaluation of the parametric solution. However, in order to obtain the parametric dynamic solution, it is necessary to have at hand the parametric solution of the static configuration problem presented in this paper.

A. The PGD constructor

The aim of this section is to explain in depth the formulation of the two problems dealt with in Section 5.1, in which the functions $\mathbf{R}_{n+1}(\tilde{\chi})$ and $L_{n+1}(l_p)$ are computed.

A.1. Computing $\mathbf{R}_{n+1}(\tilde{\chi})$ from $L_{n+1}(l_p)$

For this problem, the test function is:

$$\delta\mathbf{r} = \delta\mathbf{R}(\tilde{\chi})L_{n+1}(l_p) \tag{45}$$

where $L_{n+1}(l_p)$ in supposed to be known. Introducing equations (22) and (45) into (19), the following expression is obtained:

$$\int_0^1 \int_{\Omega_l} \left[\frac{EI}{l_p^2} L_{n+1}\delta\mathbf{R}^{''} \cdot \left(\mathbf{R}_i^{''} L_i + \mathbf{R}_{n+1}^{''} L_{n+1} \right) + \frac{EA}{2l_p^2} L_{n+1}\delta\mathbf{R}^{'} \cdot \left(\mathbf{R}_i^{'} L_i + \mathbf{R}_{n+1}^{'} L_{n+1} \right) \right.$$
$$\left. \left[\frac{1}{l_p^2} \left(\mathbf{R}_j^{'} L_j + \mathbf{R}_{n+1}^{'} L_{n+1} \right) \cdot \left(\mathbf{R}_k^{'} L_k + \mathbf{R}_{n+1}^{'} L_{n+1} \right) - 1 \right] - \rho A L_{n+1}\delta\mathbf{R} \cdot \mathbf{g} \right] l_p \, dl_p \, d\tilde{\chi} \tag{46}$$

Integrating in Ω_l, the coefficients

$$\alpha_{ijk} = \int_{\Omega_l} \frac{1}{l_p^3} L_{n+1} L_i L_j L_k \, dl_p \quad \beta_{ij} = \int_{\Omega_l} \frac{1}{l_p^3} L_{n+1}^2 L_i L_j \, dl_p \quad \gamma_i = \int_{\Omega_l} \frac{1}{l_p^3} L_{n+1}^3 L_i \, dl_p$$
$$\theta = \int_{\Omega_l} \frac{1}{l_p^3} L_{n+1}^4 \, dl_p \qquad \omega_i = \int_{\Omega_l} \frac{1}{l_p} L_{n+1} L_i \, dl_p \qquad \eta = \int_{\Omega_l} \frac{1}{l_p} L_{n+1}^2 \, dl_p$$
$$\tau = \int_{\Omega_l} L_{n+1} l_p \, dl_p \tag{47}$$

can be introduced into Eq.(46) leading to:

$$\int_0^1 \left[EI \, \delta\mathbf{R}^{''} \cdot \left(\omega_i \mathbf{R}_i^{''} + \pi \mathbf{R}_{n+1}^{''} \right) + \frac{EA}{2} \delta\mathbf{R}^{'} \cdot \left[\alpha_{ijk} \mathbf{R}_i^{'} \left(\mathbf{R}_j^{'} \cdot \mathbf{R}_k^{'} \right) + \right. \right.$$
$$\beta_{ij} \left(2\mathbf{R}_i^{'} \left(\mathbf{R}_j^{'} \cdot \mathbf{R}_{n+1}^{'} \right) + \mathbf{R}_{n+1}^{'} \left(\mathbf{R}_i^{'} \cdot \mathbf{R}_j^{'} \right) \right) + \gamma_i \left(2\mathbf{R}_{n+1}^{'} \left(\mathbf{R}_i^{'} \cdot \mathbf{R}_{n+1}^{'} \right) + \right.$$
$$\left. \left. \mathbf{R}_i^{'} \left(\mathbf{R}_{n+1}^{'} \cdot \mathbf{R}_{n+1}^{'} \right) \right) + \theta \mathbf{R}_{n+1}^{'} \left(\mathbf{R}_{n+1}^{'} \cdot \mathbf{R}_{n+1}^{'} \right) - \omega_i \mathbf{R}_i^{'} - \eta \mathbf{R}_{n+1}^{'} \right] - \tau \rho A \delta\mathbf{R} \cdot \mathbf{g} \Big] \, d\tilde{\chi} \tag{48}$$

If function $\mathbf{R}_{n+1}$ is discretized, after applying the usual Galerkin FEM a nonlinear system of algebraic equations is obtained which can be solved with the Newton-Raphson method.

A.2. Computing $L_{n+1}(l_p)$ from $\mathbf{R}_{n+1}(\tilde{\chi})$

For the next step of the fixed-point iterative process, the test function is chosen as

$$\delta\mathbf{r} = \mathbf{R}_{n+1}(\tilde{\chi})\delta L(l_p) \tag{49}$$

in which $\mathbf{R}_{n+1}(\tilde{\chi})$ is the solution of the problem solved in the previous step. In this case, the contribution of an element to the problem at hand is:

$$\int_0^1 \int_{\Omega_l} \left[\frac{EI}{l_p^2}\, \delta L\, \mathbf{R}_{n+1}^{''} \cdot \left(\mathbf{R}_i^{''} L_i + \mathbf{R}_{n+1}^{''} L_{n+1} \right) + \frac{EA}{2l_p^2} \delta L\, \mathbf{R}_{n+1}^{'} \cdot \left(\mathbf{R}_i^{'} L_i + \mathbf{R}_{n+1}^{'} L_{n+1} \right) \right.$$
$$\left. \left[\frac{1}{l_p^2} \left(\mathbf{R}_j^{'} L_j + \mathbf{R}_{n+1}^{'} L_{n+1} \right) \cdot \left(\mathbf{R}_k^{'} L_k + \mathbf{R}_{n+1}^{'} L_{n+1} \right) - 1 \right] - \rho A\, \delta L \mathbf{R}_{n+1} \cdot \mathbf{g}\, \right] l_p\, dl_p\, d\tilde{\chi} \tag{50}$$

Integrating the known functions over its corresponding domain we can define the following coefficients:

$$\begin{aligned}
I_1 &= EI \int_0^1 \mathbf{R}_{n+1}^{''} \cdot \mathbf{R}_{n+1}^{''}\, d\tilde{\chi} & I_{2i} &= EI \int_0^1 \mathbf{R}_{n+1}^{''} \cdot \mathbf{R}_i^{''}\, d\tilde{\chi} \\
\alpha_{ijk} &= \frac{EA}{2} \int_0^1 \left(\mathbf{R}_{n+1}^{'} \cdot \mathbf{R}_i^{'} \right) \left(\mathbf{R}_j^{'} \cdot \mathbf{R}_k^{'} \right) d\tilde{\chi} & \beta_{1ij} &= \frac{EA}{2} \int_0^1 \left(\mathbf{R}_{n+1}^{'} \cdot \mathbf{R}_{n+1}^{'} \right) \left(\mathbf{R}_i^{'} \cdot \mathbf{R}_j^{'} \right) d\tilde{\chi} \\
\beta_{2ij} &= \frac{EA}{2} \int_0^1 \left(\mathbf{R}_{n+1}^{'} \cdot \mathbf{R}_i^{'} \right) \left(\mathbf{R}_{n+1}^{'} \cdot \mathbf{R}_j^{'} \right) d\tilde{\chi} & \gamma_{1i} &= \frac{EA}{2} \int_0^1 \left(\mathbf{R}_{n+1}^{'} \cdot \mathbf{R}_i^{'} \right) \left(\mathbf{R}_{n+1}^{'} \cdot \mathbf{R}_{n+1}^{'} \right) d\tilde{\chi} \\
\gamma_{2i} &= \frac{EA}{2} \int_0^1 \left(\mathbf{R}_{n+1}^{'} \cdot \mathbf{R}_{n+1}^{'} \right) \left(\mathbf{R}_i^{'} \cdot \mathbf{R}_{n+1}^{'} \right) d\tilde{\chi} & \theta &= \frac{EA}{2} \int_0^1 \left(\mathbf{R}_{n+1}^{'} \cdot \mathbf{R}_{n+1}^{'} \right)^2 d\tilde{\chi} \\
\omega_i &= \frac{EA}{2} \int_0^1 \mathbf{R}_{n+1}^{'} \cdot \mathbf{R}_i^{'}\, d\tilde{\chi} & \eta &= \frac{EA}{2} \int_0^1 \mathbf{R}_{n+1}^{'} \cdot \mathbf{R}_{n+1}^{'}\, d\tilde{\chi} \\
\tau &= \rho A \int_0^1 \mathbf{R}_{n+1} \cdot \mathbf{g}\, d\tilde{\chi}
\end{aligned} \tag{51}$$

Thus, Eq. (50) can be rewritten in the following fashion:

$$\int_{\Omega_l} \left[\frac{\delta L}{l_p} \left[I_{2i} L_i + I_1 L_{n+1} + \frac{1}{l_p^2} \left(\alpha_{ijk} L_i L_j L_k + \left(\beta_{1ij} + \beta_{2ij} \right) L_{n+1} L_i L_j + \right. \right. \right.$$
$$\left. \left. \left. \left(\gamma_{1i} + \gamma_{2i} \right) L_{n+1}^2 L_i + \theta L_{n+1}^3 \right) - \omega_i L_i - \eta L_i \right] - \delta L \tau l_p \right]\, dl_p \tag{52}$$

which can be solved using an appropriate discretization technique. However, this expression can be turned into its associated nonlinear strong form:

$$\frac{1}{l_p} \left[I_{2i} L_i + I_1 L_{n+1} + \frac{1}{l_p^2} \left(\alpha_{ijk} L_i L_j L_k + \left(\beta_{1ij} + \beta_{2ij} \right) L_{n+1} L_i L_j + \right. \right.$$
$$\left. \left. \left(\gamma_{1i} + \gamma_{2i} \right) L_{n+1}^2 L_i + \theta L_{n+1}^3 \right) - \omega_i L_i - \eta L_{n+1} \right] - \tau l_p \tag{53}$$

The nonlinear system equation resulting from the result of both strategies can be solved again using the Newton-Raphson method.

B. Separation of the h function

Let h^p be a function dependent on three variables, $h^p(l_{p1}, l_{p2}, l_{p3})$. An example of such a function is depicted in Fig. 16. The domain Ω_l is discretized into $N_1 \times N_2 \times N_3$ points in which h^p could be one (vertices of shadowed squares) or zero (other points). The goal of the separation process is to obtain the functions $H_{i,1}(l_{p1})$, $H_{i,2}(l_{p2})$ and $H_{i,3}(l_{p3})$ such that:

$$h^p(l_{p1}, l_{p2}, l_{p3}) = \sum_{i=1}^{n_p} H_{i,1}(l_{p1}) H_{i,2}(l_{p2}) H_{i,3}(l_{p3}) \tag{54}$$

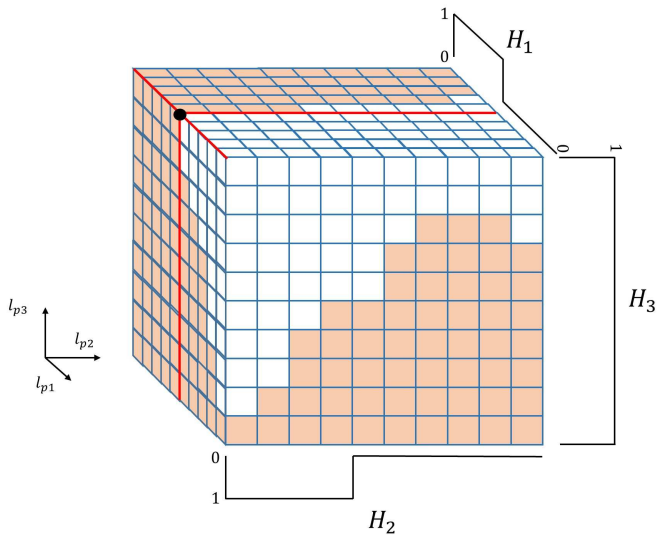

Figure 16: Example of h function and separation method. The value of h in the corners of the shadowed cubes is 1 and in the rest is 0.

All these functions are step unitary functions. Defining the residual Res_i as the difference of h^p and the right hand side of Eq. (54) for a certain value of i, the proposed algorithm reads:

1. Initialize $i = 1$, $l_{p2} = l_{p2}^-$ and $l_{p3} = l_{p3}^-$.
2. Evaluate Res_i. Three cases are distinguished:

(a) If all values are 0, there is not a new term. Go to Step 3.

(b) If all values are 1, the new term is composed of $H_{i,1}(l_{p1}) = 1$, $H_{i,2}(l_{p2}^{-}) = 1$ and $H_{i,3}(l_{p3}^{-}) = 1$. Update $i = i + 1$, and go to Step 3.

(c) If some values of Res_i are 1 and others are 0, $H_{i,1}(l_{p1}) = 1$. For the other two directions Res_i is evaluated starting from the first nonzero value of the function $H_{i,1}$ (black point in Fig. 16). Each function of the new term corresponds to the evaluation of Res_i in its direction. Update $i = i + 1$, and go to Step 3.

3. Move to the next value of l_{p2} and/or l_{p3} and repeat Step 1 until all the domain is explored. In this case, move to Step 4.

4. All the modes where $H_{i,1}(l_{p1}) = 1$ are compressed in an appropriate way in order to minimize the number of terms in (54).

Acknowledgements

The authors would like to acknowledge the financial support of the FPU program offered by the Ministerio de Educación, Cultura y Deporte under grant number (FPU13/04191). The funding from Generalitat Valenciana (PROMETEO/2012/023) are also acknowledged.

References

[1] S. Bruni, J. Ambrósio, A. Carnicero, Y. H. Cho, L. Finner, M. Ikeda, S. Y. Kwon, J. P. Massat, S. Stichel, M. Tur, *et al.*, "The results of the pantograph–catenary interaction benchmark," *Vehicle System Dynamics*, vol. 53, no. 3, pp. 412–435, 2015. 1

[2] M. Tur, L. Baeza, F. J. Fuenmayor, and E. García, "PACDIN statement of methods," *Vehicle System Dynamics*, vol. 53, no. 3, pp. 402–411, 2015. 1

[3] A. Facchinetti and S. Bruni, "Special issue on the pantograph–catenary interaction benchmark," *Vehicle System Dynamics*, vol. 53, no. 3, pp. 303–304, 2015. 1

[4] W. Zhang, G. Mei, and J. Zeng, "A study of pantograph/catenary system dynamics with influence of pre-sag and irregularity of contact wire," *Vehicle System Dynamics*, vol. 37, pp. 593–604, 2002. 1

[5] Y. H. Cho, K. Lee, Y. Park, B. Kang, and K. N. Kim, "Influence of contact wire pre-sag on the dynamics of pantograph–railway catenary," *International Journal of Mechanical Sciences*, vol. 52, no. 11, pp. 1471–1490, 2010. 1

[6] A. Ammar, B. Mokdad, F. Chinesta, and R. Keunings, "A new family of solvers for some classes of multidimensional partial differential equations encountered in kinetic theory modelling of complex fluids," *Journal of Non-Newtonian Fluid Mechanics*, vol. 144, no. 2-3, pp. 98–121, 2007. 1

[7] B. Bognet, A. Leygue, and F. Chinesta, "On the fully 3D simulations of thermoelastic models defined in plate and shell geometries," *European Journal of Computational Mechanics/Revue Européenne de Mécanique Numérique*, vol. 21, no. 1-2, pp. 40–51, 2012. 1

[8] B. Bognet, A. Leygue, and F. Chinesta, "Separated representations of 3D elastic solutions in shell geometries," *Advanced Modeling and Simulation in Engineering Sciences*, vol. 1, pp. 1–4, 2014. 1

[9] A. Ammar, A. Huerta, F. Chinesta, E. Cueto, and A. Leygue, "Parametric solutions involving geometry: A step towards efficient shape optimization," *Computer Methods in Applied Mechanics and Engineering*, vol. 268, pp. 178–193, 2014. 1, 5.1

[10] F. Chinesta, A. Ammar, A. Leygue, and R. Keunings, "An overview of the proper generalized decomposition with applications in computational rheology," *Journal of Non-Newtonian Fluid Mechanics*, vol. 166, no. 11, pp. 578–592, 2011. 1, 5.1

[11] E. Giner, B. Bognet, J. J. Ródenas, A. Leygue, F. J. Fuenmayor, and F. Chinesta, "The Proper Generalized Decomposition (PGD) as a numerical procedure to solve 3D cracked plates in linear elastic fracture mechanics," *International Journal of Solids and Structures*, vol. 50, no. 10, pp. 1710–1720, 2013. 1

[12] S. Niroomandi, D. González, I. Alfaro, F. Bordeu, A. Leygue, E. Cueto, and F. Chinesta, "Real-time simulation of biological soft tissues: a pgd approach," *International Journal for Numerical Methods in Biomedical Engineering*, vol. 29, no. 5, pp. 586–600, 2013. 1

[13] S. Niroomandi, I. Alfaro, D. González, E. Cueto, and F. Chinesta, "Model order reduction in hyperelasticity: a proper generalized decomposition approach," *International Journal for Numerical Methods in Engineering*, pp. 129–149, 2013. 1

[14] L. Boucinha, A. Gravouil, and A. Ammar, "Space-time proper generalized decompositions for the resolution of transient elastodynamic models," *Computer Methods in Applied Mechanics and Engineering*, vol. 255, pp. 67–88, 2013. 1

[15] J. Almeida, "A basis for bounding the errors of proper generalised decomposition solutions in solid mechanics," *International Journal for Numerical Methods in Engineering*, vol. 94, no. 10, pp. 961–984, 2013. 1

[16] F. Chinesta, R. Keunings, and A. Leygue, *The Proper Generalized Decomposition for Advanced Numerical Simulations: A Primer*. Springer Publishing Company, Incorporated, 2013. 1

[17] M. Tur, E. García, L. Baeza, and F. J. Fuenmayor, "A 3D absolute nodal coordinate finite element model to compute the initial configuration of a railway catenary," *Engineering Structures*, vol. 71, pp. 234–243, 2014. 3, 4

[18] A. Shabana, "Computer implementation of the absolute nodal coordinate formulation for flexible multibody dynamics," *Nonlinear Dynamics*, vol. 16, pp. 293–306, 1998. 3

[19] M. Berzeri and A. Shabana, "Development of simple models for the elastic forces in the absolute nodal coordinate formulation," *Journal of Sound and Vibration*, vol. 235, no. 4, pp. 539–565, 2000. 3, 4

[20] J. H. Seo, H. Sugiyama, and A. A. Shabana, "Three-dimensional large deformation analysis of the multibody pantograph/catenary systems," *Nonlinear Dynamics*, vol. 42, no. 2, pp. 199–215, 2005. 3

[21] J. H. Lee and T. W. Park, "Development of a three-dimensional catenary model using cable elements based on absolute nodal coordinate formulation," *Journal of Mechanical Science and Technology*, vol. 26, no. 12, pp. 3933–3941, 2012. 3

[22] I. Romero, "A comparison of finite elements nonlinear beams: the absolute nodal coordinate and geometrically exact formulations," *Multibody System Dynamics*, vol. 20, pp. 51–68, 2008. 3

[23] J. Gerstmayr and A. A. Shabana, "Analysis of thin beams and cables using the absolute nodal coordinate formulation," *Nonlinear Dynamics*, vol. 45, no. 1-2, pp. 109–130, 2006. 3

[24] A. Goetz, *Introduction to differential geometry*. Addison Wesley Publishing Company, 1970. 4

[25] F. Chinesta, A. Leygue, F. Bordeu, J. Aguado, E. Cueto, D. González, I. Alfaro, A. Ammar, and A. Huerta, "PGD-based computational vademecum for efficient design, optimization and control," *Archives of Computational Methods in Engineering*, vol. 20, no. 1, pp. 31–59, 2013. 5.1, 5.1

[26] F. Chinesta, R. Keunings, and A. Leygue, *The proper generalized decomposition for advanced numerical simulations: A primer*. Springer Science & Business Media, 2013. 5.1, 5.1, 5.1

[27] E. Nadal, F. Chinesta, P. Díez, F. Fuenmayor, and F. Denia, "Real time parameter identification and solution reconstruction from experimental data using the Proper Generalized Decomposition," *Computer Methods in Applied Mechanics and Engineering*, vol. 296, pp. 113–128, 2015. 5.1

PAPER B

Fast simulation of the pantograph-catenary dynamic interaction

S. Gregori, M. Tur, E. Nadal, J. V. Aguado, F. J. Fuenmayor and F. Chinesta

Finite Elements in Analysis and Design
Volume 129, Pages 1–13, 2017
DOI: 10.1016/j.finel.2017.01.007

Abstract

Simulation of the pantograph-catenary dynamic interaction has now become a useful tool for designing and optimizing the system. In order to perform accurate simulations, including system non-linearities, the Finite Element Method is commonly employed combined with a time integration scheme, even though the computational time required may be longer than with the use of other simpler approaches. In this paper we propose a two-stage methodology (*Offline/Online*) which notably reduces the computational cost without any loss in accuracy and makes it possible to successfully carry out very efficient optimizations or even Hardware in the Loop simulations with real-time requirements.

Key words

Catenary; Pantograph, Efficient simulation; Real-time simulations

Contents

1 Introduction **113**

2 Catenary and pantograph models **114**
2.1 Catenary model 114
2.2 Pantograph model 116
2.3 Interaction model 117

3 Static equilibrium configuration **117**

4 Dynamic interaction problem **119**
4.1 Direct time integration procedure 122
4.2 Modified time integration procedures 125
4.3 *Offline/Online* time integration methodology 126
4.3.1 *Offline* stage 126
4.3.2 *Online* stage 128

5 Numerical examples **132**
5.1 Hypothesis verification 132
5.2 Computation time study 136

6 Conclusions **137**

A The HHT time integration method **138**

B List of symbols **139**

Bibliography **141**

1. Introduction

The catenary provides the energy supply to railway locomotives through contact with the pantograph. This overhead equipment is composed of structural elements such as masts, brackets and registration arms that hold the contact wire in the desired position. However, other cables form part of the catenary. These include the messenger wire, which is hooked to the brackets, and the droppers, which suspend the contact wire from the messenger wire.

Current collection quality is vital for good performance and is usually measured by the pantograph-catenary interaction force. High contact forces cause high levels of wear on the sliding surfaces [1], while contact losses produce arcing and cut out the energy supply to the engines [2], limiting the operational railway speed. This means numerical simulations can be very useful in the design of improved pantographs and overhead equipment.

In recent decades a lot of effort has been put into the simulation of the pantograph-catenary dynamic interaction (see [3] and the references therein), and has triggered European projects (EUROPAC) and regulation in the field [4] (UNE 50318). Starting with very simple models [5, 6], the Finite Element Method (FEM) now seems to be the most suitable approach for modelling the overhead line [7]. Pantograph mathematical modelling ranges from linear lumped parameter models to flexible multibody models [8].

Computational cost is always an issue if simulations have to be performed several times as occurs in optimization procedures. In the catenary–pantograph field some authors have proposed simplified catenary models [9], modal decomposition approaches [10], models based on moving meshes [11] or even *a priori* model order reduction techniques [12] in order to reduce the computational effort. However, the common feature of all these approaches is that they are less accurate than the full FE models.

At the present time, hybrid or Hardware In the Loop (HIL) simulations are another field in which the computational cost is crucial. The main requirement of such approaches is a numerical model that can be solved in real-time. A wide range of applications can be found in many fields, such as in earthquake engineering [13], electronic engineering [14] and railway mechanics [15] to cite just a few. When testing pantographs, it is advisable to have an accurate catenary model. Although HIL simulation techniques have been implemented for pantograph-catenary dynamic interaction (see the pioneering works [10, 16]), even though they all achieve real-time performance, a somewhat simplified catenary model with a modal approach is generally used.

This paper aims to provide a realistic model of the pantograph-catenary dynamic interaction that can be solved efficiently without losing any of the accuracy achieved

by classical FE techniques. The computational cost saves can be exploited to perform efficient optimizations and furthermore, the method is suitable to be used in HIL simulations if real-time response is achieved. Extending on the idea first introduced by Collina and Bruni in [17] and used by Ambrósio et al. in [18], in which the nonlinearities of the model are moved to the right hand side of the equation of motion, the main novelty of the method proposed here relies on pre-calculating as much information as possible in an *Offline* stage. In this phase of the calculations, the catenary is treated as a linear system, and then in the subsequent *Online* stage the nonlinearities introduced by dropper slackening and loss of pantograph-catenary contact are dealt with. The pre-calculated information makes it possible to obtain the total system response by solving a system with a small set of unknowns, which notably reduces the computational cost required for the time integration.

The paper is organized as follows. After this brief introduction, the numerical models chosen for the different subsystems are described in the next section. The static equilibrium formulation is a requirement for the dynamic simulation and is detailed in Section 3. In Section 4 we explain in detail the dynamic interaction problem. The features of the new *Offline/Online* approach are deduced from what we call the classical time integration procedure and its modified versions. Some numerical examples are given in Section 5 to validate the assumed hypotheses and also to show the saving in simulation time of the proposed method. Finally, we provide some concluding remarks in Section 6.

2. Catenary and pantograph models

In this section we describe all the models used to perform the numerical simulations of the pantograph–catenary dynamic interaction. There are three different subsystems which need to be modelled: the catenary, the pantograph and the interaction between these two subsystems.

2.1. Catenary model

Among the different options found in the literature, the FEM is the method most frequently used to model realistic catenary behaviour. In the present work the catenary cables are modelled by a beam element based on the Absolute Nodal Coordinate Formulation (ANCF) first proposed by Shabana [19] and adapted for thin beams and cables in [20]. This formulation has also been used by other authors for rail-

way catenary models [21, 22]. The interested reader is referred to [23, 24] for detailed comparisons between the ANCF element and those based on the classical formulation.

For very slender beams like catenary cables, the ANCF element has only 6 degrees of freedom per node in 3D, taking into account axial and bending deformations. Hereinafter, this type of element is referred as 'cable element' and is used to model both the messenger and the contact wires. Droppers and registration arms are modelled as a single large displacement non-linear element, known as the 'bar element' throughout the paper.

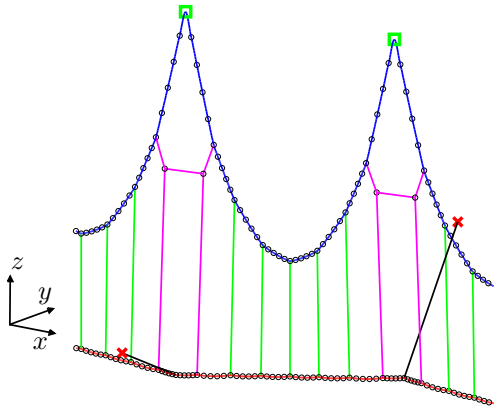

Figure 1: FE catenary model with boundary conditions.

All the supports are replaced by suitable boundary conditions. The displacements at the ends of the registration arms joined to the brackets (nodes marked with a cross in Fig. 1) are constrained.

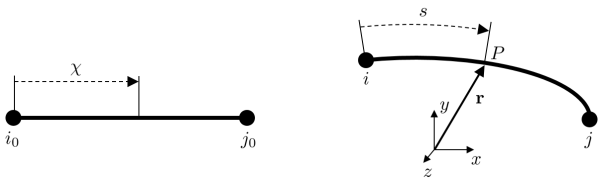

Figure 2: Reference and deformed configurations of the ANCF element.

In Fig. 2 the reference and deformed configurations for a cable element is schematically represented. The vector of degrees of freedom for an element with nodes i and j is:

$$\mathbf{q}_c = \left[\begin{array}{cccccccccccc} x_i & y_i & z_i & \frac{\partial x_i}{\partial \chi} & \frac{\partial y_i}{\partial \chi} & \frac{\partial z_i}{\partial \chi} & x_j & y_j & z_j & \frac{\partial x_j}{\partial \chi} & \frac{\partial y_j}{\partial \chi} & \frac{\partial z_j}{\partial \chi} \end{array} \right]^T \tag{1}$$

where $\chi \in [0, l_{ref}]$ is the local coordinate, l_{ref} is the initial length of the element, x_i, y_i, z_i are the coordinates of node i and $\frac{\partial x_i}{\partial \chi}$, $\frac{\partial y_i}{\partial \chi}$, $\frac{\partial z_i}{\partial \chi}$ are the slopes. In a deformed configuration, the absolute position at a given point with local coordinate χ is defined by means of a cubic Hermitian interpolation that can be written as:

$$\mathbf{r}(\chi) = \mathbf{N}_c(\chi)\, \mathbf{q}_c \tag{2}$$

where

$$\begin{gathered} \mathbf{N}_c(\chi) = [N_{c1}\mathbf{I}_3 | N_{c2}\mathbf{I}_3 | N_{c3}\mathbf{I}_3 | N_{c4}\mathbf{I}_3] \\ N_{c1}(\xi) = 1 - 3\xi^2 + 2\xi^3 \quad N_{c2}(\xi) = l_{ref}(\xi - 2\xi^2 + \xi^3) \\ N_{c3}(\xi) = 3\xi^2 - 2\xi^3 \qquad N_{c4}(\xi) = l_{ref}(-\xi^2 + \xi^3) \end{gathered} \tag{3}$$

The coordinate $\xi = \chi / l_{ref} \in [0, 1]$ denotes the normalized local coordinate and $\mathbf{I}_3$ is the 3×3 identity matrix. The C^1 continuity of the solution between elements is guaranteed with this interpolation. The degrees of freedom of a bar element are the absolute positions of the two nodes of the element only, namely:

$$\mathbf{q}_b = \begin{bmatrix} x_i & y_i & z_i & x_j & y_j & z_j \end{bmatrix}^T \tag{4}$$

In these elements, as no bending deformations are taken into account, a linear interpolation is enough to ensure continuity of the solution,

$$\begin{gathered} \mathbf{N}_b(\chi) = [N_{b1}\mathbf{I}_3 | N_{b2}\mathbf{I}_3] \\ N_{b1}(\xi) = -\frac{\xi - 1}{2} \quad N_{b2}(\xi) = \frac{\xi + 1}{2} \end{gathered} \tag{5}$$

For simplicity in the notation, subscripts c and b will not appear henceforth unless necessary.

2.2. Pantograph model

A number of accurate pantograph models can be found in the bibliography. Although these models are based on FEM or multibody approaches [8, 25] and are able to account for deformable bodies, the most widely used pantograph model in the literature is a lumped mass model with 2 or 3 vertical degrees of freedom. We have assumed a model with 3 masses, which is depicted in Fig. 3.

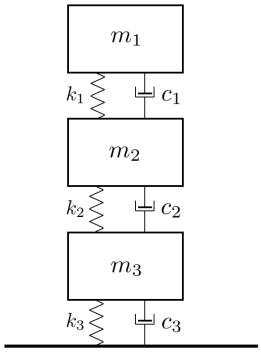

Figure 3: Lumped mass pantograph model.

2.3. Interaction model

In order to model the pantograph-catenary interaction, approaches like the imposition of unilateral constraints by Lagrange multipliers [26] or an Hertzian type contact force with internal damping [27] are found in the literature. However, in this work the pantograph-catenary interaction is simulated by a simple and widely used penalty method. This method introduces a high stiffness elastic element which connects the pantograph head with the contact wire in order to accomplish the impenetrability constraint. A scheme of this type of interaction is represented in Fig. 4. According to the reference model in [4], the value of the penalty constant is set at $k_h = 50000\,\mathrm{N/m}$. The contact or interaction force vector is assumed to be oriented vertically and its value can be computed as:

$$f_i = \begin{cases} k_h(z_1 - z_{cw}) & \text{if} \quad z_1 \geq z_{cw} \\ 0 & \text{if} \quad z_1 < z_{cw} \end{cases} \tag{6}$$

where z_1 and z_{cw} are the vertical absolute coordinates of the upper mass of the pantograph and the contact point on the contact wire respectively.

3. Static equilibrium configuration

As in any cable structure, the first step in the simulation consists of solving the so-called *shape finding* problem. During catenary stringing certain constraints must

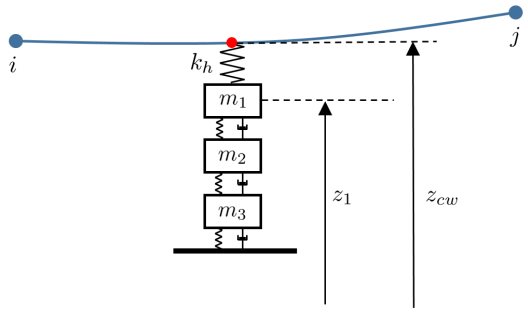

Figure 4: Pantograph–catenary interaction scheme.

be fulfilled by the cabling. In the problem at hand, the main constraints are the initial tensions of the messenger and contact wires, contact wire height and the separation between droppers. In this initial configuration problem, the non-deformed element lengths and the nodal degrees of freedom are therefore set as the unknowns. A detailed explanation of this problem is thoroughly discussed in [28].

Here we assume that the undeformed element lengths are known and that Ω represents the spatial domain of the catenary. This domain is discretized into N_e non-overlapping elements with a domain Ω^e that fulfil $\Omega = \bigcup_{e=1}^{N_e} \Omega^e$. The virtual work principle states that the virtual work produced by the internal forces must be equal to the virtual work produced by the external ones,

$$\sum_{e=1}^{N_e} \delta W_{int}^e - \delta W_{ext}^e = 0 \tag{7}$$

For a certain element e belonging to a cable with cross-sectional area A, Young's modulus E and second moment of area I, the internal virtual work is produced by a combination of axial and bending strains:

$$\delta W_{int}^e = \int_{\Omega^e} \left(EA\delta\varepsilon_a\, \varepsilon_a + EI\delta\kappa\, \kappa \right) d\chi \tag{8}$$

where ε_a is the axial strain and κ is the curvature. During catenary stringing, the cables undergo large displacements, so that a non-linear measure of the deformation is required. Using the Green strain tensor, the axial deformation is defined as:

$$\varepsilon_a = \frac{1}{2}\left(\frac{d\mathbf{r}}{d\chi} \cdot \frac{d\mathbf{r}}{d\chi} - 1 \right) \tag{9}$$

Since the cables undergo small deformations, we can assume $ds \approx d\chi$ and therefore curvature can be approximated by [29]:

$$\kappa \approx \left| \frac{d^2\mathbf{r}}{d\chi^2} \right| \tag{10}$$

The only external force applied to the system is the force of gravity. The virtual work produced by this force is:

$$\delta W^e_{ext} = \int_{\Omega^e} \delta\mathbf{r} \cdot \mathbf{g} d\chi \tag{11}$$

where the vector $\mathbf{g} = [0 \ 0 \ -gA\rho]^T$, while g is the gravitational constant and ρ is the density of the cable. By combining all the previous expressions, the static equilibrium problem consists of finding the field $\mathbf{r}(\chi)$ for any admissible $\delta\mathbf{r}$, such that:

$$\sum_{e=1}^{N_e} \int_{\Omega^e} \left[EI \frac{d^2\delta\mathbf{r}}{d\chi^2} \cdot \frac{d^2\mathbf{r}}{d\chi^2} + \frac{EA}{2} \frac{d\delta\mathbf{r}}{d\chi} \cdot \frac{d\mathbf{r}}{d\chi} \left(\frac{d\mathbf{r}}{d\chi} \cdot \frac{d\mathbf{r}}{d\chi} - 1 \right) - \delta\mathbf{r} \cdot \mathbf{g} \right] d\chi = 0, \quad \forall \delta\mathbf{r} \tag{12}$$

where the first term related with bending strain vanishes for the bar elements since $I = 0$ for them.

After the assembly process, taking into account all the Dirichlet boundary conditions, the non-linear algebraic system of equations

$$\mathbf{f}_{int}(\mathbf{q}) - \mathbf{f}_{ext} = \mathbf{0} \tag{13}$$

is obtained, which can be solved using for example the Newton-Raphson method.

4. Dynamic interaction problem

Catenary

The dynamic behaviour of the catenary system is characterized by the small cable displacements. A common assumption is to linearise the dynamic problem with respect to the static equilibrium position of the catenary cables.

Once the static equilibrium position of the catenary cabling $\mathbf{r}_0$ has been calculated by solving Eq. (12), a new absolute position $\mathbf{r} = [x \ y \ z]^T$ can be computed as $\mathbf{r} = \mathbf{r}_0 + \mathbf{u}$, where $\mathbf{u} = [u \ v \ w]^T$ are the displacements with respect to the static equilibrium position. Note that subscript 0 refers to the configuration for which the system has been linearised.

If Eq. (12) is linearised and we add the inertial term, the linear dynamic problem for the catenary consists of finding $\mathbf{u}$ for any compatible $\delta\mathbf{u}$ such that:

$$\begin{aligned} \sum_{e=1}^{N_e} \int_{\Omega^e} \Bigg[\rho A \delta\mathbf{u} \cdot \ddot{\mathbf{u}} + EI \frac{d^2\delta\mathbf{u}}{d\chi^2} \cdot \frac{d^2\mathbf{u}}{d\chi^2} + \frac{EA}{2} \frac{d\delta\mathbf{u}}{d\chi} \cdot \Bigg[2\frac{d\mathbf{r}_0}{d\chi} \left(\frac{d\mathbf{u}}{d\chi} \cdot \frac{d\mathbf{r}_0}{d\chi} \right) + \\ \frac{d\mathbf{u}}{d\chi} \left(\frac{d\mathbf{r}_0}{d\chi} \cdot \frac{d\mathbf{r}_0}{d\chi} - 1 \right) \Bigg] \Bigg] d\chi = 0, \qquad \forall \delta\mathbf{u} \end{aligned} \tag{14}$$

Introducing the interpolations defined in Section 2.1 for each type of element, the mass and stiffness matrices of the catenary are:

$$\begin{aligned}\mathbf{M}_{cat} &= \mathsf{A}_e \int_{\Omega^e} \rho A \mathbf{N}^T \mathbf{N}\, d\chi \\ \mathbf{K}_{cat} &= \mathsf{A}_e \int_{\Omega^e} \Big[EI \mathbf{N}^{''T} \mathbf{N}^{''} + EA \left(\left(\mathbf{N}^{'T} \mathbf{N}^{'} \mathbf{q}_0 \right) \left(\mathbf{q}_0^T \mathbf{N}^{'T} \mathbf{N}^{'} \right) + \right. \\ &\qquad \left. \frac{1}{2} \left(\mathbf{N}^{'T} \mathbf{N}^{'} \right) \left(\mathbf{q}_0^T \mathbf{N}^{'T} \mathbf{N}^{'} \mathbf{q}_0 \right) - \frac{1}{2} \mathbf{N}^{'T} \mathbf{N}^{'} \right) \Big] d\chi \end{aligned} \tag{15}$$

where A is the assembly operator, $\mathbf{N}$ is the shape functions matrix for both cable and bar elements whose derivatives are $\mathbf{N}^{'} = \frac{d\mathbf{N}}{d\chi}$ and $\mathbf{N}^{''} = \frac{d^2\mathbf{N}}{d\chi^2}$.

In addition to this linearisation, if we analyse Eq. (14) in more detail, another simplification can be introduced for the dropper elements. The vector $\frac{d\mathbf{r}_0}{d\chi} = \mathbf{n}_d$ has the direction of the dropper in the configuration in which the problem has been linearised (i.e. the static equilibrium position) and its modulus is $\frac{l_0}{l_{ref}}$. Therefore, the virtual work produced by axial strains can be decomposed into two terms. For a single dropper element, the first of them reads:

$$\int_{\Omega^e} EA \left(\frac{d\delta\mathbf{u}}{d\chi} \cdot \mathbf{n}_d \right) \left(\frac{d\mathbf{u}}{d\chi} \cdot \mathbf{n}_d \right) d\chi = \int_{\Omega^e} EA \left(\frac{l_0}{l_{ref}} \right)^2 \frac{d\delta\mathbf{u}}{d\chi} \left(\hat{\mathbf{n}}_d \otimes \hat{\mathbf{n}}_d \right) \frac{d\mathbf{u}}{d\chi}\, d\chi \tag{16}$$

where the unitary vector $\hat{\mathbf{n}}_d = \frac{\mathbf{n}_d}{\|\mathbf{n}_d\|}$. The second term is:

$$\begin{aligned}\int_{\Omega^e} \frac{EA}{2} \frac{d\delta\mathbf{u}}{d\chi} \cdot \frac{d\mathbf{u}}{d\chi} \left(\left(\frac{l_0}{l_{ref}} \right)^2 - 1 \right) d\chi = \int_{\Omega^e} EA\varepsilon_{a,0} \frac{d\delta\mathbf{u}}{d\chi} \cdot \frac{d\mathbf{u}}{d\chi} d\chi = \\ \int_{\Omega^e} T_0 \frac{d\delta\mathbf{u}}{d\chi} \cdot \frac{d\mathbf{u}}{d\chi}\, d\chi \end{aligned} \tag{17}$$

where $\varepsilon_{a,0}$ and T_0 are the axial strain and the tension in the static equilibrium position respectively.

If $T_0 \ll EA \left(\frac{l_0}{l_{ref}} \right)^2$, the components of (17) aligned with the dropper can be neglected. Furthermore, assuming that the movements in the perpendicular directions to the dropper are small (what is not applicable for the messenger and contact wires), the fully contribution of the term (17) is negligible and therefore, the simplified stiffness matrix for a dropper element is:

$$\mathbf{k}_d = \int_{\Omega^e} EA \left(\frac{l_0}{l_{ref}} \right)^2 \mathbf{N}_b^{'T} \hat{\mathbf{n}}_d^T\, \hat{\mathbf{n}}_d \mathbf{N}_b^{'}\, d\chi \tag{18}$$

Once the inertial and elastic properties of the catenary have been defined, proportional Rayleigh damping is also introduced. This leads to a catenary damping matrix

$\mathbf{C}_{cat} = \alpha_r \mathbf{M}_{cat} + \beta_r \mathbf{K}_{cat}$, where α_r and β_r are the damping parameters. Finally, the matrix form of the linear dynamic equations of the catenary system is:

$$\mathbf{M}_{cat}\ddot{\mathbf{u}}_{cat} + \mathbf{C}_{cat}\dot{\mathbf{u}}_{cat} + \mathbf{K}_{cat}\mathbf{u}_{cat} = \mathbf{0} \tag{19}$$

Pantograph

The lumped mass model chosen for the pantograph is linear and it only introduces vertical degrees of freedom. Applying the Lagrange equation of motion to the system, we obtain:

$$\begin{aligned} m_1\ddot{w}_1 + c_1(\dot{w}_1 - \dot{w}_2) + k_1(w_1 - w_2) &= 0 \\ m_2\ddot{w}_2 + c_1(\dot{w}_2 - \dot{w}_1) + c_2(\dot{w}_2 - \dot{w}_3) + k_1(w_2 - w_1) + k_2(w_2 - w_3) &= 0 \\ m_3\ddot{w}_3 + c_2(\dot{w}_3 - \dot{w}_2) + c_3\dot{w}_3 + k_2(w_2 - w_3) + k_3 w_3 &= F_{pan} \end{aligned} \tag{20}$$

where w_i, $i = 1, 2, 3$ denotes the displacement of the lumped masses with respect to the equilibrium position z_{ref}. This position is defined as the z_0 (third component of $\mathbf{r}_0$) coordinate of the initial interaction point in the catenary (see Fig. 4). F_{pan} is the external uplift force applied to the mass 3 of the pantograph. Besides, all three masses of the pantograph are assumed to be in equilibrium at z_{ref}. In matrix form, the previous equations become:

$$\mathbf{M}_{pan}\ddot{\mathbf{w}}_{pan} + \mathbf{C}_{pan}\dot{\mathbf{w}}_{pan} + \mathbf{K}_{pan}\mathbf{w}_{pan} = \mathbf{F}_{pan} \tag{21}$$

Interaction

The interaction force f_i depends on the position of mass 1 z_1 and the contact wire height z_{cw} which varies as the train moves. Using a penalty method, the virtual work produced by the interaction force is:

$$\delta z_i \, f_i = (\delta z_1 - \delta z_{cw}) k_h (z_1 - z_{cw}) = (\delta w_1 - \delta w_{cw}) k_h (z_{ref} + w_1 - z_{0,cw} - w_{cw}) \tag{22}$$

where k_h is the penalty constant defined in Section 2.3. The subindex cw shows that the variable is particularized at the interaction point on the contact wire. From now on, if one variable requires more than one subindex they will be separated by a comma.

From Eq. (22), the interaction stiffness matrix, which couples the catenary and pantograph degrees of freedom, is:

$$\mathbf{k}_i = \begin{pmatrix} \mathbf{k}_{i,cc} & \mathbf{k}_{i,cp} \\ \mathbf{k}_{i,pc} & k_{i,pp} \end{pmatrix} = k_h \left(\begin{array}{cccc|c} N_{c1}^2 & N_{c1}N_{c2} & N_{c1}N_{c3} & N_{c1}N_{c4} & -N_{c1} \\ N_{c2}N_{c1} & N_{c2}^2 & N_{c2}N_{c3} & N_{c2}N_{c4} & -N_{c2} \\ N_{c3}N_{c1} & N_{c3}N_{c2} & N_{c3}^2 & N_{c3}N_{c4} & -N_{c3} \\ N_{c4}N_{c1} & N_{c4}N_{c2} & N_{c4}N_{c3} & N_{c4}^2 & -N_{c4} \\ \hline -N_{c1} & -N_{c2} & -N_{c3} & -N_{c4} & 1 \end{array} \right) \tag{23}$$

where all the shape functions are evaluated in the local coordinate of the contact wire cable element particularized at the interaction point. Furthermore, a force that only depends on the static equilibrium position from Eq. (22) has also to be considered:

$$\mathbf{s}_i = [\mathbf{s}_{i,cc} \;\; s_{i,pp}]^T = k_h(z_{ref} - z_{0,cw})\,[-N_{c1} \;\; -N_{c2} \;\; -N_{c3} \;\; -N_{c4} \;\mid\; 1]^T \tag{24}$$

At this point, all the matrices are available to be combined, leading to the semidiscrete dynamic equations of the whole system. If the global vector of displacements is defined as $\mathbf{u} = [\mathbf{u}_{cat} \; \mathbf{w}_{pan}]^T$, and the different matrices $\mathbf{m}$, $\mathbf{c}$, $\mathbf{k}$, $\mathbf{f}$ and $\mathbf{s}$ presented above are assembled, the dynamic equation of the global system is:

$$\mathbf{M}\ddot{\mathbf{u}} + \mathbf{C}\dot{\mathbf{u}} + \mathbf{K}\mathbf{u} = \mathbf{F} \tag{25}$$

where:

$$\begin{aligned}
\mathbf{M} &= \begin{pmatrix} \mathbf{M}_{cat} & \mathbf{0} \\ \mathbf{0} & \mathbf{M}_{pan} \end{pmatrix} \\
\mathbf{C} &= \begin{pmatrix} \mathbf{C}_{cat} & \mathbf{0} \\ \mathbf{0} & \mathbf{C}_{pan} \end{pmatrix} \\
\mathbf{K} &= \begin{pmatrix} \mathbf{K}_{cat} & \mathbf{0} \\ \mathbf{0} & \mathbf{K}_{pan} \end{pmatrix} + \begin{pmatrix} \mathbf{K}_{i,cc} & \mathbf{K}_{i,cp} \\ \mathbf{K}_{i,pc} & \mathbf{K}_{i,pp} \end{pmatrix} \\
\mathbf{F} &= \begin{pmatrix} \mathbf{0} \\ \mathbf{F}_{pan} \end{pmatrix} - \begin{pmatrix} \mathbf{S}_{i,cc} \\ \mathbf{S}_{i,pp} \end{pmatrix}
\end{aligned} \tag{26}$$

and the capital letters denote that the variable has been expanded to the global size.

The initial conditions necessary to begin the time integration are now obtained by solving the small displacements linearised problem with the uplift force $\mathbf{F}_{pan}$ as external force. Hence, $\mathbf{u}^0$ is found after solving the linear system of equations $\mathbf{K}\mathbf{u}^0 = \mathbf{F}$. When the pantograph pushes up the catenary some droppers may be compressed. In order to consider the effect of dropper slackening we apply here the same iterative procedure as will be explained in Section 4.1. Finally, since the whole system is at rest at the initial time, $\dot{\mathbf{u}}^0$ and $\ddot{\mathbf{u}}^0$ are null.

4.1. Direct time integration procedure

In order to solve Eq. (25) and therefore obtain the displacements, velocities and accelerations of the whole system, we use the Hilber-Hughes-Taylor (HHT) time integration scheme [30]. This time integrator can be seen as a generalization of the well-known Newmark method. It uses a constant time step Δt and some parameters

α, β and γ which control the stability and the numerical damping introduced by the method.

We assume a bilinear behaviour of the droppers, as shown in Fig. 5, where the force-elongation curve for a dropper d of the linearised catenary is depicted. In this figure, f_d represents the internal force of the dropper while s_d is the value of its traction force in the static equilibrium configuration, i.e. in the configuration in which the equations are linearised. The horizontal axis denotes the elongation of the dropper, $\delta_{0,d}$ being the value of elongation at the static equilibrium position. It is also shown that in traction the dropper presents stiffness k_d, while in compression it is null.

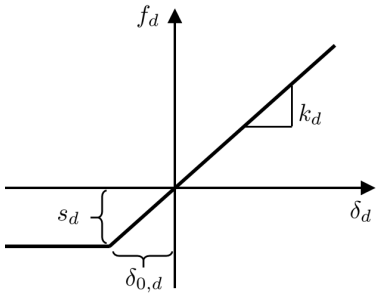

Figure 5: Force-elongation curve for dropper d in the linearised problem.

This bilinear behaviour requires the use of an iterative scheme in order to obtain the solution in each time step. Moreover, an additional non-linearity appears from the fact that the pantograph can be detached from the contact wire with the interaction force vanishing. By applying the HHT algorithm to Eq. (25), as described in A, the displacements at time step t, $t = 1, ..., N_{stp}$, and iteration j are obtained by solving the following linear system of equations:

$$\mathbf{A}_j^t \mathbf{u}_j^t = \mathbf{b}_j^t \tag{27}$$

where

$$\begin{aligned} \mathbf{A}_j^t &= \left[(1+\alpha)\left[\mathbf{K}_j^t + b_4 \mathbf{C}_j^t\right] + b_1 \mathbf{M}\right] \\ \mathbf{b}_j^t &= -\alpha \mathbf{F}^{t-1} + (1+\alpha)\mathbf{F}_j^t + \mathbf{F}_{IC}^t \end{aligned} \tag{28}$$

being

$$\begin{aligned} \mathbf{F}_{IC}^t = \alpha \left(\mathbf{K}^{t-1}\mathbf{u}^{t-1} + \mathbf{C}^{t-1}\dot{\mathbf{u}}^{t-1}\right) + \mathbf{M}\left(b_1 \mathbf{u}^{t-1} - b_2 \dot{\mathbf{u}}^{t-1} - b_3 \ddot{\mathbf{u}}^{t-1}\right) + \\ (1+\alpha)\mathbf{C}_j^t \left(b_4 \mathbf{u}^{t-1} - b_5 \dot{\mathbf{u}}^{t-1} - b_6 \ddot{\mathbf{u}}^{t-1}\right) \end{aligned} \tag{29}$$

All the b_i, $i = 1, ..., 6$ depend on the time step and the method's parameters α, β and γ.

Once $\mathbf{u}_j^t$ has been obtained we have to evaluate the state of any dropper. The internal force at node n of dropper d is $\mathbf{f}_{d,j}^t = \left[\mathbf{k}_d \mathbf{u}_{d,j}^t\right]_n$, where the operator $[\cdot]_n$ selects only the components of the force applied at the node n of the dropper. This vector is aligned with $\mathbf{s}_d$ due to the use of the simplified stiffness matrix considered in (18). Projecting it in the direction of dropper d in the static equilibrium configuration $\mathbf{n}_d$ (which is equivalent to calculating its modulus) we obtain $f_{d,j}^t$. The slackening criterion is then:

$$\begin{aligned} &\text{if } f_{d,j}^t + s_d \leq 0 \text{ then dropper } d \text{ is slackened} \\ &\text{if } f_{d,j}^t + s_d > 0 \text{ then dropper } d \text{ is tensioned} \end{aligned} \tag{30}$$

from which the slackening state $\mathcal{D}$ is defined.

The elemental stiffness $\mathbf{k}_d$ and damping $\mathbf{c}_d$ matrices of the slackened droppers have to be removed from the global ones, and also the internal force of the element in the static equilibrium position must be included in the next iteration $j+1$ in order to account for this state change. Then the given changes are:

$$\begin{aligned} \mathbf{K}_{j+1}^t &= \mathbf{K}^t - \sum_d^{N_{sd}} \mathbf{K}_d \\ \mathbf{C}_{j+1}^t &= \mathbf{C}^t - \sum_d^{N_{sd}} \mathbf{C}_d \\ \mathbf{F}_{j+1}^t &= \mathbf{F}^t + \sum_d^{N_{sd}} \mathbf{S}_d \end{aligned} \tag{31}$$

where N_{sd} is the total number of slackened droppers. These modifications imply changes in both, the global time-step matrix $\mathbf{A}_j^t$ and the right hand side of Eq. (27) $\mathbf{b}_j^t$ at every iteration.

Before moving to the next iteration, the value of the interaction force f_i must be obtained from Eq. (22) and then we enforce the contact loss criterion which defines the state $\mathcal{C}$. This consists of setting the contact force to 0 if its value is negative, i.e. if there is contact loss, or leaving it unchanged otherwise.

Now we are ready to start the next iteration $j+1$, compute $\mathbf{u}_{j+1}^t$, check the slackening criterion on each dropper, recalculate the interaction force and apply the contact loss criterion. This iterative procedure is schematized in Algorithm 1. It keeps going until the dropper slackening state $\mathcal{D}$ and the contact loss state $\mathcal{C}$ are identical in two consecutive iterations. When this happens, we can also move to the next time step $t+1$.

The main feature of this direct approach is that a different system of equations of the global problem size is solved several times in each time step, which requires a significant computational effort. Another disadvantage of this method emerges when

changes in the pantograph model are studied, because it entails a different resolution of the whole dynamic interaction problem for every change introduced in the pantograph model.

Algorithm 1 Direct time integration.

for $t = 1...N_{stp}$ **do**
  Find the interaction point;
  Initializations: $j = 0$; $\mathcal{D}_{j-1}^t = \mathcal{D}_j^t = \mathcal{D}^{t-1}$; $\mathcal{C}_{j-1}^t = \mathcal{C}_j^t = \mathcal{C}^{t-1}$;
  while $\left(\mathcal{D}_{j-1}^t \neq \mathcal{D}_j^t \text{ and } \mathcal{C}_{j-1}^t \neq \mathcal{C}_j^t\right)$ or $j = 0$ **do**
    $j = j + 1$
    $\mathcal{D}_{j-1}^t = \mathcal{D}_j^t$; $\mathcal{C}_{j-1}^t = \mathcal{C}_j^t$;
    Obtain the displacements $\mathbf{u}_j^t$ by solving (27);
    Apply the slackening criterion (30): $\mathcal{D}_j^t$;
    Update the global matrices and vectors as defined in (31);
    Apply the contact loss criterion: $\mathcal{C}_j^t$;
  end while
end for

4.2. Modified time integration procedures

As mentioned above, the main drawback of the direct approach is the reassembling the global matrix at each time step, which makes this procedure inappropriate in practice, due to the high computational cost required. Some ideas have been proposed to circumvent this issue in [17] and exploited in [18], considerably improving the computational cost. Specifically, the non-linearities of the system are moved to the right hand side of the dynamic equilibrium equation, and are therefore treated as non-linear forces. In this way, the global time-step matrix $\mathbf{A}_j^t$ does not vary in time, keeping the analysis linear. Hence, it can be factorised only once, reducing the computational effort. In practice, this modification of the direct approach can be carried out according to the following two procedures:

- Method 1: The global matrix of the system does not include the stiffness and damping of all dropper elements. They are fully treated as non-linear forces instead.
- Method 2: The droppers' stiffness and damping are fully accounted for in the global matrix of the system as in [18]. In this case, the non-linear force term added to the right hand side of the dynamic equation compensates for the slackened droppers.

Despite the clear advantages of these approaches over the direct method, in order to account for the non-linear behaviour of the droppers and the pantograph loss of contact, the iterative procedure requires solving a global size system several times in each time step in which the nodal displacements are still the unknowns of the problem.

4.3. *Offline/Online* time integration methodology

Starting from the ideas of the modified Method 2, we try to concentrate as much computational effort as possible on the *Offline* stage, leaving the minimum number of calculations to the so-called *Online* stage, in which the time integration itself takes place. Another important feature of the proposed methodology is that both the pantograph and the catenary are treated as independent systems, which makes it easier to deal with different pantograph models, or even a real system, as in HIL simulations.

In the *Offline* phase of the algorithm, the catenary is treated as a fully linear system in which the droppers are not able to slacken. Several single time step problems are solved and stored at this stage. In the *Online* calculations, the superposition principle is applied and both the initial conditions of movement and all the non-linearities of the system are considered, i.e. dropper slackening and pantograph contact loss. Using the information calculated in the *Offline* stage, these non-linearities are accounted for iteratively by solving a very small system of equations in which the unknowns are no longer the nodal displacements, but the slackening compensating forces and the pantograph-catenary interaction force. This small set of unknowns is responsible for reducing the computational cost of the solution method.

4.3.1. *Offline* stage

All the calculations which take place before the time integration loop are called *Offline* stage. In this phase we solve several sub-problems whose solution will be used afterwards in the *Online* computations. All these sub-problems are aimed at obtaining the single time-step forced response of the system under a unitary external load and null initial conditions. These unitary external forces are applied at the interaction point and at the dropper ends, as shown in Fig. 6.

As the pantograph moves forward throughout a dynamic simulation, the contact point changes in each time step. The goal of the first sub-problem in this stage is to calculate the response of the catenary system considering a unitary vertical force pushing upwards at each point at which the pantograph interacts with the contact wire (dashed arrows in Fig. 6). We have to solve as many linear problems of the form

$$\mathbf{A}_{cat}\mathbf{u}_{i,cat}^{*,t} = \mathbf{F}_{i,cat}^{*,t} \tag{32}$$

as total time steps N_{stp} in order to find the displacements $\mathbf{u}^{*,t}_{i,cat}$. Recalling the idea introduced in [17], it is important to underline that the matrix of this linear system

$$\mathbf{A}_{cat} = [(1+\alpha)\,[\mathbf{K}_{cat} + b_4\mathbf{C}_{cat}] + b_1\mathbf{M}_{cat}] \tag{33}$$

does not change in each time step t and therefore for any load position. Hence, it can be factorised as $\mathbf{A}_{cat} = \mathbf{L}_{cat}\mathbf{U}_{cat}$, where $\mathbf{L}_{cat}$ and $\mathbf{U}_{cat}$ are lower and upper triangular matrices, respectively. Applying the Cuthill-McKee reordering algorithm [31] to matrix $\mathbf{A}_{cat}$, it is possible to obtain very sparse matrices $\mathbf{L}_{cat}$ and $\mathbf{U}_{cat}$ which will reduce the computational cost in the *Online* calculations.

The other necessary catenary responses, which also will be used in the next stage, are obtained considering the unitary external forces acting on the ends of each of the N_d droppers of the catenary (solid arrows in Fig. 6). These external forces are aligned with droppers. The displacement field $\mathbf{u}^*_{d,cat}$ is obtained as the solution of the one time-step problem:

$$\mathbf{A}_{cat}\mathbf{u}^*_{d,cat} = \mathbf{F}^*_{d,cat} \tag{34}$$

in which now $d = 1, ..., N_d$. Note that $N_{stp} + N_d$ linear problems for the catenary must be solved, but as mentioned above they are performed *Offline* and only once.

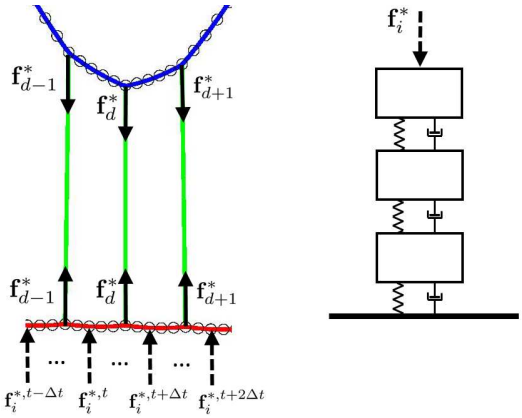

Figure 6: Unitary external forces applied in the *Offline* stage.

Finally, we only need the pantograph response under a unitary force pushing downwards on the top mass where the interaction with the contact wire takes place. The dynamic response of one time step provided by the HHT integrator is $\mathbf{w}^*_{i,pan}$, which does not depend on the time step. The only problem to solve related with the pantograph is:

$$\mathbf{A}_{pan}\mathbf{w}^*_{i,pan} = \mathbf{F}^*_{i,pan} \tag{35}$$

where the matrix

$$\mathbf{A}_{pan} = [(1+\alpha)\,[\mathbf{K}_{pan} + b_4\mathbf{C}_{pan}] + b_1\mathbf{M}_{pan}] \tag{36}$$

is also constant regardless the time step that is being solved.

The velocities and accelerations of all the sub-problems described above are also computed following the rules of the HHT time integrator.

4.3.2. *Online* stage

In this stage the time integration is carried out taking into account the non-linearities introduced by dropper slackening and pantograph contact loss. In order to obtain the formulation of the proposed approach we start from Eq. (27). Proceeding as in the modified approaches introduced in Section 4.2, the terms involving the interaction, as well as the corrections forces for the slackened droppers, are moved to the right hand side of the dynamic equation. It results in:

$$\begin{aligned}\left[(1+\alpha)\left[\begin{pmatrix}\mathbf{K}_{cat} & \mathbf{0}\\ \mathbf{0} & \mathbf{K}_{pan}\end{pmatrix}+b_4\begin{pmatrix}\mathbf{C}_{cat} & \mathbf{0}\\ \mathbf{0} & \mathbf{C}_{pan}\end{pmatrix}\right]+b_1\mathbf{M}\right]\mathbf{u}^t=\mathbf{F}_{IC}^t+\mathbf{F}_{pan}-\\ \alpha\left(-\mathbf{S}_i^{t-1}-\mathbf{K}_i^{t-1}\mathbf{u}^{t-1}+\sum_d^{N_{sd}}\mathbf{S}_d^{t-1}+\mathbf{K}_d^{t-1}\mathbf{u}^{t-1}+\mathbf{C}_d^{t-1}\dot{\mathbf{u}}^{t-1}\right)+\\ (1+\alpha)\left(-\mathbf{S}_i^{t}-\mathbf{K}_i^{t}\mathbf{u}^{t}+\sum_d^{N_{sd}}\mathbf{S}_d^{t}+\mathbf{K}_d^{t}\mathbf{u}^{t}+\mathbf{C}_d^{t}\dot{\mathbf{u}}^{t}\right)\end{aligned} \tag{37}$$

where, by the use of the hypotheses assumed in the HHT algorithm, the velocity $\dot{\mathbf{u}}^t = b_4(\mathbf{u}^t - \mathbf{u}^{t-1}) + b_5\dot{\mathbf{u}}^{t-1} + b_6\ddot{\mathbf{u}}^{t-1}$. It is also important to mention that in this rearrangement there is no coupling between pantograph and catenary degrees of freedom in the system of equations. By grouping terms, the previous equation can be rearranged as:

$$\mathbf{A}\,\mathbf{u}^t = \mathbf{F}_{kn}^t + (1+\alpha)\left(\mathbf{F}_i^t + \sum_d^{N_{sd}}\mathbf{F}_d^t\right) \tag{38}$$

where

$$\begin{gathered}\mathbf{F}_{kn}^t = \mathbf{F}_{IC}^t + \mathbf{F}_{pan} - \alpha\left(-\mathbf{S}_i^{t-1}-\mathbf{K}_i^{t-1}\mathbf{u}^{t-1}+\sum_d^{N_{sd}}\left(\mathbf{S}_d^{t-1}+\mathbf{K}_d^{t-1}\mathbf{u}^{t-1}+\mathbf{C}_d^{t-1}\dot{\mathbf{u}}^{t-1}\right)\right)\\ \mathbf{F}_i^t = -\mathbf{S}_i^t - \mathbf{K}_i^t\mathbf{u}^t\\ \mathbf{F}_d^t = \mathbf{S}_d^t + \mathbf{K}_d^t\mathbf{u}^t + \mathbf{C}_d^t\dot{\mathbf{u}}^t\end{gathered} \tag{39}$$

In this expression, $\mathbf{F}_{kn}^t$ groups all the known forces: those coming from the initial conditions, the constant uplift force and the forces arising from the previous time step. Thus, the unknown forces at time step t are the interaction force $\mathbf{F}_i^t$ and the slackened dropper correction forces $\mathbf{F}_d^t$, since they depend on the sought displacements $\mathbf{u}^t$.

The total displacement $\mathbf{u}^t$ in Eq. (38) is the response of two linear systems (catenary and pantograph) subjected to the three different actions defined in Eq. (39), two of which depend on $\mathbf{u}^t$ itself. Hence, the total response of the system can be computed as the sum of the responses caused by these forces acting separately. Denoting as $\mathbf{u}^t_{F_{kn}}$, $\mathbf{u}^t_{F_i}$ and $\mathbf{u}^t_{F_d}$ the displacement produced respectively by the forces $\mathbf{F}^t_{kn}$, $\mathbf{F}^t_i$ and $\mathbf{F}^t_d$, the total response of the system is computed as:

$$\mathbf{u}^t = \mathbf{u}^t_{F_{kn}} + (1+\alpha)\left(\mathbf{u}^t_{F_i} + \sum_d^{N_{sd}} \mathbf{u}^t_{F_d}\right) \tag{40}$$

or equivalently, taking benefit from the responses under unitary forces calculated in the *Offline* stage, and explicitly splitting the system in terms of catenary and pantograph:

$$\begin{pmatrix}\mathbf{u}^t_{cat}\\ \mathbf{w}^t_{pan}\end{pmatrix} = \begin{pmatrix}\mathbf{u}^t_{F_{kn},cat}\\ \mathbf{w}^t_{F_{kn},pan}\end{pmatrix} + (1+\alpha)\left(f^t_i\begin{pmatrix}\mathbf{u}^{*t}_{i,cat}\\ \mathbf{w}^*_{i,pan}\end{pmatrix} + \sum_d^{N_{sd}} f^t_d\begin{pmatrix}\mathbf{u}^*_{d,cat}\\ \mathbf{0}\end{pmatrix}\right) \tag{41}$$

Now, the magnitude of the interaction force f^t_i and the internal forces of slackened droppers f^t_d for $d = 1, ..., N_{sd}$ at instant t, are the set of unknowns of the problem. $\mathbf{u}^t_{F_{kn},cat}$ and $\mathbf{w}^t_{F_{kn},pan}$ are easy to compute because you only must solve the systems $\mathbf{A}_{cat}\mathbf{u}^t_{F_{kn},cat} = \mathbf{F}^t_{kn,cat}$ and $\mathbf{A}_{pan}\mathbf{w}^t_{F_{kn},pan} = \mathbf{F}^t_{kn,pan}$. Although the first of these systems of equations can be quite large, we remember that the matrix of the system has been factorized in the *Offline* stage into two sparse triangular matrices. Thus, solving the whole system consists of applying forward and backward solvers which are computationally very efficient. Besides, this global size system need only be solved once at each time step, unlike the Methods 1 and 2 defined in Section 4.2, which require several solutions of systems of this size in every time step.

To deal with the non-linearities, we define the vector $\mathbf{f} = [f^t_i\ f^t_1\ \cdots\ f^t_{N_{sd}}]^T$, which contains all the unknowns of Eq. (41). Note that although they are forces, only their magnitude is unknown, since their direction has been previously established. It is also important to emphasize that the number of unknowns is significantly smaller than the total number of degrees of freedom of the system. In order to find these unknowns, due to the non-linearities introduced by the dropper slackening and the pantograph contact loss, we must set and solve iteratively a system of equations of variable size because we do not know which droppers are slackened.

The first equation of such a system comes from the force balance at the interaction point. Looking at the second expression of Eq. (39) (or equivalently Eq. (22)) and introducing the solution in terms of Eq. (41), the external force at the contact point that must be applied is:

$$\begin{aligned} f^t_i =& k_h(z_{ref} + w^t_{pan} - z^t_{0,cw} - w^t_{cw}) = k_h\left(z_{ref} + w^t_{F_{kn},pan} + (1+\alpha)f^t_i w^*_{i,pan} - \right.\\ & \left. z^t_{0,cw} - w^t_{F_{kn},cw} - (1+\alpha)\left(f^t_i w^{*t}_{i,cw} + \sum_d^{N_{sd}} f^t_d w^*_{d,cw}\ \right)\right) \end{aligned} \tag{42}$$

The remaining N_{sd} equations of the system are derived from the third expression of Eq. (39) particularized on every slackened dropper d. By doing this we obtain the compensating forces on both nodes of the slackened dropper element. In order to obtain a scalar equation, we select only the forces on the node n and project them in the direction $\mathbf{n}_d$. Finally, introducing Eq. (41) again, and its velocity counterpart, we obtain:

$$\begin{aligned} f_d^t = \mathbf{n}_d \cdot \left(\mathbf{s}_d + \left[\mathbf{k}_d \mathbf{u}_d^t + \mathbf{c}_d \dot{\mathbf{u}}_d^t\right]_n\right) = \\ \mathbf{n}_d \cdot \left(\mathbf{s}_d + \left[\mathbf{k}_d \left(\mathbf{u}_{F_{kn},d}^t + (1+\alpha)\left(f_i^t \mathbf{u}_{i,d}^{*t} + \sum_m^{N_{sd}} f_m^t \mathbf{u}_{md}^*\right)\right) + \right.\right. \\ \left.\left. \mathbf{c}_d \left(\dot{\mathbf{u}}_{F_{kn},d}^t + (1+\alpha)\left(f_i^t \dot{\mathbf{u}}_{i,d}^{*t} + \sum_m^{N_{sd}} f_m^t \dot{\mathbf{u}}_{md}^*\right)\right)\right]_n\right) \end{aligned} \tag{43}$$

Rearranging Eqs. (42) and (43) in a matrix form leads to:

$$\begin{pmatrix} a & \mathbf{b} \\ \mathbf{c} & \mathbf{D} \end{pmatrix} \mathbf{f} = \begin{bmatrix} e \\ \mathbf{g} \end{bmatrix} \tag{44}$$

Recalling that the index $d = 1, ..., N_{sd}$, the matrix of the system is defined by

$$a = \frac{1}{k_h} - (1+\alpha)(w_{i,pan}^* - w_{i,cw}^{*t}), \tag{45}$$

the row vector $\mathbf{b}$ with the entries

$$b_d = (1+\alpha) w_{d,cw}^*, \tag{46}$$

the column vector $\mathbf{c}$ such that

$$c_d = -(1+\alpha)\mathbf{n}_d \cdot \left[\mathbf{k}_d \mathbf{u}_{i,d}^{*t} + \mathbf{c}_d \dot{\mathbf{u}}_{i,d}^{*t}\right]_n, \tag{47}$$

and the squared matrix $\mathbf{D} = \mathbf{I}_{N_{sd}} - \mathbf{G}$, being $\mathbf{I}_{N_{sd}}$ the identity matrix of size N_{sd} and $\mathbf{G}$ a matrix whose entries are

$$g_{dd} = -(1+\alpha)\mathbf{n}_d \cdot [\mathbf{k}_d \mathbf{u}_{dd}^* + \mathbf{c}_d \dot{\mathbf{u}}_{dd}^*]_n \tag{48}$$

The right hand side vector is composed of

$$e = z_{ref} - z_{0,cw}^t + w_{F_{kn},pan}^t - w_{F_{kn},cw}^t \tag{49}$$

and the column vector $\mathbf{g}$ with the components

$$g_d = \mathbf{n}_d \cdot \left(\mathbf{s}_d + \left[\mathbf{k}_d \mathbf{u}_{F_{kn},d}^t + \mathbf{c}_d \dot{\mathbf{u}}_{F_{kn},d}^t\right]_n\right) \tag{50}$$

After solving the system defined in (44), the fulfilment of the slackening (30) and the contact loss criteria are checked out. For the next iteration, only the droppers which slacken will take part in the linear system of equations (44). This iterative procedure is summarized in Algorithm 2. As in the direct approach, it lasts until in two consecutive iterations the state of all droppers $\mathcal{D}$ and the contact loss state $\mathcal{C}$ are equal, which is always achieved with only 3 or at most 4 iterations in the numerical examples that we have solved. When the iterative procedure ends, one can move to the next time step of the time integration scheme.

Algorithm 2 *Offline/Online* time integration.

OFFLINE stage:
  Assemble $\mathbf{A}_{cat}$ and calculate its LU factorization;
  Solve the N_{stp} problems (32): $\mathbf{u}^{*t}_{i,cat}$;
  Solve the N_d problems (34): $\mathbf{u}^{*}_{d,cat}$;
  Solve the equation (35): $\mathbf{w}^{*}_{i,pan}$;

ONLINE stage:
for $t = 1...N_{stp}$ **do**
  Obtain the initial conditions response: $\mathbf{u}^t_{F_{kn},cat}$, $\mathbf{w}^t_{F_{kn},pan}$;
  Initializations: $j = 0$; $\mathcal{D}^t_{j-1} = \mathcal{D}^t_j = \mathcal{D}^{t-1}$; $\mathcal{C}^t_{j-1} = \mathcal{C}^t_j = \mathcal{C}^{t-1}$;
  while $\left(\mathcal{D}^t_{j-1} \neq \mathcal{D}^t_j \text{ and } \mathcal{C}^t_{j-1} \neq \mathcal{C}^t_j\right)$ or $j = 0$ **do**
    $j = j + 1$;
    $\mathcal{D}^t_{j-1} = \mathcal{D}^t_j$; $\mathcal{C}^t_{j-1} = \mathcal{C}^t_j$;
    Set the linear system of $N_{sd} + 1$ equations (44);
    Apply the slackening criterion (30): $\mathcal{D}^t_j$;
    Apply the contact loss criterion: $\mathcal{C}^t_j$;
  end while
  With Eq. (41) obtain the total displacements $\mathbf{u}^t$;
end for

With this proposed method the pantograph and the catenary are absolutely independent, which allows us to use the proposed method with a real pantograph in a HIL simulation. In such a case, the contact force would be an input at every time step. The computational cost of this methodology is much smaller (even achieving real-time response) than the one required in the direct method and its modified versions. For every time step we only perform a unique global backward and forward resolution with very sparse triangular matrices, and a linear system of equations of the small size $N_{sd} + 1$ must be set and solved few times, instead of solving the global size system several times at each time step, as in the direct approaches.

5. Numerical examples

The numerical examples given in this section are intended to verify the simplifying hypothesis we assumed for the formulation of the dynamic problem and also, to demonstrate the significant reduction in computational cost offered by the proposed *Offline/Online* method, as compared with the classical direct approaches.

5.1. Hypothesis verification

In the beginning of Section 4, we applied two important simplifications. The first concerns the linearisation of the dynamic equations with respect to the static equilibrium position of the catenary cables. With this assumption we got rid of the geometrical non-linearity introduced by the strain measure. The second simplification is based on the small deformation undergone by the droppers in the static equilibrium configuration. This leads to an elemental stiffness matrix which is independent of the absolute position in which the system has been linearised.

To check whether or not these assumptions affect the solution, we are going to simulate the same problem formulated with the non-linear behaviour and the two versions of the linearised dynamic equations. For the simulations we use the catenary model proposed in [3], whose geometry is depicted in Fig. 7. This is a 3D catenary with a stagger of 20 cm from the centre line of the track. It is composed of 10 spans 55 m long and 9 droppers each. The material properties of the different components are listed in Table 1. A proportional Rayleigh damping model is defined by the constants $\alpha_r = 0.0125$ and $\beta_r = 0.0001$.

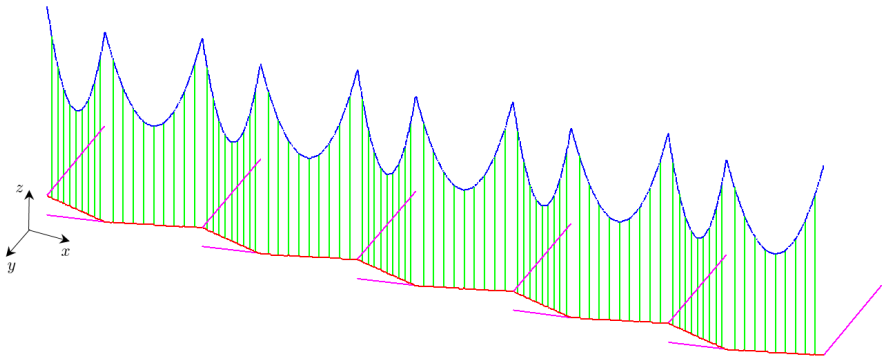

Figure 7: Catenary geometry used for the hypothesis validation.

Table 1: Material and geometrical properties of the catenary components.

Component	E (MPa)	ρ (kg/m^3)	A (mm^2)	I (mm^4)
Messenger wire	9114	$1.1 \cdot 10^{11}$	94.8	1237.2
Contact wire	9160	$1.1 \cdot 10^{11}$	150	2170
Droppers	9114	$1.1 \cdot 10^{11}$	10	0

Table 2: Pantograph model parameters.

d.o.f.	m (kg)	c (Ns/m)	k (N/m)
1	6.6	0	7000
2	5.8	0	14100
3	5.8	70	80

The parameters used for the lumped mass pantograph model are shown in Table 2. The applied uplift force is $F_{pan} = 180$ N. A time step of $\Delta t = 0.001$ s is used for the dynamic simulation. The pantograph moves at 270 km/h and the HHT parameters are set to $\alpha = -0.05$, $\beta = 0.2756$ and $\gamma = 0.55$. The penalty stiffness assigned for the interaction model is $k_h = 50000$ N/m.

The results shown in the figures below are focused on the contact force at the two central spans in order to minimize unwanted contributions from boundary effects. This magnitude is considered a good representative output of the dynamic simulation. Fig. 8 shows the interaction force obtained from two simulations, one using the non-linear formulation (solid line) and the other with the linearised formulation (dashed line). At first glance no difference is observed, but plotting the relative error between the two curves shows that it does not exceed 3.4%, confirming the validity of the linearisation hypothesis.

As regards the second assumption, Fig. 9 shows the interaction force obtained considering the full dropper stiffness matrix (solid line) or its simplified version (dashed line). Again, the differences between the two simulations are negligible, with a mean relative error around 1%.

Considering the two simplifications together, the mean of the relative error in the contact force between the linearised formulation using the simplified dropper stiffness matrix and the non-linear problem is less than 1.6%. Hence, we can conclude that using the linearised formulation along with the simplified dropper stiffness matrix (18) does not significantly affect the results.

After verifying the simplifications introduced into the formulation, we should now investigate other changes that may save computational cost. Specifically, we are going to look for the largest time step Δt in the HHT algorithm that provides accurate results.

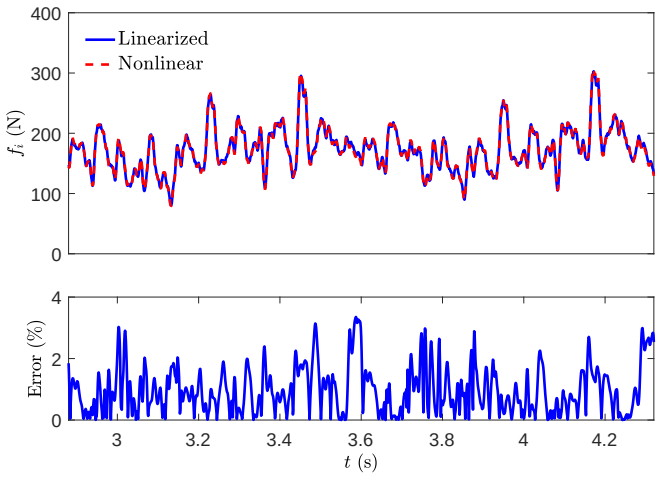

Figure 8: Interaction force from the linearised (solid blue line) and the nonlinear (dashed red line) formulation. Relative error between them.

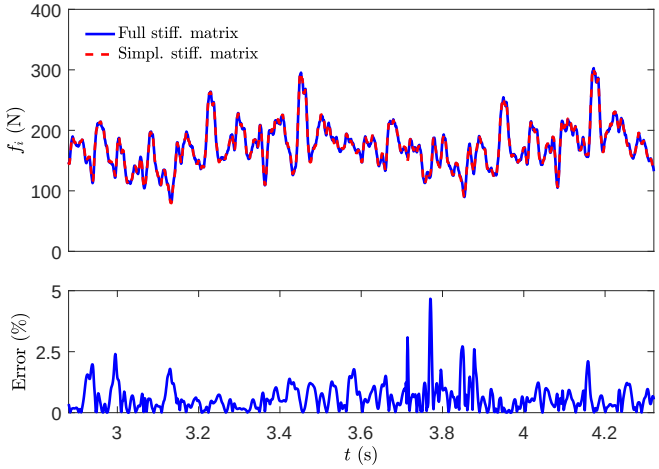

Figure 9: Interaction force using the full dropper stiffness matrix (solid blue line) or the simplified one (dashed red line). Relative error between them.

For this purpose, the interaction force obtained with three different time steps is compared in Fig. 10. The use of $\Delta t = 0.002$ s (dashed red curve), produces

quite accurate results when compared with the ones (solid blue curve) obtained with $\Delta t = 0.001$ s. However, if $\Delta t = 0.005$ s the solution does not match with the reference interaction force at all. Hence, in the light of these results, we can select the time step of 2 ms.

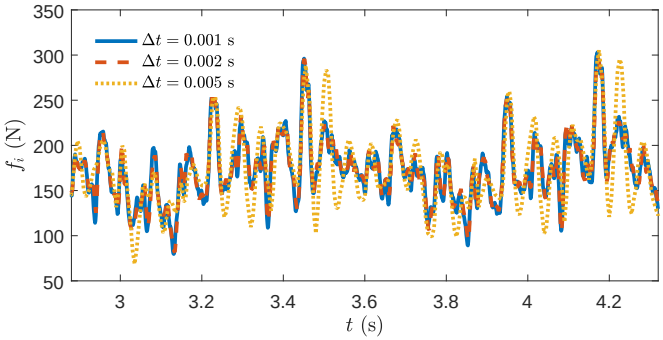

Figure 10: Interaction force using different time steps.

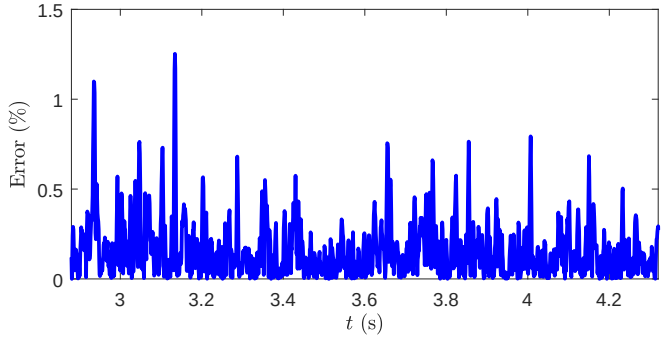

Figure 11: Relative error between the solution obtained with $\alpha = 0$ and $\alpha = -0.05$.

Another aspect to analyse is the value of the constant α in the HHT method. Fig. 11 represents the relative error of the interaction force obtained from $\alpha = 0$ (equivalent to the Newmark method) and $\alpha = -0.05$. As can be seen, this error does not exceed 1% in most of the interest interval. This means the Newmark method can be used at a lower computational cost because we do not need to include in Eq. (37) the terms evaluated in the previous time step $t - 1$.

5.2. Computation time study

The direct approach and the proposed *Offline/Online* methodology come from the same dynamic equilibrium equation. This means that there are no differences in the time history of the interaction force, obtained by both methods. This is why in this section we only compare the computational cost of the commonly used direct approaches and the proposed *Offline/Online* methodology.

To carry out this comparison, four different catenary models are studied. Three of them are 3D models with 5 (Cat.1), 10 (Cat.2) and 18 (Cat.3) spans respectively, and the other one is a 2D model 1 km in length and with 18 spans (Cat.4).

As mentioned previously, the displacements, velocities and accelerations calculated in the *Offline* stage must be stored to be used in the succeeding *Online* phase. This requires a certain amount of RAM memory available in the computer in order to avoid swapping data on the hard disk, which would slowdown the computations. For Cat.3, the biggest example studied here, approximately 2.5 GB of RAM memory is large enough to store all the results.

In Table 3 we compare the computational cost required to perform the simulations with these four catenary models. The first two rows show the number of degrees of freedom of each catenary model and the total time simulated, respectively. All the simulations are carried out with a time step $\Delta t = 0.002$ s, and the rest of the time integration parameters are equal, as in the previous section. The code was implemented in MATLAB® and launched in an Intel® Core i7-6700 CPU.

The computational time required for the direct approach time integration, the two modified methods, the *Offline* stage of the new approach and also the *Online* phase are displayed using both HHT and Newmark methods.

The remarkably high computational cost required for the modified Method 1 is about four times more than the direct integration algorithm. This is because the matrix of the system does not include any information of droppers, leading to convergence problems in the iterative procedure, which needs a large number of iterations to obtain accurate solutions. Hence, although the system matrix has been factorised, there is no improvement in computational cost, due to the large number of times the global size system needs to be solved.

However, there is a noticeable time gain with the use of the modified Method 2. In this case, the time integration can be solved more than three times faster than with the direct scheme. In this procedure, apart from taking advantage of having a factorised matrix, no more than ten iterations are usually needed to achieve convergence with a good degree of accuracy.

The good performance of the proposed *Offline/Online* method can be clearly seen in Table 3. The same simulation with exactly the same accuracy is carried out around 25 times faster than with the direct approach. This total gain factor is slightly increased for large catenary models, which require more computational effort. Focusing only on the time consumed by the *Online* stage, in most cases it comes

Table 3: Computational time comparison.

	Cat.1	**Cat.2**	**Cat.3**	**Cat.4**
d.o.f.	5996	11986	21570	14385
Simulated time (s)	3	5	10	10
HHT				
Direct (s)	56.05	205.38	802.80	412.46
Modified 1 (s)	156.76	676.1	2575.2	1405.7
Modified 2 (s)	20.98	90.58	325.47	187.35
Offline stage (s)	0.76	2.39	9.83	5.28
Online stage (s)	1.74	5.22	19.27	10.86
Newmark				
Direct (s)	52.69	218.74	785.10	417.60
Modified 1 (s)	91.99	323.89	1270	757.8
Modified 2 (s)	14.93	50.87	201.24	111.64
Offline stage (s)	0.79	2.50	9.64	5.19
Online stage (s)	1.37	4.48	15.75	9.10

close to (light green boxes), or is even less than the simulated time (green boxes), which allows real-time responses for HIL simulations. These low computational costs are due to the way we treat the non-linearities; for the four catenaries solved, they account for solving iteratively a system of maximum size of 6 equations, with only 4 iterations at most.

It is very clear that, regardless of the catenary model, the proposed approach is highly suitable for optimization purposes, when a large number of simulations must be performed.

6. Conclusions

This paper deals with the numerical simulation of pantograph-catenary dynamic interaction. The catenary is modeled by FE according to the absolute nodal coordinate formulation, while the pantograph is treated as a lumped mass system. The major difficulty in the simulations lies in the nonlinearities introduced by dropper slackening and the possible loss of contact of the pantograph. With a classical approach, a linear system of equations of the overall size of the problem must be solved

several times at each time step in order to account for these nonlinearities. This has a considerable computational cost and makes the approach useless for optimization purposes, in which many simulations are required.

Certain modifications are intended to avoid reassembling the matrix each time step by dealing with the nonlinearities as forces keeping the global matrix constant in time. Starting from these modified formulations, we developed a new strategy that notably reduces the computational effort in each simulation without any loss of accuracy. The proposed procedure is based on two stages: the *Offline* phase, performed only once, in which we solve several single time-step problems, applying unitary forces. This is followed by the *Online* stage in which we account for the initial conditions and deal with the nonlinearities by only solving a very small system of equations whose unknowns are the interaction force and the slackened dropper correction forces.

The *Offline/Online* method results in a highly computational-cost-saving approach, making it a very suitable tool for optimizing the catenary and pantograph models. Furthermore, it has been shown to be capable of computing the real-time response of the catenary unlike any other previous method in which there were no losses in accuracy. This means that the *Offline/Online* approach can be used to implement HIL simulations, in which a pantograph model is replaced by a real system.

A. The HHT time integration method

The Hilber-Hughes-Taylor (HHT) method [30] is an implicit time integration scheme widely used in structural dynamics. Given the linear system of equations of motion:

$$\mathbf{M}\ddot{\mathbf{u}} + \mathbf{C}\dot{\mathbf{u}} + \mathbf{K}\mathbf{u} = \mathbf{F} \tag{51}$$

the HHT method is based on the Newmark hypotheses:

$$\begin{aligned} \mathbf{u}^{t+1} &= \mathbf{u}^t + \Delta t\dot{\mathbf{u}}^t + \frac{\Delta t^2}{2}\left[(1-2\beta)\ddot{\mathbf{u}}^t + 2\beta\ddot{\mathbf{u}}^{t+1}\right] \\ \dot{\mathbf{u}}^{t+1} &= \dot{\mathbf{u}}^t + \Delta t\left[(1-\gamma)\ddot{\mathbf{u}}^t + \gamma\ddot{\mathbf{u}}^{t+1}\right] \end{aligned} \tag{52}$$

which depend on the coefficients β and γ and the time step Δt. The damping, elastic and external forces in Eq. (51) are weighted in two consecutive time steps by a coefficient α leading to:

$$\mathbf{M}\ddot{\mathbf{u}}^{t+1} + (1+\alpha)\mathbf{C}\dot{\mathbf{u}}^{t+1} - \alpha\mathbf{C}\dot{\mathbf{u}}^t + (1+\alpha)\mathbf{K}\mathbf{u}^{t+1} - \alpha\mathbf{K}\mathbf{u}^t = (1+\alpha)\mathbf{F}^{t+1} - \alpha\mathbf{F}^t \tag{53}$$

We can rearrange Eq. (52) in order to obtain $\ddot{\mathbf{u}}^{t+1}$ and $\dot{\mathbf{u}}^{t+1}$ as a function of the displacements $\mathbf{u}^{t+1}$ and all the variables evaluated in the previous time step as:

$$\begin{aligned} \dot{\mathbf{u}}^{t+1} &= b_4\left(\mathbf{u}^{t+1} - \mathbf{u}^{t}\right) - b_5\dot{\mathbf{u}}^{t} - b_6\ddot{\mathbf{u}}^{t} \\ \ddot{\mathbf{u}}^{t+1} &= b_1\left(\mathbf{u}^{t+1} - \mathbf{u}^{t}\right) - b_2\dot{\mathbf{u}}^{t} - b_3\ddot{\mathbf{u}}^{t} \end{aligned} \tag{54}$$

where the constants b_i are:

$$\begin{aligned} b_1 &= \frac{1}{\beta\Delta t^2} \qquad b_2 = \frac{1}{\beta\Delta} \qquad b_3 = 1 - \frac{1}{2\beta} \\ b_4 &= \gamma\Delta t\, b_1 \quad b_5 = 1 + \gamma\Delta t\, b_2 \quad b_6 = \Delta t(1 + \gamma b_3 - \gamma) \end{aligned} \tag{55}$$

Then, substituting them in (53) results in:

$$\mathbf{A}\mathbf{u}^{t+1} = \mathbf{b} \tag{56}$$

where

$$\begin{aligned} \mathbf{A} &= (1+\alpha)\left[\mathbf{K} + b_4\mathbf{C}\right] + b_1\mathbf{M} \\ \mathbf{b} &= (1+\alpha)\mathbf{F}^{t+1} - \alpha\mathbf{F}^{t} + \alpha\left[\mathbf{K}\mathbf{u}^{t} + \mathbf{C}\dot{\mathbf{u}}^{t}\right] + \mathbf{M}\left[b_1\mathbf{u}^{t} - b_2\dot{\mathbf{u}}^{t} - b_3\ddot{\mathbf{u}}^{t}\right] \\ &\quad + (1+\alpha)\mathbf{C}\left[b_4\mathbf{u}^{t} - b_5\dot{\mathbf{u}}^{t} - b_6\ddot{\mathbf{u}}^{t}\right] \end{aligned} \tag{57}$$

Once the displacements have been obtained by solving the system (56), it is easy to compute the velocities and accelerations from Eq. (54).

B. List of symbols

For the sake of clarity, in the table below we list all the symbols used throughout the paper in order of appearance:

$\mathbf{q}_c$, $\mathbf{q}_b$	Vector of degrees of freedom for cable and bar elements.
$\mathbf{r}(x, y, z)$	Absolute position vector and coordinates.
χ, s	Local reference and deformed element coordinates.
ξ	Normalized local element coordinate.
l_{ref}	Undeformed element length.
$\mathbf{N}_c$, $\mathbf{N}_b$	Shape functions matrix for cable and bar elements.
m_i, c_i, k_i, $i = 1, 2, 3$	Mass, damping and stiffness parameters of the pantograph model.
k_h	Penalty interaction stiffness.

f_i	Interaction force value.
z_1	Absolute vertical position of the degree of freedom 1 of the pantograph.
z_{cw}	Absolute vertical position of the contact wire at the contact point.
Ω, Ω^e	Catenary and element spatial domains.
N_e	Total number of finite elements.
δW^e_{int}, δW^e_{ext}	Elemental virtual work produced by internal and external forces.
E	Young's modulus.
A	Cross-sectional area.
I	Second moment of area.
ρ	Density.
$\mathbf{g}$, g	Gravitational force vector and gravitational constant.
ε_a	Axial strain.
κ	Curvature.
$\mathbf{f}_{int}$, $\mathbf{f}_{ext}$	Internal and external equivalent nodal forces.
$\mathbf{r}_0$	Static equilibrium position of the catenary.
$\mathbf{u}$	Vector of displacements from the reference position.
u, v, w	Displacements on directions x, y and z.
$\mathbf{n}_d$, $\hat{\mathbf{n}}_d$	Director vector of dropper d at the static equilibrium position and its unitary counterpart.
$\varepsilon_{a,0}$, T_0	Axial strain and tension of an element in the static equilibrium configuration.
$\mathbf{k}_d$, k_d	Stiffness matrix and stiffness constant for dropper d.
$\mathbf{c}_d$	Damping matrix for dropper d.
α_r, β_r	Proportional Rayleigh damping parameters.
$\mathbf{M}_{cat}$, $\mathbf{C}_{cat}$, $\mathbf{K}_{cat}$	Mass, damping and stiffness matrices of the catenary.
$\mathbf{u}_{cat}$, $\dot{\mathbf{u}}_{cat}$, $\ddot{\mathbf{u}}_{cat}$	Displacements, velocities and accelerations of the catenary respect to the static equilibrium configuration.
$\mathbf{M}_{pan}$, $\mathbf{C}_{pan}$, $\mathbf{K}_{pan}$	Mass, damping and stiffness matrices of the pantograph.
$\mathbf{w}_{pan}$, $\dot{\mathbf{w}}_{pan}$, $\ddot{\mathbf{w}}_{pan}$	Vertical displacements, velocities and accelerations of the pantograph d.o.f.
F_{pan}	External uplift force applied to the pantograph.
w_{cw}	Vertical displacement, respect to the static equilibrium position, of the contact wire particularized at the contact point.
$z_{0,cw}$	Static equilibrium vertical position of the contact wire at the contact point.
$\mathbf{k}_i$, $\mathbf{K}_i$	Local and global interaction stiffness matrix.
$\mathbf{s}_i$, $\mathbf{S}_i$	Local and global interaction static force vector.

$\mathbf{M}$, $\mathbf{C}$, $\mathbf{K}$, $\mathbf{F}$	Global assembled mass, damping, stiffness matrices and force vector.
$\mathbf{u}^0$, $\dot{\mathbf{u}}^0$, $\ddot{\mathbf{u}}^0$	Initial displacements, velocities and accelerations of the global system.
Δt	Time step.
N_{stp}	Total number of time steps.
α, β, γ	HHT parameters.
b_i, $i = 1, ..., 6$	Constant values depending on Δt and the HHT parameters.
$\mathbf{f}_d$, $\mathbf{s}_d$	Total internal force and internal force in the static equilibrium position for dropper d.
δ_d, $\delta_{0,d}$	Total elongation and elongation in the static equilibrium position for dropper d.
$\square^t$, $\square_j$	Any variable particularized at time step t and iteration j.
$\mathbf{A}$, $\mathbf{b}$	Global time integration matrix and force vector.
$\mathbf{F}_{IC}$	Global initial conditions force vector.
$\mathcal{D}$, $\mathcal{C}$	Dropper slackening and contact loss state variables.
$\mathbf{A}_{cat}$, $\mathbf{A}_{pan}$	Time integration matrix for the catenary and the pantograph systems.
$\mathbf{L}_{cat}$, $\mathbf{U}_{cat}$	LU factorisation of $\mathbf{A}_{cat}$.
$\square^*$	Unitary force or displacement produced by a unitary force.
N_d, N_{sd}	Number of total and slackened droppers.
$\mathbf{F}_{kn}$, $\mathbf{F}_i$, $\mathbf{F}_d$	Vectors of known, interaction and slackened dropper correction forces.
$\mathbf{u}_{F_{kn}}$, $\mathbf{u}_{F_i}$, $\mathbf{u}_{F_d}$	Displacements produced by the known, interaction and slackened dropper correction forces.
$w^*_{d,cw}$	Vertical displacement of the contact wire at the interaction point, produced by a unitary force applied on dropper d.

Acknowledgements

The authors would like to acknowledge the financial support received from the FPU program offered by the Ministerio de Educación, Cultura y Deporte under grant number (FPU13/04191), and also the funding received from the Generalitat Valenciana (PROMETEO/2016/007).

References

[1] A. Shing and P. Wong, "Wear of pantograph collector strips," *Proceedings of the Institution of Mechanical Engineers, Part F: Journal of Rail and Rapid Transit*, vol. 222, no. 2, pp. 169–176, 2008. 1

[2] G. Bucca, A. Collina, R. Manigrasso, F. Mapelli, and D. Tarsitano, "Analysis of electrical interferences related to the current collection quality in pantograph–catenary interaction," *Proceedings of the Institution of Mechanical Engineers, Part F: Journal of Rail and Rapid Transit*, vol. 225, no. 5, pp. 483–500, 2011. 1

[3] S. Bruni, J. Ambrosio, A. Carnicero, Y. H. Cho, L. Finner, M. Ikeda, S. Y. Kwon, J. P. Massat, S. Stichel, and M. Tur, "The results of the pantograph–catenary interaction benchmark," *Vehicle System Dynamics*, vol. 53, no. 3, pp. 412–435, 2015. 1, 5.1

[4] EN 50318, *Railway applications. Current collection systems. Validation of simulation of the dynamic interaction between pantograph and overhead contact line.* 2002. 1, 2.3

[5] K. Manabe and Y. Fujii, "Overhead system resonance with multi-pantographs and countermeasures," *Railway Technical Research Institute, Quarterly Reports*, vol. 30, no. 4, 1989. 1

[6] G. Gilbert and H. Davies, "Pantograph motion on a nearly uniform railway overhead line," *Proceedings of the Institution of Electrical Engineers*, vol. 113, no. 3, pp. 485–492, 1966. 1

[7] S. H. Kia, F. Bartolini, A. Mpanda-Mabwe, and R. Ceschi, "Pantograph–catenary interaction model comparison," in *IECON 2010-36th Annual Conference on IEEE Industrial Electronics Society*, pp. 1584–1589, IEEE, 2010. 1

[8] J. Ambrosio, F. Rauter, J. Pombo, and M. Pereira, "A flexible multibody pantograph model for the analysis of the catenary–pantograph contact," *Multibody Dynamics*, vol. 23, pp. 1–27, 2011. 1, 2.2

[9] O. López-García, A. Carnicero, V. Torres, and J. Jiménez-Octavio, "The influence of cable slackening on the stiffness computation of railway overheads," *International Journal of Mechanical Sciences*, vol. 50, pp. 1213–1223, 2008. 1

[10] A. Facchinetti, L. Gasparetto, and S. Bruni, "Real-time catenary models for the hardware-in-the-loop simulation of the pantograph–catenary interaction," *Vehicle System Dynamics*, vol. 51, no. 4, pp. 499–516, 2013. 1

[11] J. R. Jiménez-Octavio, A. Carnicero, C. Sánchez-Rebollo, and M. Such, "A moving mesh method to deal with cable structures subjected to moving loads and its application to the catenary–pantograph dynamic interaction," *Journal of Sound and Vibration*, vol. 349, pp. 216–229, 2015. 1

[12] S. Gregori, M. Tur, E. Nadal, F. Fuenmayor, and F. Chinesta, "Parametric model for the simulation of the railway catenary system static equilibrium problem," *Finite Elements in Analysis and Design*, vol. 115, pp. 21–32, 2016. 1

[13] R. Zhang, P. V. Lauenstein, and B. M. Phillips, "Real-time hybrid simulation of a shear building with a uni-axial shake table," *Engineering Structures*, vol. 119, pp. 217–229, 2016. 1

[14] M. Matar, D. Paradis, and R. Iravani, "Real-time simulation of modular multilevel converters for controller hardware-in-the-loop testing," *IET Power Electronics*, vol. 9, no. 1, pp. 42–50, 2016. 1

[15] R. Conti, E. Meli, and A. Ridolfi, "A full-scale roller-rig for railway vehicles: multibody modelling and Hardware In the Loop architecture," *Multibody System Dynamics*, vol. 37, no. 1, pp. 69–93, 2016. 1

[16] W. Zhang, G. Mei, X. Wu, and Z. Shen, "Hybrid simulation of dynamics for the pantograph–catenary system," *Vehicle System Dynamics*, vol. 38, no. 6, pp. 393–414, 2002. 1

[17] A. Collina and S. Bruni, "Numerical simulation of pantograph-overhead equipment interaction," *Vehicle System Dynamics*, vol. 38, no. 4, pp. 261–291, 2002. 1, 4.2, 4.3.1

[18] J. Ambrósio, J. Pombo, P. Antunes, and M. Pereira, "PantoCat statement of methods," *Vehicle System Dynamics*, vol. 53, no. 3, pp. 314–328, 2015. 1, 4.2

[19] A. Shabana, "Computer implementation of the absolute nodal coordinate formulation for flexible multibody dynamics," *Nonlinear Dynamics*, vol. 16, pp. 293–306, 1998. 2.1

[20] J. Gerstmayr and A. A. Shabana, "Analysis of thin beams and cables using the absolute nodal coordinate formulation," *Nonlinear Dynamics*, vol. 45, no. 1-2, pp. 109–130, 2006. 2.1

[21] J. Seo, A. S. Kim, I. Jung, T. Park, J. Mok, Y. Kim, and J. Chai, "Dynamic analysis of a pantograph–catenary system using absolute nodal coordinates," *Vehicle System Dynamics*, vol. 44, no. 8, pp. 615–630, 2006. 2.1

[22] J. H. Lee and T. W. Park, "Development of a three-dimensional catenary model using cable elements based on absolute nodal coordinate formulation," *Journal of Mechanical Science and Technology*, vol. 26, no. 12, pp. 3933–3941, 2012. 2.1

[23] I. Romero, "A comparison of finite elements nonlinear beams: the absolute nodal coordinate and geometrically exact formulations," *Multibody System Dynamics*, vol. 20, pp. 51–68, 2008. 2.1

[24] J. Gerstmayr and H. Irschik, "On the correct representation of bending and axial deformation in the absolute nodal coordinate formulation with an elastic line approach," *Journal of Sound and Vibration*, vol. 318, pp. 461–487, 2008. 2.1

[25] A. Collina and A. M. Carnevale, "Effect of collector deformable modes in pantograph–catenary dynamic interaction," *Proceedings of the Institution of Mechanical Engineers, Part F: Journal of Rail and Rapid Transit*, vol. 223, no. 1, pp. 1–14, 2009. 2.2

[26] Y. H. Cho, "SPOPS statement of methods," *Vehicle System Dynamics*, vol. 53, no. 3, pp. 329–340, 2015. 2.3

[27] H. Lankarani and P. E. Nikravesh, "A contact force model with hysteresis damping for impact analysis of multibody systems," *Journal of Mechanical Design*, vol. 112, no. 3, pp. 369–376, 1990. 2.3

[28] M. Tur, E. García, L. Baeza, and F. Fuenmayor, "A 3D absolute nodal coordinate finite element model to compute the initial configuration of a railway catenary," *Engineering Structures*, vol. 71, pp. 234–243, 2014. 3

[29] M. Berzeri and A. Shabana, "Development of simple models for the elastic forces in the absolute nodal coordinate formulation," *Journal of Sound and Vibration*, vol. 235, no. 4, pp. 539–565, 2000. 3

[30] H. M. Hilber, T. J. Hughes, and R. L. Taylor, "Improved numerical dissipation for time integration algorithms in structural dynamics," *Earthquake Engineering & Structural Dynamics*, vol. 5, no. 3, pp. 283–292, 1977. 4.1, A

[31] E. Cuthill and J. McKee, "Reducing the bandwidth of sparse symmetric matrices," in *Proceedings of the 1969 24th National Conference*, pp. 157–172, ACM, 1969. 4.3.1

PAPER C

An approach to geometric optimisation of railway catenaries

S. Gregori, M. Tur, E. Nadal and F. J. Fuenmayor

Vehicle System Dynamics
Published online, 2017
DOI: 10.1080/00423114.2017.1407434

Abstract

The quality of current collection becomes a limiting factor when the aim is to increase the speed of the present railway systems. In this work an attempt is made to improve current collection quality optimizing catenary geometry by means of a Genetic Algorithm. As contact wire height and dropper spacing are thought to be highly influential parameters, they are chosen as the optimization variables. The results obtained show that a Genetic Algorithm can be used to optimize catenary geometry to improve current collection quality measured in terms of the standard deviation of the contact force. Furthermore, it is highlighted that apart from the usual pre-sag, other geometric parameters should also be taken into account when designing railway catenaries.

Key words

Railway catenary; Genetic Algorithm; Optimisation; Pantograph–catenary interaction

Contents

1 Introduction **151**

2 Catenary, pantograph and interaction models **152**

3 Initial configuration problem **154**

4 Dynamic interaction problem **155**

5 Optimisation problem **157**

6 Numerical results **160**
6.1 Pre-sag optimisation 161
6.2 Benchmark catenary optimisation 163
6.3 Stitch wired catenary optimisation 166
6.4 Analysis of the optimised catenaries 168
6.4.1 Static characteristics of the optimised catenaries 169
6.4.2 Dynamic behaviour of the optimised catenaries 171

7 Conclusions **176**

A Input data of the SW catenary model **177**

Bibliography **178**

1. Introduction

The overhead equipment, commonly named the catenary, is the system in charge of providing the energy supply to the electric railway vehicle by means of a sliding contact with the pantograph, which is a mechanism located on top of the locomotive. The interaction force between the pantograph and the catenary contact wire determines the quality of the supply. High contact forces can cause excessive wear on the sliding surfaces, while too weak forces may lead to contact losses and sparking, which apart from the damage it can cause, it interrupts the energy provision.

As the maximum speed of commercial railways is mainly limited by the quality of the pantograph–catenary interaction [1, 2], an appropriate design (the reader is referred to [3] for a wide overview of the design of overhead contact lines) is crucial for the correct behaviour of such a system. This explains why in recent years a lot of effort has been put into developing accurate models capable of simulating the dynamic pantograph-catenary interaction. Among the vast diversity of studies found in the literature, the benchmark [4] and the references therein deserve special attention for the insight they provide into the present state of the art.

According to [4], Finite Element Method (FEM) and lumped mass models are the most frequently used approaches to model the catenary and the pantograph systems, respectively. Euler Bernoulli beam elements are commonly employed to model the catenary wires. However, in this work we have chosen the Absolute Nodal Coordinate Formulation (ANCF) [5]. The contact between the pantograph and the contact wire is mostly dealt with by a penalty method, although some other approaches such as kinematic constraints may be also used to this end.

This work is aimed at optimising the catenary in terms of current collection quality. This quality can be quantified by the standard deviation of the interaction force, which defines the objective function to be minimised. Current collection quality is influenced by many parameters, such as the stiffness and damping of the pan-head and frame, the contact wire tension or the static uplift force, whose influence on the contact force is thoroughly analysed in [6]. Some optimisations are found in the literature concerning the parameters which define the pantograph model. In [7] a robust design technique was used to find the optimal lumped parameters for the best current collection in catenaries with variable span lengths. By optimising the stiffness, damping and mass values of the pantograph lumped model, the standard deviation of the contact force was reduced by 11% in [8], where a Genetic Algorithm (GS) was used. A 9% of reduction was achieved in [9] using a differential evolutionary algorithm. Similar improvements are found in [10] with the use of pneumatic head suspensions instead of the classical mechanical systems.

Apart from the above mentioned parameters, the amount of initial sag (pre-sag) given to the contact wire also seems to be a key factor in current collection quality. Its

influence on the pantograph–catenary dynamics was studied in [11]. One of the main conclusions drawn from this work is that pre-sag does not improve current collection quality in the high-speed range, where the process is dominated by wave propagation rather than the stiffness variation in the catenary. In [12] the limitations of pre-sag in improving the current collection quality were also revealed. This scenario suggests it would be advisable to follow other approaches to find better catenaries, such as setting the appropriate number of droppers and their spacing, which have been practically ignored in the literature and can also affect the interaction force [13].

The present study is, up to the authors knowledge, the first attempt in finding the optimal catenary geometry, in terms of current collection quality, by exploring alternatives such as the contact wire height profile and dropper spacing. Two catenary topologies are analysed, namely, with and without a stitch wire. The catenary system is modelled by the Finite Element Method (FEM) and a lumped-parameters representation is used to model the pantograph.

When planning an optimisation, the chosen procedure is of crucial importance. Optimisation methods are mainly divided into two groups [14]: gradient-based and metaheuristic methods. Gradient-based methods need the computation of the derivatives of the objective function with respect to the optimisation variables. The problem dealt with in this work is a dynamic problem with a moving load and unilateral nonlinearities. In this case the calculation of these derivatives would be cumbersome and therefore, metaheuristic techniques [15], such as Genetic Algorithms, have been considered for the problem at hand with the addition of some operational restrictions.

The paper is organized as follows: after this brief introduction, all the mathematical models used to describe the whole system are explained in Section 2. The initial configuration problem of the catenary is treated in Section 3, while Section 4 is devoted to explain the dynamic interaction problem, which is solved efficiently. These three sections are included for the sake of completeness since they provide a summary of the models presented in [16], the shape-finding problem solved in [17] and the time integration procedure proposed in [18], respectively. The optimisation problem is set in Section 5, together with the Genetic Algorithm used to solve it. The results obtained from these optimisations are given in Section 6 for both catenary topologies. Finally, the main conclusions drawn from this work are offered in Section 7.

2. Catenary, pantograph and interaction models

The FE technique is the most widely used to model high-speed railway catenaries as can be seen from the review [19] and references in [4]. The catenary is mainly com-

posed of a messenger wire, a contact wire, steady arms, droppers and some typologies also have stitch wires as can be seen in Fig. 1. In this work, the messenger and the contact wires are modeled by beam elements based on the Absolute Nodal Coordinate Formulation (ANCF), which account for axial and bending deformations, and they are identified as 'cable elements' throughout this paper. This type of element was first proposed by Shabana [5] and adapted for thin beams and cables in [20]. Unlike other beam formulations, ANCF elements use absolute positions and their gradients as degrees of freedom instead of rotations [17]. Bar elements are used to model droppers, steady arms and stitch wires, since they only transmit axial forces.

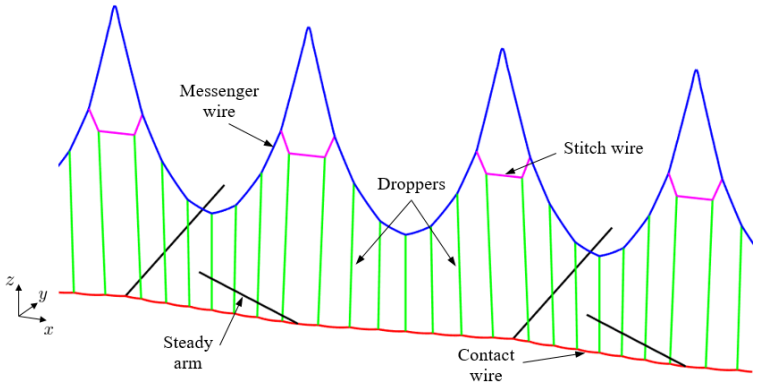

Figure 1: Finite element catenary model.

The reference and deformed configurations for a cable element are schematically represented in Fig. 2. In order to guarantee C^1 continuity, standard Hermite interpolation is used in which, the length of the undeformed element l^e_{ref} is present.

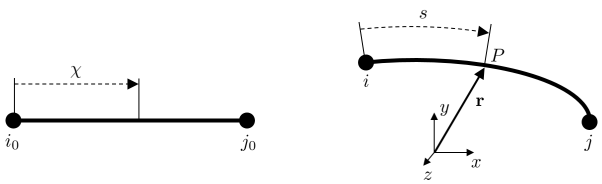

Figure 2: Reference and deformed configurations of the ANCF element.

The degrees of freedom of bar elements are only composed of the absolute positions of the two nodes of the element, so that a linear interpolation is enough to ensure the required C^0 continuity, since bending deformations are not taken into account.

A wide variety of solutions can be found to model pantographs [10]. Due to its simplicity, a linear lumped-parameters model is used in this work. It only introduces

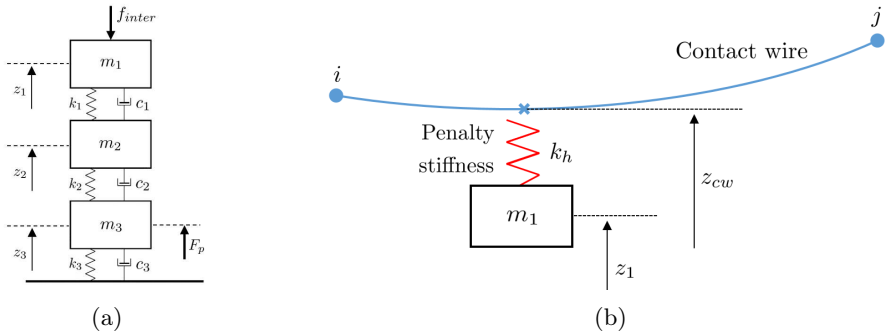

Figure 3: (a) Pantograph and (b) interaction model schemes.

three vertical degrees of freedom, as shown in the scheme depicted in Fig. 3a. F_p represents the force exerted by the uplift mechanism, which acts on the lower mass of the pantograph. This force should not be confused with the static uplift force in the contact between the pan head and the contact wire, which is obtained by solving the dynamic interaction problem.

A penalty method is considered to model the pantograph-catenary interaction. A scheme of this interaction is shown in Fig. 3b. In this model, a spring element with high stiffness, $k_h = 50000$ N/m, relates the vertical degrees of freedom of the cable element, which models the contact wire, with the pantograph upper mass. The interaction force is obtained by multiplying k_h by the interpenetration, that is:

$$f_{inter} = \begin{cases} k_h(z_1 - z_{cw}) & \text{if} \quad z_1 - z_{cw} > 0 \\ 0 & \text{if} \quad z_1 - z_{cw} \leq 0 \end{cases} \tag{1}$$

where z_1 and z_{cw} are the absolute vertical position of the upper mass of the pantograph and the interaction point on the contact wire, respectively.

3. Initial configuration problem

The initial configuration or 'shape-finding' problem, consists of finding the position of each node along with the undeformed length of each element in the mesh which fulfil both the static equilibrium equations and the constraints imposed by the stringing process. Due to the large displacements undergone by the cabling this is a non-linear problem. Despite the approach and the solution procedure are thoroughly explained in [17], some insights are given here.

Following the previous reference, the static equilibrium problem is defined by means of the non-linear equation:

$$\mathbf{F}_{int}(\mathbf{q}, \mathbf{l}^e_{ref}) + \mathbf{F}_g(\mathbf{l}^e_{ref}) = 0 \tag{2}$$

along with the appropriate essential boundary conditions. The internal forces $\mathbf{F}_{int}$ depend on the nodal coordinates $\mathbf{q}$ as well as the reference lengths of the elements $\mathbf{l}^e_{ref}$, while the gravitational forces $\mathbf{F}_g$ only depend on the latter. For a given element's length, $\mathbf{l}^e_{ref}$, Eq. (2) can be solved by using for example the Newton-Raphson method, in order to obtain the static equilibrium position of the system.

However, the final static equilibrium position of the cabling must fulfill certain constraints apart from the force equilibrium. Certain elements such as those modelling the messenger wire, contact wire and stitch wire, are pre-stressed with a tension of value T. In a given element e, this constraint can be described as:

$$c_I(\mathbf{q}, l_{ref}) = (f^e_{int_x})^2 + (f^e_{int_y})^2 + (f^e_{int_z})^2 - T^2 = 0 \tag{3}$$

where $(f^e_{int_j})$ is the j component of the internal nodal force vector. Other constraints such as the contact wire height, and the horizontal position of droppers, stitch wires, steady arms and mast supports, are imposed by means of the constraint equation:

$$c_{II}(\mathbf{q}) = q_i - P = 0 \tag{4}$$

where q_i for $i = x$, y, z is the nodal coordinate enforced to have a value of P.

Putting equilibrium equations (2) and constraints $\mathbf{c}(\mathbf{q}, \mathbf{l}^e_{ref})$ together results in the non-linear system of algebraic equations:

$$\left.\begin{array}{l} \mathbf{F}(\mathbf{q}, \mathbf{l}^e_{ref}) = 0 \\ \mathbf{c}(\mathbf{q}, \mathbf{l}^e_{ref}) = 0 \end{array}\right\} \tag{5}$$

which can be solved by the Newton-Raphson method, obtaining the nodal absolute positions $\mathbf{q}$ and the initial length of each element $\mathbf{l}^e_{ref}$, which fulfill the restrictions imposed for the catenary stringing.

4. Dynamic interaction problem

The dynamic interaction problem needs to be solved many times during the optimisation procedure, so that is crucial to have an efficient strategy in terms of computational cost to deal with this issue. The fast solution method presented in [18] is employed in this work. As pointed out in [18], apart from alleviating computational

cost, the solution given by this method is just as accurate as that obtained with a classical FEM approach. In what follows, we summarise the main features of this method.

The pantograph-catenary dynamic interaction is governed by small displacements, therefore the linear system of differential equations:

$$\mathbf{M}\ddot{\mathbf{u}} + \mathbf{C}\dot{\mathbf{u}} + \mathbf{K}\mathbf{u} = \mathbf{F} \tag{6}$$

is suitable for modelling the whole behaviour of the system [18]. The stiffness matrix $\mathbf{K}$ is obtained from linearisation of dynamic equation at the static equilibrium position resulting from solving Eq (5). $\mathbf{M}$ and $\mathbf{C}$, are the mass and damping matrices of the whole system respectively. All these three matrices contain both the pantograph and the catenary contributions. $\mathbf{F}$ is the vector of applied external forces, and $\mathbf{u}$ denotes the displacements of the pantograph-catenary with respect to its static equilibrium configuration. The proportional Rayleigh damping model stated in [4], with the constants $\alpha = 0.0125$ and $\beta = 10^{-4}$, is considered in Eq. (6) for all the catenaries studied. This ordinary differential equation can be solved by using any time integration scheme such as the commonly used Newmark method.

In order to obtain the displacements of the actual time step t, given the solution in the previous time step, $\mathbf{u}^{t-1}$, the algebraic system of equations:

$$\hat{\mathbf{K}}\mathbf{u}^t = \mathbf{F}^t_{kn}(\mathbf{u}^{t-1}) + \mathbf{F}^t_{dr}(\mathbf{u}^t) + \mathbf{F}^t_{inter}(\mathbf{u}^t) \tag{7}$$

must be solved. Matrix $\hat{\mathbf{K}}$ is obtained by applying the Newmark time discretisation to Eq. (6), (see [18]). $\mathbf{F}^t_{kn}$ is the vector of known forces, which depends on information of the previous time step. Additionally, we have moved to the right-hand side of the system the force $\mathbf{F}^t_{dr}$ necessary to compensate the slackened droppers and the interaction force $\mathbf{F}^t_{inter}$ between the pan head and the contact wire. Note that Eq. (7) is a nonlinear system since the following nonlinearities are considered: i) dropper slackening, which means that droppers only work in tension and, ii) contact loss between the pantograph and the contact wire, leading to a null interaction force.

As said above, in order to speed up the calculations, the approach proposed in [18] is fully adopted. This method is based on two fundamental ideas. The first idea was originally proposed in [21] and successfully used in [22]. It consists of moving the nonlinear correction forces of the slackened droppers, $\mathbf{F}^t_{dr}$, and also the nonlinear terms involving the interaction force, $\mathbf{F}^t_{inter}$, to the right-hand side of the system as shown in Eq. (7). In this way, the matrix $\hat{\mathbf{K}}$ does not change in time and can be precomputed and factorised only once in the algorithm.

The second idea of the method relies on the superposition principle. The displacements $\mathbf{u}^t$ at each time step can be computed as the sum of the displacements produced by the three terms present on the right-hand side of Eq. (7), that is,

$$\mathbf{u}^t = \mathbf{u}^t_{kn} + \mathbf{u}^t_{dr} + \mathbf{u}^t_{inter} \tag{8}$$

To obtain the so-called known term, $\mathbf{u}_{kn}^t$ (which is dependent on information from the previous time step, that is, it accounts for the initial conditions), it is necessary to solve the global size system:

$$\hat{\mathbf{K}}\mathbf{u}_{kn}^t = \mathbf{F}_{kn}^t \tag{9}$$

However, the other two contributions to the total displacement at time step t can be written as:

$$\begin{aligned} \mathbf{u}_{dr}^t &= \sum_{i=1}^{N_{sdr}^t} {}_i\mathbf{u}_{dr}^{*t}\, {}_if_{dr}^t \\ \mathbf{u}_{inter}^t &= \mathbf{u}_{inter}^{*t} f_{inter}^t \end{aligned} \tag{10}$$

where ${}_i\mathbf{u}_{dr}^{*t}$ is the catenary displacement vector produced by a unitary compressive force applied on the ends of the slackened dropper i, and N_{sdr}^t is the total number of slackened droppers time step t. $\mathbf{u}_{inter}^{*t}$ are the displacements produced by a unitary force applied upwards on the contact wire at the corresponding interaction point at time step t.

All these displacements produced by unitary forces can be pre-computed and stored. Therefore, at each time step, slackened droppers and loss of contact are checked and a small-sized nonlinear problem is solved iteratively, in which the values of the slackened droppers' correction forces, ${}_if_{dr}^t$, and the interaction force, f_{inter}^t, are the unknowns.

To sum up, the unilateral constraints of the system are iteratively dealt with in a nonlinear system composed of only $N_{sdr}^t + 1$ equations. This makes the approach highly efficient, requiring a low computational cost to simulate the pantograph–catenary dynamic interaction with no further simplification hypothesis other than those assumed in the classic FEM approach. The only disadvantage that should be mentioned is the need for enough available RAM memory to avoid swapping data on the hard disk, which would slowdown the calculations. Even so, it is not a big deal because 2.5 GB is a large enough memory to store the pre-computed variables for the cases discussed here.

5. Optimisation problem

As pointed out in the introduction, the main goal of this paper is to seek the best catenary geometry in terms of current collection quality. Among other parameters, the quotient between standard deviation and mean interaction force $\sigma\left(f_{inter}\right)/\bar{f}_{inter}$ is thought to be a representative statistical parameter to characterise the quality of

the interaction [8]. The standard [23] sets this parameter below 0.3, which guarantees less than a 1% probability of contact loss. This standard also establishes that the maximum mean contact force applied to the contact wire must fulfill the relationship:

$$\bar{f}_{inter} \leq 0.0097v^2 + 70 \tag{11}$$

for an alternating current catenary, where $200 < v < 320$ km/h. In this work, the interaction force is low-pass filtered at 20 Hz. Although is well known that the high frequency content has an influence on the dynamic performance of the system [10, 21, 24], we decided to stick to standard EN50367 [23] and apply the filtering in order to obtain comparable results to those of [4].

The interaction force is a magnitude that varies in time and depends on many factors such as train speed, catenary geometry, material properties and so on. In this work, the train speed, the mean contact force, the pantograph model and the wire tensions remain constant, while the geometrical parameters related to droppers (length or spacing) are considered as the optimisation variables for minimising $\sigma\left(f_{inter}\right)$.

Generally, denoting as $\mathbf{p}$ the set of parameters with respect to which it is desired to optimise the catenary, the optimisation problem reads:

$$\begin{aligned} &\min_{\mathbf{p}} \quad \sigma\left(f^t_{inter}(\mathbf{p})\right) \\ &\text{s.t.} \\ &p_i^{min} \leq p_i \leq p_i^{max} \quad i = 1, ..., N_p \end{aligned} \tag{12}$$

where p_i^{min} and p_i^{max} are the lower and upper bounds of each parameter, respectively.

To evaluate the objective function it is necessary to solve both the initial configuration problem (5) and the dynamic interaction problem (6). Obtaining the proper mean contact force value given by Eq. (11) means the dynamic simulation must be repeated and the uplift force, F_p, modified according to the ratio between the prescribed value and the mean contact force obtained in the current simulation. With only two or three re-runs the target value was achieved in all cases with acceptable accuracy. As pointed out above, the problem (12) is set for a single train speed v, which simplifies the calculations but means that the optimal geometry obtained needs to be checked for other train speeds.

Generally, two main groups of solvers are suitable for solving an optimisation problem: those based on the gradient and the so-called metaheuristic methods, among which GAs are found. The latter group of solvers was chosen in this work because a gradient-based method would require computing the derivatives of the objective function with respect to the optimisation variables $\mathbf{p}$, which could be cumbersome for this dynamic problem with high nonlinearities. On the other hand, GAs try to reproduce the stochastic process of natural selection, obtaining the global optimum even for nonlinear or discontinuous objective functions, which makes them a very attractive option.

The GA used in the present study is the one included in MATLAB® software. For a problem of N_p optimisation variables (for example N_p dropper lengths), the population size n is chosen (i.e. n different combinations of dropper lengths). The variables are taken as discrete in order to make a finite size space of variables.

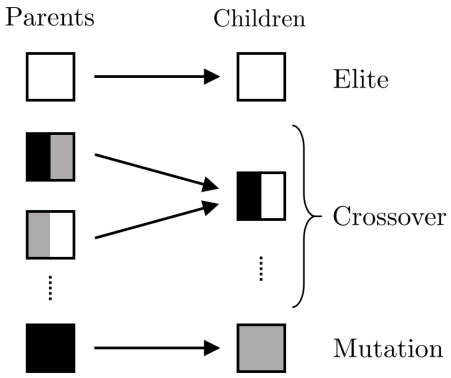

Figure 4: Scheme of the next generation creation process.

An initial population evolves towards better solutions from generation to generation following the principles of natural selection, crossover and mutation (see Fig.4). A stochastic uniform process of selection was selected. The three best-scored parents were considered as elite and were moved directly to the next generation. A crossover fraction of 0.8 has been set, which means that 80% of children came from a random combination of parent parameters. The rest of the children were randomly obtained by mutation of the parameters of a single parent.

The algorithm runs until a certain stop criterion is accomplished. Specifically, the calculations stop when the average cumulative change in value of the objective function over a certain number of generations is less than a prescribed tolerance.

During the optimisation procedure, some combination of parameters $\mathbf{p}$ could produce non-desirable catenaries from a practical point of view. In these cases, individuals that fulfill one of the following conditions are excluded from the population:

- Contact losses were not allowed, whereby the interaction force must be positive at any time t. If a contact loss is detected the individual is not valid any more.
- All the droppers must be in tension in the static equilibrium configuration. If certain dropper d is slackened in the static equilibrium position, this catenary is no longer admissible.

It is important to emphasise that any other restriction, such as the steady arm uplift, could be incorporated into the previous list without any further consideration.

6. Numerical results

The numerical results presented in this work have been obtained from two different catenary models, which are depicted in Fig. 5. The first catenary is thoroughly described in the Benchmark [4] (B), along with the pantograph model associated with it. Unlike this model, the second catenary (SW), has stitch wires at the support locations. The geometric and material properties of this catenary model and the pantograph paired with it are listed in the appendix. The Benchmark catenary has a pre-sag of 1/1000 the span length, i.e. 55 mm. The contact wire of the SW catenary remains horizontally without any static sag. Both models are composed of 20 spans and are used as reference catenaries for comparison purposes with the optimised configurations.

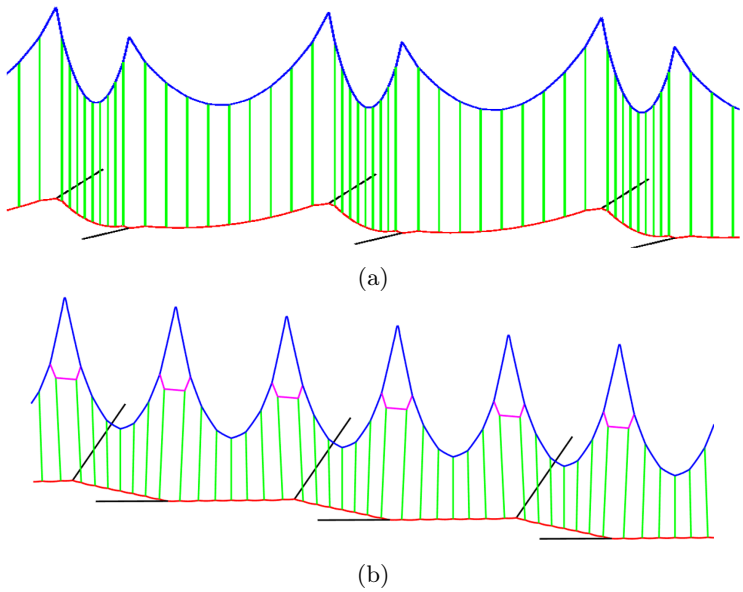

(a)

(b)

Figure 5: (a) Benchmark catenary and (b) SW catenary models.

All the dynamic simulations are carried out with a time step of 1 ms and the Newmark time integration constants are set as $\gamma = 0.5$ and $\beta = 0.25$. The contact or interaction force is measured on the 10 central spans in order to avoid boundary effects. In order to meet the standards guidelines [25], which are also followed in [4], this force is low-pass filtered at 20 Hz. A velocity of $v = 300$ km/h is considered to be the design train speed for both catenaries, which implies a mean contact interaction force $\bar{f}_{inter} =$

157.3 N as given by Eq. (11). After performing a dynamic interaction simulation, the reference Benchmark catenary presents a $\sigma_B = 40$ N, while the standard deviation of the interaction force for the reference SW catenary is $\sigma_{SW} = 22.3$ N.

In what follows, Subsection 6.1 contains a test of the optimisation algorithm carried out by optimising the pre-sag. Subsections 6.2 and 6.3 are devoted to find the best topologies of the Benchmark and the SW catenaries, respectively, that is, the contact wire height and the dropper spacing which provide the best dynamic behaviour for current collection quality purposes. Finally, in Subsection 6.4 the optimised catenaries are analysed in terms of their static and dynamic behaviour.

6.1. Pre-sag optimisation

The so-called pre-sag is the contact wire sag in the static equilibrium configuration. Pre-sag is established in order to mitigate the difference in stiffness between the centre of the span and the supports. Several dynamic problems with different pre-sag have been solved for both catenaries. As shown in Fig. 6, the amount of pre-sag strongly influences the standard deviation of the interaction force σ in the 10 central spans. For a given train speed, large values of pre-sag and also negative sags adversely affect the current collection quality for both the Benchmark (squares) and the SW (circles) catenaries.

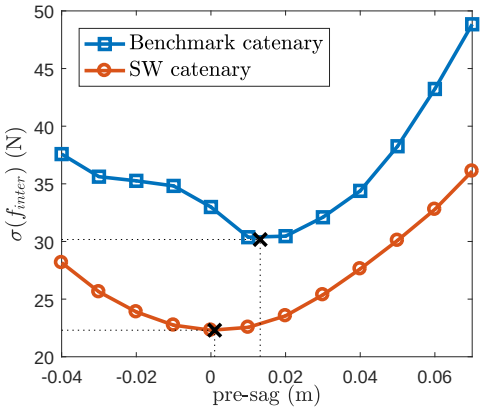

Figure 6: Pre-sag optimisation for a train speed $v = 300$ km/h.

In order to test the GA, an optimisation of the pre-sag at $v = 300$ km/h is carried out. In this academic example, there is only one optimisation variable, therefore only 8 generations with a population of 15 individuals are enough for the GA to find the global minimum. Optimal pre-sag is highlighted for both catenaries in Fig. 6 by a

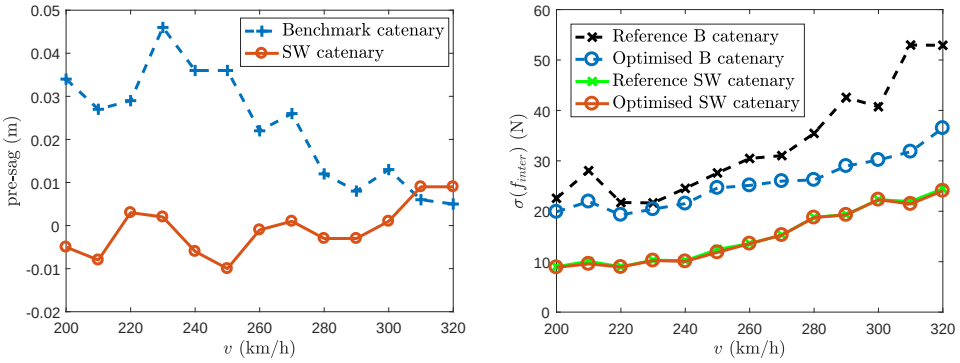

(a) (b)

Figure 7: Evolution of the (a) optimal pre-sag and (b) minimum and reference contact force σ, with respect to the train speed.

cross, in which good agreement with the expected values is observed. This optimal value matches with the reference SW model, which has no initial sag. However, the pre-sag Benchmark catenary is far from the optimal values at the speed of 300 km/h.

The optimal pre-sag is thought to be strongly affected by train speed. To investigate this relation, some optimisations are carried out at velocities ranging from 200 to 320 km/h. The optimal pre-sag (left) and the minimum σ obtained (right) are shown in Fig. 7. Looking for a smoother interaction force, it is clear that the SW catenary behaves better than the Benchmark catenary for all the studied velocities, since the optimal pre-sag is close to 0 for all the studied velocities. The Benchmark catenary gets closer to its optimal behaviour at velocities lower than 270 km/h, for which the optimal pre-sag approximates to the Benchmark catenary static sag.

For both catenary models the interaction force shows higher variability, as evidenced by the clear increasing tendency of σ, as the train speed increases. On the other hand, the optimal pre-sag shows different tendencies for each catenary type. While the optimal behaviour of the SW catenary is achieved with hardly any initial sag, for the Benchmark catenary, the lower the velocity the more beneficial pre-sag seems to be. According to the results, for this type of catenary a pre-sag between 1/1000 and 1/2000 of span length is optimal at velocities below 270 km/h.

The optimal σ can also be compared with respect to the ones obtained at the same train speed for both reference catenaries (see the curves with cross markers in Fig. 7b). This comparison reveals that for the SW catenary the greatest reduction in σ is only 5% at $v = 210$ km/h. This result confirms that with the presence of pre-sag there is no observable improvement in current collection quality for this catenary with stitch wires. Conversely, the Benchmark catenary shows a wide margin of greater improvement for high train speeds. As an example, at $v = 320$ km/h, a 31.05% of

σ could be reduced with an appropriate sag. Despite these results, it seems to be reasonable to seek some more appealing variables for which the dynamic behaviour of the catenary system could be optimised.

6.2. Benchmark catenary optimisation

The first optimisation carried out for the Benchmark catenary considers Δh_{c_i} for $i = 1, ..., N_p$ as optimisation parameters. If the height of the connection point between the steady arm and the contact wire is set as a reference, Δh_{c_i} denotes the height of the contact wire at dropper point i measured from this reference, as seen in Fig. 8. The desired catenary configuration is obtained by solving the initial configuration problem (5), in which the optimisation variable, that is, the desired contact wire height, is imposed as a constraint equation (4) (see [17]).

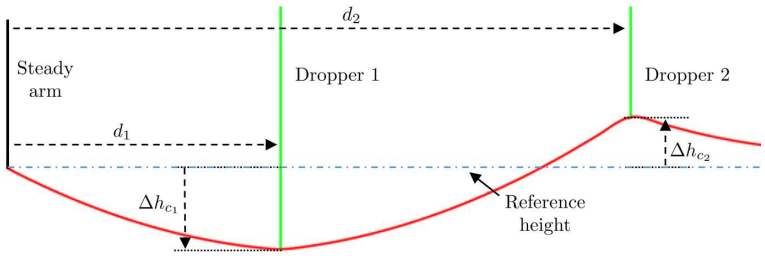

Figure 8: Graphical description of the optimisation variables: Δh_{c_i} and d_i.

Since every span must be equal and their symmetry has to be preserved, the number of variables of the problem amounts to $N_p = 5$. The five variables range from $\Delta h_{c_i}^{min} = -0.02$ m to $\Delta h_{c_i}^{max} = 0.06$ m at intervals of 1 mm. This problem is labelled as B1, and the result shown in the first row of Table 1 is obtained after 120 generations with a population of 100 individuals. A span of the B1 optimised catenary is depicted in Fig. 9, in which a non-uniform contact wire height is seen. It is important to highlight that with only changes in dropper lengths, the optimal configuration obtained produces a $\sigma_{B1} = 17.71$ N, that is, more than 56% less than that of the reference catenary with 55 mm of pre-sag.

As mentioned above, the Benchmark catenary has droppers equally spaced within a span. The second optimisation problem, labelled B2, is intended to find the optimal dropper spacing for the design speed, while keeping the pre-sag or the reference model. In this case, the distance d_i between the left steady arm of the span and the dropper i are chosen as optimisation variables. As in this catenary there is an odd number of droppers per span, the central dropper cannot be moved to preserve the catenary symmetry, therefore $N_p = 4$. In order to avoid overlapping and trying to find a

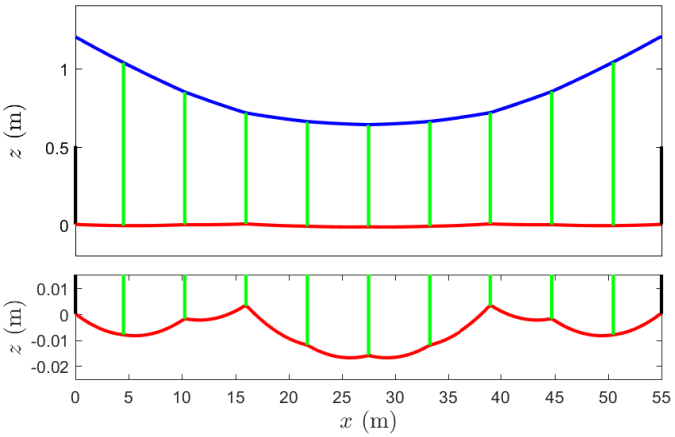

Figure 9: Optimised geometry obtained from the B1 problem.

Table 1: Optimisation results of the Benchmark catenary.

Problem identifier	Variable type	Optimal values (m)	$\sigma(f_{inter})$ (N)	σ reduction (%)
B1	Δh_c	-0.008 -0.002 0.003 -0.012 -0.016	17.71	56.52
B2	d	3.72 9.36 15.96 22.68	34.16	16.13
B3	Δh_c	-0.002 0.001 -0.018	18.44	54.73
	d	9.8 15.8		
		Reference values (m)		
B Ref.	Δh_c	0 0.024 0.041 0.052 0.055	40.73	–
	d	4.5 10.25 16 21.75 27.5		

dropper distribution as uniform as possible, the proposed range for each variable is shown in Table 2. These domains, which notably reduce the design space, are discretised into increments of 1 cm in length.

Table 2: Variable limits used in the B2 optimisation problem.

i	1	2	3	4
d_i^{min} (m)	0.1	7.4	13.2	18.9
d_i^{max} (m)	7.3	13.1	18.8	27.4

The GA stopped after 75 generations, which are composed of 80 individuals, giving the results shown in Table 1. A graphical representation of the optimised B2 catenary geometry is given in Fig. 10. In this case $\sigma_{B2} = 34.16$ N, which represents a 16.13% of reduction when compared to the reference Benchmark catenary. Although this reduction is not as large as the one obtained in the B1 optimisation, dropper spacing undoubtedly arises as an important factor in improving current collection quality.

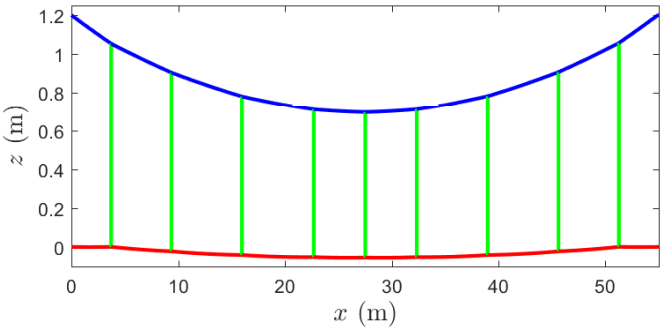

Figure 10: Optimised geometry obtained in the B2 problem.

The question remains as to whether some droppers could be eliminated without major effects on the dynamic behaviour. In order to check this scenario, we chose a Benchmark catenary with only five droppers per span. The B3 optimisation is carried out for this new catenary with fewer droppers, consisting of optimising both contact wire height, and dropper spacing. Thus, there are five optimisation variables altogether, three heights and two dropper locations. The size of the population is set to 100 individuals and the limits for each variable are listed in Table 3.

Table 3: Variable limits used in the B3 optimisation problem.

	d_i (m)		Δh_{c_i} (m)		
i	1	2	1	2	3
Min.	0.1	13.1	-0.02	-0.02	-0.02
Max.	13	27.4	0.06	0.06	0.06

After 70 generations the optimisation problem is solved, giving the optimal variables that appear in Table 1. With four fewer droppers per span, the optimised B3 catenary depicted in Fig. 11, offers almost the same good behaviour as the B1 topology in terms of σ. For this problem, the optimal solution presents $\sigma_{B3} = 18.44$ N, which is almost a 55% lower than that obtained with the reference catenary.

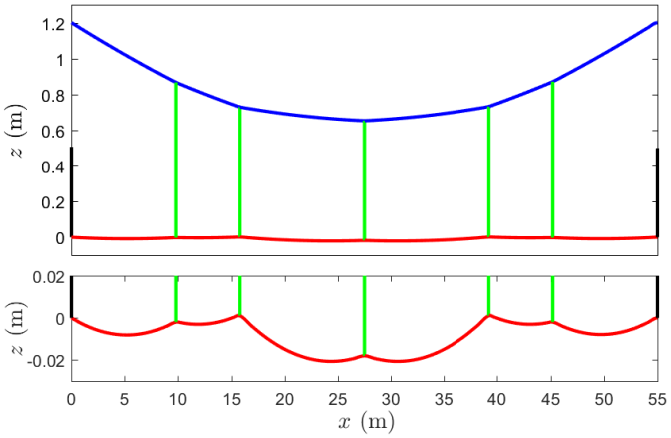

Figure 11: Optimised geometry obtained in the B3 problem.

6.3. Stitch wired catenary optimisation

In this section, the topology of the catenary with stitch wires is optimised. This catenary model has seven droppers per span and the contact wire holds horizontally. In the first place, dropper lengths optimisation is carried out, in which Δh_{c_i}, for $i = 1, ..., N_p$, are considered as optimisation variables. Again, as every span must be equal and symmetric, the number of variables in this problem is $N_p = 4$. The range of variation allowed in this case for the four variables is $\Delta h_{c_i}^{min} = -0.02$ m to $\Delta h_{c_i}^{max} = 0.02$ m. This problem is labelled as SW1, and the optimum is obtained after 90 generations with a population size of 80.

The result of the SW1 problem is given in Table 5 and Fig. 12. The SW1 catenary undergoes a smoother interaction force, as it is clear from $\sigma_{SW1} = 14.14$ N, than the reference SW catenary, with which a 36.6% greater σ is obtained. Comparing the SW1 configuration with the B1 optimised catenary (see Fig. 9), the main difference is observed in the height of the central point, being much lower for the Benchmark catenary type.

The second optimisation concerns the search for the optimal dropper spacing in terms of current collection quality. For this case there are only three optimisation variables d_i, since the dropper located at midspan cannot be moved to preserve the symmetry of this catenary, because again it has an odd number of droppers in each span. This problem is labelled as SW2 and the allowed ranges for each variable are shown in Table 4.

With a population of 60 individuals, after 54 generations the GA found the optimum, which can be seen in Table 5. In Fig. 13 a span of the optimised SW2 catenary

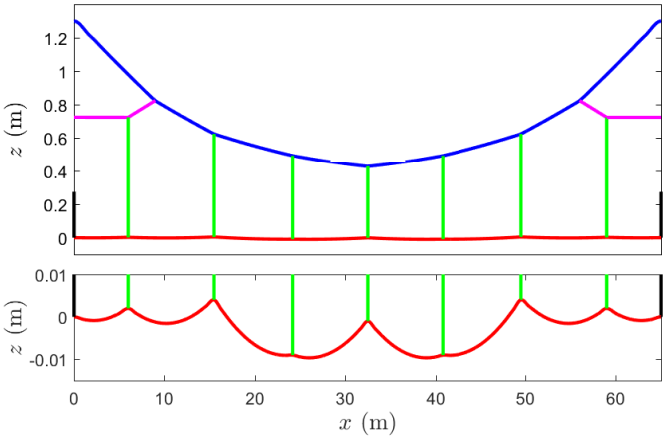

Figure 12: Optimised geometry obtained in the SW1 problem.

Table 4: Variable limits used in the SW2 optimisation problem.

i	1	2	3
d_i^{min} (m)	0.1	9.1	20.5
d_i^{max} (m)	8.9	20.4	32.4

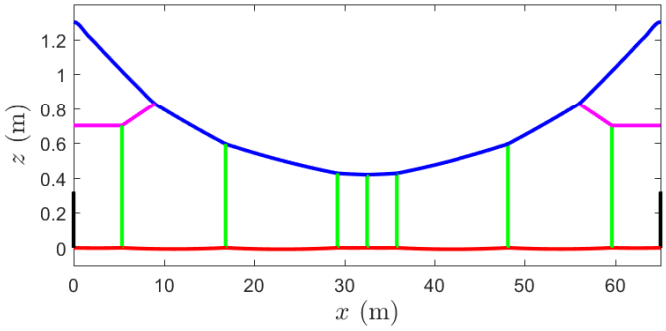

Figure 13: Optimised geometry obtained in the SW2 problem.

is plotted. The standard deviation of the interaction force is very similar to that achieved by the SW1 configuration. Specifically, $\sigma(f_{inter}) = 14.05$ N.

The location of the three droppers near the midspan indicates the possibility of removing two of them, so that the SW3 optimisation problem is carried out on an SW

Table 5: Optimisation results of the SW catenary.

Problem identifier	Variable type	Optimal values (m)	$\sigma(f_{inter})$ (N)	σ reduction (%)
SW1	Δh_c	0.002 0.004 -0.009 -0.001	14.14	36.60
SW2	d	5.36 16.83 29.21	14.05	37.00
SW3	Δh_c	0.002 0.004 0	12.42	44.31
	d	6.04 18.27		
Reference values (m)				
SW Ref.	Δh_c	0	22.30	–
	d	6 15.48 24.18 32.5		

catenary with only five droppers per span. Like the B3 problem, in this case there are five optimisation variables composed of two dropper locations and three punctual heights along the contact wire. Their ranges are listed in Table 6. Since there are 5 variables to optimise, a population of 100 individuals is set.

Table 6: Variable limits used in the SW3 optimisation problem.

	d_i (m)		Δh_{c_i} (m)		
i	1	2	1	2	3
Min.	2	10	-0.02	-0.02	-0.02
Max.	9	30	0.02	0.02	0.02

The GA have only taken 85 generations to find the optimal solution shown in Table 5. In this catenary topology the three central droppers are almost equally spaced, as can be seen in Fig. 14. The dispersion of the interaction force is the lowest of the three optimised SW catenaries, with $\sigma_{SW3} = 12.42$ N. This represents a reduction of 44.31% with respect to the value obtained for the reference SW catenary.

6.4. Analysis of the optimised catenaries

It is interesting to analyse some static and dynamic characteristics of the optimised catenary configurations obtained in the previous sections. Specifically, the stiffness of the catenary along with the internal force of the droppers in the static equilibrium position are explored and the dynamic behaviour of the optimised catenaries, even at train speeds different to the design speed, is also investigated.

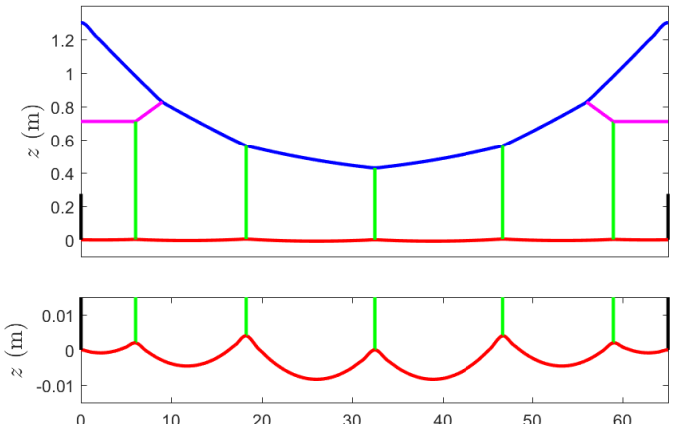

Figure 14: Optimised geometry obtained in SW3 problem.

6.4.1. Static characteristics of the optimised catenaries

The stiffness, k_{st}, at a certain point in the catenary is defined as the relationship between the vertical uplift and the upward force applied thereon. Figures 15 and 16 show this magnitude calculated in a central span subjected to a load $F = 100$ N (left) or $F = 200$ N (right) for the Benchmark and the Stitch Wired catenaries, respectively. Particularly for the former, a noticeable difference in stiffness is observed when the value of the applied force changes. This is due to the unilateral nonlinearity exhibited by the droppers, which tend to slacken making the catenary to be more flexible.

Comparing the optimised catenary configurations with respect to their reference configurations, although in the SW optimised catenaries there is a reduction in the variability of the stiffness along the span, it seems more drastic in the case of B1 and B3 optimised configurations. This means a smaller difference between the maximum k_{st}^{max} and the minimum k_{st}^{max} stiffness values. In order to quantify this effect, the stiffness variability coefficient is defined as:

$$\alpha = \frac{k_{st}^{max} - k_{st}^{min}}{k_{st}^{max} + k_{st}^{min}} \tag{13}$$

This coefficient is calculated for all the eight catenaries, as shown in Table 7. For catenary B1, this reduction largely exceeds the 50%. In contrast, the optimised B2 catenary despite showing more variability in stiffness, was demonstrated to be better in current collection quality. What emerges from these results is the benefit, although limited, of having a more uniform catenary stiffness distribution.

Another aspect that requires to be analysed is the internal force of droppers, f_d, in the static equilibrium configuration. In Fig. 17 these forces are represented for the

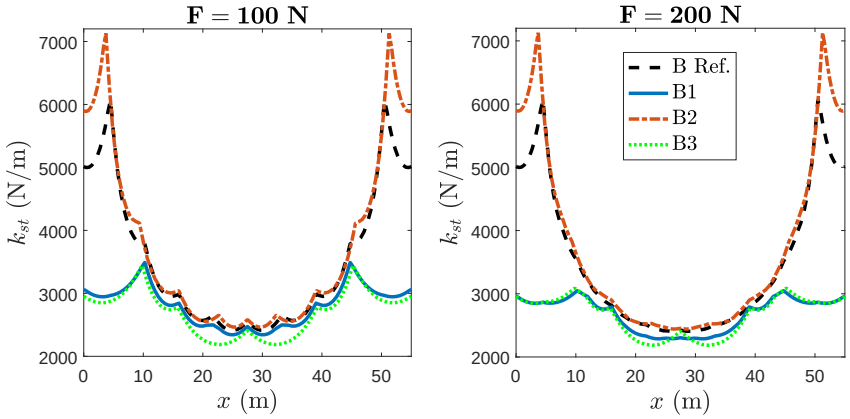

Figure 15: Vertical stiffness of the Benchmark catenaries.

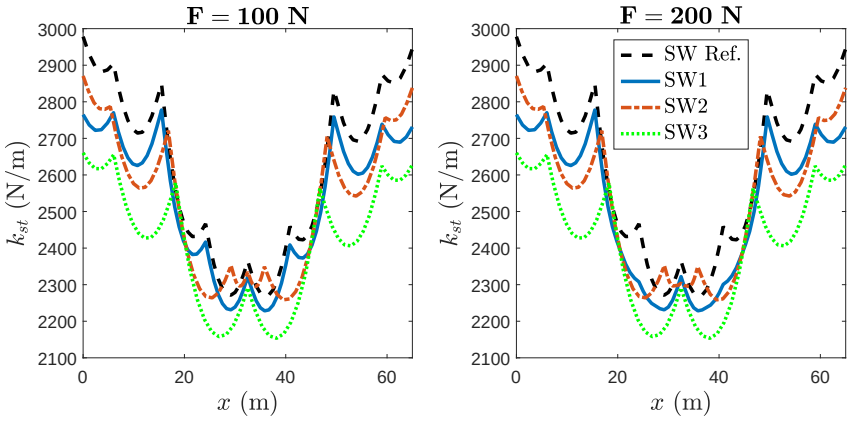

Figure 16: Vertical stiffness of the SW catenaries.

Benchmark reference and optimised catenaries. For the reference configuration, due to the initial pre-sag, the droppers located at the ends are much more tensioned than the central ones, which are almost uniformly loaded. A similar trend is observed for B2 catenary. Conversely, more irregularity in dropper tensions is present for optimised B1 and B3 catenaries. It is also noticed that certain droppers, such as the 1^{st} and 9^{th} droppers in B1, are barely loaded. Similar conclusions are drawn for SW catenaries, as shown in Fig. 18.

Table 7: Stiffness variation coefficient α of the optimised catenaries.

Cat. Label	$F = 100$ N	Reduction (%)	$F = 200$ N	Reduction (%)
B Ref.	0.431	—	0.432	—
B1	0.197	54.31	0.143	66.90
B2	0.486	-12.71	0.490	-13.43
B3	0.223	48.28	0.171	60.42
SW Ref.	0.135	—	0.135	—
SW1	0.109	19.26	0.109	19.26
SW2	0.118	12.59	0.118	12.59
SW3	0.104	22.96	0.104	22.96

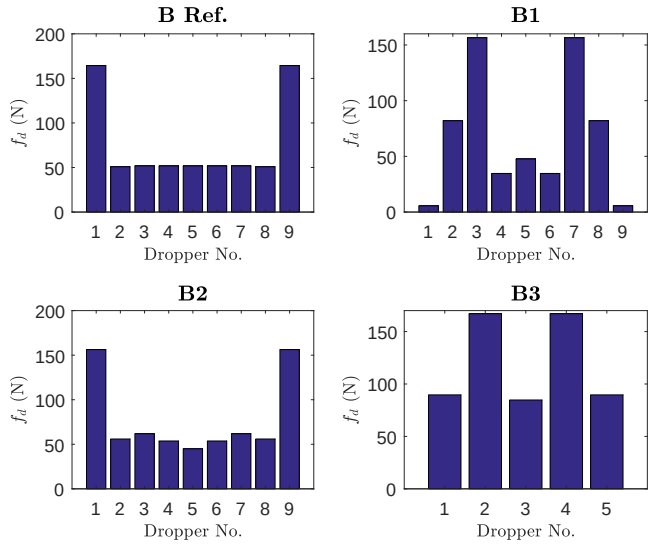

Figure 17: Dropper forces in static equilibrium configuration for Benchmark catenaries.

6.4.2. Dynamic behaviour of the optimised catenaries

Although the current collection quality has been quantified by means of the standard deviation of the interaction force, it is also interesting to see its time evolution. This is what is represented in Fig. 19 and Fig. 20 for the two central spans of the Benchmark and SW catenary models and their respective optimised catenaries, when

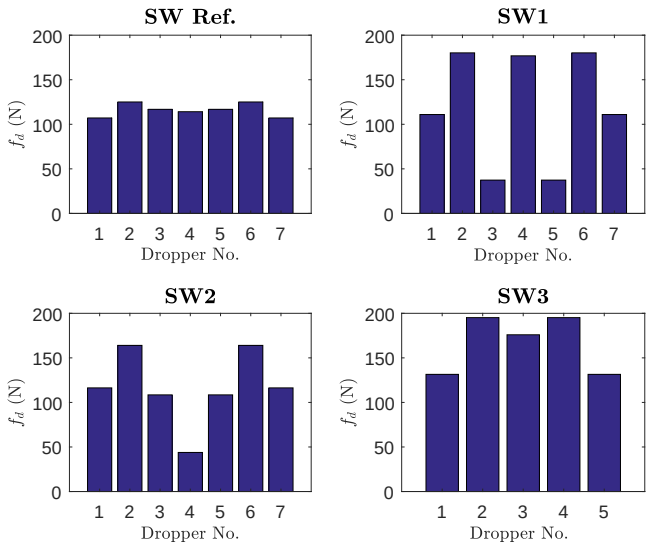

Figure 18: Dropper forces in static equilibrium configuration for SW catenaries.

the vehicle operates at the design speed. No low-pass filter has been applied to the contact force in Fig. 19, while the contact force represented in Fig. 20 has been low-pass filtered at 20 Hz. The central support is highlighted by the vertical dashed line in both figures.

For B1 and B3 catenaries, one can find lower local maxima near the supports. Additionally, higher local minima are observed near the midspan. For the SW catenaries it is more difficult to extract information from Fig. 19. However, the three important peaks present in the reference model are not generated in the optimised configurations.

Another important parameter that needs attention is the steady arm uplift. This magnitude must be controlled in order to avoid interferences with the registration arm. The vertical displacement of the central steady arm during train passage, is displayed in Fig. 21 for all the catenaries at $v = 300$ km/h.

The B1 and B3 catenaries exhibit a higher steady arm uplift. It should be noted that these optimised catenaries have a much lower stiffness on the supports region. Although this increased uplift is not a desired effect, the maximum displacement does not exceed the values recommended by the standards (between 100 and 120 mm). No notable differences are observed for the other optimised catenaries with respect to their reference cases.

As pointed out in Section 5, catenary optimisations are carried out only for a single train speed, which means that the optimised catenaries must be tested at other train

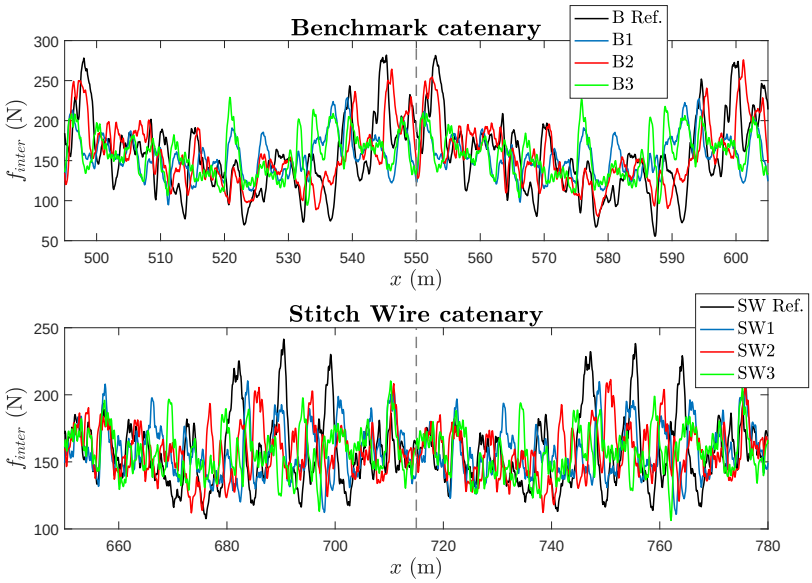

Figure 19: Interaction force at $v = 300$ km/h.

velocities. Fig. 22 shows the standard deviation σ of the interaction force for B1, B2 and B3 optimised configurations at different speeds. These results are also compared to those obtained from the reference catenary for the same range of velocities.

Fig. 22 reveals that B1 and B3 catenaries behave similarly with respect to changes in train speed. Their interaction force not only is much less oscillatory than that of the reference catenary at the design speed, but also great improvements are achieved when the train travels at velocities greater than 240 km/h. However, at velocities below 240 km/h, these catenary configurations exhibit a quite similar performance than that of the Benchmark reference topology. On the other hand, the B2 catenary barely improves its current collection quality for the design train speed. Furthermore, at all the other studied velocities any difference is found if it is compared with the reference scenario, which makes it the least promising option.

Moving to the optimised SW catenary configurations, Fig. 23 shows their dynamic behaviour in terms of σ, for the same range of train speeds. In this case, although the three optimised catenaries achieve a good improvement at the design speed, the catenary with optimised contact wire height (SW1) shows a highly oscillatory interaction force at velocities below 280 km/h. However, the SW2 and SW3 catenaries manifest a better behaviour at low train speeds, although not as good as the reference SW catenary. Unlike the SW1 catenary, these two options seem to be more stable versus velocity changes, being the SW3 the most suitable solution according to this

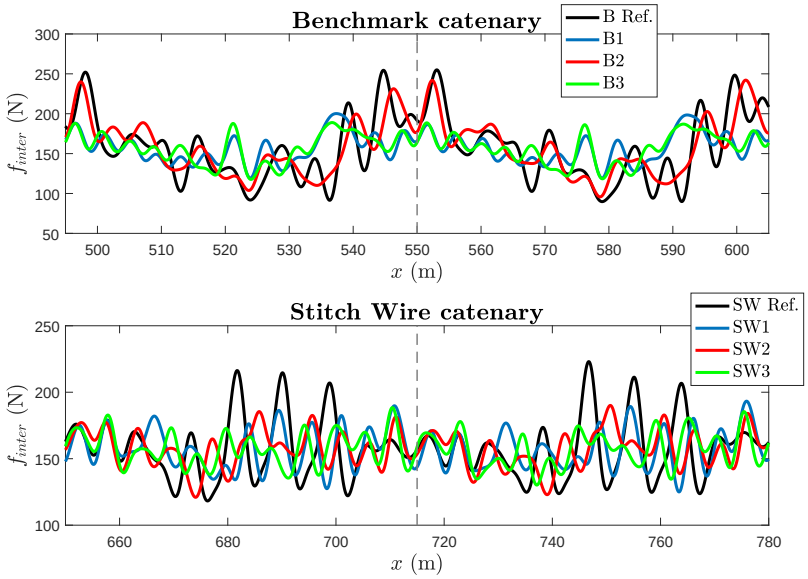

Figure 20: Interaction force low-pass filtered to 20 Hz at $v = 300$ km/h.

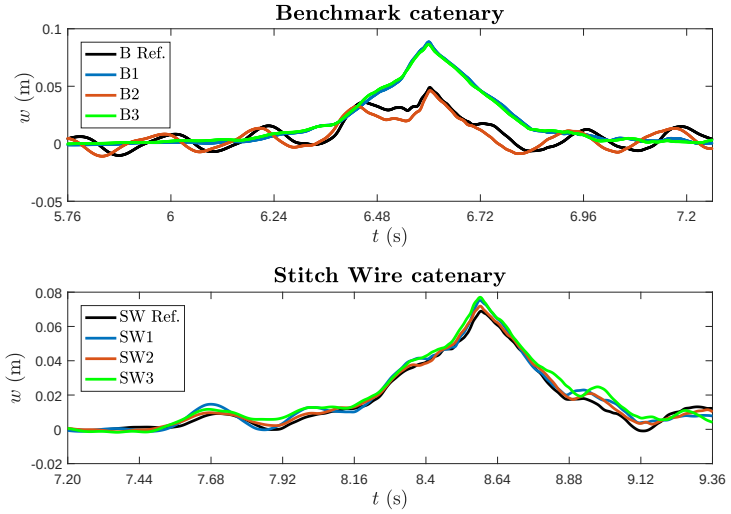

Figure 21: Central steady arm uplift at $v = 300$ km/h.

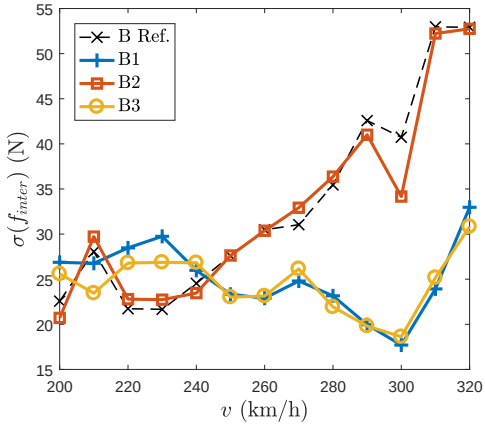

Figure 22: Optimised Benchmark catenaries behaviour at different train speeds.

criterion. In addition, the SW3 catenary presents the lowest interaction force σ at the design train speed.

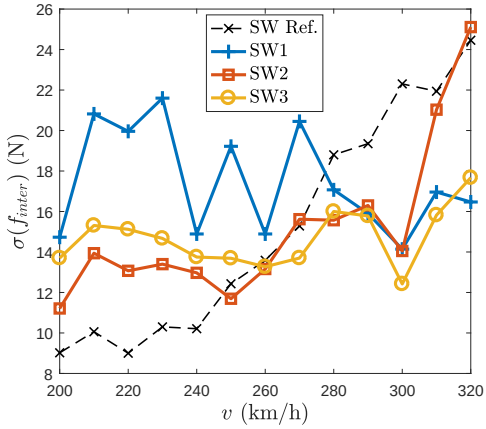

Figure 23: Behaviour of the optimised SW catenaries at different train speeds.

7. Conclusions

This paper describes an attempt to find optimised catenary configurations in terms of current collection quality for a given train speed, which does not guarantee better behaviour at other velocities. This optimisation consists in finding the catenary geometry which leads to the minimal standard deviation of the pantograph–catenary interaction force. The optimisations have been carried out by means of a GA in which contact wire height (by changes in dropper lengths), dropper spacing, or even both, are set as optimisation variables.

Several optimisations have been performed for two different catenary types: with and without stitch wires. The results of the optimisations show that current collection quality can be improved by setting the appropriate contact wire height, that moderate benefits can be obtained by varying dropper spacing and that even the removal of certain droppers can be also an appealing option to be considered.

Most of the optimised catenaries show a more uniform stiffness than their respective reference catenary geometries. The largest reduction in stiffness variation along the span is achieved in catenaries B1 and B3. Indeed, these two optimised configurations show higher uplifts of their steady arms, which, although they do not exceed the recommended limits, should be controlled to avoid mechanical interferences with registration arms.

Regarding the dynamic behaviour at different train speeds, the optimised catenaries do not worsen the current collection quality up to velocities far from the design one, specially for the Benchmark catenary type. Nevertheless, the optimised catenaries with less number of droppers seem to be the most consistent options in both Benchmark and Stitch wired catenary models. They exhibit a great behaviour not only at the design speed, but also they are the least sensitive to changes in velocity, if compared with the other optimised catenaries.

In conclusion, the results show that not only pre-sag can be a beneficial factor in current collection, but that catenary designers should also consider other geometric parameters such as contact wire height profile or dropper spacing within the span, because they can lead to great reductions in interaction force fluctuations. Besides, GAs emerge as a suitable tool that can be used to good effect in designing better catenaries.

A. Input data of the SW catenary model

The geometric input parameters needed to define the SW catenary model are shown in Table 8.

Table 8: Geometric data of the SW catenary model.

Input parameter	Value
Span length	65 m
Pre-sag	0 m
Encumbrance	1.3 m
Messenger wire stagger	0 m
Messenger wire clamp	0.21 kg
Stitch wire length	18 m
Contact wire stagger	±0.2 m
Contact wire clamp	0.21 kg
Steady arm length	1.15 m

The dropper spacing of this catenary is depicted in Table 9.

Table 9: Dropper spacing along the span.

	1	2	3	4	5	6	7
Longitudinal position of droppers (m)	6	15.48	24.18	32.5	40.82	49.52	59

Table 10 gives the material properties of the different cables which form the SW catenary.

Finally, the values of the lumped parameters defining the model of the pantograph associated to the SW catenary are displayed in Table 11.

Table 10: Material properties of the SW catenary components.

	Mass/unit length (kg/m)	Axial stiffness EA (MN)	Bending stiffness EI(Nm^2)	Tension (kN)
Messenger wire	0.864	1.042	136.09	15.75
Contact wire	1.374	1.65	238.70	31.5
Stitch wire	0.091	0.11	–	3.5
Droppers	0.091	0.11	–	–
Steady arm	1	1.1	–	–

Table 11: Lumped parameters of the pantograph model for the SW catenary.

d.o.f.	m (kg)	c (Ns/m)	k (N/m)
1	6.6	0	7000
2	5.8	0	14100
3	5.8	70	80

Acknowledgements

The authors would like to acknowledge the financial support received from the FPU program offered by the Ministry of Education, Culture and Sports of Spain (MECD), under grant number FPU13/04191, and also the funding provided by the Regional Government of Valencia (PROMETEO/2016/007).

References

[1] P. Nåvik, A. Rønnquist, and S. Stichel, "The use of dynamic response to evaluate and improve the optimization of existing soft railway catenary systems for higher speeds," *Proceedings of the Institution of Mechanical Engineers, Part F: Journal of Rail and Rapid Transit*, vol. 230, no. 4, pp. 1388–1396, 2016. 1

[2] P. Harell, L. Drugge, and M. Reijm, "Study of critical sections in catenary systems during multiple pantograph operation," *Proceedings of the Institution of*

Mechanical Engineers, Part F: Journal of Rail and Rapid Transit, vol. 219, no. 4, pp. 203–211, 2005. 1

[3] F. Kiessling, R. Puschmann, A. Schmieder, and E. Schneider, *Contact Lines for Electric Railways. Planning, Design, Implementation, Maintenance*. 2009. 1

[4] S. Bruni, J. Ambrosio, A. Carnicero, Y. H. Cho, L. Finner, M. Ikeda, S. Y. Kwon, J. P. Massat, S. Stichel, and M. Tur, "The results of the pantograph-catenary interaction benchmark," *Vehicle System Dynamics*, vol. 53, no. 3, pp. 412–435, 2015. 1, 2, 4, 5, 6, 6

[5] A. Shabana, "Computer implementation of the absolute nodal coordinate formulation for flexible multibody dynamics," *Nonlinear Dynamics*, vol. 16, pp. 293–306, 1998. 1, 2

[6] N. Zhou and W. Zhang, "Investigation on dynamic performance and parameter optimization design of pantograph and catenary system," *Finite Elements in Analysis and Design*, vol. 47, no. 3, pp. 288–295, 2011. 1

[7] J. W. Kim and S. N. Yu, "Design variable optimization for pantograph system of high-speed train using robust design technique," *International Journal of Precision Engineering and Manufacturing*, vol. 14, no. 2, pp. 267–273, 2013. 1

[8] J. Ambrósio, J. Pombo, and M. Pereira, "Optimization of high-speed railway pantographs for improving pantograph–catenary contact," *Theoretical and Applied Mechanics Letters*, vol. 3, no. 1, p. 013006, 2013. 1, 5

[9] J. H. Lee, Y. G. Kim, J. S. Paik, and T. W. Park, "Performance evaluation and design optimization using differential evolutionary algorithm of the pantograph for the high-speed train," *Journal of mechanical science and technology*, vol. 26, no. 10, pp. 3253–3260, 2012. 1

[10] J. P. Massat, C. Laurent, J. P. Bianchi, and E. Balmès, "Pantograph–catenary dynamic optimisation based on advanced multibody and finite element cosimulation tools," *Vehicle System Dynamics*, vol. 52, no. sup1, pp. 338–354, 2014. 1, 2, 5

[11] Y. H. Cho, K. Lee, Y. Park, B. Kang, and K. Kim, "Influence of contact wire pre-sag on the dynamics of pantograph–railway catenary," *International Journal of Mechanical Sciences*, vol. 52, no. 11, pp. 1471–1490, 2010. 1

[12] W. Zhang, G. Mei, and J. Zeng, "A study of pantograph/catenary system dynamics with influence of pre-sag and irregularity of contact wire," *Vehicle System Dynamics*, vol. 37, pp. 593–604, 2002. 1

[13] M. L. Yu, W. Z. Liu, J. Zhang, and C. Y. Yan, "Influence of dropper spacing on quality of pantograph–catenary current collection," in *Applied Mechanics and Materials*, vol. 654, pp. 78–81, Trans Tech Publ, 2014. 1

[14] S. Koziel and X. S. Yang, *Computational optimization, methods and algorithms*, vol. 356. Springer, 2011. 1

[15] W. Hare, J. Nutini, and S. Tesfamariam, "A survey of non-gradient optimization methods in structural engineering," *Advances in Engineering Software*, vol. 59, pp. 19–28, 2013. 1

[16] M. Tur, L. Baeza, F. Fuenmayor, and E. García, "PACDIN statement of methods," *Vehicle System Dynamics*, vol. 53, no. 3, pp. 402–411, 2015. 1

[17] M. Tur, E. García, L. Baeza, and F. Fuenmayor, "A 3D absolute nodal coordinate finite element model to compute the initial configuration of a railway catenary," *Engineering Structures*, vol. 71, pp. 234–243, 2014. 1, 2, 3, 6.2

[18] S. Gregori, M. Tur, E. Nadal, J. Aguado, F. Fuenmayor, and F. Chinesta, "Fast simulation of the pantograph–catenary dynamic interaction," *Finite Elements in Analysis and Design*, vol. 129, pp. 1–13, 2017. 1, 4, 4, 4

[19] S. H. Kia, F. Bartolini, A. Mpanda-Mabwe, and R. Ceschi, "Pantograph–catenary interaction model comparison," in *IECON 2010-36th Annual Conference on IEEE Industrial Electronics Society*, pp. 1584–1589, IEEE, 2010. 2

[20] J. Gerstmayr and A. A. Shabana, "Analysis of thin beams and cables using the absolute nodal coordinate formulation," *Nonlinear Dynamics*, vol. 45, no. 1-2, pp. 109–130, 2006. 2

[21] A. Collina and S. Bruni, "Numerical simulation of pantograph-overhead equipment interaction," *Vehicle System Dynamics*, vol. 38, no. 4, pp. 261–291, 2002. 4, 5

[22] J. Ambrósio, J. Pombo, P. Antunes, and M. Pereira, "PantoCat statement of methods," *Vehicle System Dynamics*, vol. 53, no. 3, pp. 314–328, 2015. 4

[23] EN 50367, "Railway applications. Current collection systems. Technical criteria for the interaction between pantograph and overhead line," *European Committee for Electrotechnical Standarization*, 2012. 5, 5

[24] P. Nåvik, A. Rønnquist, and S. Stichel, "Variation in predicting pantograph–catenary interaction contact forces, numerical simulations and field measurements," *Vehicle System Dynamics*, pp. 1–18, 2017. 5

[25] EN 50318, "Railway applications. Current collection systems. Validation of simulation of the dynamic interaction between pantograph and overhead contact line," *European Committee for Electrotechnical Standarization*, 2002. 6

PAPER D

Stochastic Monte Carlo simulations of the pantograph-catenary dynamic interaction to allow for uncertainties introduced during the catenary installation

S. Gregori, M. Tur, J. E. Tarancón and F. J. Fuenmayor

Vehicle System Dynamics
Accepted, April 2018

Abstract

The simulation of the pantograph–catenary dynamic interaction is at present mainly based on deterministic approaches. However, any errors made during the catenary stringing process are sources of variability that can affect the dynamic performance of the system. In this paper we analyse the influence of dropper length, dropper spacing and support height errors on the current collection quality by applying a classic Monte Carlo method to obtain the probability density functions of several output quantities. The effects of installation errors are also studied for a range of train speeds. Finally, the pre-sag that, on average, produces the best behaviour of the system is identified, allowing for the uncertainty in the catenary installation. The results obtained show the need to consider variability in pantograph–catenary dynamic simulations.

Key words

Stochastic simulation; Railway catenary; Pantograph–catenary interaction; Uncertainty propagation; Monte Carlo simulations

Contents

1 Introduction **187**

2 Catenary description and modelling **188**

3 Dynamic interaction problem **189**

4 Description of the catenary installation errors and their effects **191**
4.1 Dropper length error 192
4.2 Dropper spacing error 193
4.3 Support height error 193
4.4 Measurable effects of installation errors 194

5 Monte Carlo simulations **195**
5.1 Searching for the required number of trials 196

6 Discussion of the numerical results **200**
6.1 Statistical quantification of the effects produced by installation errors 201
6.2 Mean evaluation of the effects produced by installation errors 205
6.3 Influence of installation errors at different train speeds 206
6.4 Optimal robust pre-sag 207

7 Conclusions **209**

Bibliography **210**

1. Introduction

Current collection in high-speed trains is achieved by means of a sliding contact between the pantograph and a conductive wire. The former is mounted on the locomotive, whilst the overhead line, the catenary, is a cable structure suspended above the track. According to the standards, the interaction force generated by this sliding contact can be used to determine the quality and stability of current supply. Ideally, this force should have low force peaks to prevent component damage and wear, but at the same time it should be far enough from null values to avoid the undesirable consequences of arcing.

The simulation of the pantograph–catenary dynamic interaction has become an important tool for catenary designers in recent years (see [1] and the references therein). Simulations are helpful when different geometries, configurations and materials need to be tested or even optimized [2,3], with no need for a prototype or expensive in-line tests. However, these simulations usually provide deterministic results, such as optimized geometries or sensitivity studies [4], in which magnitudes like the interaction force or the uplift at a certain point of the catenary do not allow for the variability present in the system.

There are countless sources of variability in the pantograph–catenary dynamic interaction; for example, during catenary stringing some human errors are unavoidably made, leading to a final catenary configuration that differs from the original design. These discrepancies can have severe effects on the dynamic performance of the system, although they are not usually considered in the current software. To the authors' knowledge, very few studies can be found in the literature on the uncertainties of the catenary system. In [5] a diagnosis procedure is proposed to identify catenary defects, such as those produced by creep phenomena, wear in cables and dropper length deviations, whose impact on the catenary dynamic performance are studied in [6]. Guideline values for certain installation error rates based on real measured data were proposed in [7], while variability in pantograph–catenary dynamic simulations regarding wear, aerodynamic effects and geometry irregularities is introduced in [8], in which the need for further studies on the field is suggested.

This paper proposes an approach to deal with the variability introduced by installation errors. Dropper lengths, dropper spacing and support height errors are taken into account due to their important role in determining contact wire height [9]. The procedure is based on the application of the well-known classic version of Monte Carlo Simulations (MCS) for the propagation of uncertainty [10] and consists of evaluating the model in a sufficiently large number of simulations with a random sampling of the input quantities as described by their probability density functions (PDFs). A large number of trials are achievable by combining both a highly efficient simulation

strategy [11] and parallel computing, so that the effects of mounting errors on the system dynamics are fully characterized in a statistical sense.

The paper is organized as follows: after this brief introduction to the subject, the catenary system and its modelling are described in Section 2. The pantograph–catenary dynamic interaction problem is formulated in Section 3. We use an efficient solution method [11], which provides considerable computational cost savings (a brief description of this method is also presented for the sake of completeness). The installation errors considered and their measurable effects are defined in Section 4. Section 5 is devoted to briefly explaining the Monte Carlo simulation strategy, in which the number of simulated trials is a key factor; this issue is addressed in detail in Section 5.1. Finally, different numerical examples and results are discussed in detail and the conclusions are given in Section 6.

2. Catenary description and modelling

The railway catenary is a cable structure through which the power is supplied to the locomotive via a sliding contact with the pantograph. As shown in Fig. 1, the cabling is regularly supported by poles and brackets. In order to keep the contact wire at the desired height it is hung on droppers from the messenger wire. With the help of steady arms, the contact wire is staggered to ensure uniform wear on the pantograph collector strips. Some catenary topologies also include stitch wires near the supports to smooth out stiffness variations.

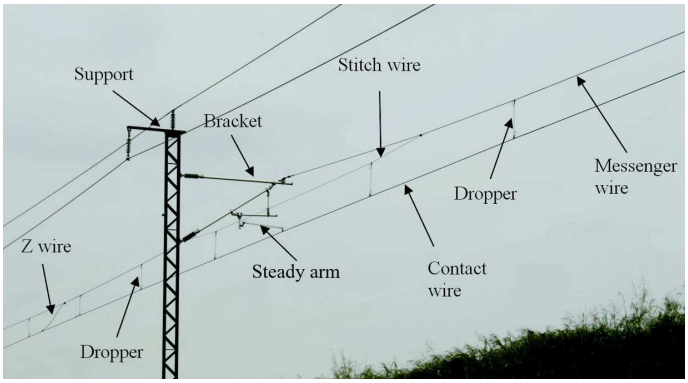

Figure 1: Real catenary with its main components.

Although mathematical models and simulations of the pantograph–catenary dynamic interaction were introduced some decades ago, it was not until the appearance of demanding high-speed requirements that an effort was made to improve these models and simulations (see for example [12, 13]). From the huge variety of studies in the recent literature, the benchmark [1] and the references therein stand out from the rest.

To model the catenary we here use the Finite Element model presented in [14], which is based on the Absolute Nodal Coordinate Formulation (ANCF) [15]. All the calculations and examples given in this paper are focused on the Benchmark catenary model, which is depicted in Fig. 2. Its geometric inputs and material properties are fully described in [1].

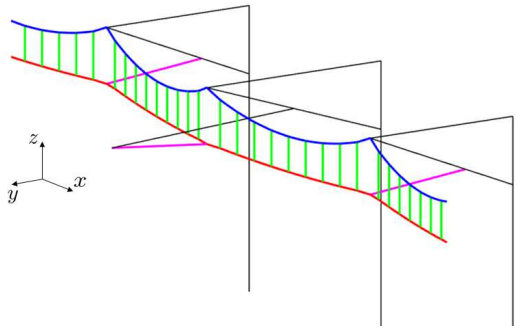

Figure 2: FE model of the benchmark catenary.

Although more complex pantograph models can be found in the literature [16], we use here a simple lumped-parameter model which only introduces three vertical degrees of freedom. Both pantograph and catenary models interact with each other by means of a penalty method with a high penalty stiffness, $k_h = 50$ kN/m, as recommended in [17]. Fig. 3 contains a sketch of both models.

3. Dynamic interaction problem

The static configuration problem consists of calculating the nodal coordinates, $\mathbf{q}$, which fulfil the nonlinear static equilibrium equations (1), that is, the internal forces must balance the gravitational forces:

$$\mathbf{F}_{int}(\mathbf{q}) + \mathbf{F}_g = \mathbf{0} \tag{1}$$

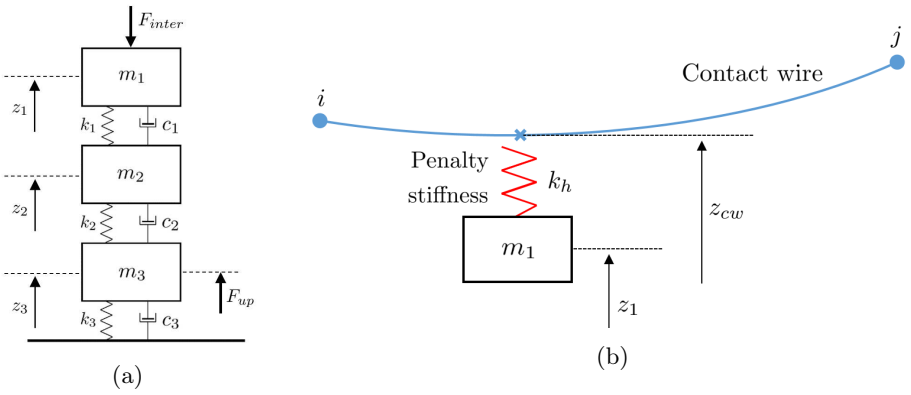

Figure 3: (a) Pantograph and (b) interaction model schemes.

Nevertheless, in a cabling structure such as the railway catenary, the usual problem to be dealt with is the so-called 'form-finding' problem, in which not only the nodal coordinates $\mathbf{q}$ are unknown, but also the finite element lengths, $\mathbf{l}^e_{ref}$, must be found to fulfil both equilibrium equations and any constraints imposed during the stringing process. Following the procedure proposed in [18] we get:

$$\begin{aligned} \mathbf{F}_{int}(\mathbf{q}, \mathbf{l}^e_{ref}) + \mathbf{F}_g(\mathbf{l}^e_{ref}) &= \mathbf{0} \\ \mathbf{c}(\mathbf{q}, \mathbf{l}^e_{ref}) &= \mathbf{0} \end{aligned} \tag{2}$$

The constraint equations $\mathbf{c}$ impose contact and messenger wire tensions, contact wire height and position of droppers and support elements.

Once the initial configuration is found, dynamic equations can be linearised with respect to this configuration due to the small displacements undergone by the cables. Therefore, if $\mathbf{u}$ denotes for the nodal displacements vector,

$$\mathbf{M}\ddot{\mathbf{u}} + \mathbf{C}\dot{\mathbf{u}} + \mathbf{K}\mathbf{u} = \mathbf{F} \tag{3}$$

models the global pantograph–catenary dynamic interaction problem, in which $\mathbf{M}$ and $\mathbf{K}$ are the mass and stiffness matrices respectively. In this paper, a proportional Rayleigh damping ($\alpha_r = 0.0125$ and $\beta_r = 10^{-4}$) is considered to build $\mathbf{C}$ [1]. Vector $\mathbf{F}$ contains the external uplift force, F_{up}, applied to the bottom mass of the pantograph model (see Fig. 3a). This dynamic problem is subject to two sources of severe non-linearities, that is, the unilateral behaviour of droppers and the contact loss between the pantograph and the contact cable.

Although the nonlinear problem stated in Eq. (3) can be solved by the commonly used Newmark method [19], its direct application would require an excessive computational cost for directly using MCS. In order to speed-up the calculations and make the approach viable, in this work we use the *Offline/Online* strategy proposed

in [11]. The solution given by this method is just as accurate as that obtained with the classical direct integration approach. The method is based on two main concepts:

- All sources of nonlinearity are shifted to the right hand side of Eq. (3). These are the interaction force and the compensating force terms coming from the slackened droppers. The idea was first proposed in [13] and exploited in [20]. This fact gives a constant system matrix which is only factorized once in the whole procedure.
- With dynamic responses under unitary forces precomputed in the *Offline* stage and the application of the superposition principle, the only unknowns are now the value of the correction forces of slackened droppers and the interaction force value at each time step. Thus, one has only to deal with a very small nonlinear system of equations which is iteratively solved during the so called *Online* stage.

The only disadvantage of this method against the traditional direct integration technique is the need for enough available RAM memory to avoid swapping data onto the hard disk, which would slowdown the calculations. For further implementation details the reader is again referred to [11].

4. Description of the catenary installation errors and their effects

During the catenary installation, technicians can make small mistakes which lead to a different static configuration from the original design. Regarding their role in achieving the desired contact wire height, of the many possible errors we consider here the three deviations from the nominal values given in Fig. 4. Namely:

1) Deviations in dropper length.

2) Deviations in dropper spacing.

3) Deviations in support height.

In order to quantify these, due to the lack of experimental measurements, we assume they are independent and follow a normal statistical distribution without any loss of generality. The mean is set as $\mu_i = 0$, for $i = 1, 2, 3$, because each error is defined as the deviation from its design value. The remainder of this section is devoted to providing further details on how each error is considered in the model plus a definition of the measurable magnitudes which can be affected by these errors.

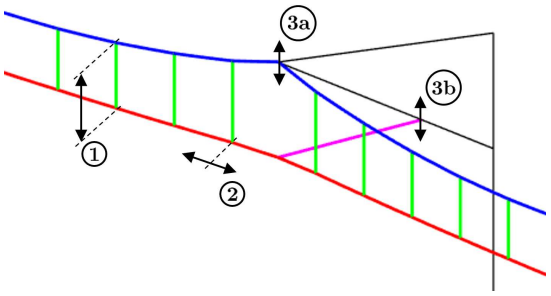

Figure 4: Scheme of installation errors.

4.1. Dropper length error

The accuracy of dropper measurements during manufacture is reported to be within about 1 cm [9]. We assume that each dropper length error is a normally distributed variable with standard deviation $\sigma_1 = 6.6$ mm, which is in accordance with the value given in [21]. Following the 3σ rule, 99.87% of the length deviations found in droppers will be within ± 2 cm.

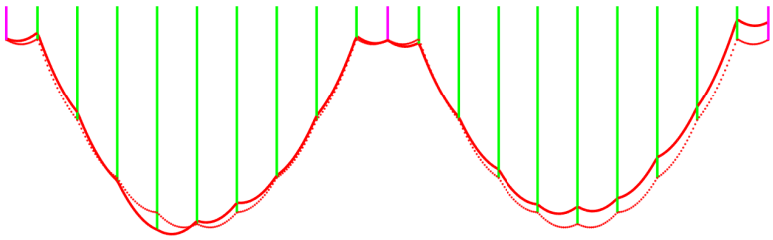

Figure 5: Catenary configuration when including dropper length error (solid line). Nominal configuration (dotted line).

From the computational point of view, in order to model this error we first solve the form-finding problem (2) to obtain the nominal contact wire height. Once the nominal lengths of the dropper elements, $\mathbf{l}^d_{ref}$, are obtained, they are modified by adding to them a value randomly sampled from the normal distribution defined for this type of installation error. The nonlinear static equilibrium problem (1) is then solved with the new dropper lengths to obtain the actual catenary configuration.

Changes in the contact wire profile can be seen in Fig. 5, which shows an example of two spans of the Benchmark catenary with and without dropper length deviations. If we define the span slope, s_s, as the difference in height per unit length between

two consecutive steady arms, it is also slightly affected, mainly by deviations in the length of the droppers near the supports.

4.2. Dropper spacing error

In a 55 m long span all the droppers are likely to be clamped to the wires at a short distance away from the point planned in the design. In the absence of experimental measurements and available information in the literature, we assume a normal distributed error with standard deviation $\sigma_2 = 20$ mm. Again, following the 3σ criterion, a deviation of within ± 60 mm with respect to their nominal position will be found in 99.87% of cases.

During installation, the dropper is initially cut to the nominal length l^d_{ref}, which guarantees the contact wire will be at the desired height. However, when the dropper is being clamped to the wires, if it is incorrectly placed, the contact wire height will not be as planned. In order to simulate the realistic features of this error, the following steps are performed:

1. Solve the form-finding problem (2) for the nominal dropper spacing in order to obtain the nominal dropper lengths $\mathbf{l}^d_{ref1}$ (dashed line in Fig. 6).

2. Solve a new form-finding problem (2) for a catenary with random deviations Δ in dropper spacing (dotted line in Fig. 6). For this obtained configuration, the obtained dropper lengths $\mathbf{l}^d_{ref2}$ differ from the nominal ones, $\mathbf{l}^d_{ref1}$.

3. Restore the nominal lengths $\mathbf{l}^d_{ref1}$ to the dropper elements and solve a static equilibrium problem (1) to obtain the final catenary configuration (solid line in Fig. 6), which has both nominal dropper lengths and a random dropper spacing error.

4.3. Support height error

The last error to be considered is the height at which cantilevers are fixed to the posts. These heights were measured in [21] and show a standard deviation of $\sigma_3 = 2$ cm. Sticking to the 3σ rule, 99.87% of the installed catenaries will not have a maximum deviation greater than 6 cm.

To model a catenary with this installation error, the form-finding problem (2) for the nominal catenary must first be solved, followed by the nonlinear static equilibrium problem (1). In the latter, the Dirichlet conditions in z direction of the support nodes of the messenger wire and the end nodes of the steady arms (3a and 3b in Fig. 4) are randomly changed to allow for the support heights error. The random change

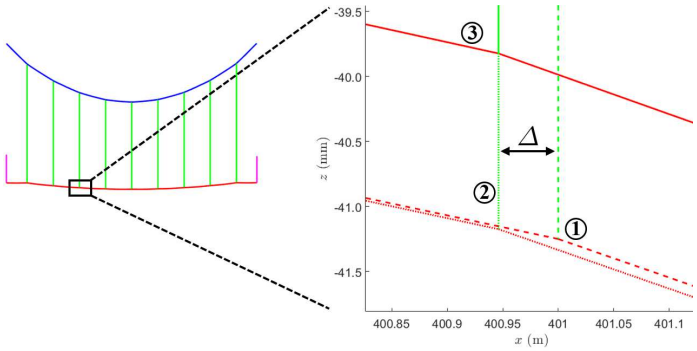

Figure 6: Representation of the catenary configurations obtained after each of the three steps followed to simulate the dropper spacing error.

in height can be either the same or different for both connections of each cantilever, depending on whether they are considered as a single installation error or as two independent deviations.

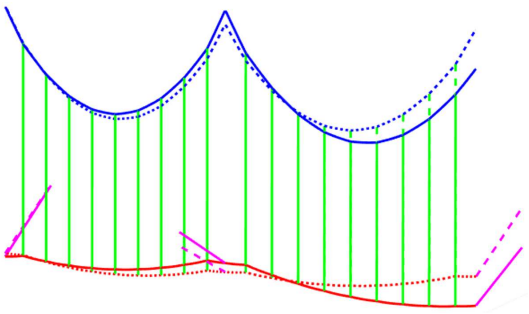

Figure 7: Catenary configuration with deviations in support heights (solid line). Nominal configuration (dashed line).

4.4. Measurable effects of installation errors

The installation errors described above affect both the catenary's static configuration and its dynamic behaviour and therefore modify the current collection performance. However, measurable magnitudes need to be defined to quantify these effects. In this study we focus on the following parameters, recommended by many standards [22, 23] and due to their important role in maintenance procedures:

- Coefficient of variation of the interaction force: defined as the ratio between its standard deviation $\sigma\left(F_{inter}\right)$, and its mean $\mu(F_{inter})$, namely:

$$\nu = \frac{\sigma\left(F_{inter}(t)\right)}{\mu(F_{inter}(t))} \tag{4}$$

  The interaction force is low-pass filtered to 20 Hz and measured in the ten central spans of a catenary with twenty spans.

- Percentage of time in which contact loss occurs: t_{cl}.
- Maximum uplift registered in steady arms: Δz^{max}.
- Maximum value of the 20 Hz filtered interaction force: F_{inter}^{max}.
- Maximum absolute value of the span slope: s_s^{max}.
- Maximum absolute value of the span slope difference between two consecutive spans: Δs_s^{max}.

The most important magnitude to be evaluated is the ratio ν, by which the current collection quality is mainly characterized. The lower the ν the more uniform the contact force. However, it is also important to avoid both contact losses and excessive wear on the components, so that t_{cl} and F_{inter}^{max} must also be checked. In order to prevent collisions between the pantograph and registration arms, Δz^{max} is usually restricted to 10 or 12 cm. The static parameters s_s^{max} and Δs_s^{max} can also be regarded as interesting output quantities due to they are limited by many standards.

5. Monte Carlo simulations

The aim of this work was to study the consequences of the errors made during the catenary installation. The widely accepted Monte Carlo (MC) technique was adopted to deal with this uncertainty propagation problem [24]. The MC method has certain advantages, such as taking the nonlinearities of the model into account and not imposing any restrictions on the output probability distributions. However, as thousands of dynamic simulations are required this method entails a high computational cost, to alleviate which we resorted to the efficient integration algorithm proposed in [11].

As can be seen in the diagram shown in Fig. 8, the starting point is the characterization of the statistical distributions X_i of the input variables (in this case installation errors). As mentioned in Section 4, they are assumed to be independent Gaussian distributed variables, and are therefore defined by their null mean and standard deviation σ_i. Vectors $\mathbf{x}_r$, $r = 1, ..., N$, are randomly sampled from the probability density

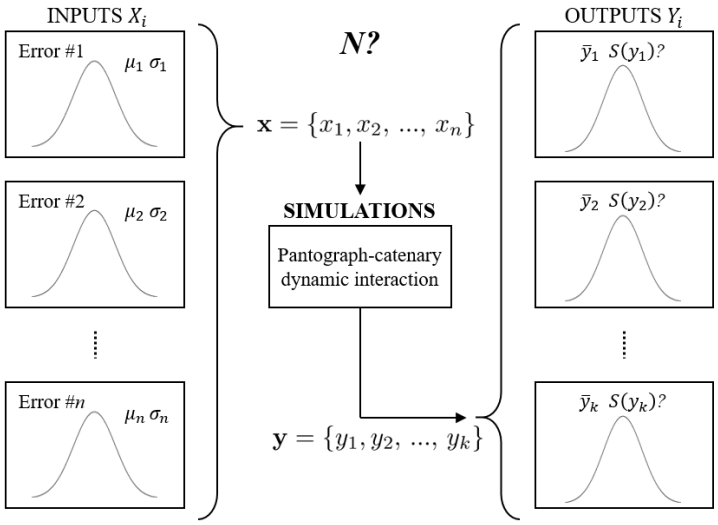

Figure 8: Uncertainty propagation flow diagram.

functions and serve as input values for the evaluation of the pantograph–catenary dynamic interaction model.

The key issue in this procedure is how to determine the number of trials, N, so that the obtained distributions of the output variables Y_i, are statistically representative. If we assume that N is chosen to provide enough accuracy in the results, one can build the probability density function (PDF) of each output variable, which can be numerically defined by its statistical moments or coverage intervals.

5.1. Searching for the required number of trials

If ν is chosen as the output quantity of interest (due to being seen as a good indicator of current collection performance), we need to obtain the value of N which provides enough accuracy in estimating both its real mean $\mu(\nu)$ and its real standard deviation $\sigma(\nu)$. In what follows, these two statistics will be referred to as 'target quantities'.

One simple strategy to asses and control the desired accuracy consists of performing M sets of N simulations, that is, M sets of N catenaries with installation errors, and then measuring the dispersion of the target quantity obtained from each of the M sets. This technique is exemplified in Fig. 9, in which ten sets are considered, $M = 10$, for three different trial sizes ($N = 500, 1000, 2000$). The $M \cdot N$ simulations

were performed with a catenary allowing for both dropper length and support height errors, which are the most influential as will be seen later.

Fig. 9 shows the estimated mean $\bar{\nu}$ (left) and standard deviation $S(\nu)$ (right) obtained from each set. Fig. 9 shows that no matter how many trials are performed, the

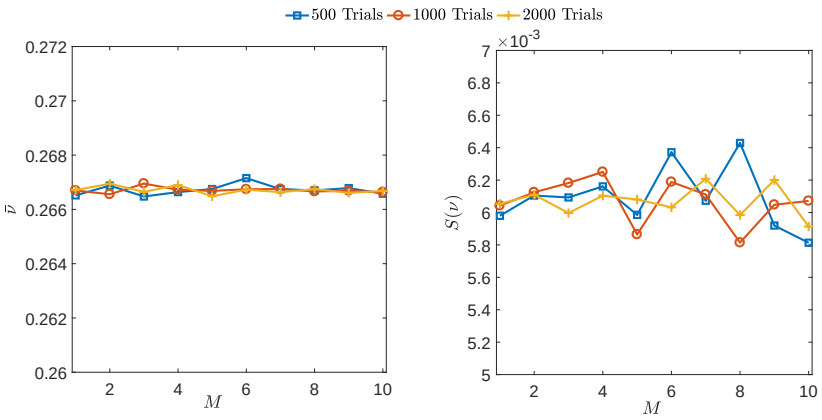

Figure 9: Mean $\bar{\nu}$ (left), and standard deviation $S(\nu)$ (right), for ten sets with different number of trials.

mean value of ν barely varies from one set to another, while the standard deviation changes considerably among the different sets, even for the largest ones, ($N = 2000$). However, these results are only able to confirm whether N provides the target quantities with a given accuracy when a huge amount of sets M are computed at a prohibitive computational cost.

In order to solve this issue we explore two different approaches. The first strategy is based on the theoretical calculation of the confidence interval of the target quantities. Regarding the unknown population mean $\mu(\nu)$, the central limit theorem [25] establishes that the mean of a sufficiently large sample, $\bar{\nu}$, follows a normal distribution with mean $\mu(\nu)$ and standard deviation $\frac{\sigma(\nu)}{\sqrt{N}}$. If α denotes the significance level, the $100(1-\alpha)\%$ confidence interval of $\mu(\nu)$ is:

$$\bar{\nu} - z_{\alpha/2}\frac{\sigma(\nu)}{\sqrt{N}} \leq \mu(\nu) \leq \bar{\nu} + z_{\alpha/2}\frac{\sigma(\nu)}{\sqrt{N}} \tag{5}$$

where $z_{\alpha/2}$ is the value with an occurrence probability lower than $\alpha/2$ in a normal standard distribution and N is the sample size. We define d as the assumable difference between the sample mean and the unknown population mean, $d = |\bar{\nu} - \mu(\nu)|$, therefore from Eq. (5) we have:

$$N = z_{\alpha/2}^2\frac{\sigma(\nu)^2}{d^2} \tag{6}$$

Although this equation needs the exact value of $\sigma(\nu)$, which is unknown, we can estimate it from a large enough population ($N = 5000$). For the catenaries studied the value of $\sigma(\nu)$ is around 0.265. Thus, if a 3% relative error is assumable in the mean estimation, the absolute difference between the estimated and real mean is approximately $d = 0.008$. After applying Eq. (6) with a significance level of $\alpha = 0.01$, in 99% of cases $\mu(\nu)$ can be estimated by only four simulations with an error of less than 3%.

Regarding $S(\nu)$, the common approach to obtain the required number of trials N to guarantee a given accuracy of the estimated standard deviation is restricted to normally distributed samples. In our case, as the PDF of ν is unknown, this normality assumption cannot be made. In this situation, different authors (see for example [26]) propose diverse strategies which only require a finite population kurtosis $\gamma(\nu)$. Among these proposals, a general and simple central limit approach [27] states that the sample variance $S(\nu)^2$ is asymptotically normally distributed with an expected value $\sigma(\nu)^2$ and a standard deviation $\sigma(\nu)^2\sqrt{\frac{\gamma(\nu)-1}{N}}$. This leads to the following nominal $100(1-\alpha)\%$ confidence interval for $\sigma(\nu)^2$:

$$\frac{S(\nu)^2}{1 - z_{\alpha/2}\sqrt{\frac{\gamma(\nu)-1}{N}}} \leq \sigma(\nu)^2 \leq \frac{S(\nu)^2}{1 + z_{\alpha/2}\sqrt{\frac{\gamma(\nu)-1}{N}}} \tag{7}$$

In order to fulfil the last relation for an assumable relative error $e = \left|\frac{S(\nu)^2 - \sigma(\nu)^2}{\sigma(\nu)^2}\right|$ in the variance, the number of trials considered in the MC method should be:

$$N = z_{\alpha/2}^2 \frac{\gamma(\nu) - 1}{e^2} \tag{8}$$

The results of applying Eq. (8) are given in Table 1 for different significance levels α and assumed relative errors e. In this case a population with 10000 trials was simulated to estimate $\gamma(\nu)$. The results reveal that this criterion is much more restrictive

Table 1: Number of trials N, required to fulfil the variance coverage interval for different relative errors e and significance levels α.

e \ α	0.05	0.02	0.01
0.05	2331	3634	4663
0.02	14571	22715	29146
0.01	58282	90861	116582

than that applied for the mean, since 12954 simulations are now needed to obtain $S(\nu)^2$ with a 3% error and 99% confidence level.

In order to validate the previous results, a second approach is used to quantify the accuracy of $S(\nu)^2$ which consists of following a classical bootstrapping strategy [28] in which no assumption of normality is required. This resampling technique is based on random sampling with replacement and can estimate the sampling distribution of almost any statistic (mean, variance, etc.) [29]. Starting from a large enough sample (of size N) of ν, one can perform N resamples $[\nu_1^*, \nu_2^*, ..., \nu_N^*]$, each one also of size N, taken from the original sample by using sampling with replacement. For each of these bootstrap samples we compute the desired statistic, in this case $[S(\nu^*)_1^2, S(\nu^*)_2^2, ..., S(\nu^*)_N^2]$, in order to obtain the histogram which provides an estimate of its PDF.

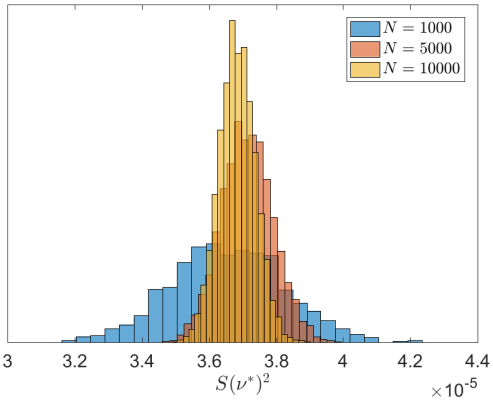

Figure 10: Bootstrap distributions of estimated variance $S(\nu^*)^2$, for samples of size $N = 1000$, 5000 and 10000.

The principle of bootstrapping assumes that for large enough N, the bootstrap PDF of $S(\nu^*)^2$ tends to its real PDF. We start from three original initial samples of nu with sizes $N = 1000, 5000$ and 10000. From these samples the histograms shown in Fig. 10 are built by the bootstrapping method. The 99% coverage intervals of these distributions are given in Table 2, in which it can be seen that they become narrower with larger sample sizes. According to the results, the maximum relative error in the estimation is also displayed in the last column of Table 2 with a 99% certainty level.

In view of the results, if $\bar{\nu}$ is the quantity of interest, using $N = 50$ trials, only about 0.002 of difference between $\bar{\nu}$ and the real $\mu(\nu)$ (less than 1% of relative error) is expected in 99% of the cases. Thus, we will use $N = 50$ trials to perform MCS when looking for $\bar{\nu}$. However, if one is interested in the PDF of ν, $N = 10000$ trials could be employed in MCS to guarantee a certain accuracy in the obtained $S(\nu)^2$. In this case, the relative error between $S(\nu)^2$ and $\sigma(\nu)^2$ is limited by 3.94% at a 99% confidence level. If this result is compared with that obtained from the analytic expression (8),

Table 2: 99% coverage interval and maximum error for the $S(\nu)$ bootstrap distribution.

	$S(\nu^*)^2$	
N	99% Cov. int.	e_{max}
1000	$3.238{\cdot}10^{-3}$ – $4.077{\cdot}10^{-3}$	11.55
5000	$3.524{\cdot}10^{-3}$ – $3.912{\cdot}10^{-3}$	5.39
10000	$3.543{\cdot}10^{-3}$ – $3.827{\cdot}10^{-3}$	3.94

with $N = 10000$ and $\alpha = 0.01$, Eq. (8) gives a relative error of 3.41% which is in good agreement with the bootstrap estimated uncertainty for $S(\nu)^2$.

6. Discussion of the numerical results

As stated in Section 2, this work analyses the Benchmark catenary model [1], although the proposed procedure can be applied to any catenary topology. The model is composed of 20 spans but the results are taken only from the 10 central spans to avoid boundary effects. Following the recommendations in [17], the interaction force is low-pass filtered at 20 Hz, so that the results are comparable to those obtained in [1].

The measurable output magnitudes for the Benchmark catenary are displayed in Table 3 and will be considered as reference values for comparison with those obtained for the actual installed catenaries with their corresponding installation errors.

Table 3: Measurable effects on the nominal Benchmark catenary when the train travels at 300 km/h .

ν	$t_{cl}(\%)$	Δz^{max} (mm)	F_{inter}^{max} (N)	$s_s^{max}(‰)$	$\Delta s_s^{max}(‰)$
0.2589	0	50.22	256.24	0	0

The first examples are carried out at a train speed of $v = 300$ km/h and an uplift force $F_{up} = 168.47$ N is applied to the bottom mass of the pantograph model to fulfil the maximum mean contact force given in [23]:

$$\mu(F_{inter}) = 70 + 0.00097v^2 \tag{9}$$

Whereas Section 6.1 gives a complete statistical quantification of the effects of installation errors on the static and dynamic features of the system, Section 6.2 only

focuses on the mean values of these measurable effects. The next section is devoted to determining the influence of error variability when the train travels at different speeds. The influence of installation errors on the optimal initial sag of the contact wire (pre-sag) is also analysed.

6.1. Statistical quantification of the effects produced by installation errors

This section characterizes the effects of installation errors by computing their full PDFs; each source of uncertainty is first considered in isolation and then the most influential errors are analysed jointly.

The first error considered is that related to dropper lengths. The PDFs of the output parameters are given in Fig. 11, after performing 10000 MC simulations. At first glance, a general deterioration of the system performance is clearly seen, since the mean of each variable is higher than the nominal deterministic values (solid lines in Fig. 11).

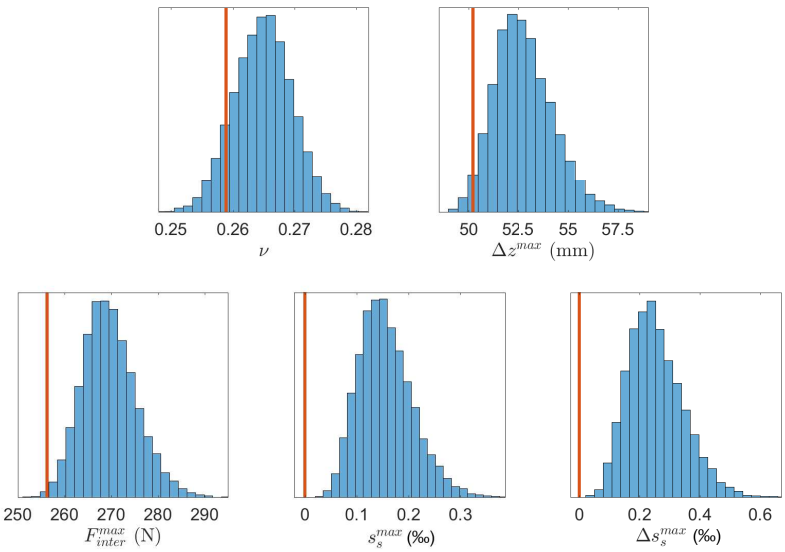

Figure 11: PDFs of output quantities for dropper length error.

The PDFs of Δz^{max}, F_{inter}^{max}, s_s^{max} and Δs_s^{max} present slightly positive skewness, while the opposite effect is found in the case of ν. This installation error hardly

produces non-desirable contact losses between pantograph and catenary. If a contact loss is considered when the contact force before filtering is null in a single time-step (1 ms in this case), they only appear in 38 of the 10000 simulations performed, and in any case exceed 7 ms throughout a simulation.

If only deviations in dropper spacing are considered, the PDFs of the measurable effects plotted in Fig. 12 are obtained. In this case neither contact losses nor span slope changes can be noted. the PDFs of ν and Δz^{max} are around the value obtained with the nominal catenary. Its most important feature is its negligible influence on all the measured output quantities. On the basis of these results, we can conclude that this error barely affects the system dynamics and therefore will be disregarded hereinafter.

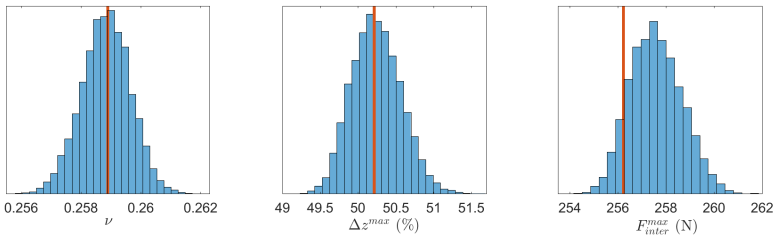

Figure 12: PDFs of output quantities for dropper spacing error.

The last error to be simulated concerns the height at which supports are placed. Considering that the same error affects both steady arm and messenger wire connections (3a and 3b in Fig. 4) gives rise to the results shown in Fig. 13. Just as when considering dropper spacing error, the pantograph does not detach from the contact wire in any case, although this error has the biggest impact on the maximum span slope. The maximum registration arm uplift has also increased more than the values obtained from the simulated dropper length error, although ν is less influenced by support height errors than dropper length errors. In fact, almost half of the simulated trials have a beneficial effect on this magnitude.

In order to split the effects of height errors on messenger wire and steady arm connections to the bracket, we applied MCS allowing only for errors in the height of the placement of the links between steady arms and supports (3b error in Fig. 4). The results obtained show almost no dispersion, indicating that relative errors between the height of steady arm and messenger wire connections to the cantilever have a negligible effect on the considered output magnitudes. The hypothesis that the same error affects both steady arm and messenger wire connections is thus confirmed.

Once each installation error has been analysed in isolation, we focus on the effects of the two most relevant errors occurring simultaneously, as can happen in practice. The results obtained are shown in Fig. 14, in which dropper spacing deviations are not considered due to their negligible influence on the measured magnitudes. In view of

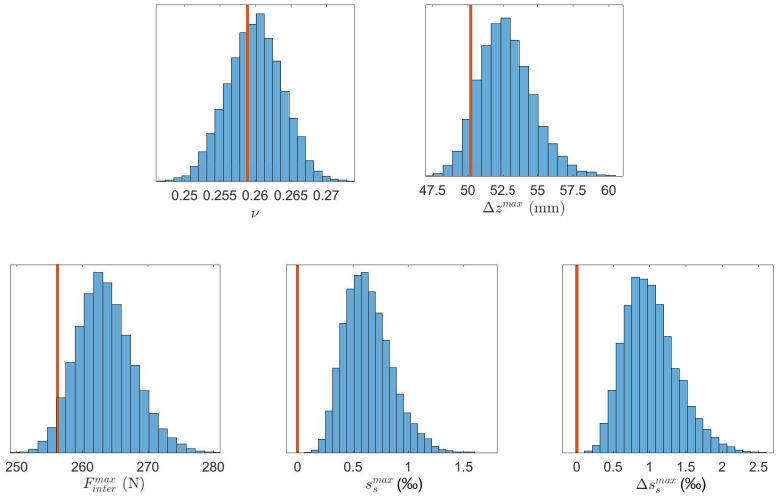

Figure 13: PDFs of output quantities for support height error.

the PDFs obtained, ν deteriorates when both errors are simulated together. However, compared to the standalone results, there is only a slight tendency to worsen the behaviour of the system in the other magnitudes. It can also be seen that variability in ν and F_{inter}^{max} is mainly dominated by dropper length error, whilst variability in Δz^{max}, s_s^{max} and Δs_s^{max} is dominated by errors in support height.

Focusing in greater detail on the coefficient of variation of the interaction force, ν, the 95% coverage interval, $[c_{min}\ \ c_{max}]$, is plotted in Fig. 15. In this figure the horizontal line represents the value of ν obtained with the nominal Benchmark catenary. The small variation of ν when dropper spacing error is considered can be clearly seen. The simulation of the support height error presents a wider 95% coverage interval, which is also centred to the nominal value. When dropper length error is allowed for, ν is more variable and most of the simulated trials show a higher value for this magnitude than the nominal one. This behaviour leads us to conclude that the dropper length error is the most harmful error, and that great care should be given to this factor during installation. The worst scenario is found when dropper length and support height errors are simulated together; this synergy produces the widest 95% coverage interval and also the highest increase in the mean of ν. Indeed, almost all the trials in the interval show worse current collection performance than the nominal catenary.

Table 4 summarises the most important results obtained for the PDF of ν. The relative distance between the maximum and minimum edges of the 95% coverage

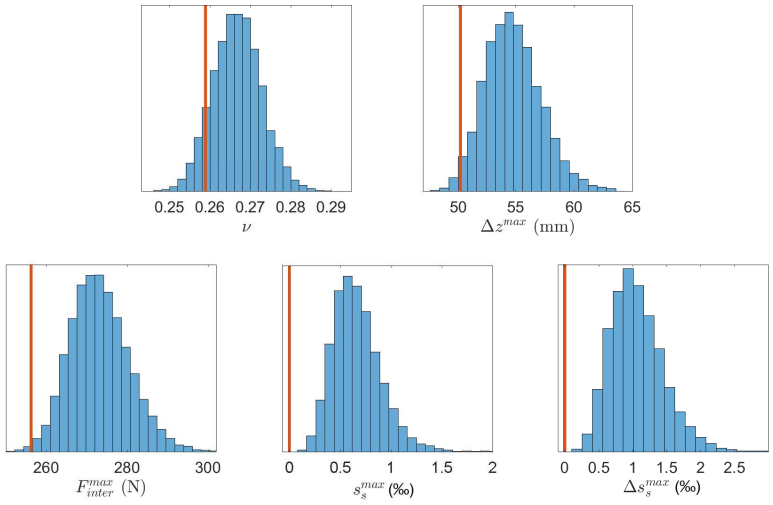

Figure 14: PDFs of output quantities accounting for both relevant installation errors, namely dropper length and support height errors.

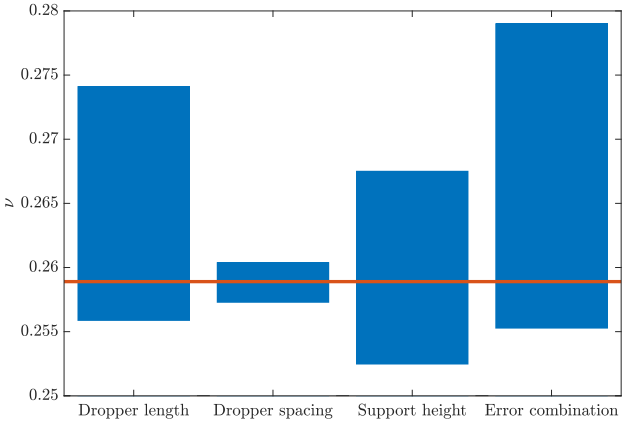

Figure 15: 95% coverage interval of ν for all the different studied scenarios.

interval,

$$\Lambda = \frac{c_{max} - c_{min}}{c_{min}} \cdot 100 \tag{10}$$

is also included as a quantifier of the variability in ν produced by each type of error.

Table 4: Summary of the statistical characterization of the PDF of ν. Mean, standard deviation, 95% coverage interval and Λ ratio for the four studied scenarios.

Error type	$\bar{\nu}$	$S(\nu)$	95% coverage interval	Λ (%)
Dropper length	0.2649	$4.711 \cdot 10^{-3}$	0.2558 - 0.2741	7.15
Dropper spacing	0.2588	$8.138 \cdot 10^{-4}$	0.2572 - 0.2604	1.24
Support height	0.2599	$3.899 \cdot 10^{-3}$	0.2524 - 0.2675	5.99
Error combination	0.2667	$6.069 \cdot 10^{-3}$	0.2552 - 0.2790	9.32

6.2. Mean evaluation of the effects produced by installation errors

As already mentioned in Section 5.1, if only the mean value of a certain output magnitude is required instead of a full PDF description, only 50 MC simulations need to be performed. With this number of simulations, the relative error expected in ν is less than 1%, with a guaranteed confidence level of 99%, although other output magnitudes may not reach this degree of accuracy.

Table 5: Comparison of estimated mean values from a population of 50 individuals and those obtained from a population of 10000 individuals.

	ν	Δz^{max} (mm)	F_{inter}^{max} (N)	s_s^{max} (‰)	Δs_s^{max} (‰)
μ	0.2667	54.76	273.21	0.665	1.065
$\tilde{\mu}$	0.2658	54.92	273.69	0.677	1.031
Rel. Err. (%)	0.34	0.29	0.18	1.80	3.19
μ/σ	43.94	22.29	37.53	2.77	2.67

The first row in Table 5 shows the mean values of the output magnitudes obtained from the PDFs in Fig. 14, which can be assumed to be the real population mean of each magnitude, since they are obtained from 10000 trials. The second row of the table gives the mean values obtained from only 50 simulations. The relative error of the latter estimation is given in the third row. It is clear that ν, Δz^{max} and F_{inter}^{max} can be accurately estimated by this procedure, while estimating s_s^{max} and Δs_s^{max} would need a larger number of trials by the MC method. This can be explained by the ratio between the mean and the standard deviation of the PDF of each magnitude. The greater this ratio, the more accurate $\tilde{\nu}$ tends to be for a given number of trials.

6.3. Influence of installation errors at different train speeds

A nominal train velocity of 300 km/h was considered in the examples discussed so far. However, any change in this parameter would affect the effects of the installation errors in the system dynamics. To study this phenomenon, the MC method was executed with 10000 trials, considering different train speeds, applying the appropriate uplift force and keeping all the other parameters constant. The simulations allow for both dropper length and support height errors.

The 95% coverage interval of ν is given in Fig. 16 for $v = 200$, 250 and 300 km/h. The uplift forces applied to the pantograph are $F_{up} = 114.07$, 138.33 and 168.47 N, respectively, to fulfil the maximum mean contact force requirement of Eq. (9). The horizontal lines denote the nominal ν value at each speed. ν clearly tends to decrease

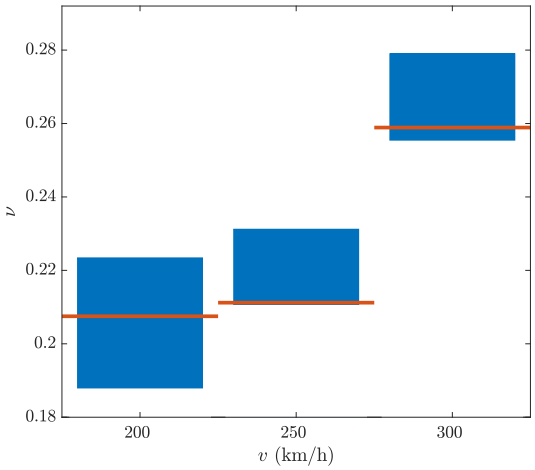

Figure 16: 95% coverage interval of ν at different train speeds including both dropper length and support height errors.

at lower train velocities. Regarding uncertainty, installation errors seem to be more detrimental at high velocities (250 and 300 km/h) since the 95% coverage interval is entirely located above its respective nominal ν, despite being narrower. This deterioration in current collection quality cannot be appreciated at $v = 200$ km/h, because most of the simulated trials have a ν value lower than the nominal.

These results indicate that careful attention should be paid to accuracy when installing high-speed catenaries, since any errors tend to have an increasingly negative effect.

6.4. Optimal robust pre-sag

A certain amount of pre-sag is beneficial for current collection quality, especially in the medium speed range [30]. Optimal pre-sag values for a given train velocity are reported in [3], but only for deterministic simulations that ignored the variability of installation errors. Here we obtained a robust optimal pre-sag value, allowing for the uncertainty present in the installed catenaries.

Fig. 17 shows a comparison between $\bar{\nu}$ computed as the mean value of 50 samples with random installation errors (circles), and ν obtained from the nominal configuration (squares) when different pre-sag values are assigned. The study was carried out at three different speeds: 200, 250 and 300 km/h. The obtained optimal pre-sag is highlighted for each case with thick crosses in Fig. 17.

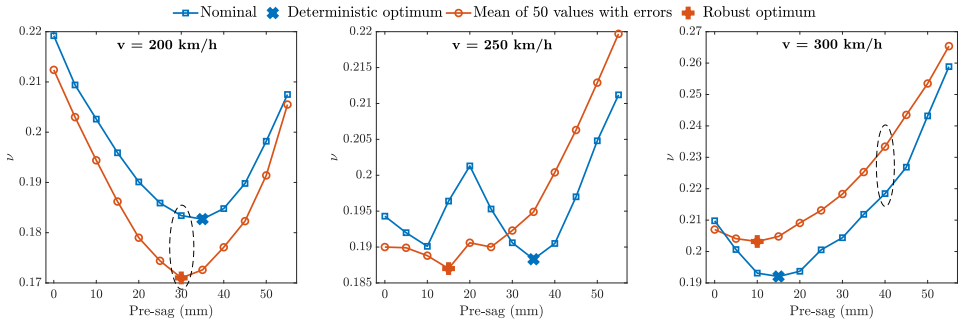

Figure 17: Comparison, for catenaries with different initial sag, between the nominal ν and $\bar{\nu}$ computed from 50 trials with installation errors. $v = 200$ km/h (left), $v = 250$ km/h (centre) and $v = 300$ km/h (right).

The first conclusion to be drawn from these results is the importance of considering the variability introduced by installation errors when seeking optimal catenary configurations. In this scenario, the optimal robust pre-sag differs from that obtained in the deterministic case.

Another interesting feature in Fig. 17 is that there are some catenary configurations in which $\bar{\nu} < \nu$, indicating that they behave better, on average, than in their corresponding nominal configuration. This unexpected behaviour occurs at low speeds (200 km/h) in all the cases studied and at medium speeds (250 km/h) in catenaries with low pre-sag (< 30 mm).

In order to explain this phenomenon, we focus on two catenaries with opposing behaviour: one with 40 mm of pre-sag at 300 km/h and another with 30 mm of pre-sag at 200 km/h (points surrounded by dashed lines in Fig. 17). The Fourier transform of the low-pass filtered interaction force for both the nominal cases (squares) and the mean of fifty configurations with installation errors (circles) can be seen in Fig. 18.

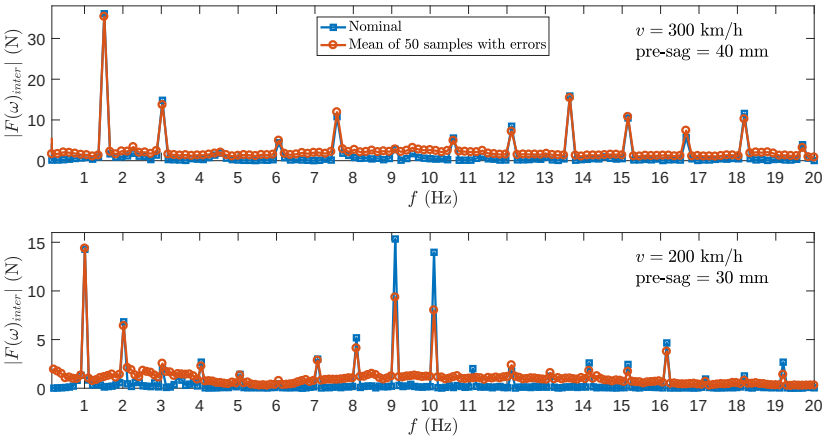

Figure 18: Frequency content of F_{inter} for catenaries with 40 mm (top) and 30 mm (bottom) of pre-sag, considering nominal and actual installed scenarios when pantograph moves at $v = 300$ km/h and $v = 200$ km/h respectively.

If $\Xi = [0, ..., 20]$ Hz, we define $h = [h_1, h_2, ..., h_{n_h}]$ as the set of the harmonics of the fundamental span-pass frequency, and $\hat{h} = \Xi - h$ is therefore the set containing the remaining frequencies. In Fig. 18 most of the frequency content of F_{inter} is located on h. The mean effect of installation errors seems to reduce the amplitudes of the h frequencies in exchange for an increase in the frequency content of $\hat{h}$ due to the elimination of periodicity in contact wire height.

In order to quantify these effects, we can decompose ν into the contribution of both h frequencies, ν_h, and the remaining frequencies, $\nu_{\hat{h}}$, so that $\nu^2 = \nu_h^2 + \nu_{\hat{h}}^2$. Fig. 19 shows the difference $\bar{\nu}^2 - \nu^2$ for both frequency set contributions: h and $\hat{h}$. The increase seen in $\nu_{\hat{h}}$ seems to be more or less constant with respect to train speed and pre-sag, although the reduction of ν_h is clearly greater at lower speeds, with the maximum at $v = 200$ km/h.

To sum up, if the decrease in ν_h overcomes the increase in $\nu_{\hat{h}}$, the catenary in which allowance is made for installation errors, on average, behaves slightly better than the nominal catenary. In the case studied, this happens at low train speeds and low pre-sag values.

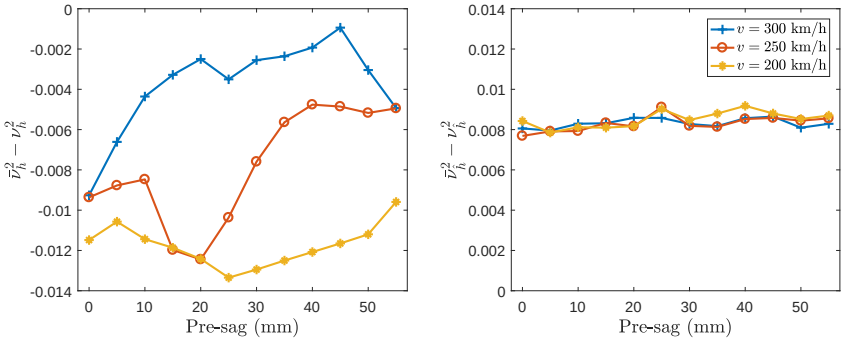

Figure 19: Difference between $\bar{\nu}^2$ and ν^2 computed with the span-pass harmonics h (left) or with the rest of the frequency content $\hat{h}$ (right).

7. Conclusions

This work proposes a method of simulating pantograph–catenary dynamic interaction that takes into account the variability introduced by catenary installation errors.

Three different error types were considered: those related to dropper length, dropper spacing and support height. After their statistical characterization, the Monte Carlo method was applied to propagate the uncertainty to the desired output quantities. A statistical study was then performed to obtain the number of MC trials required to control the accuracy of the PDF of the output quantities.

Allowing for these installation errors has a remarkable effect on the static and dynamic features of catenary behaviour. Current collection quality is clearly worse when dropper length and support height errors are simulated, whereas the spacing error has only minor effects. The results of the simulations carried out in this work indicate that the higher the speed, the more negative the effects of installation errors on current collection performance.

Another important conclusion is related to the optimal amount of pre-sag; this quantity not only varies with train speed but is also clearly affected when installation errors are taken into account in the simulations.

To summarise, all the results of this study highlight the importance of considering the uncertainty due to catenary installation and its effect on catenary dynamic behaviour.

Acknowledgements

The authors would like to acknowledge the financial support received from the FPU program offered by the Spanish Ministry of Education, Culture and Sports (MECD) under Grant Number FPU13/04191. The funding provided by the Regional Government of Valencia (PROMETEO/2016/007) and the Spanish Ministry of Economy, Industry and Competitiveness (TRA2017-84736-R) is also acknowledged.

References

[1] S. Bruni, J. Ambrosio, A. Carnicero, Y. H. Cho, L. Finner, M. Ikeda, S. Y. Kwon, J. P. Massat, S. Stichel, and M. Tur, "The results of the pantograph–catenary interaction benchmark," *Vehicle System Dynamics*, vol. 53, no. 3, pp. 412–435, 2015. 1, 2, 3, 6

[2] N. Zhou and W. Zhang, "Investigation on dynamic performance and parameter optimization design of pantograph and catenary system," *Finite Elements in Analysis and Design*, vol. 47, no. 3, pp. 288–295, 2011. 1

[3] S. Gregori, M. Tur, E. Nadal, and F. J. Fuenmayor, "An approach to geometric optimisation of railway catenaries," *Vehicle System Dynamics*, pp. 1–25, 2017. 1, 6.4

[4] J. W. Kim, H. C. Chae, B. S. Park, S. Y. Lee, C. S. Han, and J. H. Jang, "State sensitivity analysis of the pantograph system for a high-speed rail vehicle considering span length and static uplift force," *Journal of Sound and Vibration*, vol. 303, no. 3, pp. 405–427, 2007. 1

[5] A. Collina, F. Fossati, and F. Resta, "An innovative OHL diagnosis procedure based on the pantograph dynamics measurements," in *World Congress on Railway Research, Koln*, 2001. 1

[6] A. Collina, F. Fossati, M. Papi, and F. Resta, "Impact of overhead line irregularity on current collection and diagnostics based on the measurement of pantograph dynamics," *Proceedings of the Institution of Mechanical Engineers, Part F: Journal of Rail and Rapid Transit*, vol. 221, no. 4, pp. 547–559, 2007. 1

[7] M. Aboshi and M. Tsunemoto, "Installation guidelines for shinkansen high speed overhead contact lines," *Quarterly Report of RTRI*, vol. 52, no. 4, pp. 230–236, 2011. 1

[8] O. Vo Van, J. P. Massat, C. Laurent, and E. Balmes, "Introduction of variability into pantograph–catenary dynamic simulations," *Vehicle System Dynamics*, vol. 52, no. 10, pp. 1254–1269, 2014. 1

[9] O. Vo Van, E. Balmes, and J. Massat, "Statistical identification of geometric parameters for high speed train catenary," in *International Conference on Noise and Vibration*, pp. 2–11. 1, 4.1

[10] N. Metropolis and S. Ulam, "The Monte Carlo method," *Journal of the American Statistical Association*, vol. 44, no. 247, pp. 335–341, 1949. 1

[11] S. Gregori, M. Tur, E. Nadal, J. Aguado, F. Fuenmayor, and F. Chinesta, "Fast simulation of the pantograph-catenary dynamic interaction," *Finite Elements in Analysis and Design*, vol. 129, pp. 1–13, 2017. 1, 3, 5

[12] M. Arnold and B. Simeon, "Pantograph and catenary dynamics: A benchmark problem and its numerical solution," *Applied Numerical Mathematics*, vol. 34, no. 4, pp. 345–362, 2000. 2

[13] A. Collina and S. Bruni, "Numerical simulation of pantograph-overhead equipment interaction," *Vehicle System Dynamics*, vol. 38, no. 4, pp. 261–291, 2002. 2, 3

[14] M. Tur, L. Baeza, F. Fuenmayor, and E. García, "PACDIN statement of methods," *Vehicle System Dynamics*, vol. 53, no. 3, pp. 402–411, 2015. 2

[15] A. Shabana, "Computer implementation of the absolute nodal coordinate formulation for flexible multibody dynamics," *Nonlinear Dynamics*, vol. 16, pp. 293–306, 1998. 2

[16] J. Ambrosio, F. Rauter, J. Pombo, and M. Pereira, "A flexible multibody pantograph model for the analysis of the catenary–pantograph contact," vol. 23, pp. 1–27, 2011. 2

[17] EN 50318, "Railway applications. Current collection systems. Validation of simulation of the dynamic interaction between pantograph and overhead contact line," *European Committee for Electrotechnical Standarization*, 2002. 2, 6

[18] M. Tur, E. García, L. Baeza, and F. Fuenmayor, "A 3D absolute nodal coordinate finite element model to compute the initial configuration of a railway catenary," *Engineering Structures*, vol. 71, pp. 234–243, 2014. 3

[19] N. M. Newmark, "A method of computation for structural dynamics," *Journal of the Engineering Mechanics Division*, vol. 85, no. 3, pp. 67–94, 1959. 3

[20] J. Ambrósio, J. Pombo, P. Antunes, and M. Pereira, "PantoCat statement of methods," *Vehicle System Dynamics*, vol. 53, no. 3, pp. 314–328, 2015. 3

[21] O. Vo Van, E. Balmes, A. Capitaine, and X. Lorang, "Sensitivity analysis of catenary geometry on current collection quality," *The Third International Conference on Railway Technology: Research, Development and Maintenance, Cagliari, Sardinia, Italy*, 2016. 4.1, 4.3

[22] ENE TSI, "Technical specifications for interoperability relating to the 'energy' subsystem of the rail system in the union," *European Commission*, 1301/2014. 4.4

[23] EN 50367, "Railway applications. Current collection systems. Technical criteria for the interaction between pantograph and overhead line," *European Committee for Electrotechnical Standarization*, 2012. 4.4, 6

[24] M. Á. Herrador, A. G. Asuero, and A. G. González, "Estimation of the uncertainty of indirect measurements from the propagation of distributions by using the Monte-Carlo method: An overview," *Chemometrics and Intelligent Laboratory Systems*, vol. 79, no. 1, pp. 115–122, 2005. 5

[25] R. M. Dudley, "Central limit theorems for empirical measures," *The Annals of Probability*, pp. 899–929, 1978. 5.1

[26] D. G. Bonett, "Approximate confidence interval for standard deviation of non-normal distributions," *Computational Statistics & Data Analysis*, vol. 50, no. 3, pp. 775–782, 2006. 5.1

[27] S. Arnold, *Mathematical Statistics*. Prentice-Hall, 1990. 5.1

[28] B. Efron, "Bootstrap methods: another look at the jackknife," in *Breakthroughs in statistics*, pp. 569–593, Springer, 1992. 5.1

[29] B. Efron and R. J. Tibshirani, *An introduction to the bootstrap*. CRC press, 1994. 5.1

[30] Y. H. Cho, K. Lee, Y. Park, B. Kang, and K. N. Kim, "Influence of contact wire pre-sag on the dynamics of pantograph–railway catenary," *International Journal of Mechanical Sciences*, vol. 52, no. 11, pp. 1471–1490, 2010. 6.4